Investigating the interface between dynamic HES1 expression and the cell cycle

A thesis submitted to the University of Manchester for the degree of Doctor of Philosophy in the Faculty of Biology, Medicine and Health

2021

Sean A Hourihane

School of Biological Sciences
Division of Developmental Biology and Medicine

Table of contents

Word count (main text): 49702

List of figures

List of Tables

Abstract

The cell cycle is the fundamental process that underpins the generation of two daughter cells from a mother cell. Single-cell studies have revealed that genetically identical cells display differences in the time they spend progressing through the cell cycle. Deciphering how cell cycle length heterogeneity arises will have important implications for understanding aspects of cancer development and tumour relapse. Evidence from time-lapse microscopy suggests that cell cycle variation can be linked to transcription factor dynamics and how they interface with the cell cycle. This thesis sought to describe the expression dynamics and ultimately function of the transcription factor HES1 during the cell cycle in the MCF7 breast cancer cell line. Single-cell measurement of *HES1* transcription was performed using single-molecule fluorescence *in-situ* hybridisation (smFISH). A recently published HES1 inhibitor (JI051) was characterised by examining its effect on cell cycle progression, HES1 protein dynamics and HES1 target binding. *HES1* expression displayed substantial cell-to-cell heterogeneity in MCF7 cells. An increase in the number of *HES1* transcription start sites and mRNA transcripts per cell was observed in cells with a higher DNA content, indicating that *HES1* transcription is dynamic and potentially upregulated during cell cycle progression. The dominant effect of JI051 on the cell cycle was found to be a prolonged mitotic arrest without an impairment of cell cycle progression prior to mitosis. Although, nuclear expression of HES1 was decreased in a proportion of JI051-treated cells, cells arrested in mitosis regardless of any change in HES1 expression. Sustained *CCNB1* expression was identified as a notable gene expression change occurring in JI051-treated cells. Whether *CCNB1* or transcriptional activators of *CCNB1* were de-repressed due to JI051 treatment was investigated by ChIP-sequencing. No mechanistic link was identified between sustained *CCNB1* expression and HES1. Nonetheless, several novel HES1 targets were identified that will serve as useful information for the study of HES1 in a breast cancer context. Moreover, HES1 binding to its own promoter (a regulatory requirement for HES1 dynamics) was verified and found to be differentially enriched at distinct timepoints in G1, indicating that *HES1* expression may be modulated during the cell cycle by negative feedback in MCF7 cells.

Declaration

No portion of the work referred to in the thesis has been submitted in support of an application for another degree or qualification of this or any other university or other institute of learning

Copyright Statement

I. The author of this thesis (including any appendices and/or schedules to this thesis) owns certain copyright or related rights in it (the “Copyright”) and he has given The University of Manchester certain rights to use such Copyright, including for administrative purposes.

II. Copies of this thesis, either in full or in extracts and whether in hard or electronic copy, may be made only in accordance with the Copyright, Designs and Patents Act 1988 (as amended) and regulations issued under it or, where appropriate, in accordance with licensing agreements which the University has from time to time. This page must form part of any such copies made.

III. The ownership of certain Copyright, patents, designs, trademarks and other intellectual property (the “Intellectual Property”) and any reproductions of copyright works in the thesis, for example graphs and tables (“Reproductions”), which may be described in this thesis, may not be owned by the author and may be owned by third parties. Such Intellectual Property and Reproductions cannot and must not be made available for use without the prior written permission of the owner(s) of the relevant Intellectual Property and/or Reproductions.

IV. Further information on the conditions under which disclosure, publication and commercialisation of this thesis, the Copyright and any Intellectual Property and/or Reproductions described in it may take place is available in the University IP Policy (see http://documents.manchester.ac.uk/DocuInfo.aspx?DocID=2442 0), in any relevant Thesis restriction declarations deposited in the University Library, The University Library’s regulations (see http://www.library.manchester.ac.uk/about/regulations/) and in The University’s policy on Presentation of Theses

Acknowledgements

To my supervisors, Nancy and Philipp, thank you for your support during the past few years. Thank you for your patience and for keeping things moving in the right direction. It's been a challenging and rewarding experience and I appreciate all you've taught me.

During the countless times I was stuck on a problem be it experimental or theoretical, Nitin and Nathan were always hugely generous with their time when offering to help. Thank you both very much.

Thank you everyone from the Papalopulu and Kaldis labs. It's been a pleasure.

Thank you to my parents for your unending support for everything I've done in life. I would not have been able to do this without you. I'm sorry for being so grumpy the past few weeks.

Chapter 1. Introduction

1.1 Opening remarks

Advances in live-cell microscopy, single-cell analysis techniques and gene-editing have empowered research investigating the relationship between gene expression and phenotypic outcomes at the single-cell level. Researchers can now probe the mechanistic basis of cellular heterogeneity in a variety of biological contexts. Of particular interest to this thesis, is the existence of heterogeneity in cellular proliferation, namely how individual cells in a genetically similar population display differences in the rates at which they undergo cell division. This feeds into many important questions in biology and medicine such as how cells adopt different cell fates during development, or how subsets of cancer cells resist cancer treatment to then cause tumour relapse. Questions like these are now being investigated by observing the underlying gene expression dynamics that are associated with differences in how cells grow and divide.

In a similar vein, the aim of this thesis is to investigate the relationship between the cell cycle and the transcription factor HES1, a key regulator of developmental fate decisions, which has more recently been implicated in cancer development. In the introduction to the experimental work, I will describe the cell cycle and highlight recent research that has improved our understanding of its temporal regulation. I will then discuss our enhanced understanding of transcription factor function based on observation of expression dynamics and finish by focusing on HES1.

1.2 Overview of the cell cycle

A complete cell cycle encompasses successive phases of cell growth, duplication of a cell's genome and the physical division of the cell (cytokinesis) and segregation of chromosomes between each daughter cell. These phases are G1 (growth), S-phase (DNA replication), a G2 (growth) and mitosis (M-phase) (Norbury & Nurse, 1992). Mitosis comprises four distinct phases known as, prophase, metaphase, anaphase and telophase (Mitchison & Salmon, 2001). Cells can also enter a non-dividing state, known as quiescence, from which proliferation can be re-activated (Coller et al.,

2006; Cheung & Rando 2013). A well-detailed picture of the molecular mechanisms that control progress through the cell cycle phases has been developed through research that has spanned early observations of cell cycle events in model systems through to the identification of the proteins involved in the regulation of cell cycle transitions. The key proteins involved in cell cycle regulation are the Cyclin-dependent kinases (CDKs), a family of serine/threonine kinases and their binding partners, the Cyclin proteins (Satyanarayana & Kaldis 2009; Malumbres & Barbacid 2005; Martínez-Alonso & Malumbres 2020).

CDKs were first identified by research undertaken in amphibian and yeast models of cell division. In amphibians, this began with characterisation of the maturation promoting factor (MPF), a cytoplasmic extract isolated from mature *Rana pipien* oocytes. Injection of MPF into immature oocytes could stimulate meiotic divisions associated with maturation (Masui & Markert, 1971). In yeast mutant screens, the genes *cdc2* and *cdc28* from *Saccharomyces pombe* and *Saccharomyces cerevisiae* were identified for their role in promoting S-phase and mitosis (Piggott et al., 1982; Nurse & Bissett 1981; Beach et al., 1982). Expression of a human cDNA library in *S. pombe cdc2* mutants was used to identify and clone the human *cdc2* homolog, now known as CDK1 (Lee and Nurse 1987). Further purification of MPF led to the identification of the *Xenopus cdc2* homolog (Lohka et al., 1988; Gautier et al., 1988). The first cyclin protein, Cyclin A, was identified in sea urchins, aptly named due to its cyclic pattern of expression and destruction during cleavage divisions in the early embryo (Evans et al., 1983). The identification of Cyclin B in *Xenopus* and humans soon followed, and ablation of its expression was associated with defects in mitotic entry (Minshull et al., 1989; Pines & Hunter 1989). Furthermore, Inhibition of Cyclin B destruction was found to prevent exit from mitosis, demonstrating the importance of the temporal expression of cyclin molecules in maintaining the fidelity of cell cycle transitions (Murray et al., 1989).

1.3 Regulation of the mammalian cell cycle

To date, multiple CDK and Cyclin proteins have been discovered which operate at distinct phases of the cell cycle in higher eukaryotes. Their spatiotemporal activity and substrate specificity is primarily dependent on the availability of their Cyclin binding partners, which is controlled at a transcriptional level and by protein degradation (Pagano, 1997). Additionally, CDKs require phosphorylation by the CDK-activating kinase (CAK) on activating threonine residues to enable interactions with substrates (Kaldis 1999; Solomon et al., 1992; Gu et al., 1992). Transcriptional regulation of the mammalian cell cycle broadly entails repression of genes required for cell cycle progression in quiescent cells and a combination of transcriptional de-repression and induction of gene expression required for regulating the G1/S and G2/M transitions. The proteins that are central, but not exclusive, to cell cycle transcriptional regulation are: the pocket protein family (RB, p107 and p130), the E2F family of transcriptional activators (E2F1, E2F2, and E2F3A) and repressors (E2F3b, E2F4, E2F5, E2F6, E2F7, E2F8), and the MuvB protein complex (LIN9, LIN37, LIN52, LIN54, and RBBP48), an ortholog of the worm synMuvB complex (Cobrinik 2005; Attwooll et al., 2004). MuvB in complex with E2F repressors forms the DREAM (DP, RB-like, E2F and MuvB) complex that is responsible for the transcriptional repression of cell cycle genes early in the cell cycle (Sadasivam & DeCaprio, 2013). Upon S-phase entry, MuvB switches to a transcriptional activator when dissociated from the DREAM complex and bound to transcription factors B-MYB and FOXM1 (Guiley et al., 2018). Controlled protein degradation through target ubiquitination plays a pivotal role in ensuring the robustness of cell cycle transitions. The SKP1/CULLIN/F-BOX (SCF) and anaphase-promoting complex/cyclosome (APC/C) ligases are the two main complexes that regulate protein degradation (Reed, 2003). Furthermore, CDK activity can be opposed by CDK inhibitors (CDKIs), of which there are two families - the INK4 (Inhibitors of CDK4) and the Cip/Kip CDKIs (Sherr & Roberts, 1999).

1.4 Progression through G1 and S-phase

In the simplest view of cell cycle progression, entry into the cell cycle begins with mitogen stimulation of *CCND1* expression. Multiple signaling pathways induce *CCND1* transcription, these include, the mitogen-activated proteins kinase (MAPK) pathway, extracellular signal-regulated kinase (ERK) signaling, and Nuclear factor kappa B (NF-κB) signaling (Guttridge et al., 1999; Klein & Assoian, 2008). Expression of *CCND1* leads to activation of CDK4 and CDK6 which in turn initiates phosphorylation of the tumour supressor protein, Rb (Lundberg & Weinberg, 1998). The period between a cell's response to mitogenic signaling and subsequent phosphorylation of Rb is believed to encompass the restriction point (R), whereby cells commit to cell cycle progression (Blagosklonny & Pardee, 2002; Pardee, 1974). In addition to Rb phosphorylation, CDK4,6/Cyclin D1 supports cell cycle progression by promoting the dis-assembly of the DREAM complex, which represses the expression of genes required for G1/S progression (Schade et al., 2019). Transcription of *CCNE1* and subsequent CDK2/Cyclin E1 activation is associated with further cell cycle progression towards S-phase entry. *CCNE1* expression has pre-dominantly been shown to hinge on inhibitory phosphorylation of Rb to promote activation of E2F1-mediated transcription at its promoter. This was initially demonstrated in experiments where activation of *CCNE1* transcriptional reporters in late G1 was diminished in cells expressing reporter constructs where the E2F1 binding sites were abolished, indicating the requirement for E2F1 in regulating the G1 specific expression of *CCNE1* (Botz et al., 1996; Ohtani et al., 1995). However, recent research demonstrating that CDK4,6/cyclin D1 can only mono-phosphorylate Rb – an event that does not prevent Rb inhibition of E2F1 function – has questioned the reliance of *CCNE1* transcription solely on E2F1 activation (Narasimha et al., 2014). Transcription of *CCNE1* can be activated by alternative signaling pathways, such as Myc signaling (Pérez-Roger et al., 1997; Santoni-Rugiu et al., 2000). The activation of CDK2/Cyclin E1 promotes a positive feedback loop whereby E2F1 amplifies its own expression and that of *CCNE1*. This network promotes RB hyper-phosphorylation and the activation of genes required for passage through the G1/S transition, including *CCNA2* (Schulze et al., 1995; DeGregori et al., 1995; Gérard & Goldbeter 2009).

1.5 Progression through G2 and mitosis

Expression of genes required for progression through G2 and entry into mitosis is primarily coordinated by B-MYB-MuvB (MMB) and FOXM1-MuvB complexes binding to cell cycle homology region (CHR) motifs in the promoters of late cell cycle genes (Müller and Engeland 2010). Both *B-MYB* and *FOXM1* exhibit periodic expression within the cell cycle. *B-MYB* is expressed in late G1/S-phase while FOXM1 expression occurs mainly in G2 (Catchpole et al., 2002; Lam & Watson, 1993) . *B-MYB* is negatively regulated by the DREAM complex early in the cell cycle. Once its expression is de-repressed, the activity of B-MYB is enhanced through phosphorylation by CDK2/Cyclin A2 in S-phase (Ziebold et al., 1997). The *FOXM1* gene contains CHR motifs that also designate it as a target for transcriptional repression by the DREAM complex (Fischer & Müller 2017; Müller et al., 2014). It has also been demonstrated to negatively regulate its own expression, which is relieved by CDK2/Cyclin A2 and CDK1/Cyclin A2 phosphorylation of the FOXM1 protein (Laoukili et al., 2008; Park et al., 2008). ChIP-sequencing has demonstrated sequential binding of MuvB-B-MYB and MuvB-FOXM1 to the promoters of numerous G2 genes, e.g. *CCNA2*, *CCNB1, PLK1, AURORA A* and *AURORA B.* Knockdown of *B-MYB, LIN9* of MuvB, and *FOXM1* by siRNA reduced the expression of *CCNB1* and delayed entry into mitosis (Sadasivam et al., 2012). Additionally, G2 gene transcription is activated through the NF-Y transcription factor, which binds CCAATT motifs (Chae et al., 2004).

Progression into mitosis is coordinated by CDK1/Cyclin A2 and CDK1/Cyclin B1, with transcription of *CCNA2* and *CCNB1* being a key step in the initial activation of CDK1, alongside phosphorylation of CDK1 on a threonine residue (T160) by CAK (Lindqvist et al. 2009). Prior to the G2/M transition CDK1/Cyclin complexes are kept inactive by inhibitory phosphorylation on tyrosine (Y15) and threonine (T14) residues by WEE1 and MYT1 (McGowan & Russell 1993; Mueller et al., 1995). Inhibitory phosphorylation of CDK1 is reversed by CDC25 phosphatases, initiating a positive and negative feedback loop whereby CDK1 activates further CDC25 by phosphorylation and promotes the degradation of WEE1 (Izumi & Maller, 1993; Watanabe et al., 2005). Furthermore, CDK1 promotes the activation of other key regulators of mitosis,

such as the AURORA kinases and PLK1 (Van Horn et al., 2010; Tsukahara et al., 2010). PLK1 positively regulates CDK1 activity by enhancing CDC25 function and targeting MYT1 for degradation (Nakojima et al., 2003; Qian et al., 2001). Increasing CDK1 activity thereby promotes entry into mitosis (Gavet & Pines, 2010). The activity of core CDK proteins and their Cyclin binding partners during the cell cycle phases is illustrated in figure 1.1.

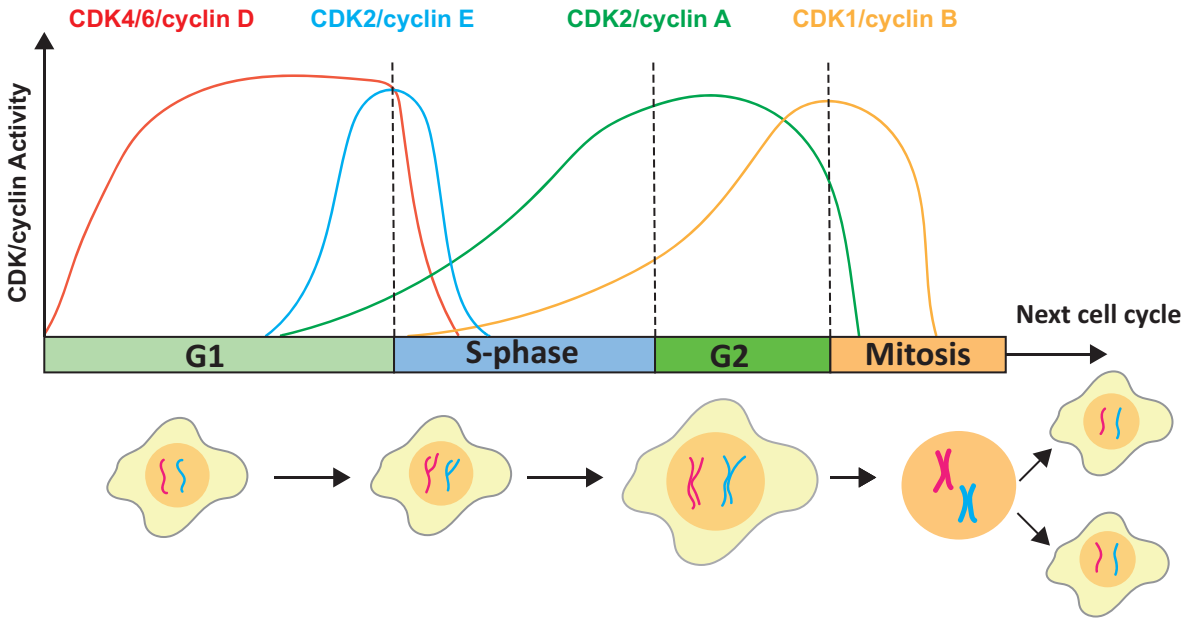

Fig 1.1 Basic overview CDK/Cyclin Activity during the cell cycle

Mitogenic signaling stimulates transcription of *CCND1* and the formation of CDK4,6/Cyclin D complexes leading to phosphorylation of RB and disassembly of the DREAM complex. De-repression of E2F1 promotes *CCNE1* transcription and subsequent CDK2/Cyclin E activity that further promotes cell cycle progression by phosphorylation of RB and inhibition of p27. Activation of CDK2/Cyclin A also targets p27 and E2F transcriptional activators for degradation during the G1/S transition. Increasing CDK/Cyclin B activity in G2 promotes entry into mitosis through phosphorylation of targets that cause cell rounding and nuclear envelope breakdown to allow sister chromatid segregation. Exit from mitosis begins when sister chromatids successfully align at the metaphase plate and CDK1 activity is reduced by degradation of Cyclin B1.

1.6 Temporal differences in cell cycle progression

Differences in proliferation rates between cells of the same cell type is a long-acknowledged phenomenon reported in early time-lapse experiments of mammalian cell cultures (Froese 1964; Dawson et al., 1965; Puck & Steffen 1963). Variability in the length of all phases of the cell cycle and between cell types has since been well described with different cellular contexts underlying cell cycle variation, for example, prolonged S-phases or G2 arrests are due to checkpoint arrest are indicative of DNA damage (Samuel et al., 2002). Cell cycle duration is also affected by cell fate decisions, for example, G1 phase lengthening and cell cycle exit are features of cellular differentiation (Buttitta & Edgar, 2007; Soufi & Dalton, 2016). With the molecular mechanisms of cell cycle control well elucidated, a more recent challenge has been to understand the relationship between the temporal activity of cell cycle regulators and the manifestation of differences in proliferation between individual cells in asynchronously cycling populations. Additionally, long-term timelapse experiments tracking cells over multiple generations have sought to identify underlying generational processes that determine cell cycle length between related cells (Chao et al., 2019; Sandler et al., 2015). This research has been made possible by imaging tools that allow direct observation of cell cycle phases and quantitative measurement of gene activity.

Describing the molecular sources of differences in G1 length has been considered of particular importance as they are thought to underly mechanisms that govern the G1/S transition or entry into quiescence (Pennycook & Barr, 2020). In cycling MCF10A cells, a mammary epithelial cell line, differences in cell cycle commitment and thus G1 length were found to result from cells entering G1 with varying levels of CDK2 activity, either increasing or low (denoted $CDK2^{inc}$ or $CDK2^{low}$) (Spencer et al., 2013). In this study CDK2 activity was measured based on the cytoplasmic to nuclear ratio of a DNA helicase B (DHB) mVENUS reporter. This reporter translocates from the nucleus to the cytoplasm when phosphorylated by CDKs, with increasing

cytoplasmic signal indicating progression through to S-phase and G2 (Hahn et al., 2009; Gu et al., 2004). Cell cycle lengths varied from 16-20 hours in $CDK2^{inc}$ cells compared to $CDK2^{low}$ cells, which displayed more heterogeneous cell cycle lengths sometimes in excess of 50 hours. Furthermore, cells that had undergone mitosis 1-3 hours before being treated with the MEK inhibitor PD032591, displayed $CDK2^{inc}$ activity and associated cell cycle progression, suggesting commitment to proliferation is determined prior to cell division and is independent of MEK-relayed mitogen sensing in G1. The bifurcation in CDK2 activity was determined to be under the control of the CDKI p21. Cells depleted of p21 decreased the number of cells exiting mitosis with CDK2 low activity and resulted in new born cells having similar cell cycle lengths to cells in control experiments born with increasing CDK2 activity (Spencer et al., 2013). This bifurcation of CDK2 activity was suggested to be a mechanism to sustain homeostasis, with entry into low-proliferative states a feature of cells that were responding to cellular stress. This scenario has been demonstrated in follow-up studies using the same CDK2 biosensor alongside live reporters for p53 and p21 (Barr et al., 2017; Yang et al., 2017). In MCF7 cells increased levels of p53 and p21 prior to mitosis were correlated with daughter cells exhibiting low CDK2 activity and delayed cell cycle progression. Mechanistically this delay is achieved when inheritance of p53 protein leads to increased levels of p21 in daughter cells which then inhibits the CDK4/cyclin D1 pathway leading to delayed CDK2 activation (Yang et al., 2017). Similarly, inheritance of p21 arising due to endogenous DNA damage was correlated with a G1 delay in hTert-RPE1 cells (Barr et al., 2017). The source of DNA damage in this case was determined to be incomplete DNA replication as judged by the appearance of 53BP1 foci in G1. p21 inheritance from mother cells could cause a G1 arrest in the case of one or both daughter cells receiving a critical level of p21 that could inhibit CDK2 activity (Barr et al., 2017).

Subsequent analysis of the CDK2 sensor determined that it reported on an accumulation of CDK2 and CDK1 activity as cells progressed into S-phase and suggested that it is more a readout of proliferation rather than CDK2 activity specifically (Schwarz et al., 2018). Furthermore, this study, showed that not all cells exhibit a mode of cell cycle progression that is determined by an inheritance of CDK2

activity. This was revealed by live-imaging of cells where 10% serum media was removed and replaced with serum free media. In RPE, MRC5 and T98G cell lines, cells born after serum removal went on to divide, indicating that they were already committed to cell cycle progression. However, in primary mouse embryonic fibroblasts, no cell born after serum removal went on to complete cell division during a 2 day imaging period. The cell cycle length of cells born before serum removal was found to be dependent on the age of the cell and on a CDK2 threshold. Cells born less than 3 hours before serum removal did not divide, instead a variable 3-10 hour range since time from division for cells was predictive of a that cell having passed the R point. A cytoplasmic-to-nuclear HDHB-EGFP ratio of >0.84 threshold for CDK2 activity at the time of serum removal was determined to be the strongest predictor of a cell completing division (Schwarz et al., 2018).

Research into the relationship between cell size and cell cycle progression has suggested that there exists a cell size threshold for cell cycle progression. In such a model, cells that are born small will spend more time in the cell cycle to achieve an optimal size for subsequent division. This has been demonstrated in numerous studies (Ginzberg et al., 2018; Liu et al., 2018; Tzur et al., 2009). Live-imaging of HeLa and RPE1 cells followed by fixation and staining for cell cycle markers and cell mass demonstrated that cells in S-phase born at the same time as cells still in G1 were significantly larger than the G1 cells, indicating that a size threshold determines entry in S-phase rather than a specific duration spent in G1. Using nuclear size measurements as a proxy for cell growth it was also shown that cells born with smaller nuclei had longer G1 phases (Ginzberg et al., 2018). Treatment of RPE1 cells with the mTORC1 inhibitor rapamycin that impairs cell growth was also found to increase the duration of G1 (Liu et al., 2018; Ginzberg et al., 2018). It has been proposed that a mechanistic consequence of increasing cell size on cell cycle length is the dilution of cell cycle inhibitors, and thus reduced function leading to the cell cycle entry (Schmoller et al., 2015; Zatulovskiy et al., 2020). Live imaging of fluorescently-labelled, endogenous Rb in immortalised human mammary epithelial cells (HMEC-hTERT1) showed that its concentration decreased as nuclear volume increased due to cell growth. *In vivo* assessment of the effect of Rb on cell size

showed that conditional knock-out of Rb in mice reduced the size of hepatocytes. KO of *Rb* in HMEC cells also reduced the duration of G1 and eliminated the inverse correlation that was observed in wild-type cells between nuclear volume after mitosis and G1 length. Conversely, constitutive-expression of Rb in HMEC-hTERT1 cells to maintain its concentration was found to increase G1 length, irrespective of nuclear size at birth (Zatulovskiy et al., 2020).

The above studies highlight different mechanisms that have been found to influence cell cycle length mainly in an *in-vitro* cell culture setting. While they differ in conclusions, they all speak to the power of single-cell analysis of gene expression and cellular properties such as size in explaining how variability in cell cycle length is generated.

1.7 Integrating transcription factor signaling dynamics with cell cycle dynamics

While the core cell cycle molecules ultimately execute decisions in cell cycle progression, they do not act in isolation. In a multicellular context, numerous signaling pathways and environmental stimuli influence the proliferative capacity of individual cells. Furthermore, the responsiveness of a cell to different signals can be dictated by its temporal position in the cell cycle (Ankers et al., 2016; Pauklin & Vallier, 2013). Our understanding of the interplay between signaling pathways and the cell cycle has benefitted immensely from live-cell reporters of both signaling molecules and cell cycle dynamics. For example, observing the temporal expression dynamics of transcription factors in living cells has opened up new ways to describe their activity and thus better understand their function with regards to the downstream effect on gene expression and cell behaviour (Purvis & Lahav, 2013). Descriptions of TF expression dynamics now incorporates parameters such as signal frequency, amplitude, and duration, which enables an understanding of TF expression variability that could not have been appreciated without live-imaging of their expression (Sonnen and Aulehla 2014; Jeknić et al., 2019). The underlying molecular mechanisms that enable such activity are based on regulatory feedback networks, time delays associated with transcription and protein synthesis and the

instability of mRNA and protein molecules that make up each network (Monk 2003; Minchington et al., 2020; Crews and Pearson 2009).

For example, the signaling dynamics of the transcription factor p53, which mediates cell cycle arrest in response to cellular stress, have been well described. A core facet of p53 signaling is its negative regulation by the E3-ubiquitin ligase MDM2, which prevents p53 from target gene regulation and promotes its degradation (Haupt et al., 1997; Chen et al., 1995). *MDM2* is transcriptionally activated by p53 thereby constituting a negative feedback loop in p53-MDM2 signaling that leads to oscillations in protein levels for each gene (Bar-Or et al., 2000; Wu et al., 1993). Live-imaging of fluorescent-reporters of p53 and MDM2 in MCF7 cells responding to gamma irradiation further described the oscillatory nature of the p53-MDM2 pathway with peaks of MDM2 protein appearing 2 hours after peaks in p53 expression (Geva-Zatorsky et al., 2006). Insights that could only be revealed by single-cell live imaging, showed a high variability in amplitude of MDM2 peaks that were not correlated with preceding p53 peaks, which was determined to arise from variation in protein production rates by mathematical modelling. Furthermore, while treated cells showed synchrony in the initial oscillatory response to irradiation, oscillations between cells became unsynchronised and a subset of cells did not display any oscillatory response to irradiation (Geva-Zatorsky et al., 2006). It was observed that in non-stressed conditions p53 exhibits protein pulses that are correlated with cell cycle progression and associated with intrinsic DNA damage and the ATM pathway (Loewer et al., 2010). Only in conditions of extrinsic stress (application of neocarzinostatin) did p53 oscillations persist at higher frequencies leading to an accumulation of p53 protein and its acetylation (Tang et al., 2008). In its acetylated form p53 had a greater capacity to induce *CDKN1A* expression and promote cell cycle arrest (Loewer et al., 2010). These results highlight the role of expression dynamics in modulating protein function and emphasise how the cell cycle can account for heterogeneity in gene expression in the case of spontaneous p53 pulses (Fig 1.2).

Nuclear factor kappa B (NF-κB) is a transcription factor that plays an important role in regulating a cell's response to immune and inflammatory stimuli that also displays dynamic expression (Taniguchi & Karin, 2018). The ability of NF-κB to regulate gene expression is negatively controlled by its cytoplasmic sequestration when bound to Inhibitor kappa B alpha (IκBα) and epsilon (IκBε) proteins. Factors that stimulate the NF-κB pathway promote the proteolysis of IκBα and IκBε, allowing NF-κB to enter the nucleus and control target gene expression (Baldwin, 1996). A negative feedback loop is instigated as a result of IκB genes being activated by NF-κB which produces oscillations in NF-κB shuttling between the nucleus and cytoplasm (Nelson et al. 2004; Sun et al., 1993). It was determined that cell cycle position plays a role in modulating a cell's response to NF-κB signal transduction (Ankers et al., 2016). In response to tumor necrosis factor alpha (TNFα) it was revealed by immunohistochemistry and live-imaging that the nuclear localistion of RelA (a subunit of NF-κB heterodimer) was reduced in cells receiving the TNFα in S-phase with no effect on cell cycle progression. Cells which had been inferred to receive TNFα at the G1/S boundary based on FUCCI-imaging exhibited a delay in cell cycle progression and RelA nuclear translocation. This was determined to result from binding of RelA to E2F1 and E2F4 at different positions in the cell cycle, with binding of RelA to E2F4 at S-phase preventing its nuclear translocation. These cell cycle dependent protein interactions were suggested to be a mechanism that dictates how a cell responds to inflammatory stimuli based on its cell cycle position. Similarly, cell cycle position has been found to affect how a cell responds to differentiation signals (Pauklin & Vallier, 2013). Using FUCCI-hESCs, it was found that cells preferentially differentiated towards an endoderm fate in early G1 and a neuroectoderm fate in late G1. Examination of SMAD2/3 signalling found that it was most highly expressed in early G1 and bound specifically to endoderm genes. The cell cycle stage specificity of SMAD2/3 binding was determined to be controlled by CDK4/6 phosphorylation with SMAD2/3 phosphorylation by CDK4/6 promoting its dissociation from chromatin (Pauklin & Vallier, 2013).

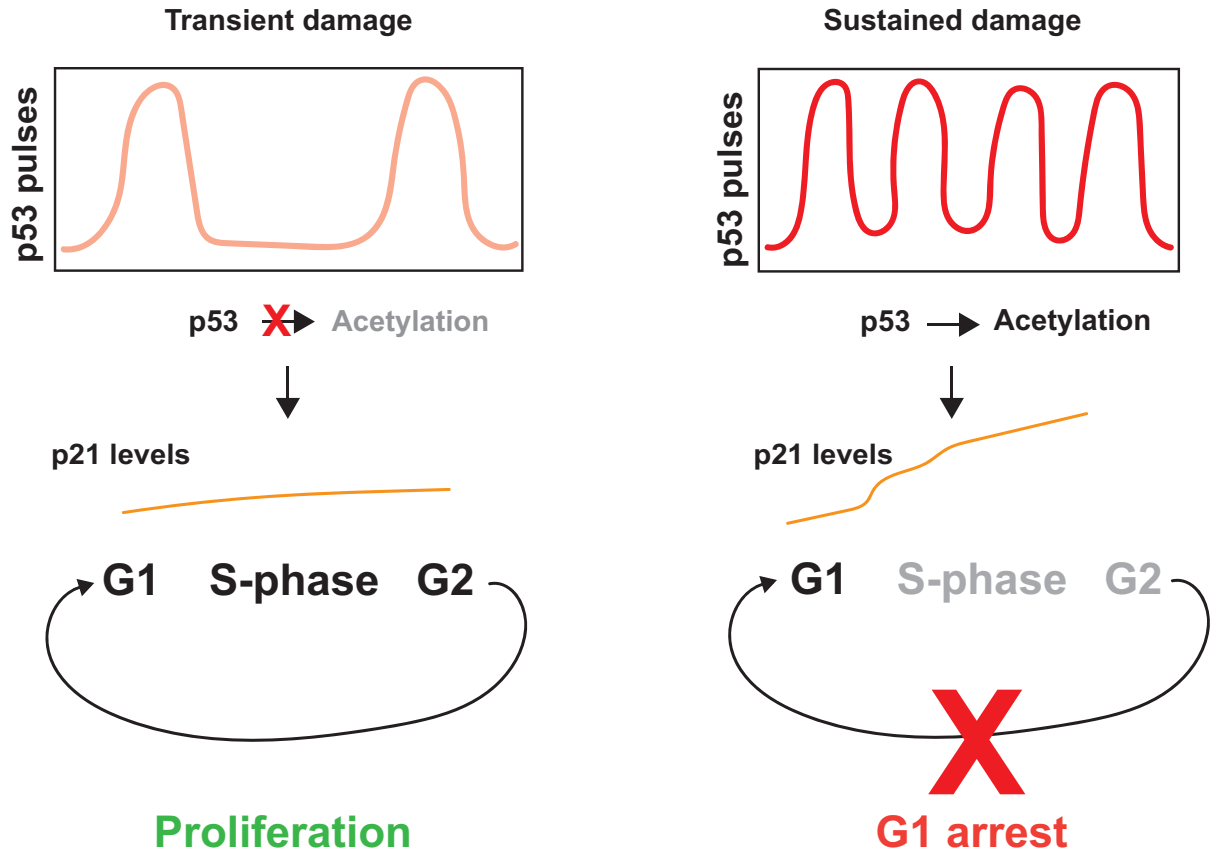

Fig 1.2 p53 dynamics with distinct cell cycle outcome
p53 protein pulses exhibit similar duration and amplitude in unstressed conditions and stressed conditions (sustained damage e.g. neocarzinostatin). Transient pulses of p53 do not inhibit proliferation. Increased pulse frequency leads to acetylation of p53 protein that enhances its ability to activate *CDKN1A* expression leading to cell cycle arrest. Adapted from (Loewer et al. 2010)

1.8 The HES1 transcription factor

HES1 is one of seven members of the mammalian *HES* gene family of basic helix-loop-helix (bHLH) transcription factors that are homologs of the Drosophila hairy and Enhancer of split [E(spl)] developmental genes (Akazawa et al., 1992; Sasai et al., 1992; Carroll et al., 1988; Rushlow et al., 1989; Ingham et al., 1985). The HES1 protein contains three domains, which are common to all HES proteins. These are the N-terminal bHLH domain, the Orange domain, and the C-terminal WRPW domain, which contains the Trp-Arg-Pro-Trp amino acid motif (Fig 1.3 A). The bHLH domain is essential for the DNA binding activity of HES1. HES1 can bind DNA at E-box (CANNTG) motifs, the common binding motif for bHLH proteins, but has been

proposed to preferentially bind DNA at C-site (CACG(C/A)G) and N-box (CACNAG) motifs (Sasai et al., 1992). The HLH domain also enables homo and hetero-dimerisation of HES proteins with other HLH proteins (Fischer and Gessler 2007). The Orange domain functions through two amphipathic helices that enable HES1 hetero-dimerisation (Dawson et al., 1995). The C-terminal WRPW domain enables binding of HES1 to the Transducin-like enhancer of split (TLE) co-repressor proteins, which are the mammalian homologs of the Drosophila Groucho protein (Grbavec and Stifani 1996; Fisher et al., 1996). The TLE proteins inhibit gene expression through chromatin modification and recruitment of histone deacetylases at target sites (Martinez and Arnosti 2008; Palaparti et al., 1997; Chen et al., 1999). HES1 activity is aimed towards the repression of genes belonging to developmental pathways. Targets of HES1 that are involved in development include the proneural genes *Mash1* and *Neurog2* and *Math1* (Ishibashi et al., 1995), *Ptf1A*, and *Neurog3,* the latter two genes being associated with pancreatic and intestinal development (Fukuda et al., 2006; Jensen et al., 2000). HES1 can also participate in passive repression (Fig 1.3 B). This occurs when HES1 binds to activators of gene expression and sequesters them from target genes, as is the case with HES1 binding to *Mash1* and *E47* (Akazawa et al., 1992). HES1 was also found to regulate its own expression in fibroblast cells by binding to multiple N-box motifs in the *Hes1* promoter. *Hes1* expression assays showed down-regulation of promoter activity when HES1 was exogenously expressed. When the N-box sequences were abolished promoter activity was unaffected by exogenous HES1 expression, indicating the autoregulatory function of HES1 (Takebayashi et al., 1994). *HES1* expression is induced downstream of multiple signaling pathways, including the sonic-hedgehog (Shh), bone morphogenetic protein (BMP), and transforming growth factor beta(TGF-β) pathways (Ostroukhova et al., 2006; Seong et al., 2021; Wall et al., 2009). Most notably, *HES1* is expressed downstream of the canonical Notch pathway and is a therefore a critical effector of lateral inhibition during development. During Notch signaling, cells communicate with each other through the expression of cell surface ligands that interact with Notch proteins on the surface of adjacent cells. In a signal transmitting cell, the expression of Notch ligands, such as the *delta-like* genes is stimulated by pro-neural factors ASCL1 and NEUROG2 (Bertrand et al., 2002). The interaction between a Notch

receptor and ligand protein on an adjacent cell ligand triggers the release of the NOTCH-intracellular domain (NICD) from the inner-membrane its translocation into the nucleus of the signal-receiving cell. In the nucleus, NICD forms a complex, known as the Notch transcription complex (NTC), with the DNA binding protein RBP-J and co-activator Mastermind like (MAML) to recruit additional transcriptional regulators that induce expression of Notch target genes, with *HES1* being a notable target. NTCs bind to Notch response elements (NREs) in target genes that consist of one or two RBP-J binding sites, with the latter being defined as sequence-paired sites (SPSs) (Cave et al., 2005; Nam et al., 2007). Once induced, HES1 will then go on to repress the expression of pro-differentiation factors in that cell (Louvi & Artavanis-Tsakonas, 2006).

1.9 The role of HES1 in development and quiescence

HES1 is expressed in multiple tissue types and plays a role during organ development. It primarily functions in the maintenance of stem cell pools by opposing pro-differentiation factors (Hatakeyama et al., 2004; Jensen et al., 2000). Homozygous null *Hes1* mice die during gestation or shortly after birth. Examination of *Hes1*-null embryos revealed defects in neural tube closure and the premature appearance of post-mitotic neurons, which was associated with the upregulation of the pro-neural factor *Mash1*, demonstrating the importance of HES1 in controlling the emergence of differentiated cell types at specific times during development (Ishibashi et al., 1995). In *Hes1*-null *Hes5*-null embryos the same phenotypes are observed but at a greater severity, additionally, when Notch signaling is constitutively activated neuronal differentiation is impaired in single mutant embryos but not in double mutant embryos, indicating the compensatory function of the *HES* genes (Ohtsuka et al., 1999). Mice that lack *Hes1*, *Hes3,* and *Hes5,* display the most dramatic phenotypes. Although neural progenitor pools form in these embryos, they undergo premature differentiation at an earlier stage than any single *Hes* mutant. The early depletion of radial glial cells in *Hes1-3* mutants leads to widespread disorganization of central nervous system structure and size (Hatakeyama et al., 2004). In the absence of functional HES1, progenitors not only undergo premature differentiation they also differentiate ectopically. In the developing central nervous system (CNS),

boundaries are formed between different regions of the brain e.g. the isthmus between the midbrain and hindbrain (Gibbs et al., 2017). A principal function of boundary regions is to partition the CNS into compartments that receive different developmental signals and thereby contain different neuronal subtypes (Kiecker & Lumsden, 2005). Loss of *HES1* and *HES3* disrupts the boundary between the mid and hindbrain and leads to early termination of FGF8 and WNT1 signaling at the isthmus that is replaced by ectopic differentiation (Hirata et al., 2001). Boundary regions consist of neuroepithelial cells that do not proliferate as rapidly as compartment cells. It was observed that HES1 displays two types of expression in boundary and compartment progenitors, with boundary cells having uniformly high HES1 expression and no proneural gene expression and compartment cells having variable levels of HES1 and MASH1 expression that were inversely proportional to each other. When progenitors were isolated from telencephalic compartments and cultured *in vitro* it was found that their proliferation could be reduced by over-expression of HES1, indicating that persistent expression of HES1 functions to maintain slowly dividing cell at boundary regions that do not differentiate (Baek et al., 2006). Further research utilising live-imaging of dissociated neural progenitors and telencephalic slice cultures expressing *Hes1* promoter-luciferase constructs revealed that *Hes1* expression was oscillatory. Furthermore, using the same methods, the pro-neural gene *Neurog2* and Notch ligand *Dll1* were found to exhibit oscillatory expression in neural progenitors. In the same study, electroporation of over-expressing HES1 constructs into the developing telencephalon caused the down-regulation of pro-neural genes and *Ccnd1* and *Ccne2* resulting in cell cycle inhibition as measured by decreased uptake BrdU compared to control electroporation (Shimojo et al., 2008). This information from a developmental context provided the first insight into how different modes of HES1 expression influenced the proliferative capacity of progenitor cells. There are numerous studies demonstrating HES1 repression of both positive (*CCND1*, *CCNE1*, *E2F1*) and negative regulators (*CDKN1A*, *CDKN1B, CDKN1C*) of the cell cycle, suggesting that HES1 regulation of two opposing cell cycle outcomes (arrest vs proliferation) is dictated by its differential binding of cell cycle regulators (Shimojo et al., 2008; Murata et al., 2005; Noda et al., 2011; Georgia et al., 2006; Hartman et al., 2004).

Further evidence that HES1 is important for cellular decisions based on cell cycle arrest vs proliferation was revealed by studies on quiescence in fibroblast cells (Coller et al., 2006). *HES1* was initially shown to be upregulated in fibroblast cells made quiescent by mitogen removal and contact inhibition (Coller et al., 2006). It was later shown that HES1 is essential for fibroblasts to maintain the ability to exit quiescence (Sang et al., 2008). Fibroblast cells that had been made quiescent by reversible expression of p21 were unable to resume proliferation when transduced with dominant-negative HES1 constructs that either blocked its ability to bind DNA or that lacked the C-terminal WRPW domain preventing HES1 from dimerising with co-repressors. A similar effect was observed when cells were made quiescent by serum starvation over a 10 day period (Sang et al., 2008).

1.10 The HES1 regulatory network

Like p53, *HES1* has been shown to exhibit dynamic or 'oscillatory' expression (Hirata et al., 2002; Kobayashi et al., 2009; Shimojo et al., 2008). Oscillatory expression of *Hes1* mRNA and protein was observed in mouse fibroblasts in timecourse experiments with samples taken every half hour after serum stimulation. Both *Hes1* mRNA and protein oscillated in 2 hour cycles with a 15 minute delay between mRNA and protein following serum stimulation (Hirata et al., 2002). The short half-lives of *Hes1* mRNA (24 minutes) and protein (22.3 minutes) were identified as contributing factors to the instability of their expression. However, based on previous evidence that HES1 negatively regulates its own expression, it was hypothesised that the mechanism generating the cyclic expression of *Hes1* was a form of negative feedback that is relieved when HES1 protein is degraded (Takebayashi et al., 1994). This was confirmed in experiments where HES1 protein was stabilised by the addition of proteosome inhibitors, which abolished *HES1* oscillations and suppressed *Hes1* mRNA expression after its initial serum response. Conversely, inhibition of HES1 protein expression by cycloheximide treatment or expression of a dominant-negative form of HES1 unable to bind DNA, resulted in sustained *Hes1* mRNA expression (Hirata et al., 2002). Regulation of *HES1* mRNA by the microRNA-9 (miR-9) is another critical component of the HES1 regulatory network. MicroRNAs are

short (~22bp) RNA molecules that can negatively regulate the expression of genes by binding to their mRNA transcripts resulting in transcript de-stabilisation and inhibition of translation (Bartel, 2004). Loss of MicroRNA function in development leads to defects in gastrulation and somitogenesis and also affects neuronal differentiation (De Pietri Tonelli et al., 2008; Giraldez et al., 2005). *Hes1* was first identified as a target of miR-9 in *Xenopus tropicalis* development, where miR-9 knockdown was found to inhibit neurogenesis by inducing apoptosis or sustained proliferation (Bonev et al., 2011). A bioinformatic screen performed in this study identified *Hairy 1* (*HES1 Xenopus troplicas* homolog), as a potential target of miR-9. It was subsequently, shown that miR-9 inhibited *Hes1* luciferase reporter activity, an effect that was prevented by co-expression of a 'target-protector' morpholino that interferes with miR-9 binding. The regulation of *Hes1* mRNA by miR-9 was examined further in mouse neural progenitors to investigate its effect on the oscillatory expression that had previously been observed for *Hes1* in this cell type (Shimojo et al. 2008). Examination of *Hes1* mRNA half live in c17.2 cells showed that its stability was increased when miR-9 was knocked down and decreased when miR-9 was over-expressed. Live-imaging of mouse neural progenitors expressing de-stabilised luciferase reporters driven by the *Hes1* promoter and containing the *Hes1* 3' UTR revealed *Hes1* oscillations that varied in period and amplitude between cells. In cells expressing wild-type luciferase constructs between 2 and 7 HES1 oscillatory cycles were captured during 20 hours of imaging. In cells expressing constructs with the miR-9 binding site removed, the number of oscillatory cycles was significantly reduced. A similar effect on the number of oscillatory cycles was observed when miR-9 was overexpressed. Furthermore, it was shown that HES1 negatively regulated miR-9 expression, with four predicted HES1 binding sites identified in a 2KB region upstream of the miR-9 hairpin. A final observation that miR-9 is the more stable transcript, with a half-life of 3 hours compared to 25 minutes for *Hes1*, led to the formulation of an elegant model of HES1 regulation that sculpts its dynamic expression. In this model oscillatory expression of HES1 is induced by a double-negative feedback loop consisting of HES1 autoregulation and regulation by miR-9. Within the same cell miR-9 expression will oscillate inversely to *Hes1* due to negative regulation by HES1. The relative stability of mature miR-9 means its levels will

gradually increase in the cell and dampen HES1 oscillations in the cell, leading to terminal down-regulation of HES1 (Bonev et al., 2012). The HES1 regulatory network described above is illustrated in Figure 1.3 C and D. Insight into the HES1 regulatory network obtained from experimental work has guided mathematical modelling of how variability in the initial levels of regulatory components, such as miR-9, in a cell can lead to different stable HES1 states that dictate a cells decision to differentiate or become quiescent (Goodfellow et al., 2014). Evidence for *Hes1* expression 'noise' in neural progenitors as observed by single-molecule fluorescent *in-situ* hybridisation (smFISH) led to the formulation of a stochastic model whereby the differentiation of clonally identical progenitors can be spread over time (Phillips et al., 2016).

Evidence that HES1 is required for quiescent exit in fibroblasts (Sang et al., 2008), and that its sustained expression maintains slow-dividing boundary cells in the mouse brain (Baek et al., 2006), has now been expanded on by examining the HES1 dynamics that are associated with quiescent cells and how they enable cells to re-enter the cell cycle (Marinopoulou et al., 2021; Sueda et al., 2019). This has been explored in the context of neural stem cells. It has previously been shown that oscillatory HES1 expression drives oscillations of the pro-neural factor ASCL in neural progenitors maintaining them in a proliferative state (Imayoshi et al., 2013). How quiescent adult stem cells in the mouse brain are maintained was shown to depend on HES1 oscillations that operate at higher levels than oscillations in proliferative cells. In this way, HES1 levels during periods of down-regulation in quiescent cells are as high as HES1 peaks in proliferative cells, leading to the sustained down-regulation of ASCL1 (Sueda et al., 2019). Live-imaging of neural stem cells derived from mice with endogenous *Hes1* fused to the mSCARLET fluorophore demonstrated that HES1 oscillations may be more important for quiescent exit than maintaining a proliferative state (Marinopoulou et al., 2021). This was demonstrated by transfecting a constitutively active UbC-mVENUS-HES1 construct into neural stem cells expressing endogenously tagged HES1-mSCARLET. Constitutively active HES1 abolished oscillatory expression of endogenous HES1 through sustained negative feedback, while expression of the UbC HES1 construct was unaffected due to

absence of negative feedback on the exogenous UbC construct. Proliferation was not impeded in cells where endogenous HES1 oscillations were abolished. When cells were cultured in the presence of BMP4 to induce quiescence, transfected cells were able to enter quiescence, as judged by a reduction in Ki-67 staining but were not able to re-enter the cell cycle when BMP4 was removed and replaced with EGF. The loss of oscillatory expression therefore prevented cells re-entering the cell cycle (Marinopoulou et al., 2021). One suggestion for this was that upstream HES1 dynamics may dictate different gene responses required for quiescent exit. Differential gene responses have previously been demonstrated to result from upstream changes in NF-κB and p53 dynamics (Lane et al., 2017; Purvis et al., 2012)

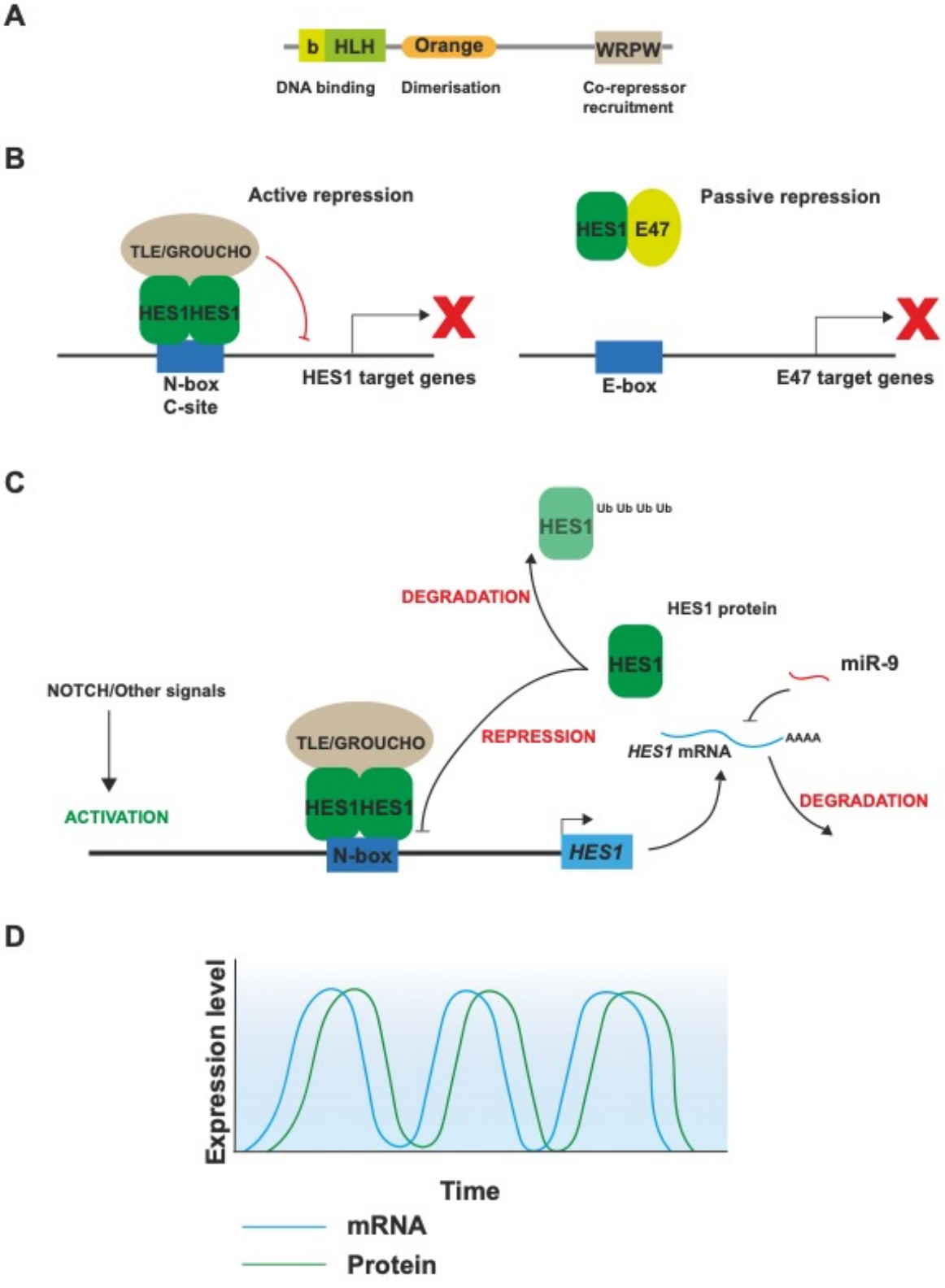

Fig 1.3 Overview of HES1 structure and function

Fig 1.3 Overview of HES1 structure and function (A) HES1 protein structure. The three conserved domains of HES proteins. The N-terminal bHLH domain is involved in DNA binding. The Orange domain regulates HES1 homo/hetero-dimerisation. The C-terminal WRPW domain enables interactions with co-repressor proteins to mediate repression of HES1-bound genes. **(B)** Modes of HES1 repression. HES1 repression of target genes can be mediated through direct and indirect methods. In direct repression, HES1 physically binds the DNA as a homo or hetero-dimer to orchestrate chromatin modification resulting in target gene repression. In indirect repression, HES1 can bind activators of gene expression (E47, shown here). When bound to HES1, activators are prevented from binding their targets resulting in indirect repression of gene expression through HES1 **(C)** The HES1 regulatory network. In response to upstream activation signals, such as NOTCH signaling, *HES1* is transcribed, *HES1* mRNA is translated into HES1 protein and HES1 protein dimerises and subsequently inhibits *HES1* expression by binding to N-box sequences in the *HES1* promoter as part of a co-repressor complex with TLE. *HES1* mRNA is de-stabilised due binding of miR-9 to the 5' end of *HES1* transcripts. HES1 protein is targeted for protein degradation by ubiquitination. **(D)** Oscillatory HES1 expression emerging from negative-feedback regulatory network. *HES1* mRNA expression signal is represented by green line and HES1 protein signal is represented by blue line. Activation of *HES1* expression leads to rising *HES1* mRNA. The subsequent expression of HES1 and its negative regulation of *HES1* combined with *HES1* mRNA instability leads toa decline in mRNA levels. Auto-regulation of *HES1* is relieved when HES1 protein levels are reduced due to degradation leading to another round of *HES1* expression. Viewed over time this leads to oscillating levels of *HES1* mRNA and protein. Figure adapted from (Kageyama et al., 2007).

1.11 A role for HES1 in cancer development

A challenge in cancer therapy is the reality that tumours are heterogeneous tissues, and as such, individual cells within a tumour will display differential responses to certain therapies (Dagogo-Jack & Shaw, 2018). Related to this, is the cancer stem cell (CSC) theory which, posits that the heterogeneous nature of tumours is initially generated and maintained by tumour cells with stem-like properties (Kreso & Dick, 2014). Encompassed within the CSC model is the idea that cells will occupy different states that can vary in their underlying gene expression state or proliferation status and that these states are plastic allowing cells to reversibly switch between states (Gupta et al., 2011; Kumar et al., 2019). A manifestation of this in a therapy setting would be the existence of dormant, or slow-cycling cells that are resistant to therapy aimed to induce apoptosis or senescence, which subsequently contribute to tumour regrowth and cancer relapse (Meacham & Morrison, 2013; Pisco & Huang, 2015).

Evidence has suggested that the efficacy of cytotoxic treatments varies depending on the proliferation or cell cycle status of cells (Granada et al., 2020). Growth of FUCCI-expressing MKN45 cells (human gastric cancer) in nude mice monitored by intravital imaging demonstrated that the proportion of cells in different cell cycle phases varied depending on their location in the tumour, with a higher percentage of cells in G0/G1 at the centre of tumours. Furthermore, treatment of tumours with cisplatinum or paclitaxel reduced the number of tumour cells in S/G/M but was ineffective at eliminating G0/G1 cells (Yano et al., 2014). In this context, a key question that has compelled further studies is how do cells that survive treatment reactivate proliferation. Examination of *MYCN*-amplified neuroblastoma cell lines uncovered a mechanism whereby cells re-enter the cell cycle following treatment with the DNA replication inhibitor, doxorubicin (Ryl et al., 2017). Although, transcriptomic analysis of *MYCN*-amplified cells revealed a gene expression profile that conferred a propensity for proliferation, only a subset of these cells was able to reactivate proliferation following treatment with doxorubicin. The reason for this was identified as the cell cycle status of cells at the time of treatment. Early G1 cells that had just exited mitosis at the time of treatment were more efficiently able to repair DNA damage and therefore prevent cell death. This example represents how

genetic factors and non-genetic heterogeneity can influence cell proliferation (Ryl et al., 2017). Evidence has also been found for distinct p53 and p21 dynamics that lead to the resumption of proliferation following irradiation. Live-imaging of RPE cells after ionizing irradiation demonstrated that re-entry into the cell cycle is heterogeneous with some cells remaining senescent and other cells undergoing more than one cell division within a 7 day imaging period. Simultaneous imaging of p53 and p21 protein dynamics in these cells showed sustained p53 oscillations that were followed by a pulse of p21 expression. As the level of the p21 pulse was correlated with the amplitude of the preceding p53 oscillation, it was determined that stochastic fluctuations in p53 amplitude around a lower average led to a decrease in p21 levels. Use of the CDK2 activity sensor described in (1.6) illustrated that the decrease in p21 levels translated to increased CDK2 activity and ultimately, cell cycle re-entry in these cells (Reyes et al., 2018).

There is increasing evidence of a role for HES1 in the tumorigenicity of different cancers (Liu et al., 2015). Much like its role in development, this evidence has pointed towards a role for HES1 in regulating cancer stem cells (Gao et al., 2014; Cenciarelli et al., 2017; Simões et al., 2015). In colon cancer biopsies *HES1* expression was positively correlated with stem cell markers such as *CD133+* and *ALDH1*. Over-expression of HES1 in colon cancer cell lines SW620 and HCT116 increased the percentage of CD133+ cells and the self-renewal properties of these cells. Furthermore, HES1-overexpressing cells caused a higher rate of tumours when injected into nude mice (Gao et al., 2014). Knockdown of *HES1* in glioblastoma stem cells was found to reduce their proliferation and invasiveness (Cenciarelli et al., 2017). In a breast cancer context, *HES1* has previously been found to be down-regulated in response to 17β-estradiol stimulation of proliferation in MCF7 and T47D cells (Ström et al., 2000). When MCF7 and T47D cells were co-treated with all-*trans* retinoic acid the proliferative effect of 17β-estradiol was inhibited and an up-regulation of *HES1* was observed. Over-expression of a dominant-negative form of HES1 that binds and inactivates wild-type HES1 reversed the effect of all-*trans* retinoic acid, indicating that the anti-proliferative effect was mediated through HES1 (Müller et al., 2002). Further work using this experimental setup found that in

response to all-*trans* retinoic acid HES1 directly repressed the expression of *E2F1* by binding to its promoter as a heterodimer with HEY1 (Hartman et al., 2004). These results suggest that HES1 can mediate between cell cycle arrest and proliferation in a breast cancer context. HES1 has been implicated in promoting the self-renewal of breast cancer stem cells in response to anti-estrogen treatment. ALDH activity, a marker for proliferative breast cancer stem cells, was found to be enriched in patient-derived ER+ tumour cells after treatment with tamoxifen and fulvestrant (Ginestier et al., 2007; Simões et al., 2015). Increased ALDH activity was also correlated with increased expression of *HES1* and *HEY1* downstream of NOTCH4 signaling. Using patient-derived xenografts and transplantation of MCF7 cells it was shown that anti-estrogen treatment combined with the Notch inhibitor RO4929097 significantly reduced the enrichment of ALDH1-positive cells and the expression of HES1 and HEY1 mRNA and protein. Furthermore, cells isolated from tumours treated with RO4929097 had decreased tumour-initiating capacity (Simões et al., 2015). HES1 over-expression has also been linked to increased proliferation and invasiveness in MCF7 cells, suggesting that changes in *HES1* expression are linked with changes in cell cycle kinetics (Li et al., 2018)

Given the functional relevance of HES1 expression dynamics in a developmental context and its role in maintaining the reversibility of quiescence (Sang et al. 2008; Hatakeyama et al., 2004; Kageyama 2007; Marinopoulou et al., 2021), further exploration of HES1 expression dynamics in a cancer context is warranted. This is substantiated by the observations described above that link HES1 expression to both pro and anti-proliferative outcomes in MCF7 cells (Hartman et al., 2004; Li et al., 2018). As described for p53, re-entry into the cell cycle can result from upstream changes in expression dynamics that induce changes in the activity of cell cycle regulators (Reyes et al., 2018). A CRISPR-generated HES1 protein reporter MCF7 cell line has recently been described by the Papalopulu lab (Sabherwal et al., 2021). Strikingly, in MCF7 cells HES1 displayed oscillatory dynamics with a periodicity of ~26 hours in contrast to the shorter ultradian dynamics previously reported in a developmental context and fibroblast cells. When HES1 expression dynamics were viewed alongside cell cycle progression, a bi-phasic pattern of expression was

observed with a peak of HES1 expression in G1 and a second peak in G2. HES1 dynamics were examined further in breast cancer stem cell subpopulations, which are typically defined as $ALDH^{High}$ (proliferative) and $CD44^{High}/CD24^{Low}$ (quiescent) (Ginestier et al., 2007). In cells enriched for the $CD44^{High}/CD24^{Low}$ sub-type, the first HES1 peak was delayed in G1, compared to cells with shorter G1 durations where the first HES1 peak occurred at mitosis. It was hypothesised that the longer G1 duration in cells with a delayed G1 HES1 peak occurs due to HES1 repression of cell cycle molecules that trigger the G1/S transition, with *CCNE1* and *E2F1* being possible candidates (Sabherwal et al., 2021). This data provided the first evidence of oscillatory HES1 expression in cancer cells and also presented a reconciled view of how HES1 can control two different cell cycle outcomes based on how HES1 dynamics are interfaced with cell cycle progression.

1.12 Overview of thesis aims

This introduction highlighted the advances that have been made towards understanding how differences in cell cycle length or proliferation are generated between cells. These advances have been made based on our improved ability to observe the temporal relationship between gene expression and the cell cycle at a single cell level.

The importance of HES1 signaling in the control of proliferation during development and an emerging role for HES1 in cancer development was also discussed. How HES1 dynamics integrate with the cell cycle to coordinate proliferation is still not fully understood. As discussed above, recent live-imaging in breast cancer cells revealed novel HES1 expression dynamics and a possible functional relationship between these dynamics and the cell cycle (Sabherwal et al., 2021). The majority of the experimental work presented in this thesis aims to complement these findings by exploring *HES1* transcription in breast cancer cells using methods of single cell measurement and cell synchronisation. Furthermore, I aim to test the functional importance of HES1 signaling through inhibition of HES1. This work is complemented by experiments analysing *Hes1* expression in immortalised mouse embryonic fibroblasts (iMEFs).

In summary, 3 broad questions motivate the experimental in this thesis.

1. How is *HES1* expression coupled with the temporal events of the cell cycle?
2. Does HES1 expression have a functional role in controlling cell cycle progression?
3. Can HES1 targets related to this function be identified?

Chapter 2: HES1 expression during the cell cycle

2.1 Introduction

2.1.1 Opening remarks

The events of the cell cycle are punctuated by characterised patterns of gene expression and protein activity, most notably, the phase-specific expression of the *cyclin* genes followed by the activation of their CDK binding partners (Bertoli et al., 2013; Satyanarayana and Kaldis 2009). Indeed, the temporal position within the cell cycle can be reliably informed by detection of *cyclin* transcription and the association of specific CDK/Cyclin complexes. The cell cycle therefore serves as a good example of how variability in gene expression and protein abundance can be understood in terms of its biological role. For example, the periodic expression of *CCNB1* and its association with CDK1 is observed and required for entry into mitosis (Fung & Poon, 2005; Ohi & Gould, 1999). For genes outside the core cell cycle molecules, population-based studies using microarray analysis have detailed global cell-cycle dependent gene expression profiles in synchronised yeast and mammalian cells that can be clustered in to different cell cycle phases (Grant et al., 2013; Spellman et al., 1998; Whitfield et al., 2002). More recently, gene and protein expression profiles during the cell cycle have been generated without prior cell synchronisation (Boström et al., 2017; Karlsson et al., 2017; Mahdessian et al., 2021)

Current descriptions of HES1 expression heterogeneity have relied on comparisons between cells with different proliferation statuses (quiescent vs proliferating). These descriptions are useful for correlating HES1 expression with the maintenance of distinct cell states but typically lack information on how *HES1* is expressed during transitions between these states. The main goal of the following chapter is to describe the dynamics of *HES1* expression within the temporal framework of a complete cell cycle. From this a relationship between the two processes can be described that can form the basis of a hypothesis on how changes in either might affect the kinetics of the other.

2.1.2 Cell cycle-dependent gene expression heterogeneity

Genetically identical cells grown in identical environments will display cell-to-cell variability in gene expression resulting in population level noise. This 'noise' in gene expression has been determined to result from 'intrinsic' and 'extrinsic' sources, with intrinsic variation due to the randomness at which transcription or translation can occur in a cell (Elowitz et al., 2002; Raj et al., 2006). Extrinsic noise reflects gene expression variation due to differences in cell size or the availability of transcription factors (Raj and van Oudenaarden 2008; Phillips, and Naef 2017). The cell cycle is a notable source of extrinsic gene expression variation. In this case, if a gene is cell cycle regulated, it's expression in one cell will differ from that in another cell that is in a different phase of the cell cycle. In an unsynchronized population of cells, this will lead to widespread cell-to-cell heterogeneity. While timecourse experiments in synchronised populations of cells have identified hundreds of genes whose overall mRNA abundance changes over the cell cycle, besides introducing unwanted artefacts, they do not inform on how the *intrinsic* process of transcription is temporally regulated for individual genes during the cell cycle.

2.1.3 Cell cycle phase specific *HES1* expression

A comprehensive analysis of how *HES1* expression varies over the cell cycle has not been performed. Hes1 expression dynamics in bulk populations have been investigated during cell cycle re-entry. Serum stimulation of synchronized mouse fibroblasts induces a 2-hour oscillatory *Hes1* response at the mRNA and protein level that is dependent on *HES1* auto-regulation. However, this approach was limited to a timecourse of 6 to 12 hours, which does not allow tracking of *Hes1* expression over a complete cell cycle (Hirata et al., 2002; Yoshiura et al., 2007). HES1 oscillations are observed in a number of contexts and have generally been associated with a proliferative cell state. In mESCs, luciferase expression driven by a *Hes1* promoter, which mimics endogenous *Hes1* expression, oscillates with a period of hours 3-5 hours, with an increase in expression observed later in the cell cycle. (Kobayashi et al., 2009). In embryonic brain development, HES1 is expressed at variable levels over the cell cycle of neural progenitors. In the mouse telencephalon, examination of fixed sections showed HES1 protein is low in early to late G1 with variable levels observed

between S-phase to G2/M. The authors reason that in the context of neurogenesis low HES1 expression early in the cell cycle may underlie asymmetric divisions, with low HES1 in one daughter cell in G1 permitting its differentiation (Shimojo et al., 2008). However, information on HES1 dynamics in this experiment was absent, as it was performed in fixed tissue, with 6 hour timepoints separating early and late G1.

In non-proliferative or quiescent cells, *HES1* expression has been shown to be upregulated compared to cycling cells. *HES1* mRNA expression was increased in fibroblasts grown in serum depleted and high confluent conditions that induce quiescence (Coller et al., 2006). Immunohistochemical staining of boundary regions in the mouse brain showed increased levels of HES1 protein compared to non-boundary regions. Cells in these regions were defined as non-proliferative based on the absence of phosphorylated histone H3 (pH3) protein (Baek et al., 2006). Phosphorylation of histone H3 on serine 10 and serine 28 residues is a feature of condensed chromatin observed in mitotic cells before chromosome segregation in mammals (Goto et al., 2002; Li et al., 2005). Using pH3 as a marker, the proliferative capacity of a tissue can be determined by observing the number of cells undergoing mitosis. Dynamic differences between high HES1 expression in quiescent cells and their proliferative counterparts have been observed via live imaging. In neural stem cells derived from adult mice, HES1 was found to oscillate at higher levels in quiescent culture conditions (BMP+) compared to cells grown in proliferative conditions (EGF+), meaning the troughs of low Hes1 expression in quiescent cells are higher than the troughs of Hes1 expression in proliferative cells (Sueda et al., 2019).

2.1.4 Improving the HES1-cell cycle relationship and experimental aims

The above examples illustrate how *HES1* expression has largely been described in a comparative manner, using different cell states to distinguish between variability in *HES1* expression and how it relates to a cell's proliferative capacity. These comparisons have often been drawn using static or population-level measurements that only describe HES1 expression levels. In the cases where live-imaging has been utilized to observe HES1 dynamics, characterisation of the cell cycle has been absent, which limits the correlation of HES1 dynamics with specific transitions within the cell

cycle. Using indicators of cell cycle progression, HES1 dynamics can be described alongside different cell cycle phases and correlated with changes in cell cycle progression. The impact of the cell cycle on HES1 expression has also not been investigated fully. Evidence that the cell cycle regulates NOTCH signaling directly in chick neural progenitors and HeLa cells (Carrieri et al., 2019; Cisneros et al., 2008), suggests that the position within the cell cycle can also affect HES1 expression. To understand this relationship, it is crucial to describe HES1 dynamics as they occur temporally over the cell cycle.

The two main objectives of the work described in this chapter are:

1. Describing how *HES1* transcription changes over the cell cycle
2. Describing HES1 protein dynamics over the cell cycle

I will first utilise established methods of cell cycle synchronisation to examine *HES1* transcription by qPCR over the cell cycle in immortalized mouse embryonic fibroblasts (iMEFs) released from G0/G1 arrest and in MCF7 released from nocodazole arrest. I will then investigate Hes1 expression in the breast cancer MCF7 epithelial cell line at the single cell level, using *in-situ* hybridization methods to detect single HES1 RNA molecules and live-imaging of endogenous Hes1 protein dynamics at defined cell cycle stages.

This will improve upon current descriptions of HES1 heterogeneity that have relied on comparisons between cells of different cycling states by providing a model that encompasses real-time dynamics within the cell cycle. This approach is also more suitable to understand how HES1 dynamics relate to cell cycle transitions from which a potential functional role can be ascertained.

2.2 Results

2.2.1 Expression of *HES1* during the cell cycle in mouse embryonic fibroblasts

To investigate changes in *HES1* transcription over the cell cycle, immortalised mouse embryonic fibroblasts (iMEFs) were synchronised at G0/G1 by serum starvation (0.1% Fetal Bovine Serum [FBS]) and contact inhibition for 72 hours. Cells were released back into the cell cycle by serum stimulation and re-seeding into new culture vessels at a lower density. RNA samples were collected every hour over a 24 hour period. Cell cycle progression was monitored by quantitative reverse transcription PCR (qPCR, hereafter) analysis of the expression *Ccne1*, *Ccna2* and *Ccnb1*. The expression profiles of each gene for three biological replicates (1-3) are shown in figure 2.2.1. For *Ccne1*, upregulation of transcription is observed at 12 hours in experiments 1 and 3. *Ccne1* expression was down-regulated at 24 hours in experiment 1 and 3 compared to 12 and 18 hours with 3.1 and 2.1-fold change measured. *Ccna2* expression begins to increase at 12 hours in experiments 1 and 3. *Ccna2* shows increased expression at 18 and 24 hours post-release from serum starvation for experiments 1 and 3 with a 16.3 and 14.25-fold change for 18 hours and 20.45 and 12.22-fold change for 24 hours. This expression profile for *Ccna2* represents passage through S-phase and entry into G2. Upregulation of *Ccnb1* expression was observed at 24 hours for experiments 1 and 2, with a 24 and 5-fold change in expression, which corresponds to late G2 and entry into mitosis. *Ccne1* and *Ccna2* expression is delayed in experiment two, suggesting that cell cycle progression occurred slower or in a less synchronised manner this timecourse. However, for experiment 1 and 3 the timecourse specific expression of *Ccne1* and *Ccna2* indicates that the 24 hour period used broadly covers cell cycle progression from G0/G1 to G2.

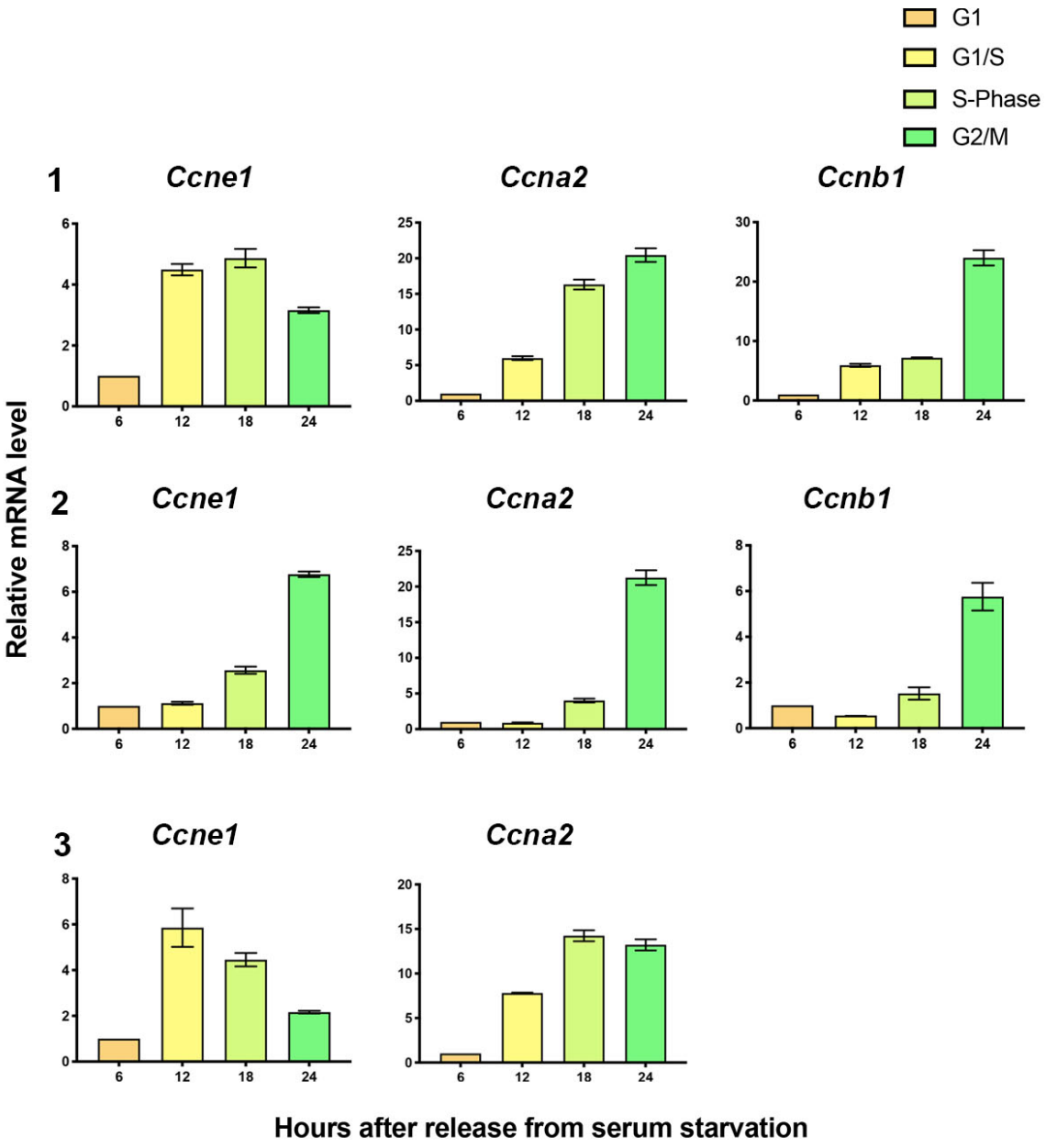

Fig. 2.2.1 Cyclin expression over the 24 hour timecoure. mRNA expression of *Ccne1*, *Ccna2* and *Ccnb1* (experiments 1 and 2) was analysed at 6, 12, 18, and 24 hours after release from serum starvation in 3 experiments (biological replicates) by qPCR. Ct values were normalised to *eEF2* at each timepoint and a fold change relative to 0 timepoint (serum starved, G0) was derived using the $2^{-\Delta\Delta Ct}$ method.

Across all 3 experiments there was a substantial increase in *Hes1* transcription (12-fold to 50-fold) immediately after serum stimulation that peaked at one hour (Fig. 2.2.2). This response is in agreement with previous studies that reported an increase

in *Hes1* expression in response to serum stimulation (Hirata *et al.*, 2002; Yoshiura *et al.*, 2007). There was inconsistency in the levels and timing of the decline between experiments. For example, at 2 hours in experiment 1, *Hes1* levels dropped to a 4-fold increase compared to timepoint 0. In experiment 2, *Hes1* levels showed an almost 30-fold increase compared to timepoint 0.

Judging the expression levels for *Hes1* in relation to the cell cycle, higher levels were observed in the first half of the timecourse, corresponding to G1. However, the inconsistency in *Hes1* expression between experiments during this period makes it difficult to ascribe a particular mode of expression to *Hes1* as it may be obscured by the strong serum response. While my expression analysis of *Ccne1*, *Ccna2,* and *Ccnb1* (Fig 2.2.1)display expression profiles that indicate between 0 and 24 hours cells traverse G1 and enter G2, there are still differences in expression levels for these genes. This likely indicates a degree of asynchrony at the population level. For this reason, *Hes1* dynamics at 1 hour intervals are unlikely to be informative, although the general expression levels indicate that *Hes1* expression is decreased in G2.

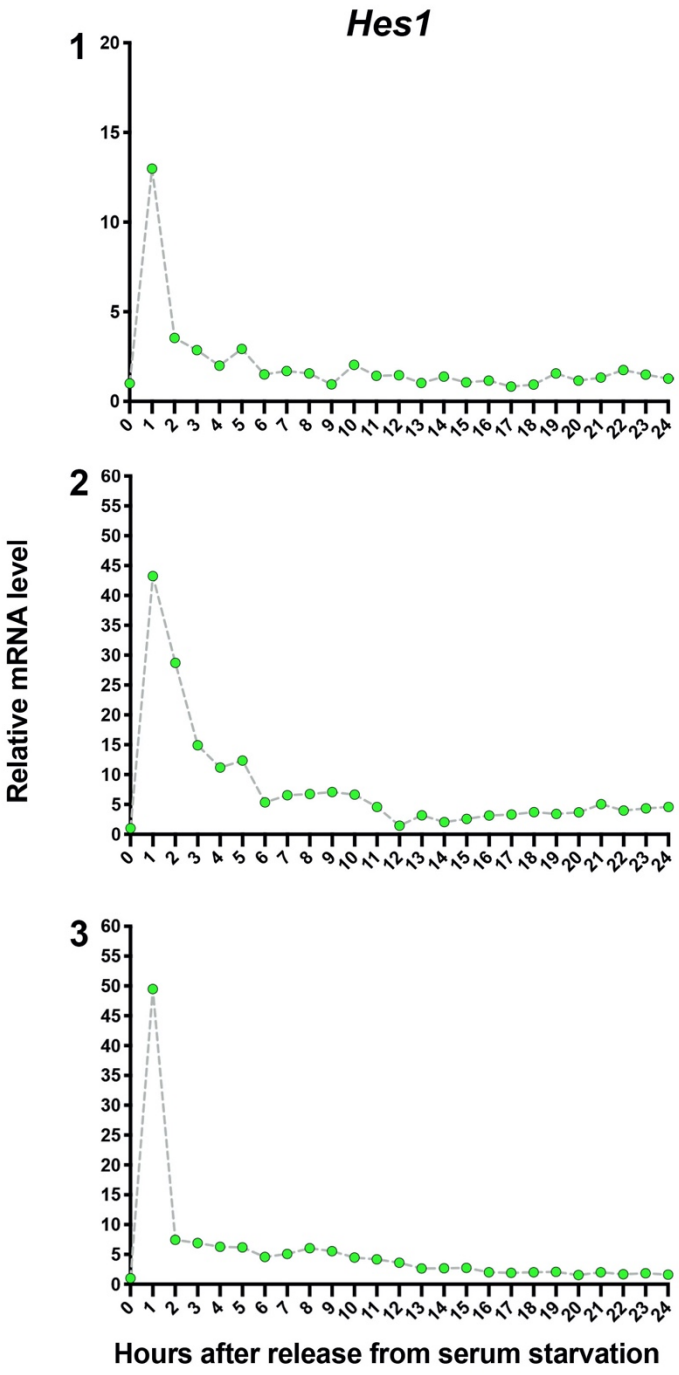

Fig. 2.2.2 *Hes1* mRNA expression over the cell cycle in iMEFs. *Hes1* expression over a 24 hour timecourse was analysed by qPCR. Ct values were normalised to *eEF2* at each timepoint and a fold change relative to 0 timepoint (serum starved, G0) was derived using the $2^{-\Delta\Delta Ct}$ method. Each data point for all 3 experiments indicates mean of two technical replicates.

2.2.2 Analysis of *HES1* expression from mitosis to G1 in MCF7 cells

Although, the iMEF timecourse in 2.2.1 was consistent with previous studies that reported a peak *Hes1* expression in response to serum stimulation, the inconsistency in *Hes1* expression during the G0/G1 transition limited characterisation of *Hes1* dynamics. For this reason, I decided to move away from a system that introduces a strong serum response. Instead, I chose the mitosis to G1 (M – G1) transition in MCF7 cells to study the expression of *HES1* in early G1. The expression of *HES1* has not been investigated during this transition, as past studies have focused more on the G0/G1 transition (Hirata et al., 2002; Sang et al., 2008). Studying the M-G1 transition can potentially reveal differences in *HES1* expression when entering G1 from mitosis or quiescence. Moreover, use of a cancer cell line such as MCF7 cells was desirable based on the evidence discussed in 1.11 of a role for HES1 in regulating proliferation in MCF7 cells. The MCF7 breast cancer cell line is characterised as being both estrogen and progesterone receptor positive. MCF7 cells are aneuploid and are generally described as hypertriploid or hypotetraploid, with reported chromosome variations ranging from 60 to 120 (Comşa et al., 2015; Nugoli et al., 2003).

MCF7 cells were synchronised in prometaphase by treatment with 200nM nocodazole for 15 hours. Mitotic cells were collected by physically washing off rounded-up cells from the culture plate. Collected cells washed twice in PBS to remove nocodazole and released into fresh, nocodazole-free media. The expression of Hes1 was analysed 1-2 hours after nocodazole washout at half hour intervals by qRT-PCR. Hes1 increased gradually over the 2 hour timecourse. Exit from mitosis over this period was confirmed by western blot analysis of mitotic markers. Decreased protein expression for Cyclin B1 and phospho-histone H3 (ser10) occurs at 2 and 4 hours compared to the 0 timepoint, which represents nocodazole arrested cells, is an event associated with exit from mitosis (Fig. 2.2.3. B). Unlike, in iMEFs released from serum starvation, *HES1* expression did not peak at 1 hour after release from nocodazole arrest. Its upregulation was also lower for corresponding timepoints after release. The 2 hour pulse of *Hes1* expression observed after release from serum starvation has been attributed to HES1 auto-regulation (Hirata et al., 2002), therefore the pattern of *HES1* expression observed here may represent

differences in HES1 negative feedback between the G0-G1 and M-G1 transitions. However, these differences could also be based on variability between species. The period of p53 protein oscillations has been found to differ between mouse and human cell lines with 'faster' oscillations observed in mouse cell lines due to smaller periods of expression (Stewart-Ornstein et al., 2017). The expression of *HES1* during the M-G1 transition is explored further in chapter 4.

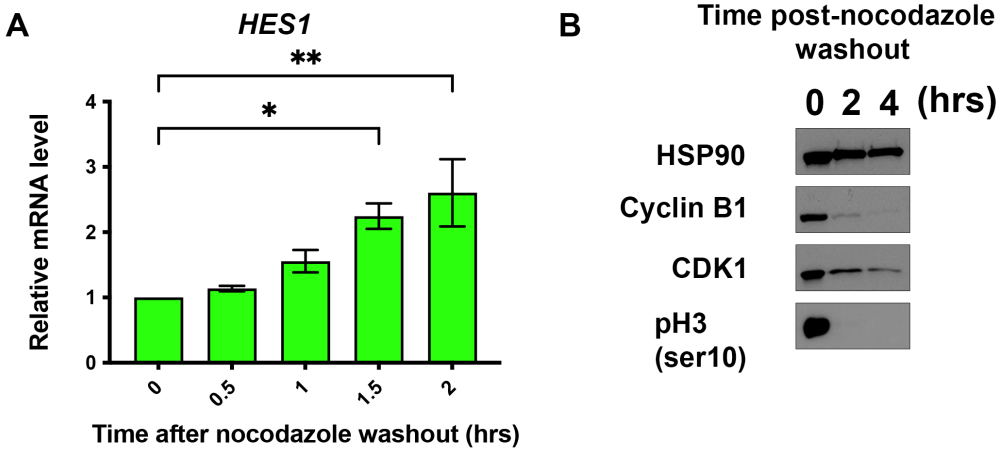

Fig. 2.2.3 *HES1* mitosis to G1 (M-G1) expression in MCF7 cells
(A) qPCR analysis of *HES1* mRNA expression 2 hours after release from nocodazole arrest. mRNA expression was analysed at half hour intervals. Ct values were normalised to *18S rRNA* at each timepoint and a fold change relative to 0 timepoint (nocodazole-arrested) was derived using the $2^{-\Delta\Delta Ct}$ method. Significance was determined by 1-way ANOVA using Tukey's multiple comparisons. Error bars indicate ±SEM from 3 biological repeats **(B)** Western blot analysis of Cyclin B1, CDK1 and pHistone-H3 (pH3) 0, 2, and 4 hours after nocodazole washout. HSP90 was used as a loading control. Blot is representative of 3 biological repeats.

2.2.3 Single-cell analysis of *HES1* transcription in MCF7 using single molecule fluorescent in-situ hybridisation (smFISH)

Analysis of gene expression at the single cell level is required to accurately decipher cell-to-cell heterogeneity that cannot be detected by population-based methods (Jeknić et al., 2019). It has been previously reported that *Hes1* exhibits substantial cell-to-cell variability in mRNA expression in mouse neural progenitor cells using single molecule fluorescent *in-situ* hybridization (smFISH) (Phillips et al., 2016). Differences in expression over the cell cycle may not be detectable if they are masked

by the population averages at different timepoints in qRT-PCR experiments. For this reason, I investigated *HES1* expression in MCF7 cells using smFISH, which allows for absolute quantification of RNA abundance at the single-cell level. This is achieved by hybridisation of multiple fluorescent probes to single *HES1* transcripts (Fig 2.2.4 A). Human *HES1* probes were designed by former Papalopulu Dr Tom Pettini using Stellaris Probe Designer (LGC Biosearch Technologies). Two probe sets were designed, labelled with Quasar 570 and Quasar 670, which targeted *HES1* exons and introns, respectively. Co-localisation of exonic and intronic signal in the nucleus of cells indicates the positions of transcription start sites (TSS) (Fig 2.2.4 A). This information can be used to infer changes in the kinetics of transcription rather than relative fold changes of mRNA (Munsky et al., 2012).

Following staining and image acquisition, images were analysed using the custom Matlab toolbox, FISH-quant, to detect both mature and nascent *HES1* RNA (Materials and methods 7.8) (F. Mueller et al., 2013). Quantification of *HES1* mRNA expression by smFISH showed that there is substantial cell-to-cell variability in *HES1* expression in MCF7 cells, consistent with what has been reported for smFISH *Hes1* expression measurements in mouse neural progenitors (Phillips et al., 2016). Representative data illustrating *HES1* heterogeneity is presented in Fig 2.2.4. Similar to what has been reported in mouse neural progenitor cells (mean 72 *Hes1* mRNA/cell), *HES1* copy number is low in MCF7 cells (mean 40 mRNA molecules per cell). *HES1* variability and low copy number is shown in three representative cells and compared with the highly abundant mRNA transcripts of the 'house-keeping' gene, *GAPDH* in the same three cells (Fig 2.2.4). In this example, *GAPDH* mRNA was detected using Q670 smFISH probes (Stellaris Biosearch). Sites of active *HES1* transcription were visualised by co-localisation of the fluorescent signal from probes targeting exonic regions of the *HES1* transcript and probes targeting intronic on nascent *HES1* transcripts. Spot size intensity often appears larger and brighter due to the fact that numerous transcripts are found at TSS (Fig. 2.2.4 C). From an example experiment of 164 cells, the distribution of *HES1* mRNA and TSS is illustrated in Fig 2.2.4 D**.** The long-tail mRNA distribution shown here may be indicative of slow-switching from an active to inactive transcriptional state (Munsky et al., 2012). Indeed, the distribution

for *HES1* TSS per cell indicates that 70% of cells have at least 1 *HES1* TSS. Overall, initial examination of smFISH data illustrates that in asynchronously growing MCF7 cells *HES1* transcription exhibits a substantial degree of cell-to-cell variability, in line with observations that transcription is an inherently stochastic process (Raj et al., 2006). The insight that *HES1* mRNA expression in MCF7 cells is characterised by low copy number and substantial cell-to-cell variability is useful as these are two properties that have previously been used to model how stochasticity in *HES1* expression affects cell differentiation (Phillips et al., 2016).

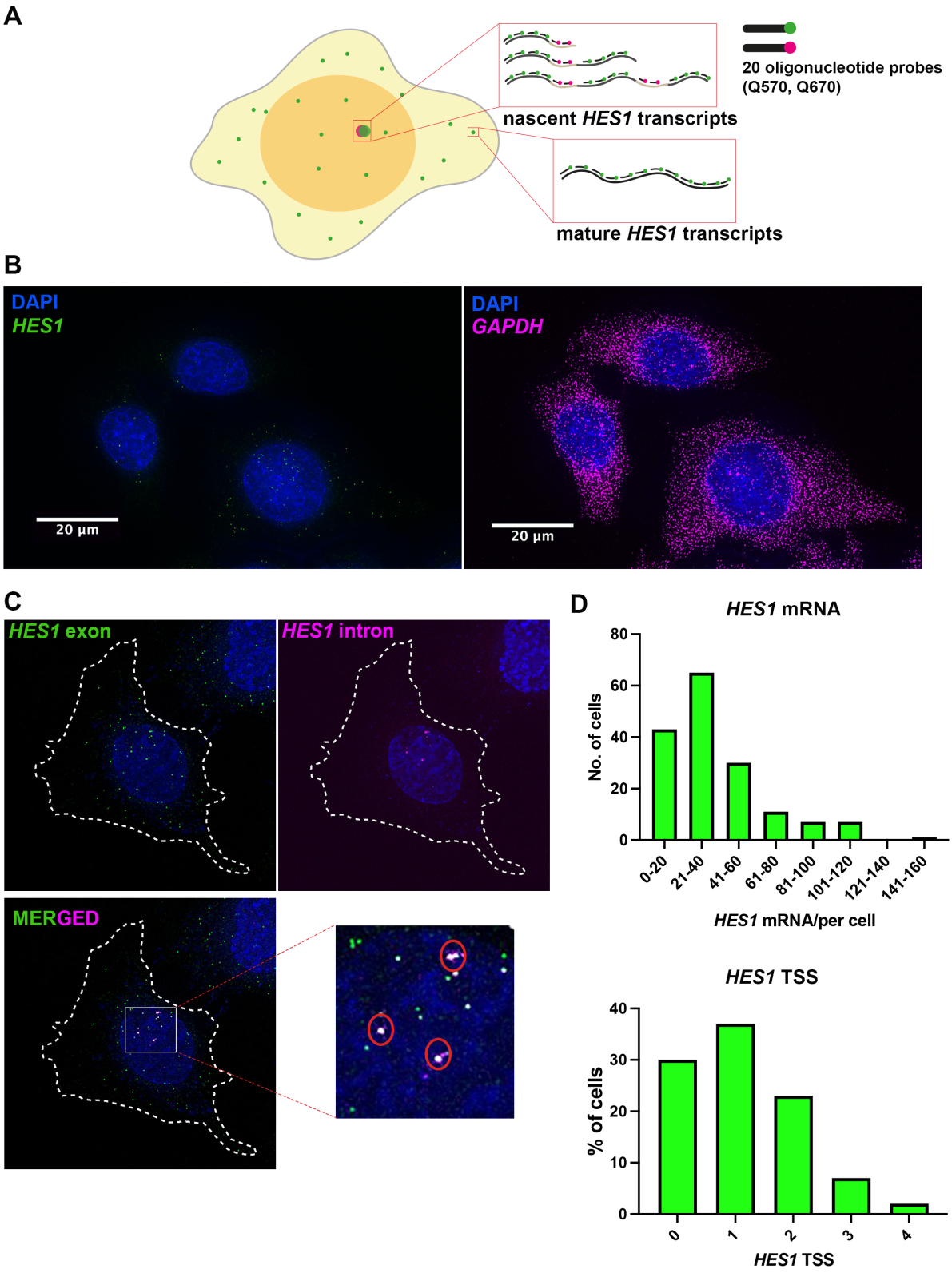

Fig 2.2.4. smFISH detection of single *HES1* RNA transcripts in MCF7 cells (A) Cartoon of smFISH detection of single *HES1* RNA transcripts and transcription start sites (TSS) in a single cell. 32 x 20 Quasar 570-conjugated oligonucleotide probes (green) were designed against *HES1* exonic sequences and 35 x 20 Quasar 670 probes (magenta) were designed against *HES1* intronic sequences. Green dots are observed in the

nucleus and cytoplasm where exonic probes have bound mature *HES1* transcripts. Sites of exonic (green) and intronic (magenta) co-localisation indicate nascent transcripts at TSS **(B)** Qualitative smFISH image. Left, three cells with *HES1* mRNA detected. Right, same three cells with *GAPDH* mRNA detected**.** Scale bar = 20 μm. **(C)** Left to right, single cell with *HES1* mRNA and *HES1* nascent RNA detected. Bottom left, exonic and intronic channels merged. Co-localised signal in nucleus highlighted. Images from **(B)** and **(C)** are z-projections of 41 images taken at 0.2 μm intervals **(D)** Distributions of *HES1* mRNA (mean 40 mRNAs per cell) and transcription start sites from sample experiment of n=164 cells.

2.2.4 Inferring the cell cycle status of MCF7 cells

To investigate if the non-genetic heterogeneity observed for *HES1* expression can be understood based on the cell cycle, I sought to categorise individual cells from smFISH experiments based on DNA content and nuclear size, two parameters which scale positively with cell cycle progression (Ginzberg et al., 2018; Gut et al., 2015). To better understand how DNA content and nuclear size relate to the cell cycle in MCF7 cells, I performed independent immunofluorescence staining of proliferating cell nuclear antigen (PCNA) and Cyclin B1 with identical DAPI staining to my *HES1* smFISH experiments. PCNA has a distinct temporal pattern of expression during the cell cycle. In S-phase it is associated with replication forks and can be observed as distinct foci in the nucleus of cells undergoing DNA replication (Bravo et al., 1987; Leonhardt et al., 2000). Cyclin B1 protein expression is observed in early G2, initially in the cytoplasm, before it localises to centrosomes and to the nucleus upon entry into mitosis where it is subsequently localised to unattached kinetochores and spindle poles at various points during mitosis (Pines and Hunter 1994; Bentley et al., 2007; Chen et al., 2008). To extract DNA content and size information, nuclei from single cells were segmented using the surfaces feature in IMARIS and the sum of total DAPI fluorescence was extracted to provide a measure of the total DNA content of each cell alongside measurements for nuclear size. Cyclin B1 expression (Top panel, left to right Fig 2.2.5) was observed in the cytoplasm of interphase cells (cells 1-6 Fig 2.2.5), the nucleus of a representative prophase cell (cell 7) and was closely associated with the condensed chromatin characteristic of prometaphase cells (cell 8-9). Analysis of total DAPI intensity and nuclear size of Cyclin B1 positive cells in interphase (G2 cells) revealed that G2 cells had a significantly higher sum of DAPI intensity (mean 7.2 versus 4.6, arbitrary units) and nuclear area size (mean 468 versus 360 μm²) than

Cyclin B1 negative cells. PCNA expression (bottom panel, left to right Fig 2.2.5) appeared as bright foci in the nucleus of cells, indicating the cell was in S-phase (white arrows) or was smooth in appearance (red arrows), indicating the cell was in G1 or G2. Analysis of the DAPI content for PCNA cells shows that S-phase (PCNA foci) cells had a significantly higher sum of DAPI intensity than non-S-phase cells (smooth PCNA) (mean 5.3 versus 4.3 arbitrary units). For non-S-phase cells, the scatter plot appears to show two distinct groups. The group above the median (22 cells) more likely indicates G2 cells as the DAPI content for these overlaps with data in the Cyclin B1 + scatter plot. Analysis of nuclear area for PCNA cells shows that cells in S-phase (PCNA foci) have a significantly higher nuclear area than non-S-phase cells (203 versus 329 μm^2). Given the likelihood that the smooth PCNA group contains a higher percentage of G1 cells than G2, this may skew the nuclear area mean towards a lower value (Fig 2.2.5).

Plotting the sum of DAPI intensity and nuclear area from Cyclin B1 images against each other showed that these two parameters were positively correlated ($r = 0.66$) as determined by Pearson correlation analysis (Fig 2.2.5 D). Overall, this data indicates that DNA content, as measured by DAPI intensity, and nuclear area are two parameters that scale with cell cycle progression in MCF7 cells as both show higher values in G2 (Cyclin B1 +) cells. Thus, DAPI intensity and nuclear area information from smFISH experiments can be used to infer the cell cycle status of individual cells in these experiments.

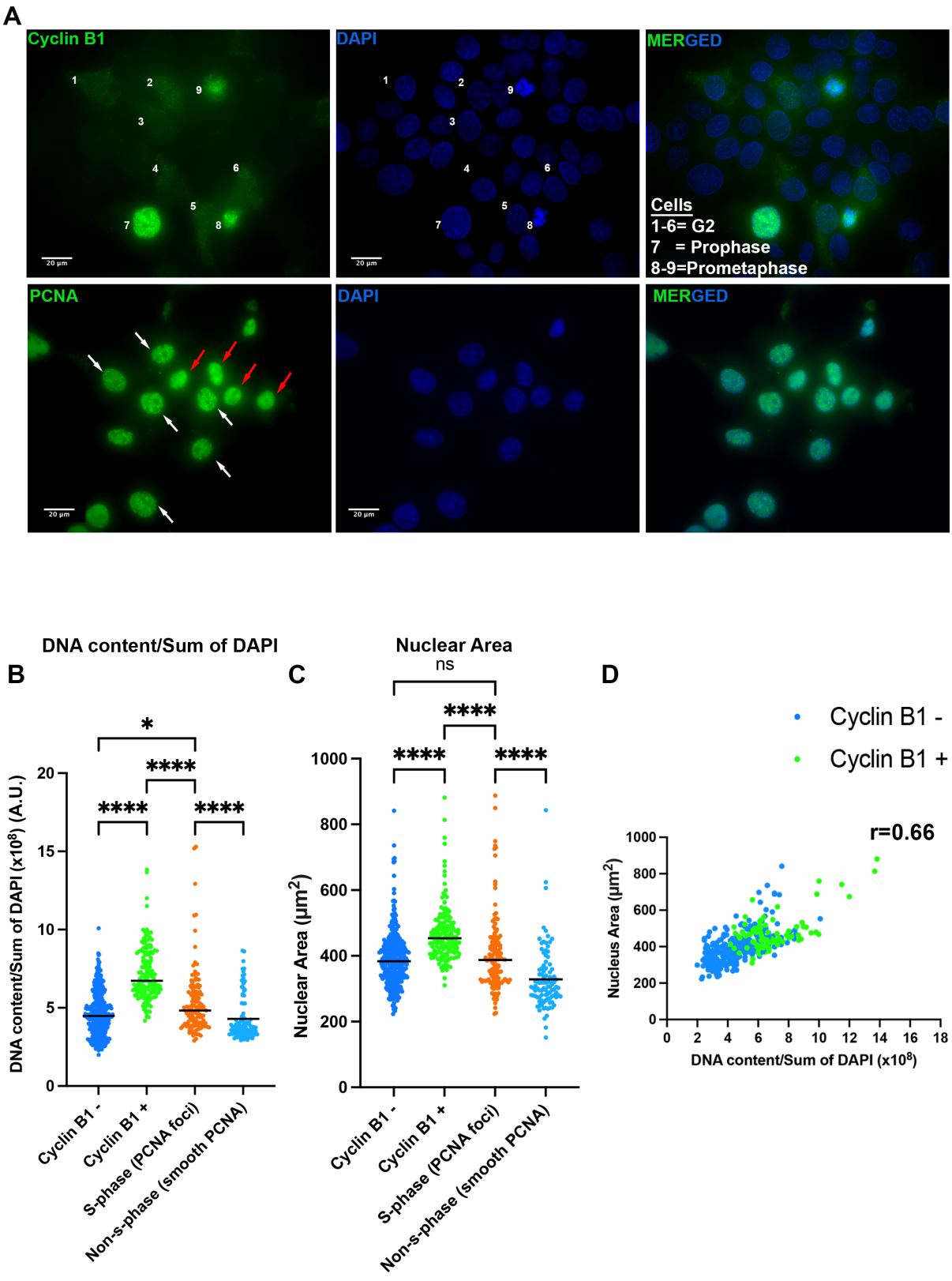

Fig. 2.2.5 Relationship of Cyclin B1 and PCNA expression with DAPI intensity and nuclear area in MCF7 cells. (A) Expression of Cyclin B1 and PCNA in different cells. Images are z-projections of 41 images taken at 0.2 µm intervals. Cyclin B1 images are displayed in the top panel left to right. Cells 1-6 show cytoplasmic Cyclin B1

expression, indicative of G2. Cell 7 is a prophase cell. Cells 8 and 9 are in prometaphase. PCNA images are displayed in the bottom panel, left to right. White arrows indicate S-phase cells as determined by appearance of PCNA foci. Red arrows indicate non-S-phase cells with smooth PCNA expression **(B-C)** Scatter plot showing distribution of sum of DAPI intensity (DNA content) and nuclear volume between Cyclin B1 positive (Cyclin B1 +, green dot), Cyclin B1 negative (Cyclin B1 -, blue dot), PCNA foci (orange dot) and PCNA smooth (light blue dot) cells. Each dot represents measurement from single cell. Black line represents median value**.** Significance was determined using Kruskal-Wallis One-way ANOVA with Dunn's multiple comparisons. The black square, circle and triangle symbol denote the mean value from each biological replicate for each group **(D)** Pearson's correlation between nuclear area and sum of DAPI intensity. For Cyclin B1 staining, 526 cells were analysed in total (373 Cyclin B1 - and 153 Cyclin B1 +). For PCNA staining 231 cells were analysed in total (133 PCNA foci and 98 PCNA smooth)

2.2.5 *HES1* mRNA abundance increases with DNA content and nuclear volume

Knowing that nuclear volume and DNA content scale with cell cycle progression in MCF7 cells, I extracted this information from individual MCF7 cells from smFISH experiments and examined how *HES1* mRNA abundance related to the two parameters. This allowed me to infer how *HES1* expression changes over the cell cycle. A moderate positive correlation was observed between *HES1* mRNA/cell and sum of DAPI intensity (r = 0.5) and nuclear area (r = 0.47), indicating that cells with larger nuclei and increased DNA content tend to have a higher amount of *HES1* mRNA (Fig 2.2.6 A). I examined this relationship further by binning sum of DAPI intensity and nuclear area values into groups of increasing size for both. In this way the increase in both parameters can be viewed as a proxy for cell cycle progression, given that higher values for both are more likely to be a G2 cell based on the Cyclin B1 immunostaining (Fig 2.2.5 B). For sum of DAPI, 1 A.U. bins were set, and for nuclear area, 50 μm^2 bins were set. An exception to this was the lowest and highest groups for both sum of DAPI and nuclear area, where the bin ranges were increased. This was done as the number of cells at the lower and higher end of these ranges for both parameters was very low, for example, 5 cells were observed with a nuclear area over 650 μm. Based on DAPI staining, I also identified mitotic cells by their characteristic chromatin structure, although this group contained a low number of cells (23 cells). Mean *HES1* mRNA abundance increased significantly with increasing

DAPI content. For cells with a sum of DAPI value between 2 and 4, the mean *HES1* mRNA/cell was 23. This increased to 33, 42, 52, 57 and 87 over the increasing sum of DAPI groups. A mean of 18 *HES1* mRNA molecules existed in mitotic cells. A similar pattern of *HES1* expression was observed with increasing nuclear area. In the smallest group (200-300 μm^2), a mean of 29 *HES1* mRNA/cell was observed. This decreased slightly to 25 mRNA/cell in 300-350 but increased to 30, 38, 42, 60 and 82 mRNA/cell over the remaining groups of nuclear area. For ease of viewing and so as not to cramp the corresponding graph, given the number of tests statistically significant comparisons between group means are listed in table form (Fig 2.2.6 C).

A

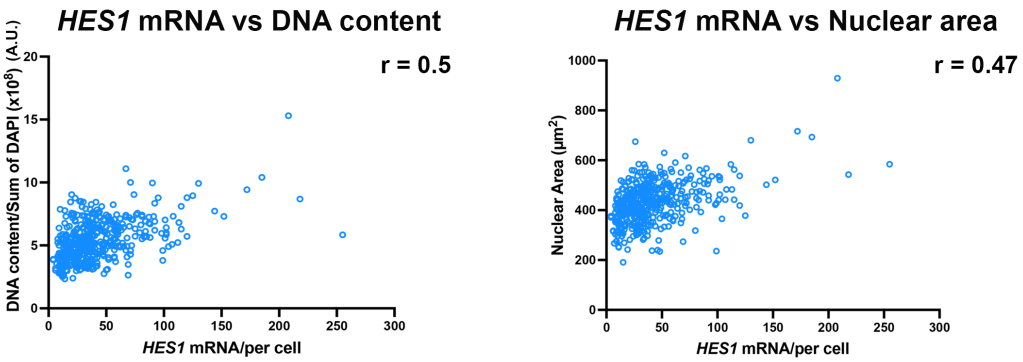

B

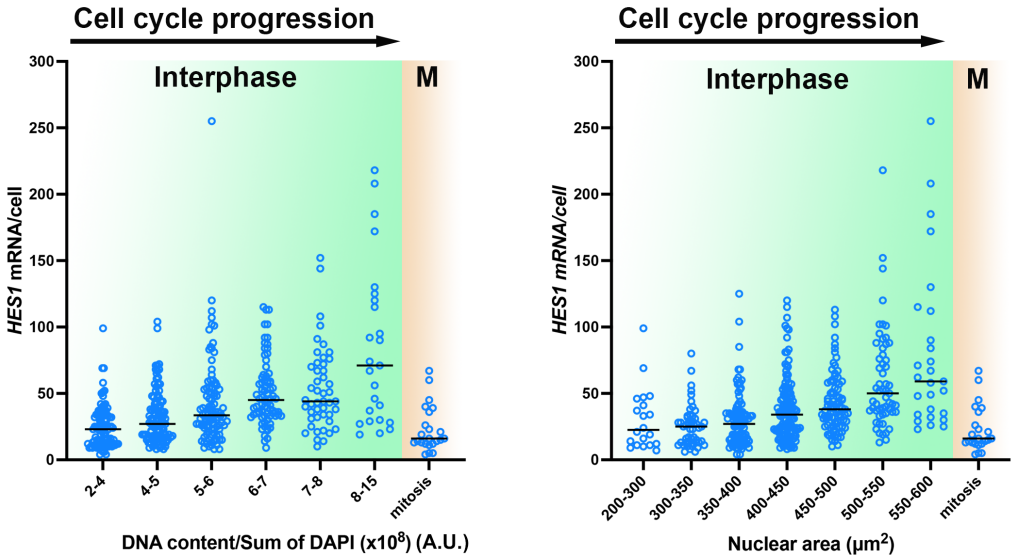

C

HES1/DNA content

Comparison	Summary	Adjusted P Value
2-4 vs. 5-6	****	<0.0001
2-4 vs. 6-7	****	<0.0001
2-4 vs. 7-8	****	<0.0001
2-4 vs. 8-15	****	<0.0001
4-5 vs. 6-7	****	<0.0001
4-5 vs. 7-8	***	0.0002
4-5 vs. 8-15	****	<0.0001
5-6 vs. 6-7	*	0.0346
5-6 vs. 8-15	*	0.0135
5-6 vs. mitosis	*	0.0146
6-7 vs. mitosis	****	<0.0001
7-8 vs. mitosis	****	<0.0001
8-15 vs. mitosis	****	<0.0001

HES1/Nuclear area

Comparison	Summary	Adjusted P Value
200-300 vs. 500-550	**	0.0012
200-300 vs. 550-600	***	0.0008
300-350 vs. 400-450	*	0.013
300-350 vs. 450-500	****	<0.0001
300-350 vs. 500-550	****	<0.0001
300-350 vs. 550-600	****	<0.0001
350-400 vs. 450-500	***	0.0003
350-400 vs. 500-550	****	<0.0001
350-400 vs. 550-600	****	<0.0001
400-450 vs. 500-550	***	0.001
400-450 vs. 550-600	**	0.0023
400-450 vs. mitosis	*	0.043
450-500 vs. mitosis	***	0.0006
500-550 vs. mitosis	****	<0.0001
550-600 vs. mitosis	****	<0.0001

Fig 2.2.6 *HES1* mRNA abundance over range of DAPI intensity and nuclear area (A) Left, correlation between *HES1* mRNA/cell and DNA content/sum of DAPI intensity

for corresponding cell. Right, correlation between *HES1* mRNA/cell and nuclear area of corresponding cells. Pearson's r is indicated in top right of graph for each comparison. **(B)** Scatterplots representing *HES1* mRNA per cell grouped by DNA content/Sum of DAPI intensity (right) and nuclear area (left). Each dot represents a single cell. Black lines over data represent population median **(C)** Results of Kruskal-Walls 1-way ANOVA with Dunn's multiple comparisons test to compare means between groups of *HES1* mRNA/cell and DNA content (left) and nuclear area (right). Only statistically significant results ($p < 0.05$) are listed. In total 456 interphase cells and 23 mitotic cells were analysed from 3 biological replicates.

2.2.6 Increased *HES1* transcription is associated with higher DNA content and larger nuclear area

Having established that *HES1* mRNA scales with DNA content and nuclear volume, I next aimed to investigate the transcriptional status of *HES1* in MCF7 cells and assess how it relates to *HES1* mRNA abundance and the DNA content and nuclear area of each cell. As mentioned previously, TSS were identified by observing co-localisation of exonic and intronic signal in cell nuclei. I characterised each cell based on the number of TSS, with cells having 2 or more TSS classified as multi-allelic and cells with 1 TSS classified as mono-allelic. Furthermore, I identified a subset of cells that expressed a 'doublet', this being two TSS in close proximity to one another (Fig 2.2.7 A). Doublets are indicative of actively transcribing alleles on sister chromatids following DNA replication and their identification here is evidence that a cell is in G2. *HES1* mRNA abundance was significantly higher in cells that contained a doublet or were multi-allelic with a mean of 65 and 57 *HES1* mRNA molecules per cell, respectively. Mono-allelic cells had a mean of 38 *HES1* mRNA molecules per cell, while cells with no TSS had a mean of 28 *HES1* mRNA molecules per cell. However, as illustrated in the scatter plot diagrams for each group, a high amount of variability exists, as some cells with no TSS also had a high *HES1* mRNA count (Fig 2.2.7). For sum of DAPI, the highest mean values were observed in the doublet and multiallelic groups, 7.q and 6.3 A.U., respectively and these were both significantly higher than mean values in mono-allelic cells (mean 5.2) and cells with no *HES1* TSS (mean 5). Similarly, cells with larger nuclei were associated with doublet (477.6 μm^2) and multi-allelic cells (453.7 μm^2). Doublet containing cells were significantly larger than cells

with no TSS. None of the other groups for nuclear area showed a significant difference, indicating that DNA content as measured by sum of DAPI may be a better differentiator of G2 and non-G2 cells. Using the information obtained from Cyclin B1 immunostaining in (Fig 2.2.5) I set a threshold based on sum of DAPI intensity to split cells into two groups, G1-S and G2. A sum of DAPI value of 6.5 was set on the normalised frequency scale shown in (Fig 2.2.7 C). Using the DAPI information from Cyclin B1 immunostaining, this scale illustrates the frequency of cells being Cyclin B1 + or Cyclin B1 – for a given value for sum of DAPI. The value of 6.5 was picked based on the frequency of Cyclin B1 + from this value. However, this is not a precise threshold and some overlap with non-G2 cells will occur. Using this threshold to split cells from my smFISH experiments into G1-S or G2 cells, I then calculated the percentage of cells from each group that had a certain number of *HES1* TSS (0-6). For G1-S, the majority of cells had either 0 or 1 *HES1* TSS, 38 and 35%, respectively. This percentage decreased from 1 TSS. For cells placed in the G2 category, 2 *HES1* TSS per cell constituted the highest percentage of cells. The percent of G2 cells with 2 TSS was significantly higher than G1-S cells. Overall, this data suggests that transcription occurring from more than one allele is a potential mechanism driving increased *HES1* expression, as measured by mRNA abundance. The fact that DNA content and nuclear area shared a similar relationship with cells with more than one *HES1* TSS is evidence that a switch to multi-allelic expression occurs as cells progress through the cell cycle and grow in size.

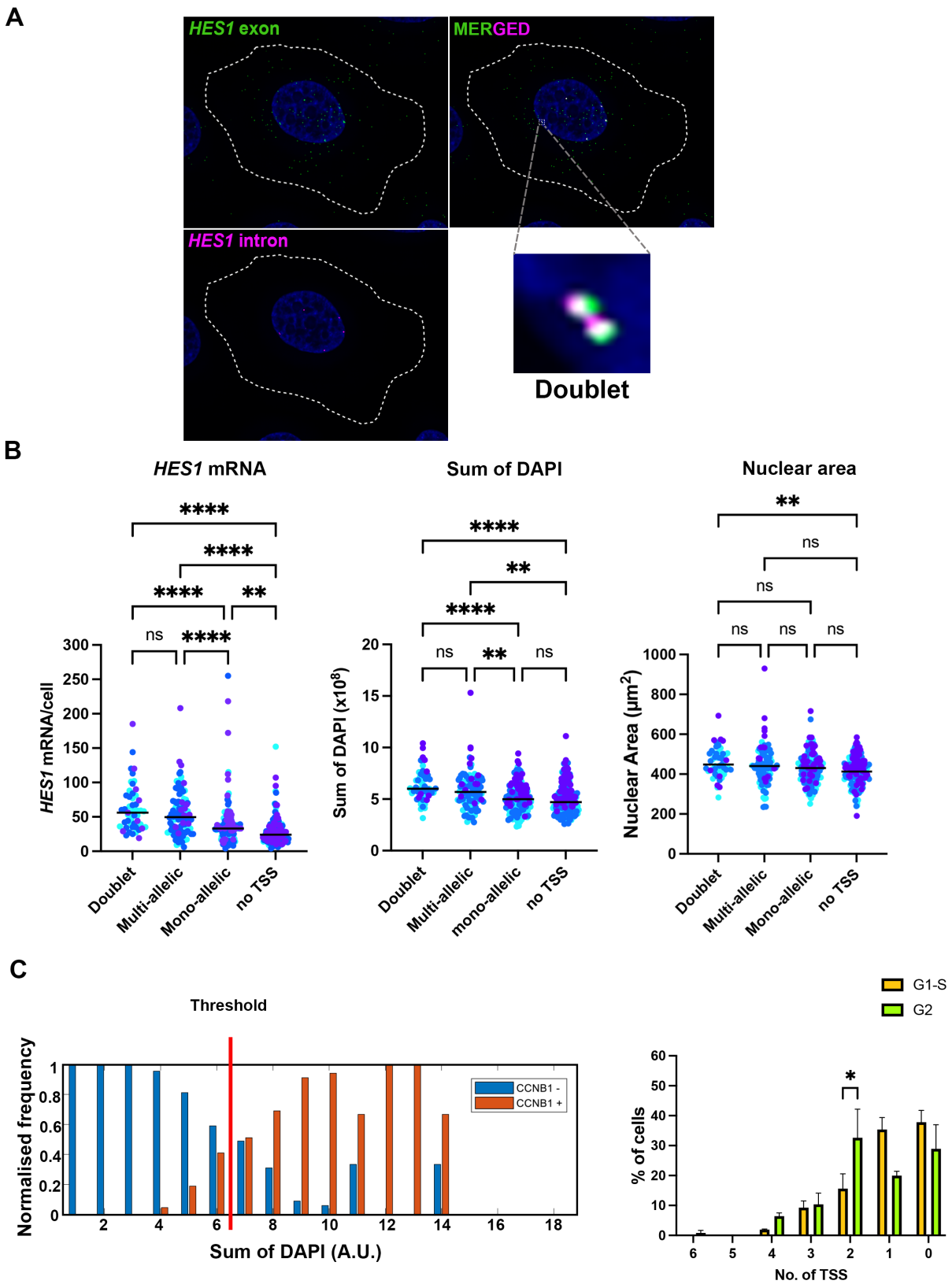

Fig 2.2.7. Characterisation of *HES1* TSS (A) Representative MCF7 cells with multiple *HES1* TSS. images are z-projections of 41 images taken at 0.2 intervals **(B)** From left

to right, scatter plots depicting the distribution of *HES1* mRNA, sum of DAPI, and nuclear area values per *HES1* TSS group. Black line on each scatterplot indicates population media. Dots in each group are colour coded to represent cells from different biological replicates. Significance was determined by Kruskal-Wallis 1-way ANOVA using Dunn's multiple comparisons **(C)** Left, graph depicting range of sum of DAPI values (2 A.U. intervals) observed in Cyclin B1 immunostaining (Fig 2.2.5) and the corresponding normalised frequency of Cyclin B1 +/- cells at each interval. Threshold of 6.5 set to split smFISH data into G1-S and G2 populations. Right, The percentage of cells from G1-S and G2 and the corresponding number of *HES1* TSS. Significance determined using 2-way ANOVA using Tukey's multiple comparisons.
In total 456 interphase cells from 3 biological replicates.

2.2.7 Live-imaging of HES1 protein dynamics in MCF7 cells

The above smFISH experiments illustrate the substantial cell-to-cell variability in *HES1* transcription. I observed an increase in *HES1* mRNA abundance and transcriptional activity as cells increased their DNA content and nuclear size, indicating that the increase in expression is concomitant with cell cycle progression. To investigate how the transcriptional profile of *HES1* during the cell cycle relates to its protein expression, I performed live-imaging to monitor endogenous HES1 expression in MCF7 cells. Live-imaging of endogenous HES1 protein dynamics was facilitated by integration of the coding sequence for the mVENUS fluorophore at the N-terminal of the HES1 locus using the CRISPR/Cas9 system in MCF7 cells (Fig. 2.2.8). Cell cycle dynamics were observed in the same cell line by lentiviral expression of a mCherry-PCNA construct. Live-imaging of the punctate expression of PCNA during S-phase (Fig 2.2.8) allowed the delineation of G1 and G2 cell cycle phases. Hes1-mVENUS and mCherry-PCNA MCF7 line was generated by Dr Nitin Sabherwal of the Papalopulu lab. Genotyping of this cell line determined it to be hemizygous for HES1. Sequencing of the *HES1* locus following CRISPR tagging identified one allele with the in-frame mVENUS insertion and a second allele with multiple mutations and a premature stop codon. HES1 dynamics have been extensively characterised in this cell line. HES1 exhibits bi-phasic expression during the cell cycle, with a peak occurring in G1 and G2 and period of lower expression occurring as cells enter S-phase (Sabherwal et al., 2021). In my independent live-imaging, I characterised the

levels of HES1 expression in each cell cycle phase. Representative traces of HES1 expression are shown in (Fig 2.2.11 A)

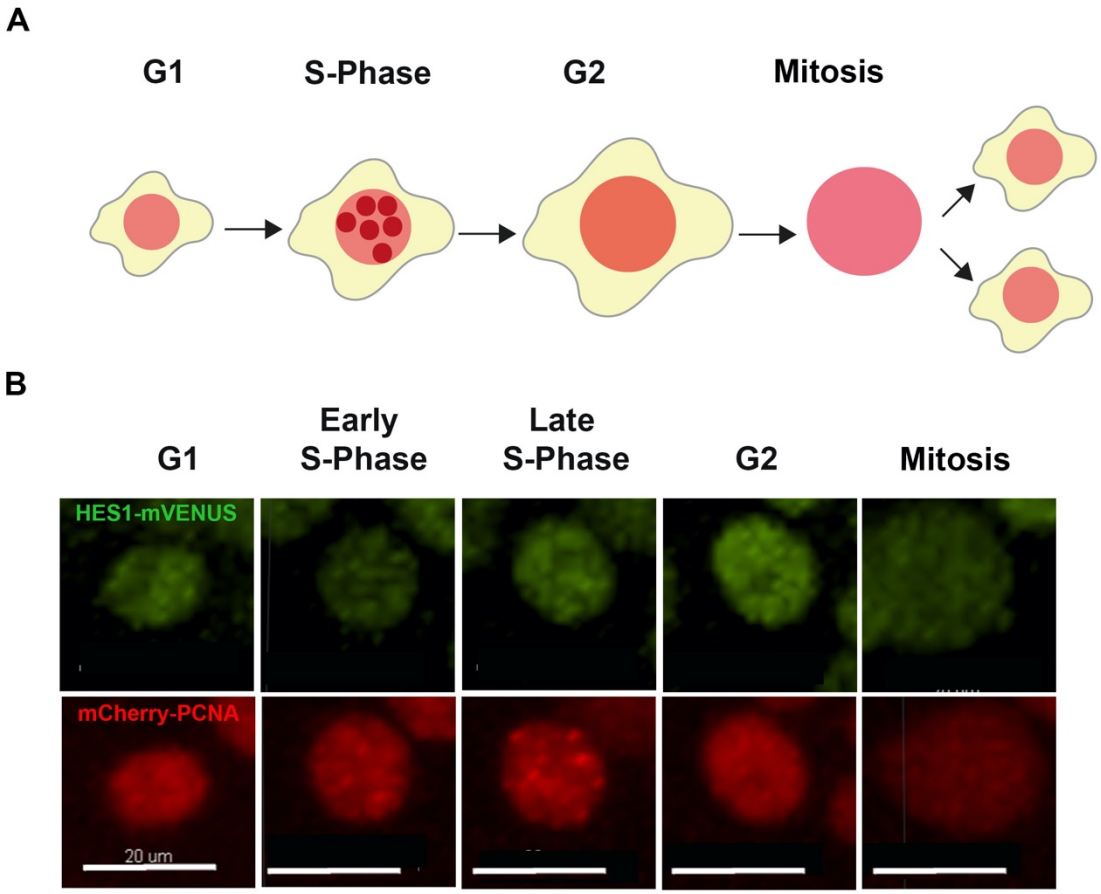

Fig 2.2.8. PCNA cell cycle expression profile in MCF7 cells. (A) Schematic of PCNA expression during the cell cycle. **(B)** Expression of HES1 and PCNA during the cell cycle in representative MCF7-HES1-mVENUS cell. is localized in the nucleus throughout the cell cycle. In S-phase PCNA is expressed as numerous bright foci due to its interaction with DNA replication machinery. Scale bars = 20 µm

MCF7-HES1-mVENUS cells were imaged every 20 minutes at 20x magnification using a Nikon A1 inverted confocal microscope. Measurements for mean HES1 intensity representing HES1 concentration in cell nuclei of MCF7 cells were obtained using the spot tracking function in IMARIS software (Materials and Methods 5.8). Cell cycle lengths (exit from mitosis to entry into mitosis) varied for individual cells ranging from less than 20 hours up to 50 hours (Fig 2.2.9). G1 had the longest duration with a mean of 14.3 hours, S-phase was the second longest with a mean of 8.8 hours and

G2 was the shortest cell cycle phase with a mean duration of 4.3 hours. Furthermore, each cell cycle phase showed a moderate correlation with other cell cycle phases (r = 0.5) for each comparison (Fig 2.2.9).

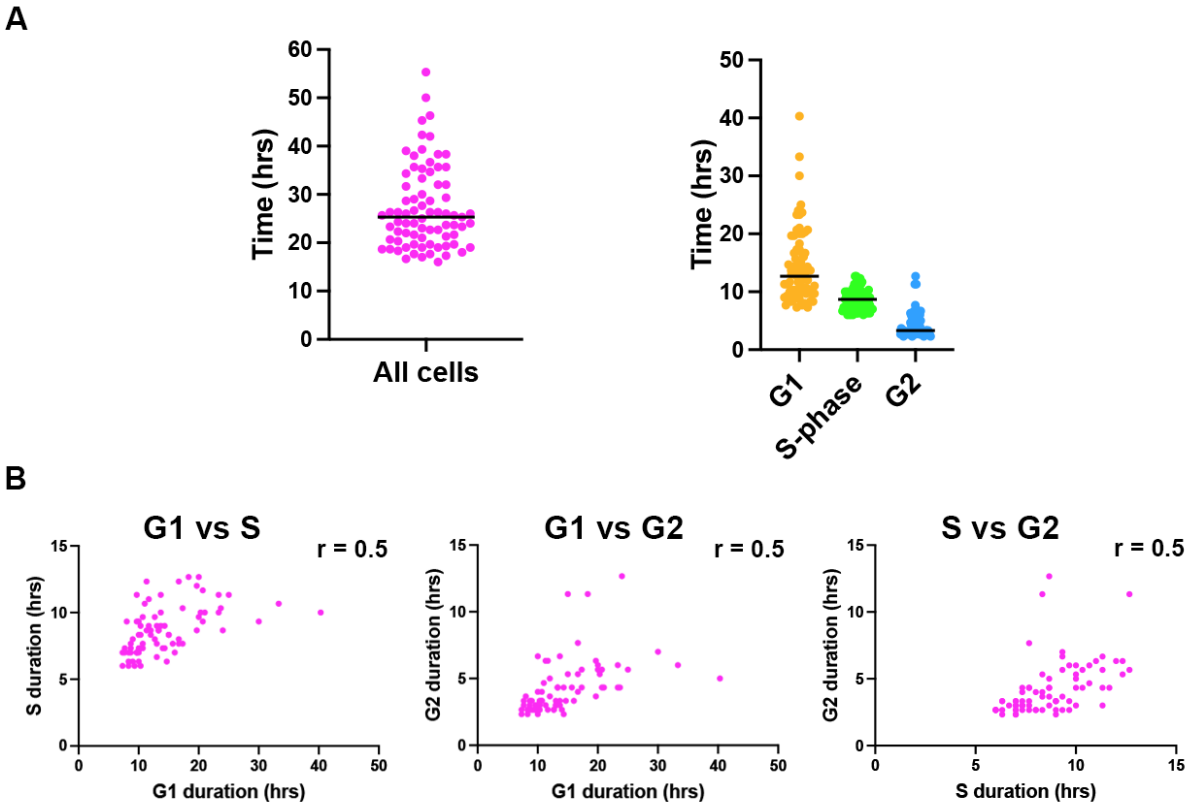

Fig. 2.2.9 Characterisation of cell cycle lengths in MCF7-HES1-mVENUS cells (A) Left, duration (hrs) of complete interphase cell cycle (exit from mitosis to entry into mitosis) in individual cells. Each dot represents a single cell (n=72). Right, the duration (hrs) of each cell cycle phases. Black line represents population median. **(B)** Correlation between cell cycle phases in individual cells. Left to right, G1 vs S, G1 vs G2, S vs G2. Pearson's r is indicated in top right of each graph.

HES1 expression was variable over the cell cycle in single cells as illustrated by the single cell traces in (Fig 2.2.10 A). In the representative traces, cell 7 and cell 9 illustrate how HES1 levels decrease from the beginning of G1 to S-phase. In cell 3 and cell 6, HES1 expression increases at the beginning of G1 before reaching a peak and declining before S-phase. In all cells, bar cell 8, an increase in HES1 expression was observed as cell progressed through S-phase. In cell 8 the increase in HES1 started at the beginning of G2. Overall, mean HES1 intensity changed per cell cycle phase and was lowest in S-phase cells, consistent with characterisation of HES1 expression in

this cell line that identified a dip in expression over-lapping with the G1/S transition (Sabherwal et al., 2021) (Fig 2.2.10 B). In MCF7 cells, I observed an increase in *HES1* transcription in cells inferred to be at later stages of the cell cycle (Fig 2.2.6 B and Fig 2.2.7 B). This suggests that the increase in HES1 expression as cells progress through S-phase and G2 might be facilitated by increased transcription of *HES1*. I did not observe a dip in *HES1* transcription in interphase cells occurring before its increase that would explain a dip in HES1 protein expression. However, without a distinct marker to identify S-phase or G1 cells the identification phase-specific *HES1* transcription could be obscured. In Fig 2.2.5 the sum of DAPI and nuclear area for S-phase cells overlapped substantially with Cyclin B1- cells, which are a mixture of G1 and S-phase cells, indicating that the difficulty to distinguish G1 and S-phase cells in the absence of a distinct marker. Additional factors, such as post-translational modification of HES1, might be involved in regulating its expression during the cell cycle.

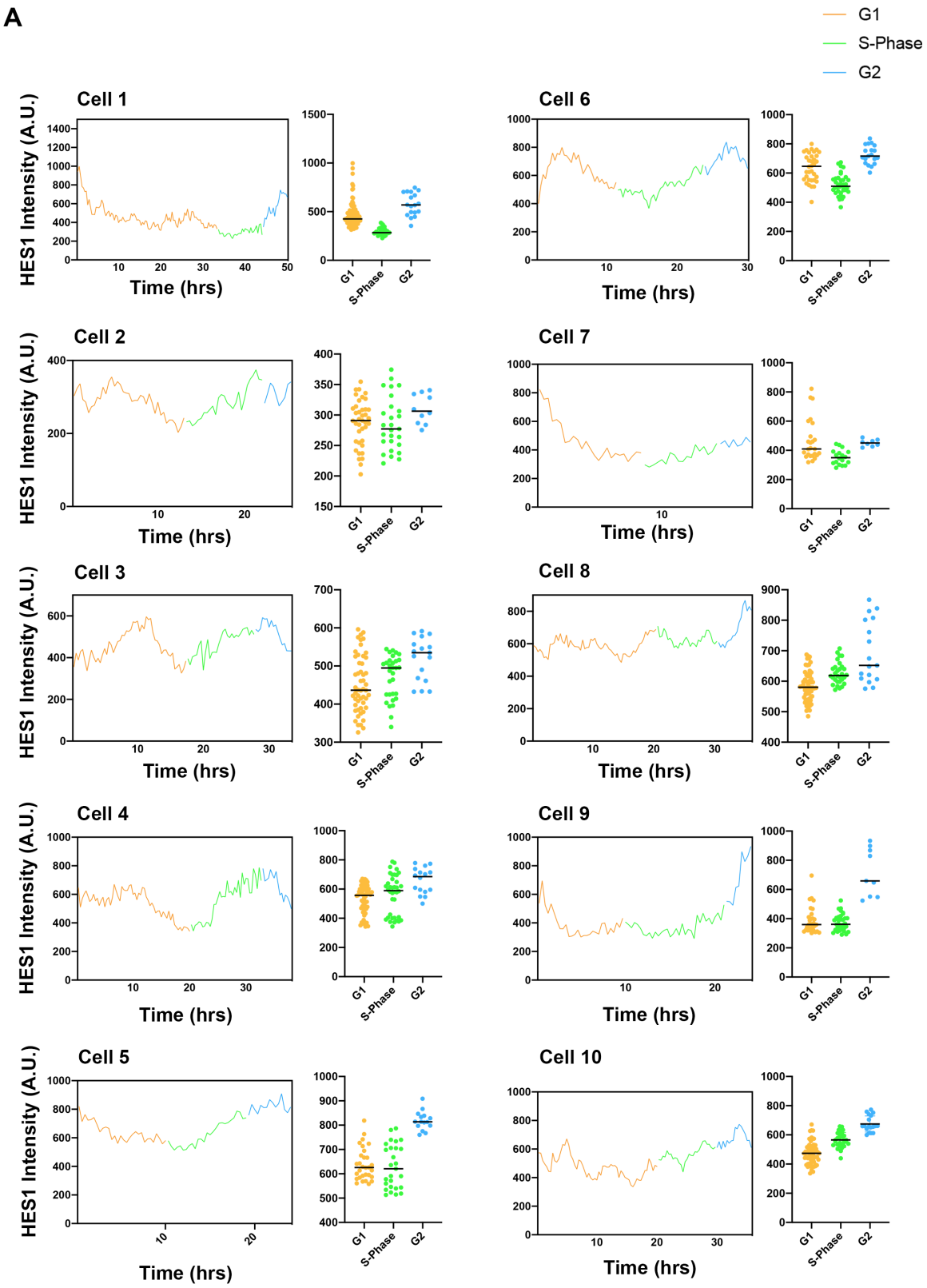
A
G1
S-Phase
G2
Cell 1
Cell 6
Cell 2
Cell 7
Cell 3
Cell 8
Cell 4
Cell 9
Cell 5
Cell 10
HES1 Intensity (A.U.)
Time (hrs)
G1
S-Phase
G2

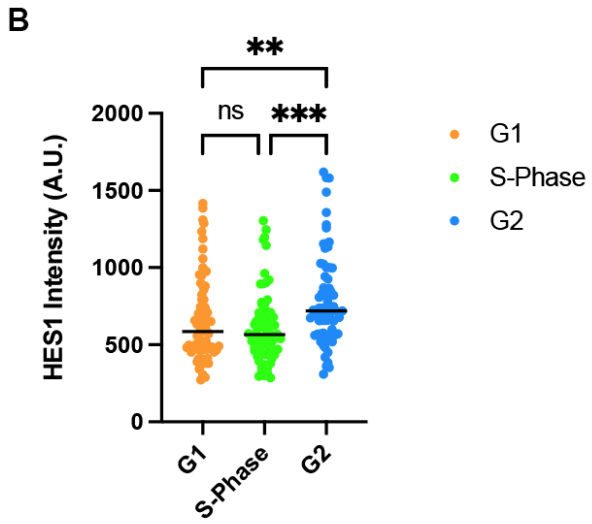

Fig 2.2.10 HES1 expression dynamics from mitosis to mitosis in MCF7 cells (A) MCF7 cells were imaged from mitosis to mitosis and values for HES1 mean intensity at each timepoint (20 mins) were recorded. Representative traces for Hes1 protein dynamics are shown for 10 cells. Traces are colour-coded to indicate transitions through cell cycle phases. On the right of each graph is scatterplot depicting HES1 intensity at each timepoint during each phase of the cell cycle **(B)** Scatter plot of mean HES1 intensity for each cell cycle phase. Each dot represents mean HES1 intensity in a single cell for the indicated cell cycle phase. Black line represents median of each group. Significance was determined using Kruskal-Wallis 1-way ANOVA with Dunn's multiple comparisons.

2.3 Discussion

HES1 is a widely studied transcription factor involved in the regulation of cell fate during development (Kobayashi & Kageyama, 2014). More recently, *HES1* has been implicated in regulating cancer stem cells (Gao et al., 2014; Simões et al., 2015; Cenciarelli et al., 2017). Cell fate diversification during development and the contribution of cancer stem cells to cancer development are cellular events that occur due to modulation of the cell cycle (Soufi & Dalton, 2016). How the cell cycle responds to dynamics in *HES1* signaling is not fully understood. Additionally, the extent to which *HES1* expression variability is dependent on the cell cycle has not been investigated.

The work presented is based on the argument that the best way to understand the potential coupling of *HES1* dynamics and the cell cycle, is by observing the two processes side-by-side. To this end, *HES1* transcription at a population and single cell level was investigated at different stages of the cell cycle in iMEFs and MCF7 cells, respectively. Endogenous HES1 protein dynamics were observed in real-time over the cell cycle in MCF7 cells in order to establish a relationship between *HES1* gene expression with protein expression.

2.3.1 *Hes1* expression over the cell cycle in iMEFs

Hes1 expression was significantly upregulated (up to 50-fold increase) when MEFs entered the cell cycle after serum stimulation. The levels of *Hes1* peaked at 1 hour post release and declined thereafter for the remainder of the 24 hour time-course.

This *Hes1* response to serum stimulation has been observed previously in studies using C3H10T1/2 mouse fibroblasts (Hirata et al., 2002; Yoshiura et al., 2007; Babaei et al., 2018). In these studies *Hes1* levels were increased up to 10-fold after serum stimulation. The difference between these results and those presented here may be due to the quiescent state of cells prior to serum stimulation. Quiescence was induced in the above studies by serum deprivation for 24 hours before release, whereas for the iMEFs used in this study, quiescence was induced by 72 hours of serum deprivation and contact inhibition. The longer duration of cell cycle arrest

used here may induce a so-called 'deeper' quiescence. The depth of quiescence has been found to limit the rate at which cells re-enter the cell cycle (Coller et al., 2006). If iMEF cells were less able to re-enter the cell cycle, it may explain the larger up-regulation of *Hes1* in this case. Such as scenario has been demonstrated for E2F1, where higher activation thresholds are needed for progression through the R-point (Kwon et al., 2017). The requirement of *Hes1*, in terms of activation levels, may scale with how readily cells can exit quiescence. The 3 experiments in Fig 2.2.2 were performed under identical conditions, the differences in the *Hes1* peak may be indicative of differences in the rate at which cells exited quiescence. This might be particularly relevant for experiment 2, where Hes1 levels are still relatively high up to 5 hours post-serum stimulation, compared to the other two experiments. The cells at these timepoints may still be quiescent/exiting quiescence and the sustained high levels of *Hes1* transcription observed a feature of this. A delay in cell cycle progression due to slow exit from quiescence would also explain the delayed expression *Ccne1* and *Ccna2* in this experiment.

2.3.2 Potential methods to study the G0-G1 transition in MCF7 cells

In this chapter, *HES1* expression during cell cycle re-entry was monitored when cells exited mitosis after release from nocodazole. This was done for two reasons: first, MCF7 cells were readily arrested in mitosis with nocodazole, and secondly, *HES1* expression during the M-G1 has not been studied before. Studying *HES1* expression during the G0-G1 transition in MCF7 cells would also be of interest since cell cycle re-entry from quiescence is believed to underlie cancer dormancy and treatment resistance (Sosa et al., 2014). Previous reports have achieved growth arrest in MCF7 cells by methods such MEK inhibition or treatment with 12-O-Tetradecanoylphorbol-13-acetate (TPA) (Alblas et al., 1998; Zhao et al., 2017). Drug treatment of MCF7 cells to achieve cell cycle arrest could be tested in future experiments and live-imaging of treatment periods followed by drug removal could capture G0-G1 transitions when cells reactivate proliferation. To overcome artefacts associated with cell cycle synchronisation, the use of live-cell markers of proliferation would also be advantageous when potentially investigating the G0-G1 transition in MCF7/MCF7 HES1-mVENUS cells. As described in the thesis introduction, a reporter for CDK2

activity has been employed in live-imaging studies using MCF10A cells (Spencer et al., 2013). Spencer et al. showed that cells exiting mitosis display a bifurcation in CDK2 activity with $CDK2^{low}$ cells entering a 'quiescent' state that is characterised by a delay in cell cycle progression and elongated cell cycle lengths (Spencer et al., 2013). The CDK2 reporter has been used in MCF7 cells in a study which examined the accumulation of Ki67 as cells progress through G1 from a $CDK2^{low}$ state , demonstrating the utility of this system for studying the G0/G1 transition in MCF7 cells (Miller et al., 2018). More recently, a CDK4/6 activity reporter has been developed. This reporter consists of a fluorescent mCherry tag fused to nuclear export and import sequences fused to a C-terminal made from a fragment of Rb bearing a docking site and phosphorylation sites that are specific to cyclin D/CDK4 but not cyclin E/CDK2 (Yang et al., 2020). Simultaneous Live-imaging of the CDK4/6 and CDK2 in MCF10A cells showed that the CDK4/6 is active before CDK2, indicating that it is a more precise reporter of when a cell enters the cell cycle (Yang et al. 2020). This reporter could be utilised in the MCF7 HES1-mVENUS cell line used in this thesis to study HES1 dynamics in cells that have spontaneously entered a G0-like state. Previous studies using breast/breast cancer cell lines, such as MCF10A, SUM149, HCC1594 and MCF7 cells, have characterised the stem-like or CSC sub-populations that exist in these cell types (Ginestier et al., 2007; Liu et al., 2014; Al-Hajj et al., 2003). These sub-populations are generally considered as two separate cell states, $CD24^{-}/CD44^{+}$ and ALDH+, with the former being described quiescent and the latter being described as proliferative. Furthermore, these two cell types have been found to spontaneously interconvert (Liu et al., 2014). Live-imaging using the CDK4/6 reporter could be a reliable marker to detect the interconversion between quiescent and proliferative cell states in MCF7 cells. CRISPR-modified MCF7 cell lines bearing endogenous fluorescent tags for CSC markers could also be generated for live-imaging studies examining cell state transition like G0/G1 in MCF7 cells.

2.3.3 Single cell analysis of *HES1* transcription in MCF7 cells

The expression of *HES1* has not been characterised in a cell-cycle dependent manner before in MCF7 cells. In this chapter I investigated changes in *HES1* transcription at the single cell level and established that they are correlated with an increase in

nuclear size and DNA content. Viewing these findings in relation to cell size, they are in agreement with multiple reports that gene expression scales with increases in cell volume in yeast and animal cells (Schmidt & Schibler, 1995; Zhurinsky et al., 2010). This agreement comes with the caveat that in my experiments I used nuclear area measurements from z-projected images rather than the 3D volume of entire cells. However, it is generally accepted that nuclear size and overall cell size is proportional (Huber & Gerace, 2007). Furthermore, increasing values for nuclear area have previously been used to track cell cycle progression from fixed cell analysis (Ginzberg et al., 2018; Gut et al., 2015). Recent smFISH experiments have identified transcriptional mechanisms behind size-dependent scaling of mRNA expression for multiple genes in fibroblast cells and fission yeast (Padovan-Merhar et al., 2015; Sun et al., 2020). The abundance of mRNA for high expressing genes, such as *GAPDH*, and low expressing genes, with less than 30 mRNAs per cell, showed a positive correlation with cell volume. The mechanism behind this scaling was determined to be an increase in the burst size of transcription as measured by TSS intensity. This effect on transcription was observed in larger G1 and G2 cells. TSS burst intensity did not change in a cell-cycle dependent manner as the volume of fibroblast cells used in this study did not change significantly during the cell cycle (Padovan-Merhar et al., 2015). In my smFISH analysis of *HES1* expression, transcription changed based on an increase in the number of actively transcribing *HES1* loci, which was correlated with increased expression of mature *HES1* mRNA and nuclear size. As mentioned previously, MCF7 cells are aneuploid with chromosome numbers reported to range from 60 to 120 (Comşa et al., 2015). This adds an element of uncertainty when analysing MCF7 cells, as larger cells with higher numbers of *HES1* loci could represent subpopulations of cells with increased ploidy rather than cells in G2 that have undergone DNA replication. Furthermore, previous work has demonstrated that transcription scales with cell size as a mechanism to maintain similar concentrations of mRNA between cells of different sizes (Padovan-Merhar et al., 2015; Kempe et al., 2015; Marguerat and Bähler 2012; Sun et al., 2020). However, this isn't the case for all genes, Miettinen et al. showed that mitochondrial genes decrease expression as cell size increases (Miettinen et al., 2014).

To more precisely examine whether the increased *HES1* expression observed here is cell cycle or cell size dependent, subsequent experiments would need to be performed that discriminate between gene expression measurements from cells of varying size versus cells that are definitively characterised as being in a specific cell cycle phase. This has previously been performed in MCF7 cells using single-cell FACS for cell size and cell cycle phase followed by qPCR (Dolatabadi et al., 2017). In this paper, single cells were sorted into different cell cycle phases based on increasing levels of Vybrant DyeCycle DNA stain. Concurrently, cell size was measured using the CellVue lipid membrane marker. Using this approach, the authors showed increased expression for cell cycle genes, such as *CCNA2 and CCNB1* in MCF7 cells sorted as G2 using qPCR (Dolatabadi et al., 2017). Following this experimental protocol and analysing *HES1* expression by qPCR alongside cell cycle genes would provide insight into cell cycle dependent *HES1* expression. To maintain experimental similarity with the smFISH results presented in this thesis, additional markers could be probed for to provide a specific read-out of cell cycle phase. Candidate cell cycle genes whose expression could be measured by smFISH alongside *HES1*, include *CCNA2* and *CCNB1.* Padovan-Merhar et al used a threshold of *CCNA2* mRNA counts combined with *HIST1H4E* mRNA counts to designate cells as being in G1, S-phase or G2 (Padovan-Merhar et al., 2015). *HES1* DNA-FISH could be utilized to assay *HES1* loci on sister chromatids as the identification of 'doublets' (fluorescently-labelled sites in close proximity/adjacent to each other) would mark cells that have undergone DNA replication. DNA-FISH has previously been utilized to detect and measure the distance between loci on sister chromatids (Stanyte et al., 2018). Combined with smFISH analysis of *HES1* expression analysis of co-localisation of *HES1* DNA-FISH and smFISH signal, would allow for a more robust assessment of how *HES1* is expressed in relation to the number of *HES1* copies per cell.

Analysis of transcription in single cells using smFISH and MS2 live-imaging has revealed how changes in the mRNA abundance of cell cycle genes reflect changes in how their respective genes are expressed. This has been demonstrated for *CCNA2* and *CCND1* (Dhuppar & Mazumder, 2020; Yunger et al., 2010). smFISH analysis of *CCNA2* expression in HeLa cells captured its cell cycle regulated increase in mRNA

expression and demonstrated that the increase is correlated with cells with more transcriptionally active copies of the *CCNA2* gene as measured by co-localisation of RNA and DNA FISH signal in the nucleus (Dhuppar & Mazumder, 2020). Live-imaging using *CCND1* promoter-driven MS2-GFP constructs in HEK293 revealed the burst-like nature of transcription as periods of expression were interspersed with shorter periods where no transcription occurred. As cells progressed through the cell cycle, expression was observed from 2 alleles at lower intensities than pre-replication indicating the cell cycle regulated reduction in *CCND1* expression in G2 (Yunger et al., 2010). The relationship between *HES1* mRNA abundance and *HES1* TSS with DNA content indicated that increased *HES1* expression occurred at later stages in the cell cycle. In this way, the expression of *HES1* is similar to what has been observed for *CCNA2* expression as measured by smFISH in HeLa cells, where a higher abundance of *CCNA2* mRNA was associated with more actively transcribing copies of the gene in G2 (Dhuppar & Mazumder, 2020). Similarly, I reported on the appearance of *HES1* TSS doublets, which I speculated to be expression occurring from *HES1* alleles on sister chromatids after DNA replication. The observation that these cells had the highest sum of DAPI intensity (Fig 2.2.7 B) provided further evidence that these were G2 cells. Expression from alleles on sister chromatids observed by live-imaging for *CCND1* transcription in HEK293 cells expressing MS2 constructs driven by the *CCND1* promoter, indicates that this type of expression can occur. However, in this case, expression of *CCND1* in cells after replication was associated with a decrease in promoter firing and lower amounts of mRNA, indicating that an increased number of alleles does not mean an increase in expression (Yunger et al., 2010).

In mouse embryonic stem cells (mESCs) transcription kinetics are altered for the pluripotency genes *Nanog* and *Oct4* along the cell cycle to effectively off-set gene dosage. Here a two-state model was used, which infers the time both genes spend in the transcriptionally 'on' and 'off' states (Munsky et al., 2012). After DNA replication, a decrease in the probability of *Oct4* and *Nanog* being on was predicted to maintain a consistent level of cell-to-cell variability between cells at different cell cycle stages. (Skinner et al., 2016). My observation here that *HES1* transcription is

more likely to be on in G2, suggests that HES1 is not regulated in such as a way as to maintain a constant level of expression during the cell cycle, at least the mRNA level.

Gene-expression studies in HeLa and U2OS cells have identified enriched gene expression profiles at different stages of the cell cycle using cell synchronization and microarray analysis (Grant et al., 2013; Whitfield et al., 2002). These studies characterised gene expression in G1/S, S, S/G2, G2/M, and M/G1 and assigned periodicity scores based on the expression profiles of genes in different clusters. The data presented here suggests that if *HES1* expression were to cluster into one of the above cell cycle groups it would be S/G2. *HES1* was not identified in these studies as having periodic expression within the cell cycle. This could be due to low expression of *HES1* or due to the fact that these experiments determined periodicity based on a threshold in fold-change in gene expression between cell cycle phases. In my smFISH data differences in mean *HES1* mRNA/per cell were significant between cells judged to be at early stages of the cell cycle versus later stages (Fig 2.2.6), however, fold-change difference may be below what has been used as a cut-off in these studies. ChIP-seq analysis has identified the target genes of transcription factors B-MYB and FOXM1, which activate late cell cycle (G2/M) gene expression. *HES1* was not identified as a target, indicating that its expression is not specifically enriched in G2 in these cell types (Sadasivam et al., 2012). More recent studies have moved away from cell synchronisation and have employed techniques for more precise measurement of gene expression such as single-cell RNA-seq (Boström et al., 2017; Karlsson et al., 2017; Mahdessian et al., 2021). In these studies a 'pseudo-time' for temporal progression of the cell cycle is determined based on reference data such as specific *cyclin* RNA expression or FUCCI measurements in single cells (Karlsson et al., 2017; Mahdessian et al., 2021). In a study describing gene expression during the cell cycle for developmental TFs in HeLa and U2OS cells, *HES1* and *HES7* were identified as having peak expression in G1 in HeLa cells with *NOTCH2* being expressed in G2/M (Boström et al., 2017). However, another study using U20S cells did not identify any cell cycle-dependent expression for *HES1* RNA and protein in U2OS cells (Mahdessian et al., 2021). These results could reflect differences introduced by experimental approach, Boström et al, FACs sorted cells based on FUCCI-markers

before performing RNA-seq, while Mahdessian et al, used a pseudotime model to determine cell cycle position.

Lastly, I sought to relate my findings on *HES1* transcription in MCF7 cells to HES1 protein dynamics observed in the MCF7-HES1-mVENUS cell line (Sabherwal et al., 2021). One of the key findings in this paper was the bi-phasic expression of HES1 during the cell cycle, with a peak observed in G1 and G2 with an intervening period of down-regulation that occurred during S-phase entry in the majority of cells (Sabherwal et al., 2021). In this chapter I showed that *HES1* levels increase significantly in a manner reflective of cell cycle progression, leading me to speculate that the increase in HES1 protein expression could result from increased *HES1* transcription I observed in cells with a higher DNA content. In mouse fibroblasts a delay between *Hes1* transcription and protein expression has been measured as approximately 15 minutes after serum stimulation, indicating that mRNA levels are indicative of subsequent protein expression within a short timespan (Hirata et al. 2002), This has informed subsequent studies that modelled ultradian oscillations in HES1 (Goodfellow et al., 2014; Monk, 2003). For cell cycle regulated proteins and transcripts, Mahdessian et al determined a delay of 8.6 hours delay between peak mRNA expression and peak protein expression (Mahdessian et al., 2021). Using smFISH combined with protein immunofluorescence in HeLa cells a correlation of r = 0.714 between mRNA levels and protein levels in single cells was observed for 23 genes tagged endogenously with GFP (Popovic et al., 2018). Direct observation of *HES1* expression and HES1 protein in MCF7 will be necessary to definitively comment on the relationship between *HES1* RNA and protein expression.

With regards, to the down-regulation of HES1 during the G1/S transition in MCF7 cells, there is evidence that this could occur due to cell cycle-dependent down-regulation of Notch signaling. The stability of *Notch1* and *Dll1* mRNA decreases during S-phase in dissociated chick and mouse neural precursors along with the capacity to induce *HES1* expression (Cisneros et al., 2008). Additionally, the Notch intracellular domain (NICD) is negatively regulated by the cell cycle. Phosphorylation of NICD in HeLa cells by CDK1 and CDK2 targets it for degradation during S-phase

(Carrieri et al., 2019). Although, this study didn't analyse the downstream effect of NICD degradation on *HES1* expression, it can explain how activation of *HES1* expression through NOTCH signaling could be diminished based on cell cycle position. Using increasing nuclear area and DNA content as a proxy for cell cycle progression, I did not observe a subset of cells that displayed a dip in *HES1* expression, however, the overlap between S-phase cells and G1 cells for these two parameters (Fig 2.2.5) indicates that a change in transcription would be difficult to observe during the transition from G1 to S-phase. Aside from transcriptional means, HES1 expression could be modified by post-translational modifications. HES1 stability has been found to be enhanced by SUMOylation and de-ubiquitination (Kobayashi et al., 2015). It's SUMOlytation was found to increase protein stability leading to enhanced repression of *GADD45a* in HEK293 cells (Chiou et al., 2014). Studying the post-translational modification of HES1 in a cell cycle-dependent manner and identifying periods during the cell cycle where its stability varies could uncover mechanisms underlying its expression dynamics during the cell cycle that are independent of its transcription. Overall, my data is supportive of a potential role for increased *HES1* transcription in HES1 upregulation in G2 but cannot account for changes in HES1 protein expression that may occur earlier in the cell cycle due to the lack of markers that could discriminate G1 and S-phase cells.

2.3.4 Concluding remarks

In this chapter, I investigated *HES1* transcription during the cell cycle using cell synchronisation and qPCR (iMEFs) and smFISH (MCF7) for single-cell analysis. In iMEFs, *HES1* exhibited a strong serum response, that has previously been described. However, in these experiments the inconsistency in expression limited insight into a potential dynamic pattern of *HES1* transcription in this experiment. In MCF7 cells, identification of *HES1* expression variability at the single cell level is an important finding that substantiates the possibility that *HES1* is dynamically expressed in cancer cells. Furthermore, I related my findings on *HES1* transcription to HES1 protein dynamics in the MCF7-HES1-mVENUS line. I concluded that increased protein expression in S/G2 in MCF7-HES1-mVENUS cells could be facilitated by upregulation of transcription.

Chapter 3: HES1 function over the cell cycle

3.1 Introduction

3.1.1 Opening remarks

In chapter 2, I demonstrated the utility of the MCF7-HES1-mVENUS cell line for observing the expression of HES1 during the cell cycle. As a follow-up objective, I will investigate if there is any regulatory relationship between these dynamics and cell cycle control. The importance of *HES1* in the control of cell proliferation is underscored by *in vivo* models, where loss or mis-expression of *HES1* leads to depletion of progenitor pools or abnormal organ development (Hatakeyama et al., 2004; Jensen et al., 2000). Despite these observations, how *HES1* expression dynamics are directly linked to cell cycle control is still not fully understood.

Live-imaging of protein dynamics has enabled the parameterization of gene expression signals that is more attuned to their temporal and spatial properties (Purvis & Lahav, 2013). There is now significant research demonstrating the functional stratification of different signaling molecules as a result of their expression dynamics. For example, how cells respond to cellular stress is mediated, in part, by changes in the dynamics of p53 expression that have been directly linked to changes in downstream expression of cell cycle regulators. Frequent pulses of p53 expression have been linked to activation of *CDKN1A*, while sustained expression results in activation of p53 targets associated with apoptosis and permanent cell cycle exit (Loewer et al., 2010; Purvis et al., 2012). A number of cell cycle regulators have been reported to be targets of HES1, however, no research has investigated the corresponding HES1 dynamics that may dictate target binding/repression or the timing of these events within the cell cycle.

3.1.2 The functional relationship between *HES1* and cell cycle regulators

HES1 has a paradoxical functional relationship with the cell cycle as it has been shown to transcriptionally repress both positive and negative regulators of the cell cycle (Ström et al., 2000; Baek et al., 2006; Georgia et al., 2006). HES1 represses the expression of *CDKN1B* to maintain proliferation in HeLa cells. This was shown under conditions where *HES1* was exogenously expressed from a tetracycline promoter. Induction of HES1 led to repression of p27 protein levels that could not be restored by co-treatment with proteasome inhibitors, indicating that loss of p27 occurred through transcriptional repression. Repression of *CDKN1B* by HES1 was determined to occur at the transcriptional level through HES1 binding to a class C site in the *CDKN1B* promoter. Mutation of this site blocked HES1 repression of luciferase activity driven by 3.5 kb 5' flanking region of *CDKN1B*. Expression of HES1 protein with a mutated WRPW C-terminal domain still resulted in luciferase repression, indicating that repression was mediated independently of the TLE-1 co-repressor (Murata et al., 2005). Conversely, HES1 represses the expression of the positive regulator of the cell cycle *E2F* that is activated through estrogen signaling in these cells, leading to a G1 phase cell cycle arrest in the T47D breast cancer cell line (Hartman et al., 2004). HES1 was determined to bind an N box consensus site in the *E*2F*1* promoter and subsequently repress luciferase activity driven by a *E2F1* promoter region containing the HES1 binding site. Repression was reversed when the N box sequence was mutated. In this study it was determined that HES1 bound the *E2F1* promoter as a heterodimer with the related HERP-1/2 protein. The HES1-HERP-1/2 heterodimer was previously shown to have greater repressive activities than either protein acting alone or as a homodimer (Iso et al., 2001). However, so far there is little research on whether HES1 binding partners dictate its targeting to different cell regulators. These two examples of HES1 repression were performed using Tet-inducible expression systems and therefore do not mimic endogenous HES1 expression. The function of HES1 may also vary due to cell type. The anti-proliferative effect of HES1 over-expression in T47D cells mimics the induction of Hes1 by All-*trans*-retinoic acid, which suppresses cell proliferation by estrogen signaling.

One way to resolve the contradictory activity of HES1 in cell cycle control is to view its potential targets in a manner that is reflective of their temporal activity in the cell cycle. For example, p27 and E2F1 are two molecules that can have temporally distinct expression and activity profiles in the cell cycle. During cell cycle arrest, p27 can inhibit the activity of Cdk4/6 prior to its phosphorylation of Rb and therefore earlier in the cell cycle than when E2F1 is released from Rb inhibition prior to G1/S (Ekholm & Reed, 2000). Therefore, HES1 regulation of these molecules may be influenced by the temporal expression of HES1 during G1 progression. A similar line of thinking was reached through modeling of how Hes1 can promote both cell cycle arrest and proliferation (Pfeuty, 2015). High HES1 in early G1 results in G0/G1 arrest, while oscillatory expression in late G1 promotes proliferation. In this model cell cycle progression can be opposed during windows of low HES1 in late G1 that relieves p27 repression facilitating stabilisation of NEUROG2 to induce cell cycle arrest and differentiation (Pfeuty, 2015). This approach to HES1 cell cycle control emphasises the importance of describing the temporal relationship between the two processes, where the outcome of HES1 dynamics is also dependent on the cell cycle position. Indeed, a key finding from the characterisation of the MCF7-HES1-mVENUS cell line was that cell cycle length is modulated based on the position of the G1 HES1 peak. In cells where the G1 HES1 peak occurred later in G1 a longer cell cycle was observed (Sabherwal et al., 2021).

Observing gene expression dynamics alongside cell cycle progression can help characterise heterogeneity in a gene's expression in relation to the cell cycle but it is not completely sufficient to assign a functional role. Perturbing dynamics, observing their corresponding change and the subsequent change in cellular response is one method to attribute a functional role to gene expression dynamics. This has been demonstrated using optogenetic approaches that modulate gene expression signals in neural progenitors. In multipotent, dividing neural progenitors HES1 and ASCL1 are co-expressed and oscillate. Sustained expression of a light-inducible ASCL1 versus oscillatory expression leads to neuronal differentiation. Altering the levels of ASCL1 pulses was not able to promote differentiation, indicating that the change in

dynamics was behind the switch from proliferation to differentiation (Imayoshi et al., 2013).

3.1.3 Perturbing gene expression dynamics

HES1 expression dynamics have been modulated through inhibition of upstream Notch signaling. Functional Notch signaling is dependent on cleavage of the NOTCH intracellular domain (NICD) at the intracellular membrane of cells by gamma-secretase prior to NICDs translocation to the nucleus where it regulates Notch targets like *HES1*. Gamma-secretase inhibitors e.g. DAPT, ultimately prevent translocation of the NICD to the nucleus and transcriptional activation of Notch targets (De Strooper et al., 1999). The amplitude of HES1 oscillations in mouse pancreatic explants was reduced by treatment with DAPT. This change in dynamics was associated with changes in the proportion of pancreatic progenitor cells (Seymour et al., 2020). Similarly, *Hes1* mRNA oscillations were ablated upon DAPT treatment of mesenchymal tissue from chicken limbs, which was associated with disruption to the spatial growth of these micromass cultures. *In ovo*, DAPT treatment, resulted in the impaired digit morphogenesis indicating that Hes1 oscillations are required for the correct patterning of the avian limb (Bhat et al., 2019). HES1 dynamics have also been altered by manipulation of transcriptional time-delays. Generation of mice expressing an 'intronless' *HES1*, thereby shortening the time for transcription, was reported to dampen Hes1 oscillations. These mice had smaller brains but neurogenesis proceeded similarly to control mice based on staining for genes associated with different neuronal subtypes. HES1 levels in these mice were lower than control but similar to HES1 heterozygous mice which do not present a reduction in body or brain size, again indicating a distinctive role for Hes1 expression dynamics (Ochi et al., 2020).

3.1.4 Experimental aims

The MCF7 HES1-mVENUS cell line is an excellent model for experimental perturbation of HES1 dynamics, as these can be readily visualised by live-imaging. Furthermore, the mCherry-PCNA reporter can provide a readout of the effect of HES1 perturbation on cell cycle progression. Recently, a small molecule inhibitor of

HES1 was described, named JI051 that arrested HEK293 cells in G2/M and caused the appearance of multinucleated cells, suggesting a potential regulatory role for HES1 in the G2/M transition (Perron et al., 2018). The proposed action of the inhibitor was to interfere with HES1 target repression due to stabilisation of a novel HES1 heterodimer with the scaffold protein PROHIBITIN 2 (PHB2), leading to decreased nuclear levels of HES1. Inhibition of functional HES1 DNA binding would lead to widespread de-repression of HES1 targets, including disrupting its ability to negatively regulate its own expression (Bavelloni et al., 2015; Perron et al., 2018). Such a scenario could have downstream effects on the HES1 auto-regulatory network and subsequent expression dynamics (Sturrock et al., 2014).

The aim in this chapter is to investigate a functional role for HES1 expression dynamics in cell cycle progression. The system of G0/G1 synchronisation and release into the cell cycle will be utilized for iMEFs. To assess the dependence of quiescence exit and cell cycle progression after serum stimulation on HES1 expression, I will modulate its expression using the gamma-secretase inhibitor, DAPT.

I will also determine the effect of JI051 on iMEF and MCF7 proliferation to assess if the G2/M arrest reported for JI051 is consistent in these cell lines. Both iMEF and MCF7 cells will then be used to assess the genes expression changes downstream of HES1 inhibition that precede any changes in cell cycle progression. The overall aim is to modulate HES1 expression and examine changes in cell cycle dynamics and gene expression to better describe how HES1 signaling integrates with cell cycle control.

3.2 Results

3.2.1 Inhibition of Notch signaling in iMEFs down-regulates *Hes1* expression

HES1 has previously been shown to be essential for the G0/G1 transition (Sang et al. 2008). In chapter 2, I observed a pulse of *HES1* transcription when iMEF cells entered the cell cycle after serum stimulation (Fig2 .2.2). To assess a functional role for *Hes1* expression during this transition, I used DAPT inhibition of Notch to attenuate *Hes1* transcription. DAPT (GS1-IX) is an inhibitor of gamma-secretase, a protease that cleaves the Notch intracellular domain (NICD) at inner-membrane surface of the cell. Preventing NICD translocation to the nucleus inhibits the activation of Notch targets, such as *HES1* (Borggrefe & Oswald, 2009). Additionally, the effect of reduced Notch signaling and *Hes1* expression on cell cycle progression will be investigated.

To synchronise cells in G0/G1, iMEFs were grown to confluency in normal 10% FBS media and then serum deprived for 72 hours using 0.1% FBS DMEM, as previously described. DAPT was added to cells at a concentration of 20 µM for the last 24 hours of serum deprivation. After 72 hours G0/G1 arrested iMEFs were re-plated at sub-confluent densities into new 10% FBS DMEM containing plates and treated with 20 µM DAPT or DMSO for control. iMEFS were collected every half hour after release for up to 2 hours after release from serum starvation and RNA was harvested to analyse gene expression via qPCR over the G0/G1 transition. iMEFs were also collected 6, 12, 18, 24, 30 and 48 hours after release from serum starvation and RNA was harvested to analyses gene expression via qPCR over the cell cycle.

The two hour *HES1* response was observed in control cells with a 27, 48, 21.5 and 13.5 mean fold increase in *HES1* expression at occurring at 0.5, 1, 1.5 and 2 hours post release from serum starvation, respectively. This two hour response is observed in DAPT treated cells, however, levels of *Hes1* were significantly reduced. There was a 1.7, 8.6, 1.5 mean fold increase relative to 0 hours control observed at 0.5, 1 and 1.5 hours post release from serum starvation, respectively. At 0 and 2 hours post release in DAPT treated cells *Hes1* expression was reduced by 70 and 40% relative to 0 hour control.

In control cells mean *Notch1* expression increased 7.3 and 12.8 fold at 1.5 and 2 hours, respectively, post release from serum starvation (1 hour later than *Hes1* upregulation). *Notch2* levels did not significantly change over the two hour timecourse. Only *Notch1* expression levels were significantly down-regulated by DAPT treatment compared to control cells. This reduction in expression was observed at 1.5 and 2 hours post release where the fold change relative to 0 hours was 1.3 and 1.8, respectively. *Notch1* is a reported transcriptional of target of Notch signalling and it's expression is down-regulated upon treatment with gamma secretase inhibitors (Borggrefe & Oswald, 2009; Weng et al., 2007). The delay in *Notch1* expression with respect to *Hes1* (1.5 versus 0.5 hours after release from serum starvation) could simply reflect differences between transcriptional responsiveness of *Hes1* and *Notch1* to Notch signaling after cells have been released from serum starvation. Activation of Notch signaling In the *Drosophila* DmD8 cell line has previously revealed temporal differences in the expression of Notch targets, with the *enhancer of split* genes identified as early-responders (Housden et al., 2013). Furthermore, the presence of SPS elements in the prompters of Notch targets has been speculated to dictate responsiveness to Notch signaling. Promoter assays testing the activation of Notch targets in response to different Notch proteins showed that the *HES1* promoter, which contains an SPS site, had higher fold activation responses than the *HES1* promoter (Ong et al., 2006). Although not tested, these mechanisms of differential gene activation in response to Notch signaling can explain how differences in the temporal expression of *Hes1* and *Notch1* exist in this experiment, with down-regulation of *Notch1* due to DAPT being observed later.

Hes1 expression was reduced over the cell cycle relative to expression at 6 hour. Expression was reduced by 38, 35, 51, 55 and 64% at 12, 18, 24, 30 and 48 hours respectively. This reduction was increased in DAPT treated cells. At 6, 12, 18, 24, 30 and 48 hours, *Hes1* expression was reduced by 72, 78, 82, 79, 75 and 71%. The most significant reduction was observed early in the cell cycle at 6 and 12 hours post release from serum starvation. *Notch1* expression was reduced by in control cells. In DAPT treated cells, levels were also reduced but the only significant reduction was

observed at 6 hours where *Notch1* expression was reduced by 50% relative to 6 hour control. *Notch2* expression levels weren't significantly affected by DAPT treatment over the cell cycle. A comparable expression profile for *Ccnb1* was observed between DMSO and DAPT. A 3.9, 5.2 and 4.5 fold increase in in *Ccnb1* expression was observed at 18, 24 and 30 hours after release from serum starvation in control cells, indicating passage through G2/M. Similarly in DAPT treated cells, a 3.2, 6.4 and 4 fold increase in expression relative to 6 hours control was measured at 18, 24 and 30 hours. This data indicates that iMEF cells are able to enter the cell cycle when *HES1* expression is significantly reduced. Furthermore, it informs on the temporal relationship between Notch-HES1 signaling and the cell cycle, specifically NOTCH1, as DAPT treatment only affects *Hes1* expression early in the cell cycle at 6 and 12 hours.

To better characterise Notch signaling during the above timecourse experiments, western blot analysis of NICD could indicate when Notch signaling is active and when DAPT is effective at inhibiting NICD cleavage. Furthermore, analysis of Notch1 and Hes1 protein expression would be useful to examine whether the observed down-regulation in *Hes1* and *Notch1* mRNA expression has a significant effect on corresponding protein expression. This would strengthen the conclusion reached above that reduced expression of *Hes1* and *Notch1* after DAPT treatment doesn't significantly affect cell cycle progression in iMEFs when released from serum starvation. Analysis of HES1 protein expression was hampered by a failure of commercial antibodies tested to detect Hes1 protein in western blot experiments.

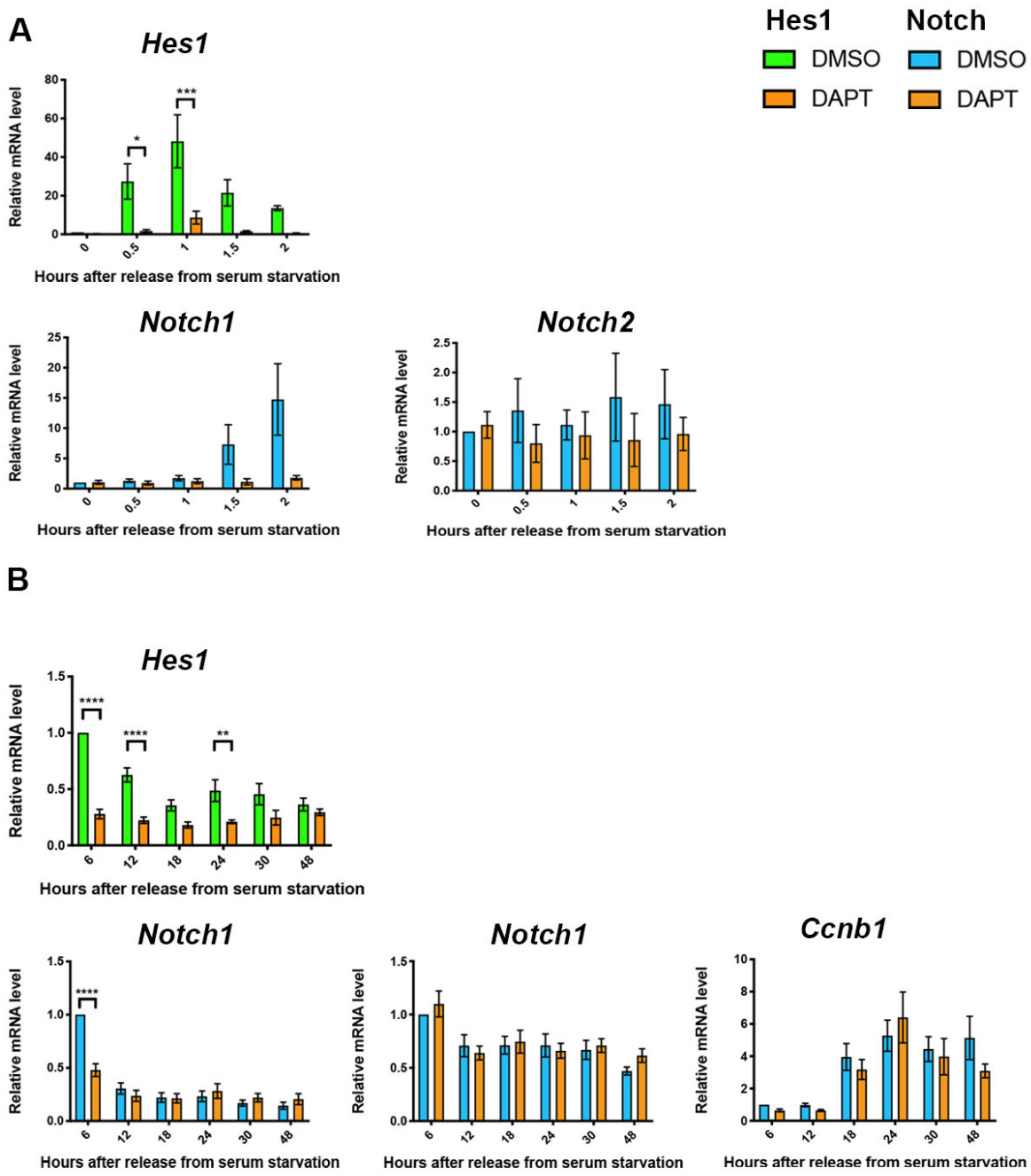

Fig. 3.2.1 Analysis of gene expression in iMEFs released from G0/G1 and treated with Notch inhibitor, DAPT. (A) Analysis of *Hes1*, *Notch1*, and *Notch2* expression during G0-G1 transition in iMEFS. Gene expression was analysed by qPCR at half hour intervals up to 2 hours after release from serum starvation **(B)** Analysis of *Hes1*, *Notch1*, and *Notch2* expression during the cell cycle in iMEFs. Gene expression was analysed at indicated timepoints after release from serum starvation in iMEFs.
Ct values were normalised to *eEF2* at each timepoint and a fold change relative to 0 timepoint (serum starved, G0) was derived using the $2^{-\Delta\Delta Ct}$ method. Significance was determined by 2-way ANOVA using Šidák's multiple comparisons. Error bars indicate ±SEM from 3 biological repeats.

3.2.2 JI051 reduces cell proliferation in MCF7 cells

The anti-proliferative effect of JI051 HES1 inhibition, first shown in HEK293 and pancreatic cancer MIA PaCa-2 cells (Perron et al., 2018), has not yet been tested in breast cancer cells. As mentioned in Chapter 2 2.2.3, evidence of a role for HES1 in cancer development formed part of the motivation to characterise *HES1* expression during the cell cycle in MCF7 cells. If JI051 has the same effect on MCF7 cells, a functional role for HES1 in controlling the cell cycle can be explored further in breast cancer using JI051.

Cell proliferation was assessed using live-imaging and the alamarBlue proliferation assay in MCF7-HES1-mVENUS and MCF7 cells. For live-imaging MCF7-HES1-mVENUS cells were seeded into 12 well plates at similar densities in triplicate and treated with 2 µM. Untreated (DMSO) and JI051 cells were imaged every 45 mins for 3 days. In control cells, cell confluence at time 0 was calculated ~27%. Cell confluence increased over 3 days reaching ~50% confluence when the last image was captured. JI051-treated cell did not grow significantly past the initial ~25% confluence they were seeded (Fig 3.2.2). For the alamarBlue assay, MCF7 cells were seeded into 96 well plate and treated with 1 µM JI051. Cells were grown in normal 10% FBS DMEM at 37 degrees for up to 5 days. Each day normal media was replaced with 10% FBS DMEM and 1x alamarBlue reagent. Cells were incubated at 37 degrees for 4 hours and proliferation was assessed by measuring alamarBlue reduction with a fluorescent plate reader. In Fig 3.2.2 (A) day 1 represents 24 hours after cells were seeded into wells. By day 2 both control and JI051 cells showed the same rate of proliferation. Proliferation increased for control cells up to day 5, however at days, 3, 4 and 5 proliferation was reduced for JI051 treated cells with 0.88, 0.72, and 0.46 percent proliferation compared to control on each day as measured by alamarBlue reduction. This indicates that JI051 has a similar anti-proliferative effect on MCF7/MCF7-HES1-mVENUS growth rates and can be utilised further to explore the role of HES1 in cell proliferation in these cells.

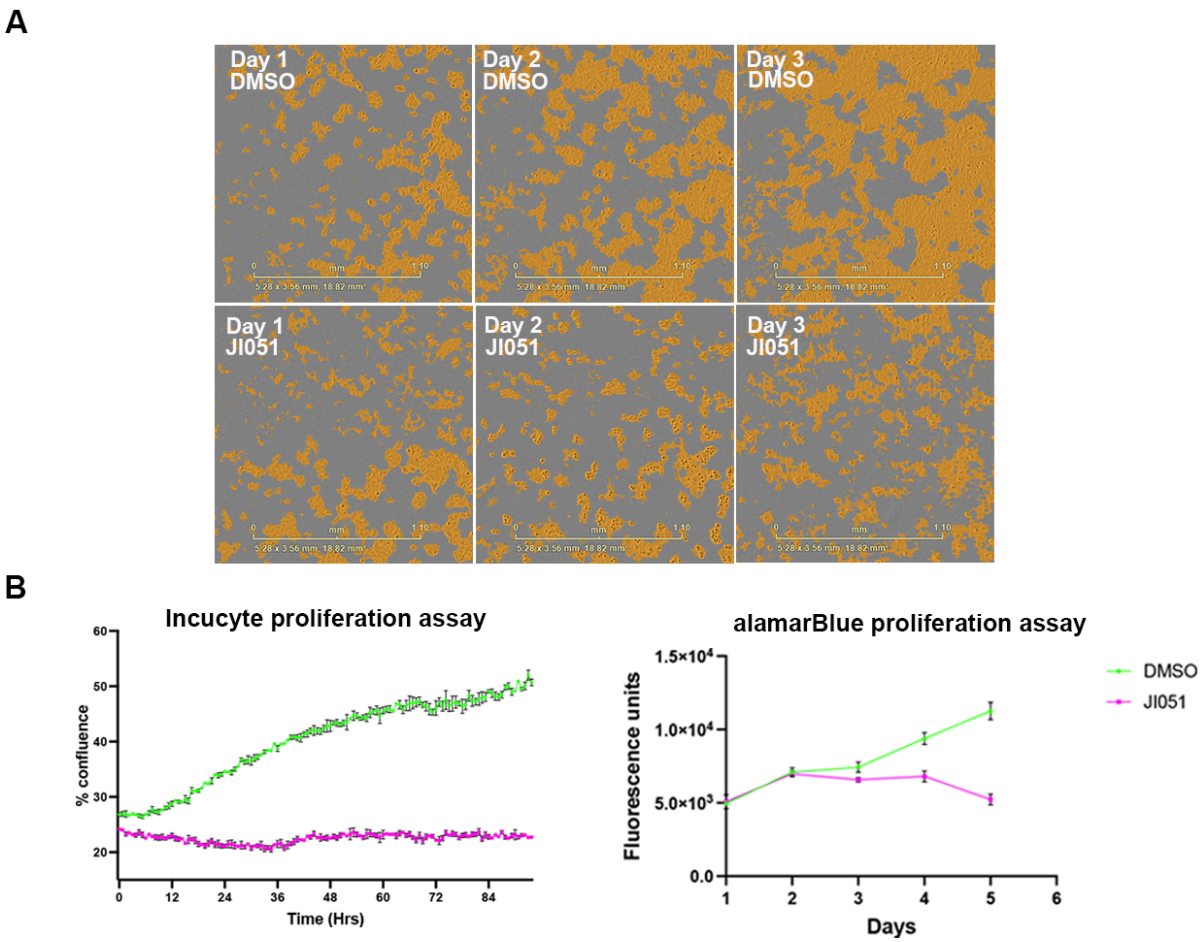

Fig 3.2.2 Reduction in proliferation in JI051 treated cells (A) Analysis of growth rates over 3 days in control and JI051-treated cells (2 µM). Cells were imaged every 45 mins at 4x magnification. Using incucyte software, a confluence mask was overlayed on cells from which a %confluence was calculated at each timepoint. **(B)** Right, line graph showing the increase in %confluence of cell populations in control (green) and JI051-treated (magenta) cells as calculated in **(A).** Graph is representative of 3 biological repeats performed in MCF7-HES1-mVENUS cells. Left, alamarBlue proliferation assay. Line-graph represents plate reader measurements of fluorescence due to reduction of resazurin. alamarBlue proliferation assay was performed once in MCF7 cells. Each point on line-graphs represents mean of triplicate measurement (incucyte analysis) and quintuplicate measurement (alamarBlue). Error bars indicate ±SEM.

3.2.3 Analysis of cell cycle progression and gene expression prior to mitotic arrest in iMEFs

The first published data on JI051 described a G2/M arrest of HEK293 cells after treatment with JI051 (Perron et al., 2018). However, no analysis of changes in cell cycle progression or gene expression prior to the arrest was conducted. Also, there

was no analysis of changes in mRNA expression of *HES1* to assess whether JI051 interferes with HES1 negative feedback. To investigate potential changes in gene expression that may underlie the G2/M arrest and to identify where in the cell cycle JI051 has an effect on *Hes1* expression, timecourse experiments were performed in iMEFs released into the cell cycle after serum starvation. G0/G1 arrest and release was performed as previously described (Materials and methods 7.1). iMEFs were re-plated in 10% FBS DMEM media containing DMSO (negative control) or 0.8 µM JI051.

To assess cell cycle progression in iMEFS, cells were treated with bromodeoxyuridine (BrdU) for one hour prior to indicated timepoints followed by fixation and staining with propidium iodide (Fig 3.2.3). Fluorescence-activated cell sorting (FACS) analysis of cells indicate that from 18 hours to 30 hours post-release from G0/G1 there was an increase in the proportion of G2/M cells in control and JI051 treated cells. For control cells the percentage of cells in G2/M increases 15 to 38 to 54 at 18, 24 and 30 hours post-release, respectively. This increase is similar in JI051 treated cells, where the percentage of G2/M cells increases from 18 to 34 to 59 percent at 18, 24 and 30 hours, respectively. At 48 hours post-release the majority of control cells were in G1 or S-phases, as expected for a cycling population of cells (52% G1/S versus 30% G2/M) In JI051 treated cells the majority of cells were still in G2/M (60% G2/M vs 15% G1/S), indicating that they were unable to progress beyond G2/M into a new cell cycle after release from serum starvation. This data confirms that JI051 has the same anti-proliferative effect in iMEFs. It also indicates that cell cycle progression is not inhibited prior to the G2/M arrest.

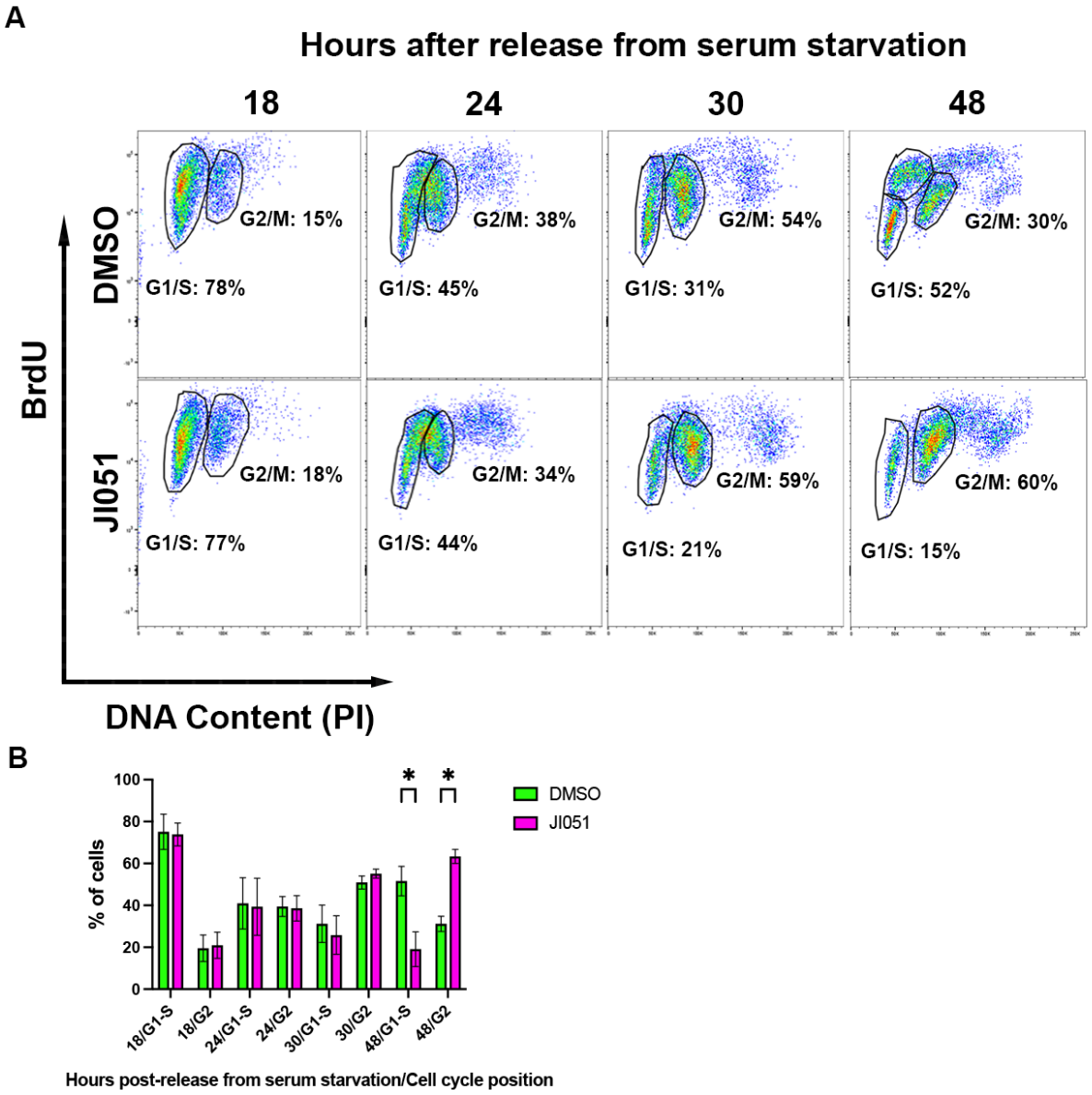

Fig. 3.2.3 FACS analysis of iMEF cell cycle progression after release from G0/G1 and JI051 treatment. Cell cycle distribution in iMEFs was assessed at 18, 24, 30 and 48 hours after G0/G1 release by BrdU staining and propidium iodide staining of DNA. iMEF cells were treated with 0.8 µM JI051. Significance was determined by 2-way ANOVA using Šidák's multiple comparisons. Error bars represent ±SEM from 3 biological repeats.

The expression of genes shown in figure 3.2.4 was assessed by qPCR at 6, 12, 18, 24 and 30 hours release from G0/G1 arrest. *Hes1* expression was not affected by treatment with JI051. In control samples, an approximately half-fold decline in *Hes1* expression was observed at 12 hours compared to 6 hours. At 18, 24 and 30 hours expression levels remained low with a reduction of approximately 85% observed compared to 6 hours. This *Hes1* expression pattern was also observed in cells treated

with JI051. *Hes1* expression levels were reduced by 50% at 12 hours and remained low at 18, 24 and 30 hours post-release (~85% decrease). There were no expression levels changes between control and JI051 treated cells at each timepoint. This indicates that *Hes1* transcription is not altered by JI051 treatment prior to the G2/M arrest. Moreover, it suggests that JI051 does not interfere with HES1 negative feedback

In line with progression through G2/M, there was an increase in expression of the mitotic regulators *Ccnb1*, *Cdk1* and *Plk1* at 18, 24 and 30 hours post release from G0/G1. *Ccnb1* expression increased 2.1, 8.5, 14.4 and 13.7 fold at 12, 18, 24 and 30 hours post-release in control cells. In JI051 treated cells a 1.5, 6.7, 13 and 13.2 fold increase in expression was observed at 12, 18, 24 and 30 hours post release, respectively. *Cdk1* expression increased 2.5, 9.5, 11 and 8.3 fold in control cells relative to 6 hours. In JI051 treated cells a 1.8, 8.3, 10 and 11 fold increase was observed at 12, 18, 24 and 30 hours post release, respectively. *Plk1* expression increased 2.5, 3.4 and 3 fold at 18, 24 and 30 hours post release in control cells. A similar increase was observed in JI051 treated cells with a 2.6, 3.3 and 2.9 fold increase observed at 18, 24 and 30 hours respectively.

Cyclin B1 and CDK1 protein expression was analysed by western blot at 16, 18, 22, 24 30 and 48 hours post release from serum starvation. Cyclin B1 protein levels were increased from 22 hours and comparable levels were observed between control and JI051 treated cells. CDK1 levels were present earlier in the timecourse at 16 in control cells. In JI051 treated cells these levels appeared slightly lower Comparable expression for CDK1 was observed at 22, 24, 30 and 48 hours for control and treated cells (fig. 3.2.5). There was no significant change to this pattern of expression for these genes in JI051 treated cells.

To investigate if DNA damage was a contributing factor to the G2/M arrest phenotype observed after JI051 treatment, the expression levels of several DNA damage response genes was analysed in the iMEF timecourse. These genes included *p53*, *Cdkn1a*, *Atm*, *Atr*, and *Fancc*. There was no difference in expression for these

genes between control and JI051 treated cells, suggesting that no DNA damage response was launched after JI051 treatment. Transcription for *p53* rose by approximately 1.5 fold at 12 and 18 hours post release from serum starvation in both control and JI051 cells. This *p53* expression is expected for normal progression through the cell cycle is accompanied by intrinsic DNA damage. Cell cycle arrest in response to DNA damage is mediated through the activity of the Cyclin-dependent kinase inhibitor, p21, which is transcriptionally activated by *p53* (Espinosa & Emerson, 2001). There was no increase in *Cdkn1a* transcription in JI051 treated cells to suggest increased *Cdkn1a* activity. There was no also no change in transcription for *Atm* and *Atr*, two kinases that regulate *p53* activity by phosphorylation at serine 15 of *p53* in response to DNA damage (Banin et al., 1998; Tibbetts et al., 1999). In both control and JI051 cells transcription for both of these genes was upregulated over the cell cycle. An approximately 3-fold increase was observed for *Atr* and *Atm* at 24 and 18 hours post release from serum starvation. Transcription levels were also assessed for the fancomi anemia protein (*Fancc*), which is involved in homologous repair of damaged DNA (Niedzwiedz et al., 2004). Transcription increased over the cell cycle and peaked at 24 hours post-release. There was no significant change in transcription between control and treated cells.

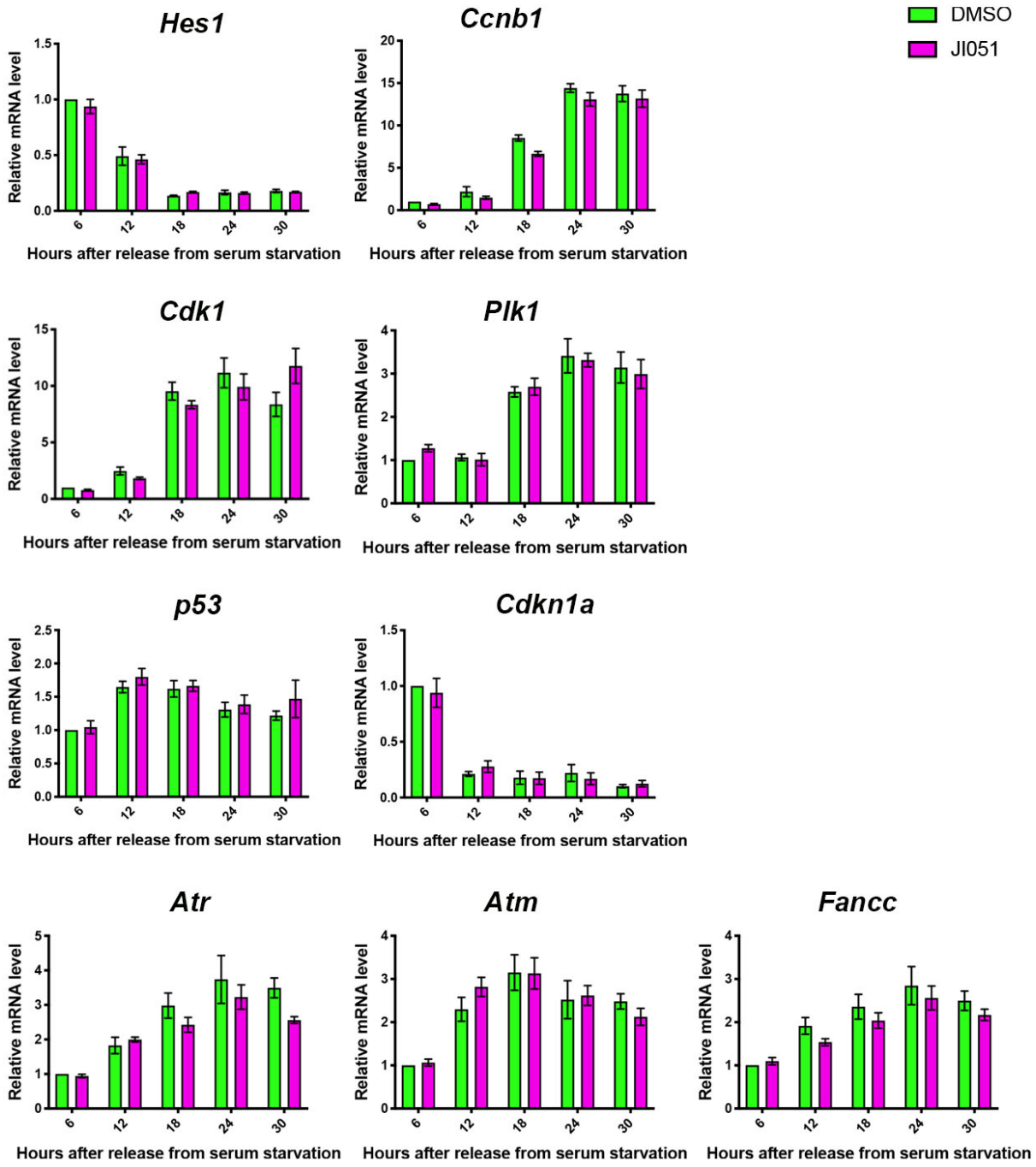

Fig 3.2.4. Analysis of gene expression in iMEFs released from serum starvation and treated with JI051. mRNA expression was analysed by qPCR for indicated genes after release from serum starvation at indicated timpoints. Ct values were normalised to *eEF2* at each timepoint and a fold change relative to 0 timepoint (serum starved, G0) was derived using the $2^{-\Delta\Delta Ct}$ method. iMEF cells were treated with 0.8 µM JI051. Significance was determined by 2-way ANOVA using Šidák's multiple comparisons. Error bars indicate ±SEM from 3 biological repeats.

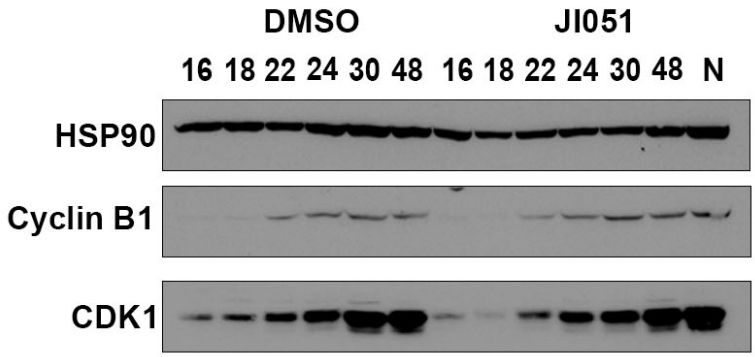

Fig. 3.2.5 Cyclin B1 and CDK1 protein expression after release from G0/G1 arrest in JI051 treated iMEF cells Western blot analysis of Cyclin B1 and CDK1 protein expression at indicated timepoints after release from serum starvation. iMEF cells were treated with 0.8 µM JI051

3.2.4 JI051 treated cells enter a prolonged mitosis

JI051 was reported to affect HES1 localisation, specifically Perron et al, 2018 observed loss of nuclear HES1 in HEK293 and increased cytoplasmic HES1 based on immunofluorescent staining. As this observation was based on fixed cells 24 hours after JI051 treatment, no information on the effect of JI051 treatment on cell cycle progression or on HES1 expression dynamics prior to arrest is known. In (Fig. 3.2.3), I showed that JI051-treated iMEFs showed similar cell cycle distributions after release from serum starvation prior to their arrest at G2/M. However, this analysis did not give a precise readout of the time spent in individual cell cycle phases and broadly depicts the arrest as occurring in G2/M. To investigate exactly where JI051-treated cells arrest and if HES1 expression dynamics are altered during the cell cycle, live-imaging of MCF7 HES1-mVENUS cells was performed. 1 µM or 2 µM of JI051 was added to cells in a glass-bottom dish immediately before the dish were transferred to a Nikon A1 inverted confocal microscope. MCF7 cells were imaged as previously described (2.2.6), with images captured every 20 minutes at 20x magnification. Expression of mCherry-PCNA in the same cell line allowed visualisation of progression through S-phase based on nuclear PCNA foci.

JI051 treated cells progressed through the cell cycle based on characteristic PCNA expression during S-phase. S-phase and G2 lengths were slightly shorter in JI051-

treated cells. Control cells had a mean S-phase of 7.8 hours, while JI051-treated cells had a mean S-phase duration of 7.3 hours. G2 duration in control cells was 4.3 hours, while in JI051-treated cells the mean duration was 3.8 hours (Fig. 3.2.7 B) JI051-treated cells were also able to enter mitosis, as indicated by cell rounding and diffusion of PCNA and HES1 signal throughout the cell, suggesting nuclear envelope breakdown (NEBD) had also taken place. The majority of control cells underwent cell rounding, cell division, and a return to an interphase morphology within 2 hours. JI051 treated cells were delayed in mitosis and remained in a rounded-up, mitotic state with the duration of the delay ranging from 6 to over 20 hours. After a sustained mitosis, JI051 treated cells returned to a 'flat' interphase cell morphology without under-going cytokinesis, indicative of mitotic slippage (Brito & Rieder, 2006). These cells were consistently multi-nucleated after exit from the mitotic state (Fig. 3.2.7 A). The multi-nucleated 'daughters' of JI051 treated cells did not appear to progress to S-phase or undergo any subsequent divisions as no characteristic S-phase PCNA was observed in the nuclei of these cells. However, timelapse imaging was only performed for up to 48 hours in these experiments, which prevented observation of further progression of the multi-nucleated cells.

It was not possible to observe a complete cell cycle from mitosis to mitosis prior to JI051-treated cells entering mitosis. Cells that entered mitosis early in the timelapse encountered a sustained mitosis and subsequent imaging of these cells captured their delayed mitosis and subsequent time spent in a multi-nucleated state. For this reason, no complete G1 was captured in JI051 cells before they entered mitosis. For equal comparison between control and JI051-treated cells analysis of cell cycle phase duration was confined to S-phase and G2. HES1 expression was based on traces obtained from the start of S-phase to G2/M. As described previously, measurements for mean HES1 intensity were obtained from regions of cell nuclei segmented by the spot object function in IMARIS software.

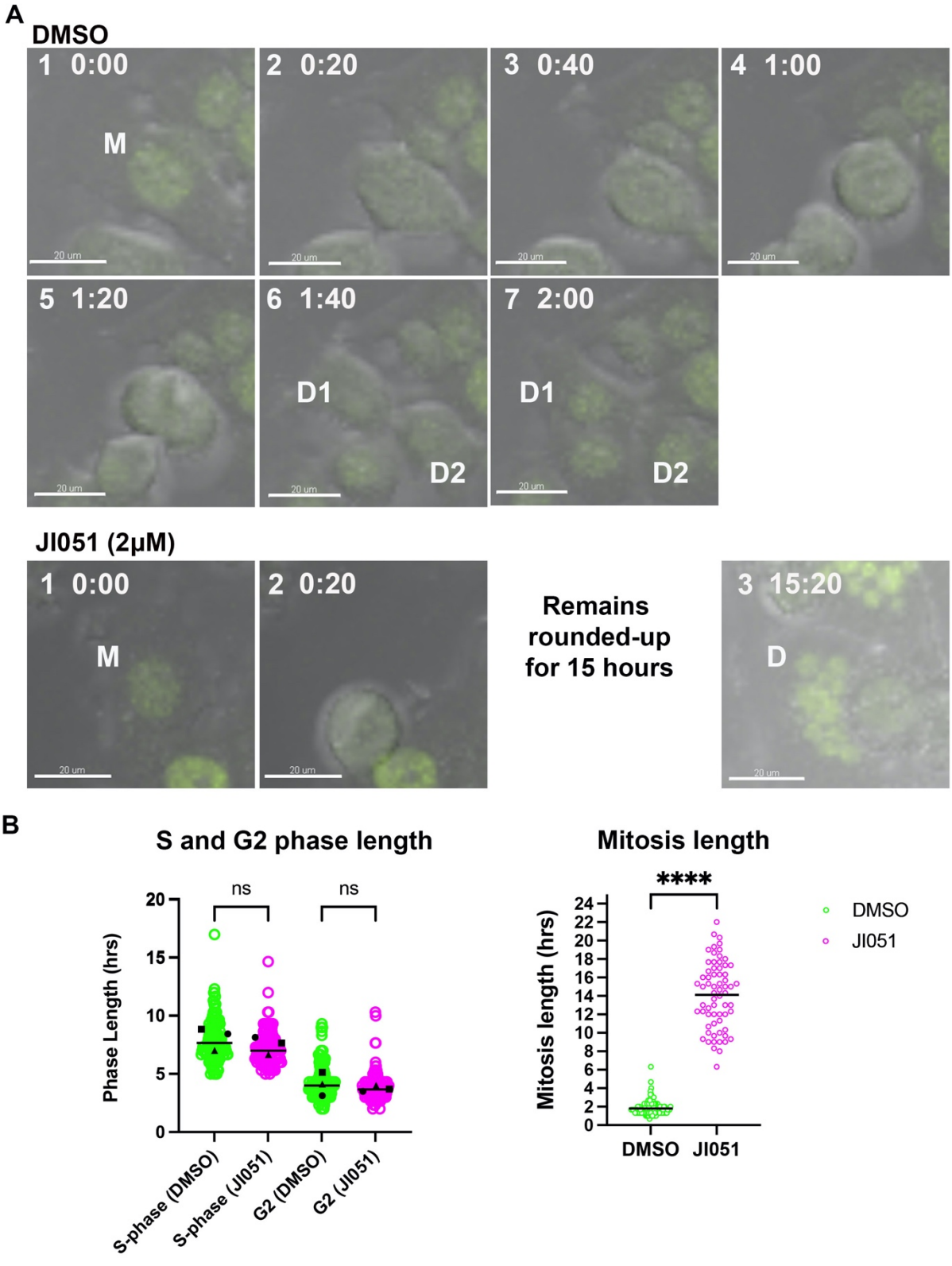

Fig 3.2.7 Cell cycle progression and mitosis entry in JI051 treated cells (A) Top panels (1-7) indicate progression of control (DMSO) mother (M) cell through mitosis. Each panel represents image captured at 20 minute interval. The M cell rounded up and underwent cytokinesis to produce 2 daughter cells (D1 and D2) panels (2-5). Lower panels (1-3), representative JI051-treated cell entered mitosis but remained

rounded up for 15 hours. The cell did not undergo cytokinesis and appeared multi-nucleated upon return to a flattened, interphase morphology. **(B)** Left, S and G2 phase duration (hrs) of control and JI051-treated cells (2 µM). Line represents overall mean from 3 biological repeats. Number of cells per group: S-phase DMSO = 125, G2 DMSO = 129, S-phase JI051 = 105, G2 JI051 = 124. Higher number of cells in G2 represents measurements from cells where the start of S-phase was unknown and therefore only G2 length was recorded. **(B)** Right, Duration (hrs) of mitosis (from start of rounding up until return to interphase morphology of daughter cells) in control and JI051-treated cells. Line represents median duration from 118 cells (DMSO) and 66 cells (JI051). Significance determined by Kruskal-Wallis 1-Way ANOVA using Dunn's multiple comparisons (S and G2 Length) and Mann Whitney unpaired t-test (mitosis length). Mean from each biological replicate is indicated by a black circle, square, and triangle symbol (Phase length). Breakdown of number of cells per group: **Circle**, DMSO n = 20, JI051 n = 24 (S-phase and G2). **Square**, DMSO n = 45 (43 S-phase), JI051 n = 44 (31 S-phase) **Triangle** DMSO n = 64 (62 S-phase), JI051 n = 56 (50 S-phase).

3.2.5 Investigating the effect of JI051 treatment on HES1 protein expression

As observed in the HES1 traces presented in Fig 2.2.10, HES1 nuclear expression is characterised by a dip that overlaps approximately with entry into S-phase and which is followed by an increase in expression as a cell exits S-phase and enters G2. I showed that this pattern of expression can be represented by an increase in mean HES1 intensity in G2 compared to mean HES1 intensity in S-phase in cell nuclei (Fig 2.2.10 B). I examined whether this S-G2 increase in mean HES1 intensity occurs in JI051-treated cells. For this experiment, data is presented for two concentrations of JI051, 1 and 2 µM. The experiment using 1 µM was performed once. Treatment using 2 µM was performed in 3 biological replicates. For control and JI051-treated cells an increase in mean HES1 intensity occurred from S-phase to G2. In the 1 µM experiments consisting of 37 control cells (both S-phase and G2 imaged) and 27 JI051-treated cells (22 where a complete S-phase was imaged), the increase in mean HES1 intensity between S-phase and G2 was significant in control and JI051-trated cells. When cells from the 2µM experiments were tested collectively, the mean increase in HES1 intensity was not significant. Moreover, mean HES1 intensity in control G2 cells was higher than JI051-treated G2 cells (Fig 3.2.8 A). For individual cells where a full S

-phase and G2 could be recorded (125 control cells) and (105 JI051-treated cells), I determined the percent of cells that exhibited an increase (S-G2 increase) and decrease (S-G2 decrease) in mean HES1 intensity between S-phase and G2. For control cells, 86% of cells analysed exhibited an S-G2 increase. In JI051-treated cells the percent of cells exhibiting an increase in HES1 intensity was decreased to 74% (Fig 3.2.8 B). I next determined whether cells treated with 2 µM JI051 entered mitosis with different levels of HES1, I measured total HES1 intensity (sum of intensity) in mitotic cells at the first timeframe when they displayed a rounded-up morphology. Total HES1 levels in mitotic cells were decreased in JI051 cells compared to S-phase cells (Fig 3.2.8 C).

To examine the effect of JI051 on HES1 expression kinetics at the single cell level, HES1 traces from individual cells were visualised in a heatmap format with normalised HES1 intensity values presented for each trace. (Fig 3.2.9). On each trace (read from top to bottom), the transition between G1 and S-phase (appearance of PCNA foci) is indicated by a blue dot and the transition from S-phase to G2 (return to smooth PCNA expression) is indicated by a black dot. In the few cases where no blue dot is shown, this means the trace began at the start of S-phase. All traces are aligned to a common end point, which is the last timeframe from which a nuclear HES1 measurement could be obtained before cells entered mitosis. As mentioned above, no full cell cycle could be recorded for JI051 treated cells due to the fact that no cell division occurred in these cells, indicating that JI051 is immediately effective at causing a mitotic arrest. In control cells the bi-phasic expression of HES1 is visualised by higher intensities at the start of each trace (occurring in G1) and at the end of each trace before cells enter mitosis. In the majority of cells, a period of down-regulation can be observed that overlaps with the transition between G1 and S-phase. This pattern of HES1 expression is reproducible in JI051 treated cells, with the exception that more cells display diminished HES1 expression in G2 before entering mitosis, as I previously indicate in Fig 3.2.8 B.

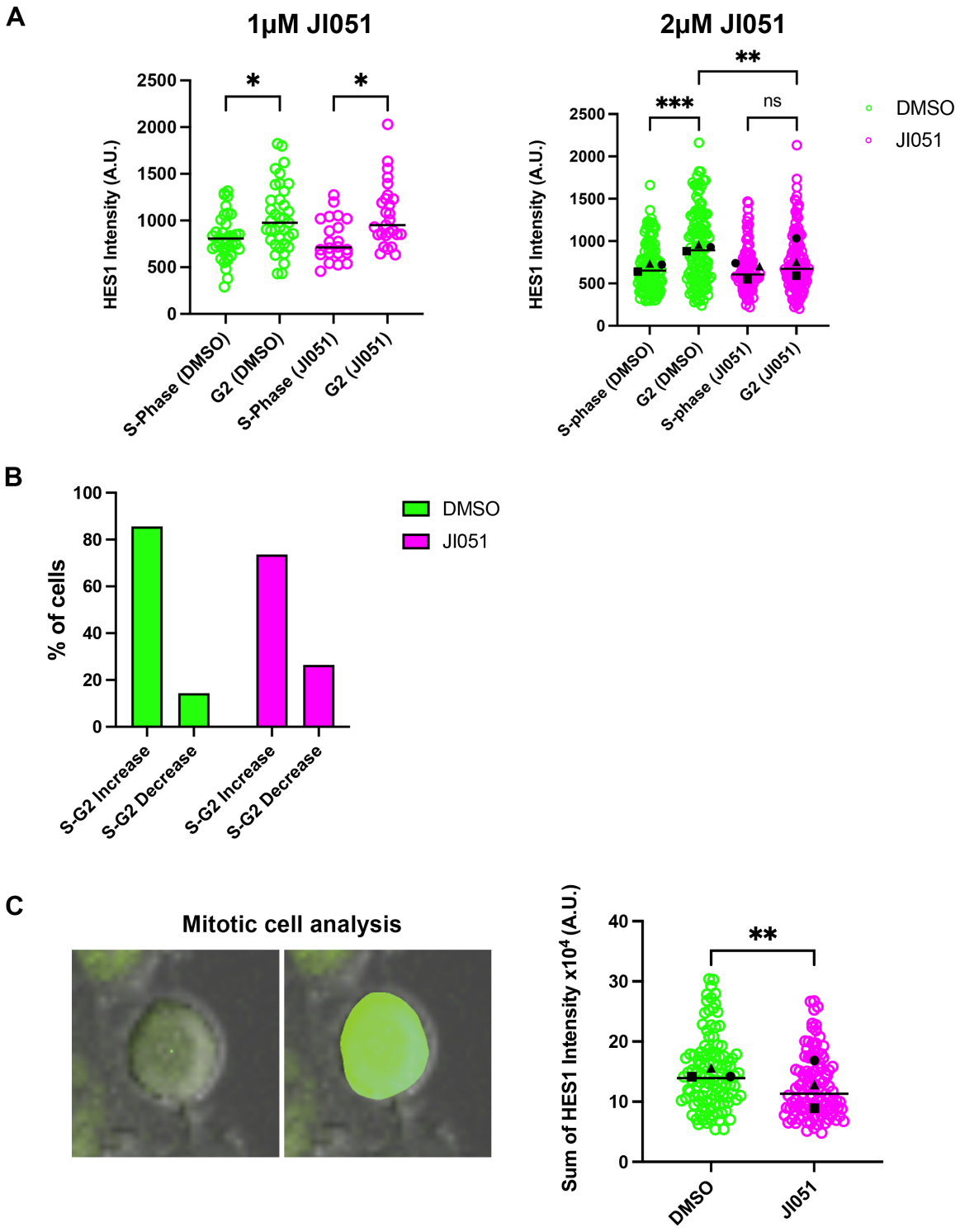

Fig. 3.2.8 Analysis of HES1 expression in JI051-treated cells

(A) Left, mean HES1 intensity per S-phase and G2 in control and JI051-treated cells (1 µM). Right, mean HES1 per S-phase and G2 in control and JI051-treated cells (2 µM) **(B)** Percent of cells from either control and JI051-treated cells (2 µM) that showed either an increase or decrease in mean HES1 levels in G2 compared to S-phase. **(C)** Right, measurement of total HES1 intensity in rounded-up, mitotic cell

using surface analysis function in IMARIS. Left, Comparison of total HES1 (sum of intensity) in control and JI051 treated cells. Mean from each biological replicate is indicated by a black circle, square, and triangle symbol. Number of cells in each group stated in Fig 3.2.7 legend. Significance determined by Kruskal-Wallis 1-Way ANOVA using Dunn's multiple comparisons (HES1 phase intensity comparison) and Mann Whitney unpaired t-test (Total HES1 intensity). Lines on data indicate median.

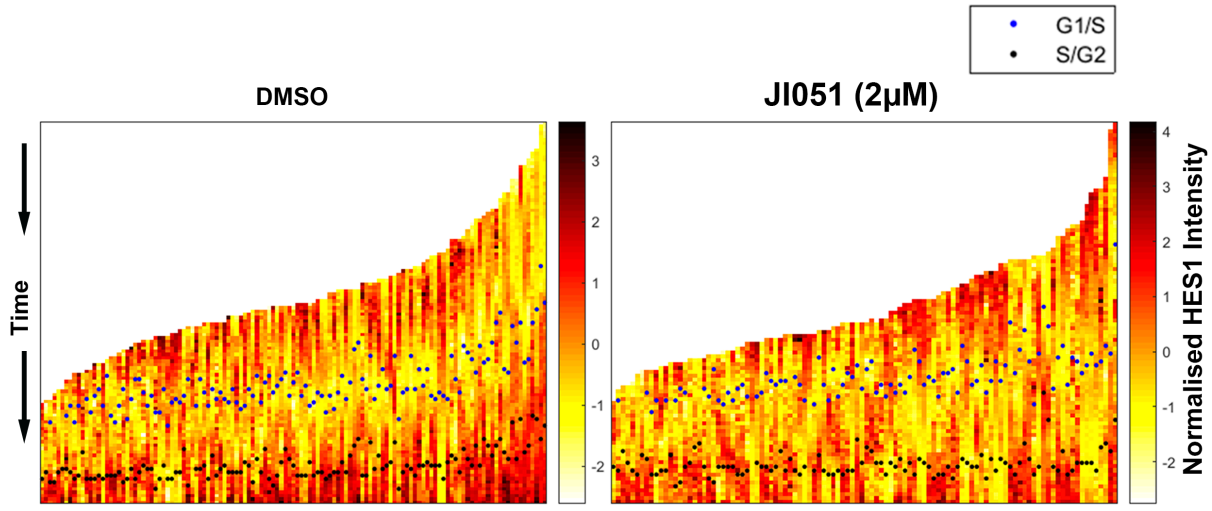

Fig 3.2.9 Analysis of HES1 dynamics in JI051-treated cells

Heatmap displaying normalised HES1 intensity traces in single cells. Each column represents a single cell. HES1 intensity values at each timepoint were normalised using Z-scores [(raw intensity – mean trace intensity)/standard deviation]. G1/S and S/G2 transitions are indicated on each trace by a blue and black dot respectively.

3.3 Discussion

By using methods of HES1 inhibition, I assessed the function of HES1 expression dynamics in cell cycle progression in iMEFs and MCF7 cells. The work presented in this chapter primarily sought to assess the activity of recently published HES1 inhibitor, JI051 (Perron et al., 2018).

3.3.1 Regulation of *Hes1* expression by Notch signaling over the cell cycle in iMEFs

In chapter 2 a transcriptional profile was generated for *Hes1* over the cell cycle in iMEFS. A peak in *Hes1* mRNA expression was observed at 1 hour post-release from serum starvation. *Notch1* was also upregulated at this 1 hour timepoint, suggesting that *Notch1* acts upstream of *Hes1* in this context. To investigate this relationship, iMEFs were treated with the NOTCH inhibitor DAPT during the G0/G1 transition (0 - 2 hours) and over the cell cycle (6 – 48 hours). From these experiments, a regulatory role for NOTCH signaling in activating *Hes1* can be described as reduced expression of *Hes1* was observed alongside reduced *Notch1* expression. However, in these experiments, cell cycle progression did not appear to be disrupted, suggesting that the reduced levels of *Notch1* and *Hes1* mRNA have a negligible impact on their protein expression or that Notch-HES1 signaling in this system is not essential for cell cycle progression.

HES1 has previously been reported to be essential for maintaining the reversibility of quiescence. Human fibroblasts maintained in serum deprived conditions for 10 days failed to re-enter the cell cycle when transduced with a dominant-negative HES1 construct that prevented binding of HES1 to its co-repressor TLE-1 (Sang et al., 2008). The importance of the *Hes1* transcriptional response after serum stimulation has been tested previously. In NIH/3T3 cells, *Hes1* transcription is upregulated after serum stimulation during treatment with hydrogen peroxide (Babaei Khalili et al., 2018). In this experiment, the duration of the *Hes1* mRNA response exceeded the initial 2 hour response in control cells as down-regulation was not observed until 3 hours in treated cells. HES1 protein expression was down-regulated in these cells despite the increase in *Hes1* transcription, suggesting that H_2O_2 treatment inhibited

translation. Subsequent cell cycle analysis 24 hours post release showed that H_2O_2 treated cells did not progress beyond G1 phase, indicating that the initial loss of HES1 protein impeded cell cycle progression (Babaei Khalili et al., 2018). Both these examples suggest initial expression of functional HES1 protein is essential for exit from G0/G1 and cell cycle progression. In the DAPT experiments presented here *Hes1* mRNA expression is not completely abolished. Although, the fold-change at the 1 hour peak was much lower than control (mean 8.6 compared to 48), this may produce a sufficient level of functional HES1 protein required to re-enter the cell cycle. As no protein expression analysis was performed for these experiments this cannot be fully concluded. However, as the 2 hour *Hes1* response was unchanged i.e. 1 hour peak and down-regulation at 2 hours, it suggests that the HES1 negative feedback network is operational (Hirata et al., 2002).

No functional evidence for Notch-HES1 regulating the G0/G1 transition and subsequent cell cycle progression can be derived from the DAPT iMEF experiments. However, they do provide insight into the temporal activity of the Notch-HES1 regulatory relationship within the cell cycle. *Notch1* was significantly down-regulated at 6 hours post-release from serum starvation in DAPT treated cells. For the rest of the timecourse *Notch1* mRNA levels were comparable between control and DAPT treated. This indicates that *Notch1* expression occurs early in the cell cycle, which agrees with the role of *Notch1* expression in regulating the G1/S transition (Joshi et al., 2009; Sarmento et al., 2005). The drop in *Notch1* expression from 12 hours and over the rest of the timecourse is consistent with previously observed cell cycle regulation of NOTCH signaling. In chick neural precursors *Notch1* mRNA stability is reduced during S-phase (Cisneros et al., 2008). NICD has also been found to be targeted for degradation by CDK2 and CDK1 in HeLa cells, leading to reduced levels in S-phase (Carrieri et al., 2019). If Notch signaling is attenuated in a cell cycle specific manner it would explain why there is no difference between *Notch1* expression between control and DAPT treated cells. However, *Hes1* was significantly down-regulated at 6, 12 and 24 hours (fig 3.2.1), indicating that early down-regulation of *Notch1* early in the cell cycle might have a more lasting impact on *Hes1* expression

at later stages of the cell cycle or that *Hes1* has Notch-independent inputs later in the cell cycle.

3.3.2 JI051 treated cells progress through the cell cycle but enter a delayed mitotic state

A primary aim of this chapter was to further characterise the function of the recently published HES1 inhibitor, JI051 on cell cycle and HES1 dynamics. JI051 is a small molecule that has been demonstrated to stabilise a HES1-PHB2 complex in HEK293 cells, leading to decreased nuclear levels of HES1. The stabilisation of HES1-PHB2 was demonstrated by co-immunoprecipitation and immunofluorescence suggested that HES1-PHB2 co-localisation increased in the cytoplasm (Perron et al., 2018). Furthermore, *HES1*-promoter luciferase assays in HEK293 cells demonstrated that JI051 treatment increased luciferase activity, indicating that HES1 negative feedback was impaired by JI051 (Perron et al., 2018).

MCF7 and iMEF cells treated with JI051 showed reduced proliferation and a mitotic arrest re-affirming the first descriptions of JI051 by Perron, et al. 2018. What was not investigated in this paper was whether there were changes in cell cycle progression and gene expression preceding the arrest. I investigated the response of *Hes1,* cell cycle and DNA damage genes to JI051 treatment in iMEF cells. I did not observe a change in *Hes1* transcription during the timecourse, indicating that negative feedback by HES1 was not impaired. Expression of dominant-negative HES1 constructs that do not bind DNA has previously been shown to lead to an increase in *Hes1* expression (Hirata et al., 2002). HES1 has been shown to regulate p53 and FANCC previously so its misexpression after JI051 treatment could alter the activity of these proteins and impair DNA damage pathways (Huang et al., 2004; Tremblay, 2009). No change in expression for *p53*, *Cdkn1A*, *Atm/Atr* and *Fancc* was observed, however, to properly assess whether DNA damage occurred, evaluation of downstream targets of DNA damage response genes should be performed to thoroughly assess any induction of DNA damage. For example, the phosphorylation status of p53 on s15 and phosphorylation of H2AX are better indicators of a DNA

damage response than transcription of DNA damage response genes (Awasthi et al., 2016; Podhorecka et al., 2010).

Transcription of *Ccnb1* and *Plk1* is cell cycle regulated and does not occur until late S-phase and G2 (Golsteyn et al., 1995; Minshull et al., 1990; Pines & Hunter, 1989). *Ccnb1* and *Plk1* transcription is activated by upstream regulators such as FOXM1, B-MYB and NF-Y (Laoukili et al., 2008; Chae et al., 2004; Sadasivam et al., 2012). These transcription factors are themselves activated by CDK2/Cyclin A2 during S-phase (Park et al., 2008; Ziebold et al., 1997). The increase in *Ccnb1* and *Plk1* transcription 18 hours post-serum stimulation in both control and JI051 treated cells indicates that both cell cycle progression and the molecular mechanisms involved in activating late cell cycle genes is not impeded by JI051 treatment. Of course, correct timing of gene expression does not automatically equate to the proper function/activity of the corresponding proteins. The live-imaging I performed in MCF7-HES1-mVENUS cells, demonstrates that JI051 treated cells can enter mitosis and that the G2/M arrest originally described by Perron *et al* occurs exclusively in mitosis, at least in MCF7 cells. This indicates that as well as displaying the correct temporal gene expression, CDK1 is functional to at least trigger entry into mitosis and disassembly of the nuclear envelope, as indicated by rounding up of cells and diffusion of nuclear PCNA/HES1 signal. Both of these morphological changes require CDK1 phosphorylation of targets such as the nuclear lamins and Ect2 (Matthews et al., 2012). Entry into mitosis can be achieved by CDK1/Cyclin A2 activity in the absence of B-type Cyclins (Gong et al., 2007; Hégarat et al., 2020; Soni et al., 2008). However, CDK1/Cyclin B1 activity is critical for completing mitosis. In RPE-1 cells depleted of Cyclin B1 and B2, CDK1 substrate phosphorylation is reduced with loss of correct localisation of proteins, such as AURORA B and TPX2 (Hégarat et al., 2020). The mitotic specific functions of CDK1/Cyclin B1 are associated with increased activity of CDK1 as measured by APC phosphorylation and FRET-based sensors (Gavet & Pines, 2010; Lindqvist et al., 2007). Lindqvist *et* al, 2007, demonstrated that cells arrested in mitosis with attenuated CDK1 activity have reduced APC phosphorylation and are delayed in progressing through anaphase. This delay was less than 2 hours, which is substantially shorter than the mitotic delays I recorded for JI051 treated cells.

However, diminished CDK1 activity cannot be ruled out in JI051 treated cells even after they have entered mitosis as an initial cause of the delay in mitosis. Furthermore, the live-imaging I performed does not inform on other early mitotic events, such as DNA condensation, kinetochore formation, and assembly of the spindle apparatus. These mitotic events, require CDK1 activity alongside mitotic kinases such as AURORA A and B, PLK1 And NEK2 (Kishi et al., 2009; Rellos et al., 2007). That a mitotic delay subsequently occurs after JI051 treated cells enter mitosis indicates that at least one of these processes is disrupted. Multinucleated cells, like those observed after the prolonged mitotic arrest can arise through mitotic slippage, when cells exit mitosis without undergoing cell division (Brito & Rieder, 2006). In future experiments live-imaging of chromatin dynamics using reporters for H2B would address uncertainties as to how far JI051 treated cells progress through mitosis.

3.3.3 The effect of JI051 treatment on HES1 expression

The increase in HES1 protein expression as MCF7 cells progress through S-phase and G2 has not been described before (Sabherwal et al., 2021). As JI051 was demonstrated to induce a G2/M arrest (Perron et al., 2018), It seemed a useful method to test the function of HES1 expression during this transition. I sought to analysis whether a change in HES1 dynamics through JI051 could be associated with the mitotic arrest. HES1 has not previously been linked to the control of mitotic events and its inhibition has not resulted in the robust mitotic arrest observed upon JI051 treatment. Knockdown of *HES1* in CUTLL1 cells, which are a T-ALL cell line expressing constitutively active *NOTCH1*, resulted in a slight increase in G2/M cells as assessed by flow cytometry, and an increase the pro-apototic factor *BBC3* associated with increased cell death (Schnell et al., 2015). *HES1* knockdown by shRNA glioblastoma CSCs obtained from patients reduced proliferation with an increase in the proportion of G1 cells (Cenciarelli et al., 2017). In MDA-MR-321 breast cancer cells *HES1* knockdown results in decreased proliferation and migration (Li et al. 2018). Similarly, shRNA knockdown of *HES1* in nasopharyngeal carcinoma cells reduced migration of these cells as assessed by Transwell migration and Boyden invasion assays (Wang et al., 2015).

In my analysis of HES1 expression, I observed an increase in the number of cells that showed diminished S-G2 expression of nuclear HES1 when treated with 2 μM JI051 (Fig 3.2.8 A). This resulted in cells entering mitosis with reduced levels of HES1 (Fig 3.2.8 C). However, regardless of any changes in nuclear HES1 expression all JI051-treated cells entered a prolonged mitosis. Nonetheless, The G2/M arrest observed here could be the result of the novel form of HES1 inhibition by JI051-stabilisation of a HES1-PHB2 complex. HES1 and PHB2 have not previously been identified as interacting proteins. If a HES1-PHB2 interaction occurs in a cell cycle dependent manner then JI051 may only be functional at times in the cell cycle when HES1 complexes with PHB2. This may not affect HES1 expression specifically, but it may inhibit HES1 function by preventing it from interacting with other proteins and limiting its ability to induce gene repression. Perron et al, validated JI051 using *HES1*-promoter luciferase assays that showed increased expression during JI051 treatment in HEK293 cells. However, I did not observe increased expression of *Hes1* in my iMEF timecourse, so cannot conclude that negative feedback is disrupted.

Previous methods of *HES1* inhibition using shRNA in asynchronous populations may have predominantly targeted G1 phase cells and led to cell cycle arrest early in the cell cycle (Cenciarelli et al., 2017). If HES1 is functional later in the cell cycle as well as in G1/S progression, knockdown of Hes1 in asynchronous cells may only inform on its G1 function. To my knowledge no HES1 knockdown has been performed in cells which have already progressed through S-phase. Inducible knockdown of *HES1* in cells which have already gone through S-phase, e.g. cells arrested by double thymidine block and subsequently, would be useful for probing HES1 function later in the cell cycle

3.3.4 Concluding remarks

Here I have demonstrated that JI051 does not significantly impair cell cycle progression prior to the mitotic arrest, suggesting that regulatory events specific to mitosis are impaired. Gene expression analysis in mitotis during JI051 treatment will

be explored in more detail in the following chapter as well as a potential regulatory role for HES1.

Chapter 4: Investigating gene expression during mitosis exit in JI051-treated MCF7 cells

4.1 Introduction

4.1.1 Opening remarks

The sustained mitotic arrest and subsequent mitotic slippage observed in MCF7 cells treated with JI051 indicates that the regulation of mitotic events is disrupted in these cells. In the following chapter, I will describe the regulation of mitosis in more detail to highlight aspects of mitotic control that could be compromised upon treatment by JI051.

4.1.2 Regulation of mitosis

A successful mitosis is dependent on a cell orchestrating structural changes associated with cell-rounding, DNA condensation, nuclear envelope breakdown breakdown and re-assembly at the end of mitosis (Batty & Gerlich, 2019; Ramkumar & Baum, 2016). Segregation of sister chromatids is initiated at the metaphase/anaphase transition. This transition is blocked until sister chromatids have aligned correctly at the metaphase plate. Each sister chromatid must also secure microtubule attachments from opposing cell poles via its kinetochore to ensure faithful segregation of chromosomes between daughter cells (Nicklas, 1997). The completion of these events is monitored by the spindle assembly checkpoint (SAC), which is enacted by the mitotic checkpoint complex (MCC) (Musacchio & Salmon, 2007). The MCC functions by inhibiting APC/C-mediated protein degradation of Cyclin B1 and SECURIN, and is comprised of the proteins MAD2, BUBR1, BUB3, and CDC20, which is also a co-activator of the APC/C (Sudakin et al., 2001; Hagting et al., 2002; King et al., 1995; Morgan 1999). Activation of the MCC stems from CDK1/Cyclin B1 phosphorylation of the kinase Mono-Polar Spindles 1 (MPS1) (Hayward et al., 2019; Morin et al., 2012). Phosphorylated MPS1 is recruited to unattached kinetochores where it phosphorylates the outer kinetochore protein KNL1, which serves as a dock for formation of the MCC (Yamagishi et al., 2012). The

APC/C is primed by phosphorylation by CDK1/Cyclin B1, which enables the recruitment of its CDC20 co-activator (Zhang et al., 2016; Fujimitsu et al., 2016). However, while the SAC is still active, the MCC operates by binding to APC/C and preventing substrate recognition of the APC/C bound CDC20. The ubiquitination activity of the APC/C is also inhibited by BUBR1-mediated interference of binding with UBCH10, a ubiquitin-conjugating enzyme that assists the APC/C in target ubiquitination (Alfieri et al., 2016; Summers et al., 2008).

Localisation of MPS1 to unattached kinetochores is also facilitated by AURORA B, which serves as the catalytic component of the chromosomal passenger complex (CPC) that includes INCENP, BOREALIN and SURVIVIN (Nijenhuis et al., 2013). AURORA B plays a role in inhibiting error-prone microtubule attachment to kinetochores, which would otherwise impede MPS1 function at kinetochores. This is achieved by AURORA B phosphorylation of outer kinetochore complexes KLN1, MIS12, and NDC80, which prevents microtubule attachment to the kinetochore (Welburn et al., 2010). The ability of AURORA B to promote microtubule dis-attachment is reduced when spatially separated from its kinetochore substrates. This separation occurs due to tension created when microtubules from opposite poles attach to kinetochores on sister chromatids (Liu et al., 2009). The activation of AURORA B and its localisation with other CPC components to the centromeres is mediated by CDK1, PLK1, and AURORA A (Tsukahara et al., 2010; Kunitoku et al., 2003). PLK1 has been found to phosphorylate SURVIVIN, which in turn mediates the activation of AURORA B (Chu et al., 2011). CDK1 and PLK1 promote CPC recruitment through phosphorylation of the mitotic kinase, HASPIN. Activated HASPIN then phosphorylates a threonine residue on HISTONE-H3, which serves as a binding site for CPC (Zhou et al., 2014). HASPIN and PLK1 further facilitate AURORA B function by phosphorylating AURORA B substrates that inhibit AURORA B autophosphorylation (Rosasco-Nitcher et al., 2008).

AURORA A and PLK1 also have distinct roles in establishing a functional mitotic spindle and promoting centrosome maturation and separation upon mitotic entry. AURORA A facilitates spindle microtubule nucleation when bound to co-factor TPX2

(Kufer et al., 2002). PLK1 phosphorylates pericentrin, which enables recruitment of AURORA A to centrosomes (Lee and Rhee 2011). At mitotic centrosomes AURORA A is activated through the scaffold protein CEP192, which triggers its autophosphorylation (Joukov et al., 2010). In turn AURORA A phosphorylates PLK1, which promotes docking of PLK1 on CEP192. Phosphorylation of CEP192 by PLK1 initiates the recruitment of periocentriolar material (PCM) components, such as γ-TuRC, NEDD1, CKAP5, and XMAP215, which are essential for microtubule nucleation and attachment of microtubules to centrosomes (Joukov et al., 2014; Wieczorek et al., 2015)

The SAC is silenced upon successful bi-orientation of sister chromatids and microtubule attachment to kinetochores (Foley & Kapoor, 2013). The completion of these events results in declining levels of CDK1/Cyclin B1 activity due to Cyclin B1 degradation by APC/C^{CDC20} and the dephosphorylation of CDK1 targets by a trio of phosphatases, PP1, PP2A-B55, and PP2A-B56 (Holder et al., 2019). In early mitosis both PP1 and PP2A-B55 are inhibited by CDK1 phosphorylation prior to SAC silencing. PP1 is directly phosphorylated by CDK1 while PP2A-B55 inhibition occurs indirectly through the kinase MASTL (Dohadwala et al., 1994; Mochida et al., 2010). CDK1 activation of MASTL during mitosis results in MASTL phosphorylation of the molecules ARRP19 and ENSA. These molecules bind PP2A-B55 and inhibit its phosphatase activity towards CDK1 targets during mitosis (Blake-Hodek et al., 2012; Gharbi-Ayachi et al., 2010; Mochida et al., 2010). Key de-phosphorylation events that promote the meta/anaphase transition are the removal of inhibitory phosphorylation on CDC20, which activates APC/C^{CDC20} thereby accelerating Cyclin B1 destruction (Labit et al., 2012). Dephosphorylation of MPS1 by PP2A-B55 and PP2A-B56 terminates SAC signaling at kinetochores (Espert et al., 2014; Hayward et al., 2019). Furthermore, dephosphorylation of PRC1, a binding partner of PLK1 in anaphase, and INCENP by PP2A-B55 promote the anaphase functions PLK1 and translocation of AURORA B from centromeric chromatin to the anaphase central spindle (Cundell et al., 2013; Gruneberg et al., 2004).

.

The aim of the following chapter is to examine the effect of JI051 treatment on mitotic gene expression. To achieve this, JI051 treatment will be instigated specifically in cells released from prometaphase arrest. Concurrently, I will expand on the M-G1 *HES1* expression results presented in (Fig. 2.2.3) to investigate how M-G1 *HES1* expression responds to JI051 treatment and whether this response can be functionally linked to the regulation of mitosis.

4.2 Results

4.2.1 Nocodazole released MCF7 cells do not exit mitosis in presence of JI051

The timecourse and live-imaging experiments presented in chapter 3 demonstrate that JI051 treated cells enter a prolonged mitosis that is followed by the appearance multi-nucleated cells. To investigate if JI051 treatment of mitotic cells without any prior exposure to the drug also inhibits mitotic progression, MCF7 cells were synchronized in prometaphase using nocodazole and mitotic cells were re-plated in nocodazole-free media to allow progression through mitosis and into G1 of the next cell cycle. Cells grown under normal conditions (DMEM 10%FBS) were treated with 200nM nocodazole for 15 hours. Rounded-up mitotic cells were collected by shake-off and re-plated in fresh media containing DMSO or 1μM JI051. The ability of cells to exit mitosis following treatment with JI051 was assessed by FACS analysis of DNA content 6 hours post-nocodazole washout. Figure 4.2.1 shows that there is an increase in the percentage of cells entering G1 in the control (50% G1 versus 25.3 G2/M). The majority (66.67 G2/M versus 6% G1) of JI051 treated cells remained in mitosis 6 hours after collection, in line with live-imaging observations. This data indicates that JI051 is effective at causing a mitotic arrest without cells being exposed to the drug before entering mitosis.

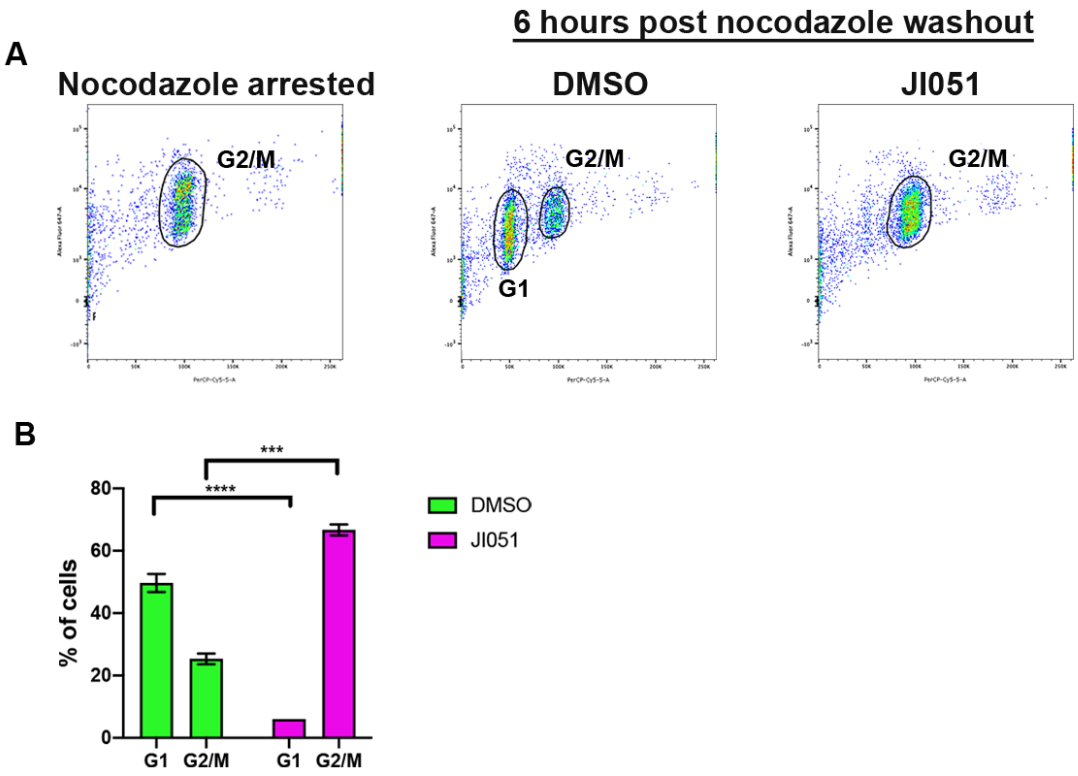

Fig. 4.2.1 FACS analysis of G1 entry in nocodazole released MCF7 cells. (A) Representative FACS analysis of JI051-treated MCF7 cells released from nocodazole arrest. Cell cycle entry was assessed by BrdU and propidium iodide staining of DNA **(B)** Quantification of FACS data from 3 biological replicates. Significance was determined by 2-way ANOVA using Šidák's multiple comparisons. Error bars represent ±SEM from 3 biological repeats

To investigate gene expression changes that are associated with the JI051-induced mitotic arrest, RNA and protein levels from control or JI051 treated cells were analysed at different timepoints following re-plating of MCF7 mitotic cells in nocodazole free media. Before mitotic shake-off and re-plating into JI051 media, MCF7 cells were also treated with 1 µM JI051 for one hour (JI051 0 timepoint). An additional experiment is presented, which was performed in the MCF7-HES1-mVENUS cell line to validate that results are similar between parental MCF7 cells and the HES1-mVEUS reporter cell line. No pretreatment of nocodazole arrested cells was performed in this experiment (Fig 4.2.2 B II). JI051 treated cells showed sustained expression of mitotic proteins after nocodazole washout and during JI051 treatment compared to DMSO. Phosphorylation of serine 10 in Histone 3 was absent 2 hours post-nocodazole washout in control cells. In JI051 treated cells

phosphorylation was observed up to the 4 hour timepoint (Fig. 4.2.2 B 1) Histone H3 (Ser10) phosphorylation occurs alongside chromosome condensation during early mitosis (Hendzel et al., 1997). The persistence of HISTONE H3 (Ser10) phosphorylation indicates that JI051 cells are arrested before anaphase when the Ser10 phosphorylation is reversed by PP1/Repoman (Qian et al., 2011). Conversely, the persistence of ser10 phosphorylation could represent disruptions to PP1 function or other processes involved in DNA decondensation in anaphase. In MCF7 and MCF7-HES1-mVENUS cells Cyclin B1 levels declined from 2 hours after nocodazole washout, indicative of Cyclin B1 degradation after cells undergo the meta/anaphase transition. Cyclin B1 protein expression was still present in JI051-treated cells in MCF7 (up to 2 hours) and MCF7-HES1-mVENUS cells (Up to 6 hours). As indicated by HSP90 expression, 4 hour JI051 sample had low protein concentration due to technical error. PLK1 expression was still present at 4 hours in control cells, although at lower levels than nocodazole arrested cells. As PLK1 is degraded in upon mitotic exit by APC/C^{CDH1}, this residual expression indicates that not every cell had exited mitosis completely four hours post-nocodazole washout. MASTL protein expression is present in control cells at 2 and 4 hours post nocodazole washout. At 0 hours, the slightly higher and weaker band for MASTL indicates the phosphorylated form of MASTL which is present during active CDK1/Cyclin B1 signaling in early mitosis (Blake-Hodek et al., 2012). This band is absent after 2 hours in control cells while in JI051 treated cells it persists (Fig. 4.2.2 B I, II).

To assess the response of gene expression during the JI051-induced mitotic delay, *HES1*, *CCNB1*, *PLK1*, *MASTL* and *CDC20* expression was assessed every half hour after nocodazole washout by qPCR (Fig 4.2.2 A). These genes were chosen based on their roles in regulating aspects of mitosis and whose dysregulation is associated with cell division defects (de Cárcer et al., 2018; Mondal et al., 2007; Rogers et al., 2018). A 4 hour 'pulse' of *HES1* expression was observed after release from nocodazole arrest. In control cells, *HES1* levels increased from 0.5 hours post nocodazole washout and peaked at 2 hours with a 2.9 fold increase relative to the 0 hour timepoint (nocodazole arrest). *HES1* levels declined from the 2 hour 'peak' to 4 hours where a 1.28 fold increase relative to 0 hours was measured. *HES1* levels were significantly

increased at the 2 hour timepoint compared to JI051 treated cells. Furthermore, there was a shift in the 'peak' of the *HES1* response in JI051-treated cells from 2 hours to 1 hour, with a 2.6 fold increase compared to 0 hours control measured. In control cells, *HES1* levels show a continuous decline after 2 hours until the last timepoint at 4 hours where levels are increased 1.28 fold relative to 0 hour control. This decline isn't as pronounced in JI051 treated cells. Indeed, a 2.3 fold decrease from 'peak' control *HES1* levels at 2 hours to 4 hours was statistically more significant than the 1.5 fold change decrease from 'peak' JI051 *HES1* levels at 1 hour to 4 hours in JI051 treated cells. This data indicates that *HES1* down-regulation is impaired in JI051 treated cells and that a lack of transcriptional repression may contribute to the mitotic arrest.

In control cells, *CCNB1* expression was reduced during the timecourse. At 2 hours *CCNB1* mean levels were reduced by 24%, at 4 hours this reduction increased to a 45% drop in expression levels from 0 hours. *CCNB1* exhibits sustained transcription in JI051 treated cells compared to control. At 4 hours post nocodazole washout a reduction of 26% was measured in JI051 treated cells compared to 45% in control cells. In control cells *PLK1* levels declined over the timecourse post nocodazole washout. At 4 hours mean *PLK1* levels were reduced by 35% compared to 0 hours. In JI051 treated cells, *PLK1* expression also declined over the 4 hour timecourse. Mean levels were elevated at 4 hours compared to control with a smaller 15% reduction in expression from 0 hours measured. *MASTL* levels declined over the 4 hour timecourse in control cells. At 4 hours post nocodazole washout levels were reduced by 55% compared to the 0 hour timepoint. *MASTL* expression was elevated in JI051 treated cells at 4 hours compared to control cells with a smaller 40% reduction measured. Similarly, *CDC20* levels declined over the 4 hour timecourse. In control cells, *CDC20* expression was reduced by 45% at 4 hours post nocodazole washout. In JI015 cells expression was elevated with a smaller 27% reduction measured.

Based on these results, failure to exit mitosis in the presence of JI051 is also associated with changes in transcription from *HES1* and *CCNB1*, that may mechanistically stem from impaired HES1 repression. Sustained *CCNB1* expression in

this scenario may subsequently maintain the mitotic arrest if it causes sustained Cyclin B1 expression that keeps CDK1 activity high.

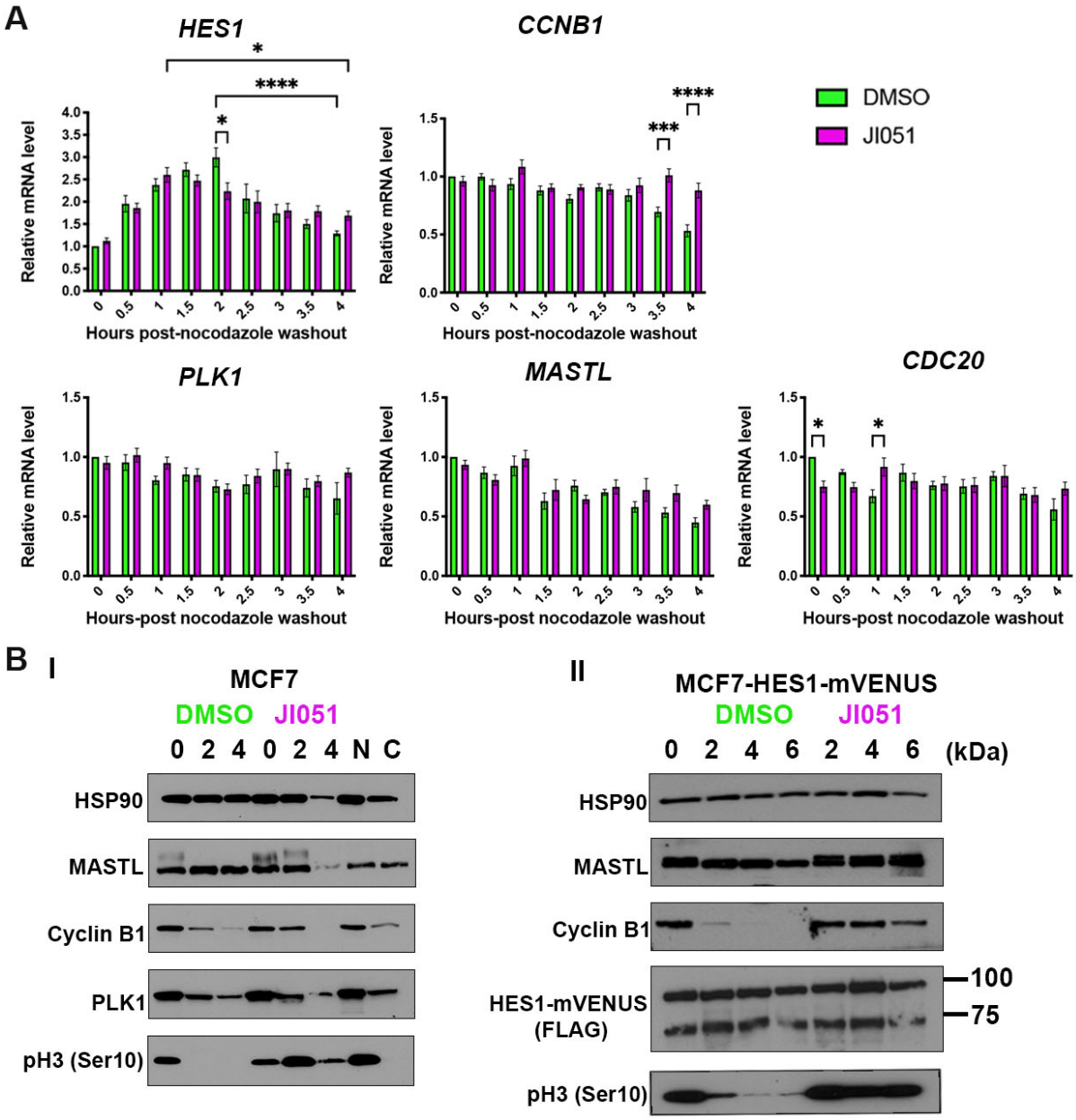

Fig. 4.2.2 Gene expression analysis in MCF7 cells after nocodazole release. (A) Gene expression was measured every half hour for 4 hours after nocodazole washout for genes indicated by qPCR. Ct values were normalised to *18S rRNA* in each condition and a fold change relative to the 0 timepoint in DMSO cells was derived using the $2^{-\Delta\Delta Ct}$ method. Significance was determined by 2-way ANOVA using Tukey's multiple comparisons. Error bars represent ± SEM from 3 biological replicates **(B)** Left, western blot analysis of indicated protein expression in nocodazole-arrested MCF7 cells (0) and cells 2 and 4 hours post-nocodazole release in MCF7 cells. 'N' and 'C' indicate protein expression in nocodazole-arrested (independent arrest) and cycling

cell populations. Right, western blot analysis of indicated protein expression in nocodazole-arrested MCF7-HES1-mVENUS cells 2, 4, and 6 hours after nocodazole washout. **(B I)** is representative of 3 biological replicates. **(B II)** was performed once. HSP90 was used as a loading control.

4.2.2 CDK1 activity persists in JI051 mitotic cells

CDK1/Cyclin B1 activity is a feature of cells in early mitosis, while de-phosphorylation of CDK1 targets and degradation of Cyclin B1 by APC/C^{CDC20} initiates exit from mitosis (Yang & Ferrell, 2013). The experiments described in (4.2.1) demonstrate that JI051 treated cells arrest in mitosis. The ser10 phosphorylation status of HISTONE H3 and elevated levels of Cyclin B1 and PLK1 suggests that this arrest occurs prior to anaphase. To test if this is the case, I aimed to evaluate the dependence of the JI051 arrest on CDK1 signaling. I assessed the ability of JI051 treated cells to maintain a mitotic arrest in the absence CDK1 activity. Nocodazole released cells were treated with JI051 in the presence of a CDK1 inhibitor, R0-3306, an ATP-competitive inhibitor of CDK1 activity that has previously been shown to force nocodazole arrested cells out of mitosis through loss of CDK1 kinase activity (Vassilev et al., 2006). Nocodazole arrest and release experiments were performed as described in 4.2.2 using the MCF7 HES1-mVenus cell line. Mitotic cells were collected by shake-off after nocodazole treatment and re-plated into three different conditions, DMSO, JI051, and JI051 + RO-3306. Protein and RNA samples were collected for each of the three conditions 4 hours post-nocodazole washout. The level of phosphorylated CDK substrates was evaluated using an antibody that recognizes substrates phosphorylated at threonine residues (p-CDK substrates pTPXK/R). Levels of phosphorylated CDK (pCDK) substrates were reduced in control DMSO cells and cells treated with JI051 and RO-3306 (Fig. 4.2.3 A I, II). In these two conditions there was also a loss of serine 10 phosphorylation on HISTONE H3 (Fig. 4.2.3 B I), indicating that these cells had exited mitosis. JI051 treated cells showed comparable levels of phosphorylated CDK substrates to nocodazole arrested cells, indicating that JI051 arrests cells in mitosis when CDK1 activity is still high. Ser10 phosphorylation of HISTONE H3 was still present and protein expression of Cyclin B1 and PLK1 was higher in JI051 treated cells compared to DMSO control cells, although this was not significant, and levels

were reduced compared to prometaphase cells (Fig. 4.2.3 B I, II). Cyclin B1 and PLK1 protein expression was still present 4 hours post nocodazole washout in JI051 + RO-3306 treated cells. R0-3306 has been shown to promote mitotic exit in the presence of the proteasome inhibitor MG132, indicating that APC-mediated degradation of Cyclin B1 or PLK1 isn't necessary when cells are forced out of mitosis due to de-phosphorylation of CDK targets (Vassilev et al., 2006). This data demonstrates that the JI051 arrest occurs with levels of CDK activity similar to that of nocodazole-arrested cells, indicating it occurs in the presence of SAC signaling. This indicates that the arrest occurs prior to the metaphase/anaphase transition.

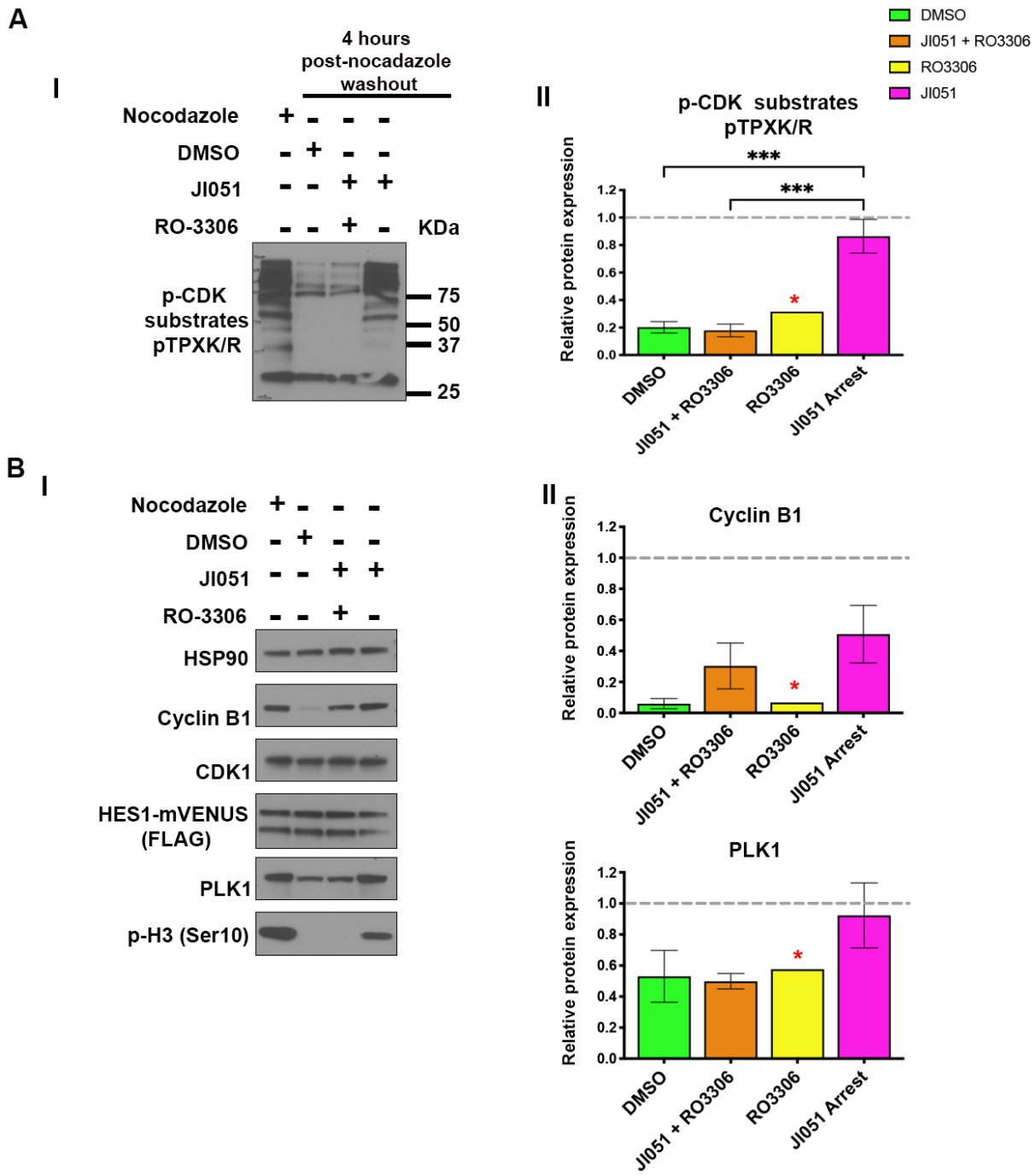

Fig. 4.2.3 CDK substrate phosphorylation and protein expression in nocodazole released cells (overleaf) (A) 1, Representative western blot for pCDK threonine substrates in each condition. 2, Signal quantification of pCDK substrates in conditions indicated 4 hours after nococdazole-washout. **(B)** I, Representative western blot for proteins indicated in each condition. II, Protein quantification of Cyclin B1 and PLK1. For signal quantification, the relative level per condition was quantified by densiometric analysis of band intensity normalised to HSP90 and expressed as a ratio relative to nocodazole arrested cells (dashed, gray line). Error bars represent ± SEM from 3 biological replicates. Significance determined by 1-way ANOVA with Tukey's

multiple comparisons. Only significant differences are indicated. Red asterick above 'R03306' in **A 2** and **B 2** indicates measurement from n=1.

HES1 transcription was elevated 4 hours after release from nocodazole arrest in control and JI051 treated cells. In control cells a mean 1.62 fold increase was measured, while in JI051 treated cells a mean 1.63 fold increase was measured. Cells co-treated with JI051 and R0-3306 showed a 26% reduction in transcription from nocodazole arrested cells (Fig. 4.2.4). The 1.62 fold increase in *HES1* expression in control cells was slightly higher than the 1.28 fold increase that was observe in 4.2.2, where *HES1* expression was lower than JI051 levels at 4 hours post nocodazole washout. The expression data for JI051 and RO3306 treated cells indicates that the upregulation observed in DMSO and JI051 conditions isn't solely the result of a serum effect. DMSO, JI051, JI051 + RO-3306 treated cells were all re-plated in fresh media. The differences observed may be indicative of cell fate. DMSO and co-treated cells are no longer in mitosis at 4 hours but have different levels of *HES1*. This may be an indication of how *HES1* is transcribed in a more 'normal' early G1 when cells have progressed through mitosis compared to JI051 + RO-3306 cells that are forced out of mitosis and do not undergo cytokinesis which was observed in (Vassilev et al., 2006). JI051 cells are still in mitosis 4 hours after nocodazole release as indicated by sustained pH3 and HES1 levels are significantly higher than nocodazole arrested cells. This supports the idea that in JI051 mitotic cells transcriptional repression is impaired.

As observed in previous timecourse experiments (Fig 4.2.2), *CCNB1* transcription was reduced in controls cells with an 84% reduction observed compared to nocodazole arrested cells. In JI051 treated cells *CCNB1* transcription was elevated compared to cells which had exited mitosis with a smaller reduction 41% reduction measured compared to prometaphase arrested cells (Fig 4.2.4). *CCNB1* and *PLK1* transcription was reduced by over 80% in cells treated with JI051 and RO-3306. This likely reflects the cessation of late cell cycle transcriptional programme when cells are forced out of mitosis through dephosphorylation of CDK targets. The levels of *FOXM1* and *B-*

MYB transcription were also assessed. Both of these proteins are involved in the up-regulation of *CCNB1* expression. In control cells *FOXM1* expression was reduced by 58% 4 hours after nocodazole washout. In JI051 treated cells, *FOXM1* transcription was slightly higher than control cells with a smaller reduction of 48% measured. In JI051 and RO-3306 treated cells, *FOXM1* expression was reduced by 63%. *B-MYB* expression increased 1.37 fold in control cells and 1.27 in JI051 treated cells. In cells treated with JI051 and RO-3306, *B-MYB* transcription was reduced by 14% compared to nocodazole arrested cells. Comparable transcription levels for *FOXM1* and *B-MYB* in control and JI051 treated cells indicates that the sustained *CCNB1* expression is not associated with a change in expression of upstream transcriptional activators.

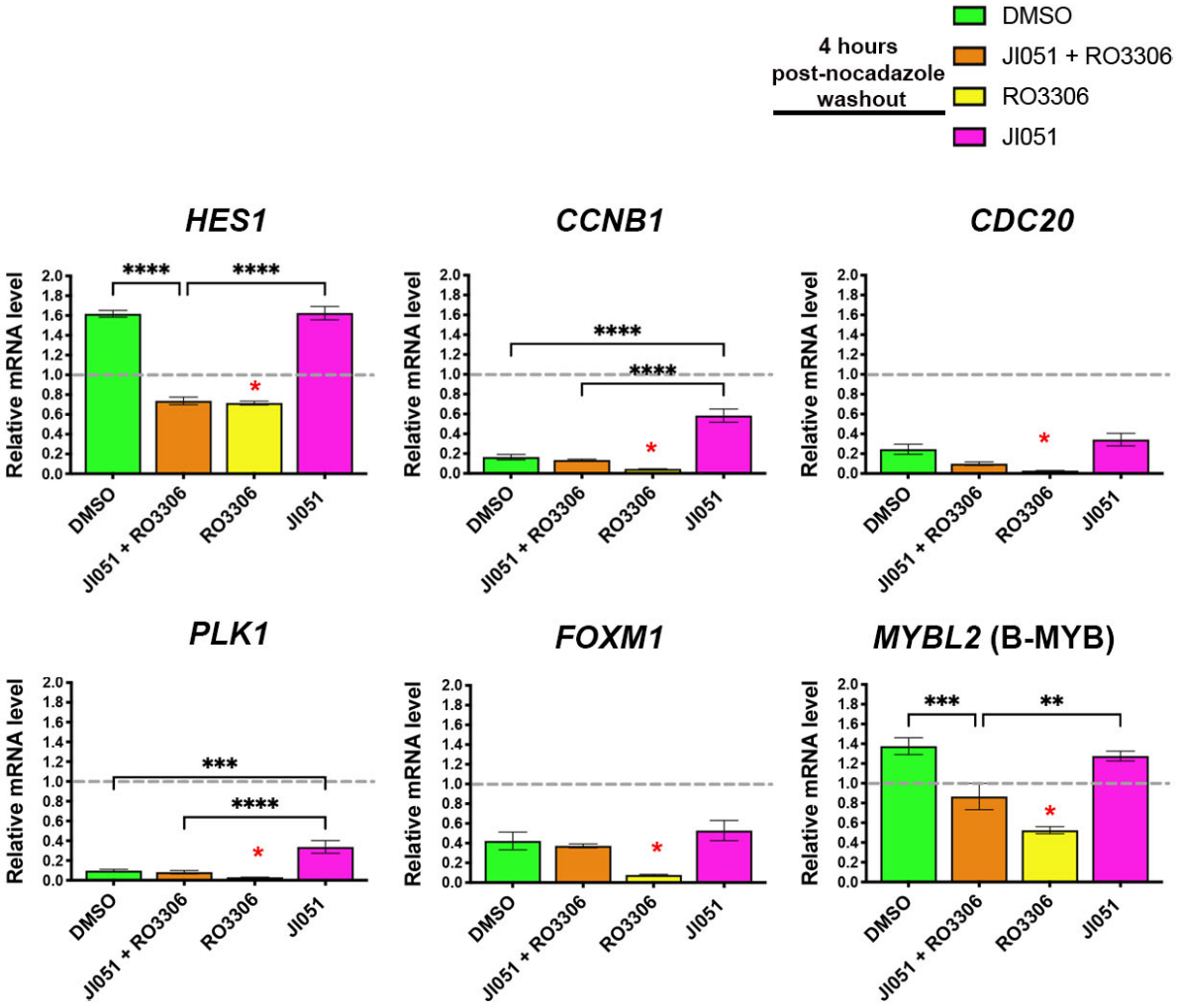

Fig. 4.2.4 Gene expression in MCF7 cells treated with JI051 and CDK1 inhibitor RO3306 The relative expression of the genes indicated was assessed by qPCR 4 hours

post-nocodazole washout in conditions indicated. Ct values were normalised to *18S rRNA* in each condition and a fold change relative to nocodazole arrested (dashed, gray line) was derived using the $2^{-\Delta\Delta Ct}$ method. Error bars represent ± SEM from 3 biological replicates. Significance was determined by 1-way ANOVA using Tukey's multiple comparisons. Red asterick above 'R03306' indicates measurement from n=1.

4.3 Discussion

4.3.1 Sustained CDK1 activity as a mechanism preventing mitotic exit in JI051-treated cells

A combination of live-imaging and gene expression analysis clearly shows that JI051 induces a prolonged mitotic arrest. This arrest occurs when cells are exposed to JI051 prior to entering mitosis and when mitotic cells are released from nocodazole arrest and treated with JI051. The latter observation suggests that JI051 acts specifically on regulatory events required for proper exit from mitosis. The evidence presented here indicates that persistent CDK1 activity is a potential mechanism behind the prolonged mitotic arrest. Furthermore, I showed by qPCR that *CCNB1* and *PLK1* expression is not down-regulated in JI051 treated cells compared to control cells. This also indicates that the transcriptional programme involved in G2/M cell cycle gene expression, which up-regulates genes such as *CCNB1*, *PLK1* and *FOXM1* is still active (Grant et al., 2013). Sustained expression of *CCNB1* could therefore act as a source of keeping CDK1 active. As detailed in the introduction (4.1) exit from mitosis is dependent on de-phosphorylation of CDK1/Cyclin B1 targets and silencing of the SAC after sister chromatids are successfully oriented on the metaphase plate and properly attached the mitotic spindle. Degradation of Cyclin B1 and SECURIN by APC/C^{CDC20} releases SEPARASE, which subsequently cleaves centromeric cohesion allowing chromosome segregation and entry into anaphase (Gorr et al., 2005; Hauf et al., 2001; Stemmann et al., 2001). Additionally, degradation of Cyclin B1 protein expression will lead to a decrease in CDK1 activity. CDK1 phosphorylation targets, crucial to maintaining an active SAC, such as MPS1, will no longer function to activate the MCC and cells will progress through to anaphase (Hayward et al., 2019; Morin et al., 2012).

Sustained CDK1 activity in JI051 cells could induce a prolonged mitosis by promoting MCC formation, which would prevent full activation of the APC/C (Alfieri et al., 2016). It would also reduce dephosphorylation events required for mitotic exit as both PP1 and PP2A-B55 are inhibited directly and indirectly by CDK1 activity. Furthermore, CDK1 negatively regulates the translocation of the CPC from centromeres to the

spindle midzone by preventing CPC interaction with the kinesin MKLP2 (Hümmer & Mayer, 2009). Preventing CPC translocation would maintain AURORA B signaling at kinetochores and thus prevent the formation of stable kinetochore-microtubule attachments.

CCNB1 has been shown to be transcriptionally active in mitotic cells and its expression has been found to be necessary for a sustained SAC in early mitosis (Sciortino et al., 2001; Mena et al., 2010). This was shown in HEK293 cells arrested in prometaphase with nocodazole that underwent mitotic slippage when treated with either cycloheximide or actinomycin D, which inhibit protein synthesis and transcription, respectively. Cyclin B1 protein and mRNA levels were down-regulated in cells that had undergone slippage following treatment with the above inhibitors. Exogenous expression of Cyclin B1 alongside inhibition of transcription decreased the levels of mitotic slippage, indicating that transcription of *CCNB1* is required to maintain the SAC. This is a contentious conclusion as mitosis has generally been thought of as a transcriptionally silent phase of the cell cycle (Liang et al., 2015; Parsons & Spencer, 1997). However, a recent study has challenged this belief by demonstrating active transcription during mitosis, adding support to the notion that transcription could play a role in mitotic signaling prior to satisfaction of the SAC (Palozola et al., 2017). Despite these reports, the conclusions of Sciortino et al and Mena et al. have been questioned based on experiments that examined the effect of actinomycin treatment on nocodazole arrested cells (Novais-Cruz et al., 2018). In line with Sciortino et al and Mena et al, nocodazole arrested cells HeLa cells undergo mitotic slippage when treated with actinomycin D. However, instead of inhibiting transcription, actinomycin D and other DNA intercalating agents, were found to interfere with localisation of the CPC, thereby preventing AURORA B signaling at centromeres and preventing SAC function. Furthermore, In the same study, live-imaging experiments demonstrated that mitotic slippage could be prevented when actinomycin D treated cells were co-treated with the proteasomal inhibitor MG132. Further live-imaging of HeLa cells expressing an endogenous Cyclin B1 VENUS tag demonstrated that when cells entered a prolonged mitosis after treatment with nocodazole, levels of Cyclin B1-Venus were comparable between cells subsequently

treated with nocodazole and the proteasomal inhibitor MG132 versus cells treated with nocodazole, actinomycin D and MG132 (Novais-Cruz et al., 2018). This result suggests that *CCNB1* is not expressed during mitosis and that protein degradation rather than inhibition of de novo transcription promotes exit from mitosis.

Expression of Cyclin B1 constructs that are resistant to destruction delay mitotic exit (Clijsters et al., 2014; Wolf et al., 2006). If JI051 The results presented here suggest a scenario whereby HES1 inhibition leads to transcriptionally active *CCNB1*. If this leads to continuous Cyclin B1 protein expression, as I have demonstrated, it could create a situation reminiscent of experiments, where non-degradable forms of Cyclin B1 prevent exit from mitosis by maintaining CDK1 activity. Although the results in Fig 4.2.3 B 2 show that Cyclin B1 levels decline in JI051-treated cells compared to nocodazole arrested cells, they do not show as substantial a reduction as control cells. Chromosome segregation occurs once Cyclin B1 levels fall below a threshold, which has been experimentally measured in HeLa cells (Hayward et al., 2019). In JI051-treated cells an unstable mitotic state could be created whereby Cyclin B1 levels do not readily drop below a critical threshold due to sustained transcription. The live-imaging performed in Fig 3.2.7 shows that cells undergo mitotic slippage indicating that Cyclin B1 levels do eventually drop below a 'mitotic exit' threshold in JI051 treated cells (Gascoigne & Taylor, 2008). However, at this point, It cannot be ruled out that the sustained CDK1 activity observed here is instead a response to JI051-treated cells failing to complete other mitotic events, such as chromosome congression at the metaphase or the establishment of a functional mitotic spindle after release from nocodazole. In these scenarios, *CCNB1* expression would be sustained not because of inhibition of transcriptional repression but because cells are delayed in mitosis for the reasons mentioned above. The possibility of other mitotic defects occurring through JI051 treatment will be elaborated on in chapter 5 discussion.

4.3.2 Concluding remarks

In this chapter I have characterised further the effect of a recently published HES1 inhibitor that was described to arrest HEK293 cells at G2/M (Perron et al., 2018). In

the above discussion, I argue that exit from mitosis is prevented by sustained CDK1 activity and expression of key mitotic genes, notably *CCNB1* and *PLK1*, which could potentially stem from inhibition of transcriptional repression. HES1 has not been implicated in the regulation of mitosis before, either as a transcriptional regulator or more generally. In the following chapter (Chapter 5) I will investigate further direct targets of HES1 in cells exiting mitosis/early G1. Furthermore, I will characterise genome-wide gene expression changes that result from JI051 treatment and which may contribute to the mitotic arrest to elucidate a potential role for HES1 in the regulation of mitosis.

Chapter 5: HES1 function at the target gene level

5.1 Introduction

5.1.1 Opening remarks

The data presented in chapter 4 contends that sustained expression of *CCNB1* and subsequent CDK1 activity prevents exit from mitosis in cells treated with the HES1 inhibitor, JI051. If this stems from inhibition of HES1 transcriptional repression, then *CCNB1* or transcriptional activators of *CCNB1* may be subject to HES1 transcriptional repression. The hypothesis that this regulation occurs specifically in mitosis, is contingent, first on HES1 DNA binding in mitosis, and secondly, on continued transcription during mitosis in the absence of HES1 regulation.

The *CCNB1* promoter has been shown to be transcriptionally active in mitotic cells as a mechanism to maintain *CCNB1* levels to maintain activation the SAC (Sciortino et al., 2001). However, as discussed in 4.3.1, these results have been called into question given evidence that DNA intercalating agents disrupt CPC localisation in mitosis (Novais-Cruz et al., 2018). In chapter 4, I also showed that *CCNB1* transcription is sustained in JI051 arrested cells compared to control cells that have exited mitosis. These observations imply that down-regulation of *CCNB1* transcription in mitosis alongside its protein degradation may also be required for exit from mitosis in MCF7 cells. Investigating HES1 DNA binding and the potential transcriptional regulation of *CCNB1* during mitosis is the main objective of the following chapter.

5.1.2 Regulation of *CCNB1* transcription

CCNB1 transcription is regulated temporally within the cell cycle with transcription occurring from the end of S-phase and increasing during the G2/M transition (Pines & Hunter 1989; Minshull et al., 1990). Early characterisation of the *CCNB1* promoter using chloramphenicol acetyltransferase (CAT) reporter assays in Hela cells, revealed E-box consensus sites for Upstream stimulatory factor (USF) and, putative binding sites for MyoD, SP-1 and AP-2. Deletion of E-box consensus sites led to reduced

expression, indicating that they are required for *CCNB1* transcription. Furthermore, the binding affinity for USF was increased 4-fold in G2/M enriched cells, indicating that increased promoter activity is due to cell cycle dependent binding of transcription factors (Cogswell et al., 1995). Further characterisation, identified two CCAAT consensus sites present in both mouse and human that are crucial for the cell cycle specific induction of *CCNB1* transcription at the end of S-phase, and which are bound by the NF-Y transcription factor (Katula et al., 1997). In terminally differentiated C2C12 myoblast cells, NF-Y binding to the CCAAT regulatory sites is reduced alongside transcription of CAT reporters driven by the *CCNB1* promoter compared to proliferating C2C12 cells (Farina et al., 1999). Luciferase promoter assays demonstrated that NF-Y activates *CCNB1* transcription with p300 with increased activation observed when both proteins were transfected concurrently rather than NF-Y alone. The same paper reported that mutation of a cell cycle gene homology region (CHR) leads to early activation of human *CCNB1* promoter activity and a decrease in G2 fold-change compared to control cells (Wasner et al., 2003). Additionally, over-expression of FOXM1 in Hela cells promotes activation of the *CCNB1* promoter that is also dependent on the presence of a CCAAT sequence. (Leung et al., 2001).

While low levels of *CCNB1* transcription prior to the end of S-phase/start of G2 are associated with a lack of transcriptional induction, negative regulation of *CCNB1* transcription can also occur to arrest cells at the G2/M border (Innocente et al., 1999). p53 has been shown to mediate negative regulation of *CCNB1*. Human SKOV3 cells expressing a temperature sensitive p53 that has wild-type p53 function at 32°C, were arrested in G2 phase of the cell cycle when incubated at 32°C. This arrest was associated with decreased CDK1 activity and decreased *CCNB1* mRNA and protein expression, which could be rescued by over-expression of an exogenous Cyclin B1 construct. The activity of a CAT reporter containing 1,050 bp of the human *CCNB1* promoter was repressed at 32°C, indicating that the G2 arrest occurred through p53 regulation of *CCNB1* transcription (Innocente et al., 1999). In C2C12 cells, DNA damage induced by adriamycin led to a G2 arrest that was associated with decreased expression of *CCNB1* promoter CAT constructs. Expression of a dominant negative

p53 construct, which lacks a DNA binding domain, decreased the down-regulation of *CCNB1* and led to loss of the G2 arrest in response to Adriamycin treatment and an increase in mitotic cells with nuclear defects. In the same study, down-regulation of *CCNB1* promoter activity was abrogated when two CCAAT motifs, recognized by the cyclin transcriptional activator, NF-Y, in the *CCNB1* promoter were mutated, indicating that functional NF-Y is also required for p53 regulation of *CCNB1*. (Manni et al., 2001). In mouse myeloma 32D cells, over-expression of c-MYC in combination with the expression of a temperature sensitive mutant p53 leads to a 10-fold *CCNB1* over-expression compared to p53 mutants alone. Analysis of *CCNB1* over-expression these cells also showed them to be tetraploid, indicating that regulation of Cyclin B1 through p53 is important for preventing chromosomal instability (Yin et al., 2001). In human glioblastoma U87 cells, over-expression of MXI1, a negative regulator of MYC, inhibits G2/M progression through down-regulation of *CCNB1* mRNA expression. Expression of CAT reporter driven by a *CCNB1* promoter was decreased in MXI1 over-expressing cells. This repression was abolished when the E-box sequence in the promoter construct was mutated. *In-vitro* binding of MXI1 and Max heterodimers to the E-box sequence was verified by EMSA, suggesting that this complex competes with activators of *CCNB1* transcription (Manni et al., 2002).

5.1.3 A role for HES1 in regulating mitotic gene expression and experimental aims

The nocodazole release experiments in chapter 4 demonstrate that cells not exposed to JI051 prior to mitosis entry fail to exit mitosis efficiently in the 4 hour timespan analysed. This indicates that the HES1 function inhibited by JI051 occurs specifically in mitosis. Using restriction enzyme accessibility assays, the *CCNB1* promoter region was shown to exhibit an 'open' chromatin structure in mitotic Hela cells. In the same study, ChIP assays demonstrated that the NF-Y protein was bound to CCAAT regions of the *CCNB1* promoter in mitotic cells (Sciortino et al., 2001). This data indicates that *CCNB1* can be regulated transcriptionally during mitosis. As mentioned above, NF-Y binding is required for negative regulation of *CCNB1* by p53 (Manni et al., 2001), therefore its binding in mitotic cells could serve a dual purpose of keeping *CCNB1* transcription active but also facilitating binding of negative regulators to enable its down-regulation to coincide with mitotic exit.

Transcriptional regulation of mitotic gene expression by HES1 has not previously been investigated. The proposed action of JI051, cell cycle specific effect, and gene expression changes observed in mitosis after treatment are supportive of a role for HES1 in mitosis, with the caveat that JI051 is specific to HES1. A method of gene expression control that occurs during mitosis is 'mitotic bookmarking', which involves transcription factor binding or epigenetic changes on mitotic chromatin before cytokinesis that is carried over into daughter cells (Zaidi et al., 2018). This has been demonstrated for a number of transcription factors, including *RUNX2, GATA1*, and *RBPJ* (Kadauke et al., 2012; Lake et al., 2014; Young et al., 2007). This is an appealing way to think about HES1 control of transcription and will be explored in the experiments below, which examine the extent of HES1 chromatin binding in mitosis.

A working hypothesis for the following chapter is that transcriptional repression through HES1 is required for mitosis exit, which is impaired in JI051 arrested cells. To investigate this hypothesis, I aim to characterise HES1 DNA binding in mitosis and early G1 and assess the impact of JI051 treatment on this binding. I will employ ChIP-seq to identify early G1 HES1 targets, whose repression is potentially necessary for mitosis exit. RNA-seq will also be used to characterise global transcriptional changes that occur in JI051 treated cells. Ultimately, I aim to describe a HES1 regulatory network consisting of direct and indirect HES1 targets, whose regulation is necessary for mitotic progression.

5.2 Results

5.2.1 HES1 binds its promoter in early G1

MCF7 cells released from nocodazole arrest do not exit mitosis when treated with the HES1 inhibitor JI051. In line with observations that JI051 disrupts the nuclear localisation of HES1 (Perron et al., 2018), I hypothesised that the cause of the mitotic arrest stemmed from de-repression of HES1 targets. I didn't observe mis-localisation of HES1 in my live-imaging experiments prior to delayed the mitosis. However, I did observe sustained *CCNB1* expression and a change to the *HES1* expression profile in JI051 arrested cells after release from nocodazole leading me to speculate that the effect of HES1 inhibition may occur specifically in mitosis. To test this, I evaluated HES1 DNA binding during exit from mitosis. ChIP-qPCR was performed in MCF7 HES1-mVENUS cells released from nocodazole arrest (Fig 5.2.1). HES1 DNA binding was also assessed in cells treated with JI051 to investigate if changes in DNA binding were correlated with gene expression changes. In chapter 4. I argued that HES1 negative feedback on its own promoter was potentially impaired in JI051 treated cells after release from nocodazole, therefore identification of HES1 binding to its own promoter was used as a proxy to determine the effect of JI051 on HES1 DNA binding. HES1 primers were designed to target a region in the *HES1* promoter recently identified as a HES1 binding site in human embryonic stem cells (hESCs) (Lichtenberg et al., 2018).

MCF7-HES1-mVENUS cells were arrested in prometaphase, collected by mitotic shake-off and released as described in (Materials and Methods 7.1). Cells were fixed in prometaphase (nocodazole arrested) and 4 and 8 hours after nocodazole washout in untreated cells. HES1-bound DNA was immunoprecipitated using a GFP antibody that recognized the N-terminal mVENUS tag on endogenous HES1. Isolated DNA was amplified by qPCR using *HES1* specific primers (Fig 5.2.1 A). Enrichment of HES1-bound DNA at each timepoint was quantified as a percentage of recovered input, calculated based on the amplification seen in 1% of input DNA. Enrichment was observed in mitosis and at 4 and 8 hours post-nocodazole release. Hes1 bound DNA was most enriched at 4 hours 4.6%, compared 1.6 and 1.2 % for nocodazole and 8

hours, respectively. This enrichment was not observed in chromatin samples immunoprecipitated using rabbit IgG antibody (Fig 5.2.1 C). I also performed one independent negative control ChIP-qPCR using parental MCF7 cells (no HES1-mVENUS tag). Mitotic cells were collected from MCF7 and MCF7-HES1-mVENUS cells and released separately into fresh media. Cells were fixed and lysed 4 hours post-nocodazole washout. DNA from lysates was immunoprecipitated using the indicated antibodies (Fig. 5.2.1 B). In parental MCF7 cells no enrichment of HES1 was observed at the *HES1* promoter in parental MCF7 lysates, demonstrating that the enrichment observed in MCF7-HES1 mVENUS cells is specific to detection of the CRISPR-modified HES1 protein (Fig. 5.2.1 B)

To assess the effect of JI051 on HES1 DNA binding, additional ChIP experiments were performed in cells treated with 1µm JI051 for 4 hours after nocodazole release. In control ChIP experiment enrichment of HES1 bound DNA at 4 hours was 6.9%. This enrichment was reduced by 5.3% in JI051 treated cells. Again, enrichment of HES1 bound genomic loci using non-specific IgG antibody was absent (~0.2%).

This data indicates that HES1 binding, at least to its own promoter, occurs in mitosis and is increased when cells enter G1, implicating a role for HES1 autoregulation of *HES1* transcription as cells enter G1. This agrees with the 4 hour *HES1* expression profile observed in (Fig 4.2.2 A) as *HES1* mRNA expression is reduced at four hours. Moreover, HES1 binding to its promoter could be differentially regulated at different stages during G1, as enrichment at 8 hours was decreased compared to 4 hours (Fig 5.2.1 C) When cells are released from nocodazole and treated with JI051, blocking exit from mitosis, HES1 binding to its own promoter was reduced. This suggests that HES1 DNA binding with a potential regulatory function could be required for mitotic exit, however as enrichment of HES1 on its promoter was comparable between nocodazole and JI051 treated cells, it could also be a reflection of HES1 binding in mitotic cells as opposed to specific inhibition.

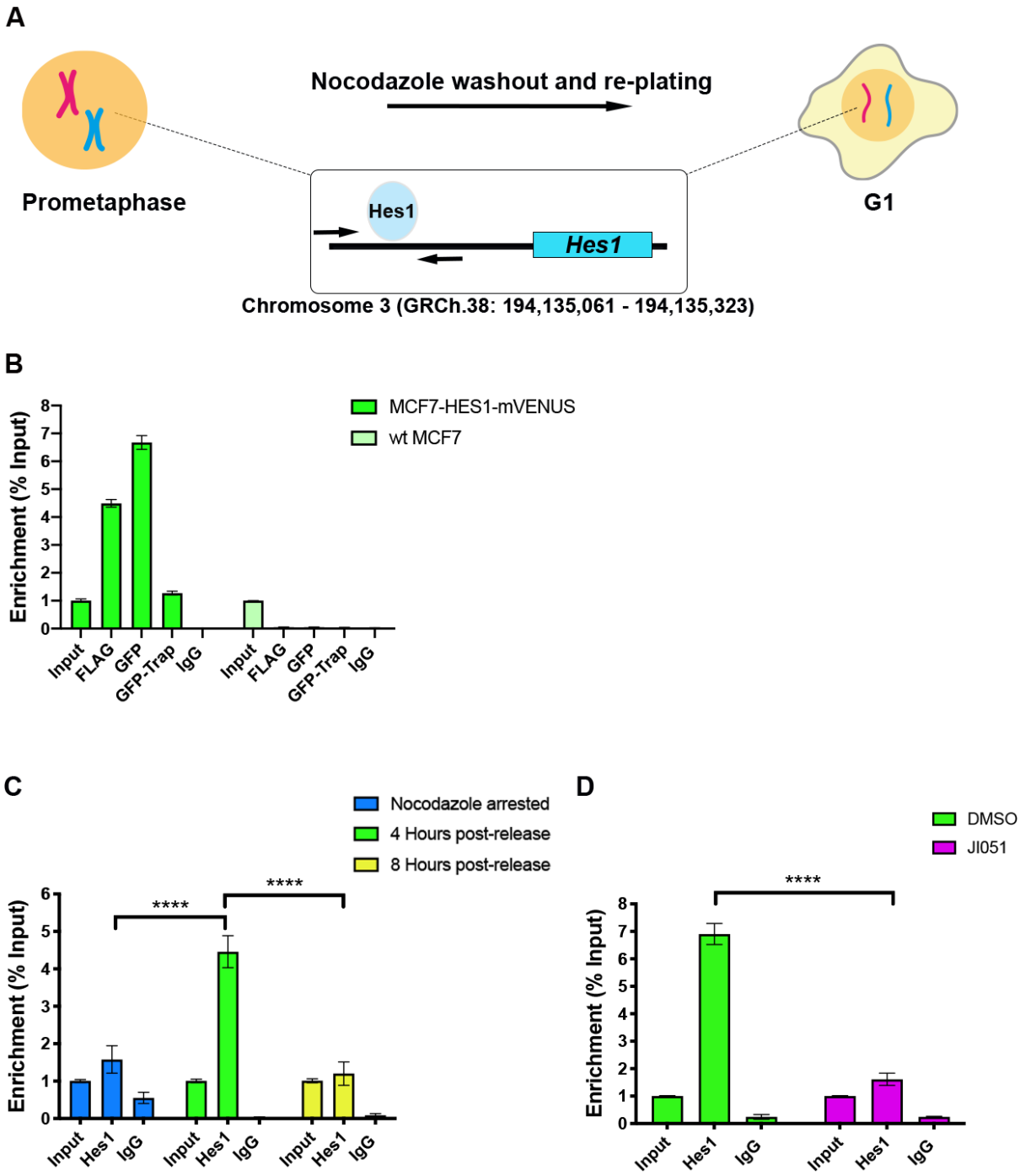

Fig. 5.2.1 Evaluation of HES1 binding to its own promoter (A) Enrichment of HES1-bound DNA in prometaphase and early G1 was measured by ChIP-qPCR using primers targeting the *HES1* promoter. **(B)** DNA was immunoprecipitated from MCF7 and MCF7-HES1-mVENUS lysates using the indicated antibodies 4 hours post-nocodazole washout. **(C)** HES1 promoter binding in prometaphase and early G1 (4 and 8 hours post-nocodazole release) in HES1 and non-specific IgG immunoprecipitated samples **(D)** HES1 binding in control (DMSO) and JI051 treated cells, 4 hours post-nocodazole release in HES1 and IgG immunoprecipitated samples. In all experiments, enrichment was calculated as a percentage of recovered input. Non-specific IgG

immunoprecipitation was used as a negative control. Significance was determined by 2-way ANOVA. Error bars represent ± SEM from at least 3 biological replicates.

5.2.2 Genome-wide identification of HES1 targets

While binding of HES1 to its own promoter in early G1 is indicative of autoregulation of *HES1* expression, identification of other targets, principally late cell cycle genes, is required to ascribe a regulatory role for HES1 in the M – G1 transition. To identify HES1 targets in early G1, ChIP-seq was performed in MCF7-HES1-mVENUS cells 4 hours post-nocodazole washout using anti GFP and FLAG antibodies recognizing the VENUS and FLAG tags on endogenous HES1. The 4 hour post-nocodazole washout timepoint was chosen based on the enrichment profile of HES1 on its own promoter in Fig 5.2.1. Using the 4 hour timepoint was also motivated by my observations in Fig 4.2.2, where expression of both *HES1* and *CCNB1* showed the most significant down-regulation in the 4 hour timecourse.

ChIP-Seq was performed for 12 samples: 3 samples immunoprecipated using a GFP antibody, 2 samples using a FLAG antibody and 1 sample using the GFP-Trap and their corresponding input samples (Materials and Methods 7.12). Peak calling using MACS2 was performed using a q-value threshold of 0.05. The number of high-confident peaks varied between samples. For the three samples immunoprecipitated using a GFP antibody (GFP1-3), 351, 881, and 4507 peaks were selected, respectively. For samples immunoprecipitated using a FLAG antibody (FLAG 1-2), 275 and 734 peaks were selected, respectively. 1224 peaks were selected in the GFP-Trap immunoprecipitated sample after sequencing. To compile a list of high confidence HES1 targets between biological replicates the Irreproducibility Discovery Rate (IDR) framework was applied to the 3 GFP biological replicates to examine peak consistency between replicates (Li et al. 2011). IDR analysis was performed in combination with a MACS2 q-value threshold of 0.05 to create 3 new datasets of high confidence HES1 targets: GFP1 GFP2, GFP1 GFP3, and GFP2 GFP3. In GFP1 GFP2 221 peaks were identified, mapping to 200 unique genes. In GFP1 GFP3 182 peaks were identified, mapping to 175 unique genes. In GFP2 GFP3 371 peaks were identified, mapping to 244 unique genes. High confidence HES1 target genes for the

GFP IDR analysis are presented as 3 tables (GFP1 GFP2, GFP1 GFP3 and GFP2 GFP3) in supplementary information (table S2). The lower number of 'unique' genes results from peaks being observed more than once in the same gene and the removal of genomic regions that weren't annotated. Variation was observed in the proportions of genomic loci bound by HES1 between samples. For each sample, the percentage of peaks within specific genomic loci was characterised (Fig. 5.2.2 A). For GFP-immunoprecipitated samples (1-3), approximately 60, 50, and 25% of peaks were located in promotor regions, or within 3kb of transcription start sites (TSS). The remaining peaks were characterised as intergenic or intragenic. For FLAG-immunoprecipatated samples (1-2), approximately 36 and 30% of peaks were located in promoter regions. For GFP-trap samples, the majority of peaks were located in intragenic regions and intragenic regions, approximately 20% of peaks were located in promoter regions. The relative location of peaks from TSS for each sample is further described in (Fig 5.2.2 B)**.** An average peak profile for each sample was characterised using a +/- 1000 bp window relative to TSS to define the frequency of HES1-bound loci within this region (Fig 5.2.2 C).

Gene-ontology analysis was performed for each sample to identify HES1 target genes with shared function. HES1-bound genes were significantly associated with GO terms relating to developmental processes, e.g. 'cell morphogenesis involved in neuron differentiation' and 'gland development', p values, 4.79e-09 and 2.82e-09, respectively (Fig 5.2.3 A). The list of genes for GO term 'cell morphogenesis involved in neuron differentiation', which includes *HES1*, is shown in supplementary table 1 (S1). To characterise genomic sequences bound by HES1, motif enrichment was performed using DREME (Discriminative Regular Expression Motif Elicitation) from MEME-suite (Motif-based sequence analysis tools). Discovered motifs were compared to known motifs from the JASPAR database using HOMER (Hypergeometric Optimisation of Motif Enrichment). Representative enriched motifs are shown in (Fig 5.2.3 B). Motif enrichment was also performed using sequence data from a combined analysis of GFP 1 and GFP 2. Here peak data from GFP 1 and GFP 2 was combined based on similarity of peaks after Irreproducibility Discovery Rate (IDR) analysis with a relaxed peak calling threshold of ($p = < 0.05$) (Fig 5.2.3 B). In

both cases motifs were discovered with high significance with similarity to known HES protein DNA binding motifs (GFP 1 p = 1e-22, GFP 2 p = 1e-32, GFP 1-2, p =1e-2984). Of the motifs listed, the HES/BHLH-related motifs (highlighted in red) were the most abundant in targets identified by ChIP-seq as indicated by '% of targets' (Fig 5.2.3 B).

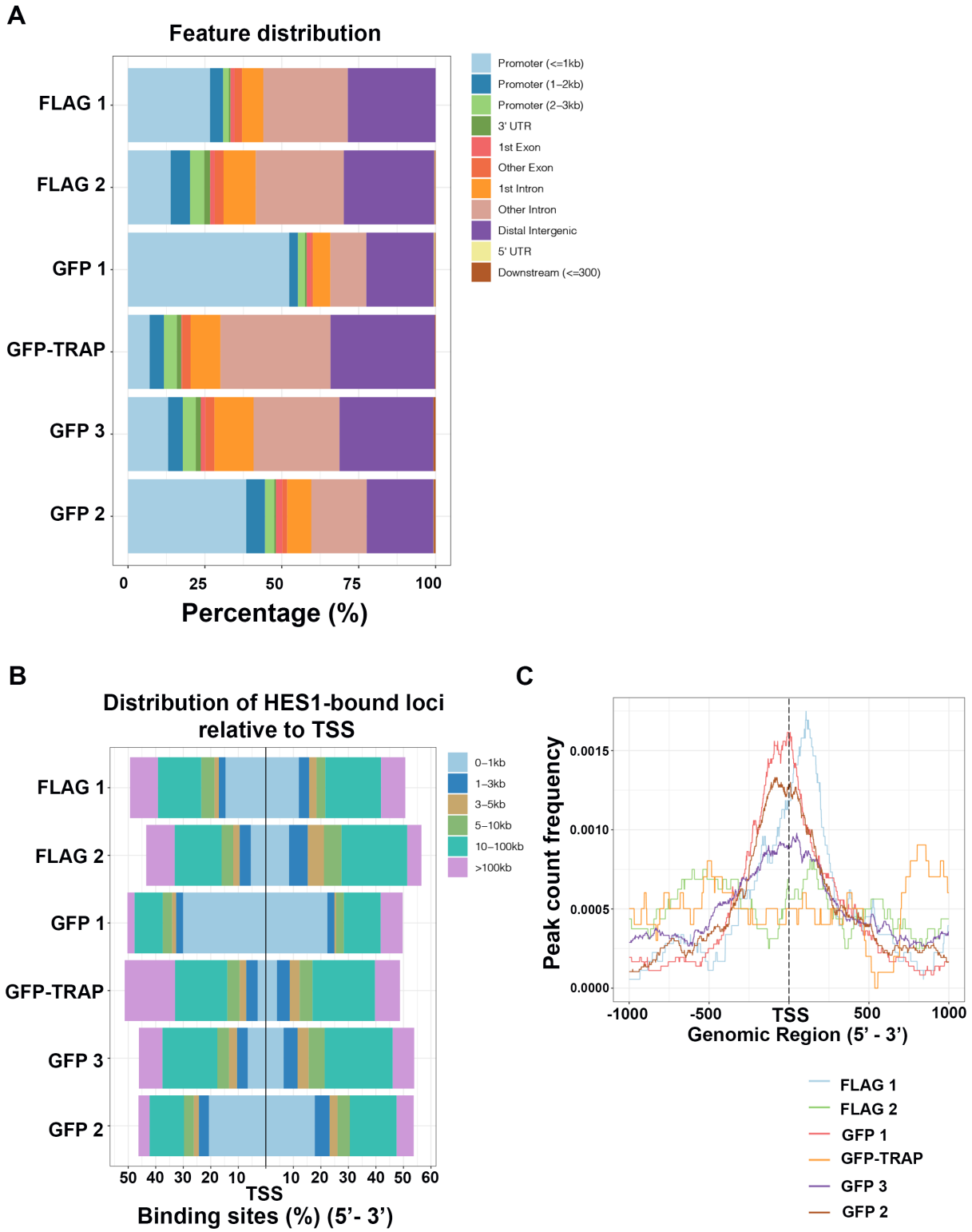

Fig. 5.2.2 Distribution of genomic loci bound by HES1

(A) Percentage of genomic regions bound by HES1. Promoter regions are defined as +/- 3kb (kilobases) from TSS. Other regions were classified as exonic, intronic, distal intergenic, or belonging to 5' and 3' UTRs **(B)** Distance of HES1 bound loci from TSS for each sample **(C)** Average peak profile for each HES1 ChIP-seq sample. Peak frequencies for each sample were plotted relative to TSS sites within a +/- 1000 bp

window. ChIP-seq analysis was performed by Dr. Soumita Ghosh, a former member of Dr. Hyungwon Choi's lab at National University Singapore.

A

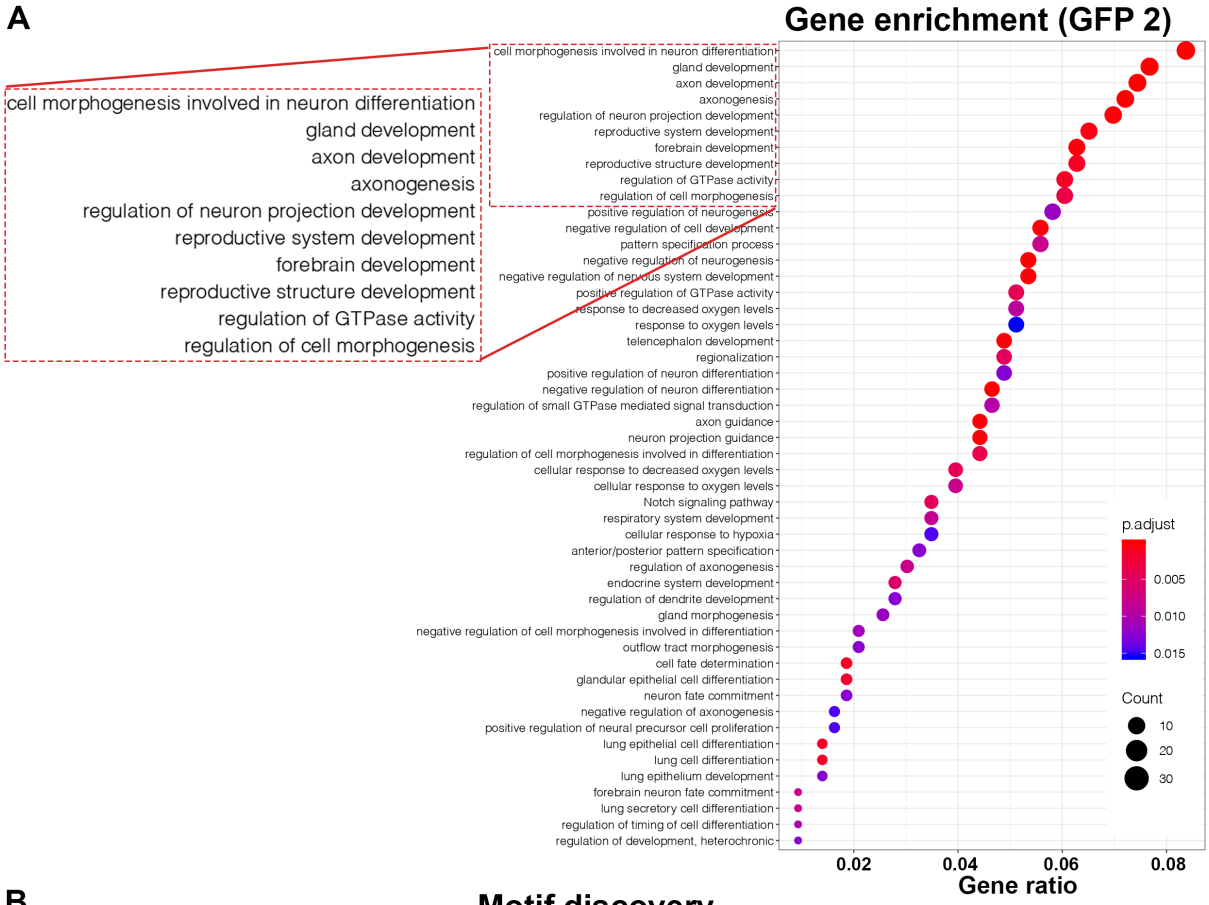

B

Motif discovery

1. GFP 1

Rank	Motif	P-value	log P-pvalue	% of Targets	% of Background	STD(Bg STD)	Best Match/Details
1		1e-65	-1.516e+02	7.00%	0.00%	46.6bp (2.7bp)	ZNF410/MA0752.1/Jaspar(0.583) More Information | Similar Motifs Found
2		1e-44	-1.018e+02	7.33%	0.03%	52.4bp (56.3bp)	DUX4/MA0468.1/Jaspar(0.618) More Information | Similar Motifs Found
3		1e-43	-1.003e+02	7.33%	0.03%	51.8bp (69.6bp)	PB0176.1_Sox5_2/Jaspar(0.723) More Information | Similar Motifs Found
4		1e-22	-5.099e+01	49.00%	22.97%	52.0bp (78.4bp)	HES2/MA0616.2/Jaspar(0.953) More Information | Similar Motifs Found

2. GFP 2

Rank	Motif	P-value	log P-pvalue	% of Targets	% of Background	STD(Bg STD)	Best Match/Details
1		1e-36	-8.476e+01	2.05%	0.00%	49.3bp (0.0bp)	PB0169.1_Sox15_2/Jaspar(0.633) More Information | Similar Motifs Found
2		1e-32	-7.384e+01	28.70%	11.78%	50.3bp (68.7bp)	HES1/MA1099.2/Jaspar(0.926) More Information | Similar Motifs Found
3		1e-26	-6.054e+01	2.34%	0.02%	57.1bp (56.9bp)	PB0096.1_Zfp187_1/Jaspar(0.553) More Information | Similar Motifs Found
4		1e-15	-3.570e+01	15.81%	6.77%	54.0bp (56.0bp)	Wt1/MA1627.1/Jaspar(0.639) More Information | Similar Motifs Found

3.GFP 1-GFP 2 IDR (p=0.05)

Rank	Motif	P-value	log P-pvalue	% of Targets	% of Background	STD(Bg STD)	Best Match/Details
1		1e-3908	-8.999e+03	17.84%	2.38%	47.9bp (71.6bp)	Srebp1a(bHLH)/HepG2-Srebp1a-ChIP-Seq(GSE31477)/Homer(0.759) More Information | Similar Motifs Found
2		1e-3096	-7.130e+03	11.49%	1.09%	52.7bp (72.5bp)	POL013.1_MED-1/Jaspar(0.753) More Information | Similar Motifs Found
3		1e-2984	-6.873e+03	12.65%	1.48%	39.3bp (71.0bp)	HES1/MA1099.2/Jaspar(0.719) More Information | Similar Motifs Found
4		1e-2912	-6.706e+03	12.94%	1.62%	53.5bp (69.8bp)	Ddit3::Cebpa/MA0019.1/Jaspar(0.558) More Information | Similar Motifs Found

Fig 5.2.3 Gene enrichment and motif discovery in HES1 ChIP-seq analysis (overleaf) **(A)** GO analysis of HES1 bound loci. Each dot represents specific GO term with the colour and size indicating p-value and number of genes associated with term, respectively. **(B)** Representative result of motif discovery in HES1 ChIP data using HOMER. ChIP-seq and motif analysis was performed by Dr. Soumita Ghosh, a former member of Dr. Hyungwon Choi's lab at National University Singapore.

To validate the ChIP-seq data, targets identified in all 4 samples were selected for additional ChIP-qPCR analysis in HES1-immunoprecipitated chromatin. Primers were designed to amplify genomic regions for each gene identified as a HES1 binding site (see table 6 page 197). These targets included genes known to be HES1 interactors such as the pro-differentiation genes *ASCL1* and *NEUROG3* and the pioneer factor *FOXA1* (Lichtenberg et al. 2018; Chen et al. 1997; Lee et al. 2001). Targets, which to my knowledge have not been described before include, the basic helix-loop-helix transcription factor *BHLHE41*, a transcription factor involved in regulation of circadian proteins CLOCK/BMAL1, CDK5 regulatory subunit-associated protein 1, *CDK5RAP1*, and the zinc-finger transcription factor, *PRDM10* (Honma et al., 2002; Reiter et al., 2012). Relevant to the control of *CCNB1* transcription was the identification of a HES1 binding site in the transcription factor *MYB* (c-MYB) promoter, which has been shown to induce *CCNB1* expression in drosophila and hematopoietic cells (Nakata et al., 2007; Okada et al., 2002). The pseudokinase *TRIB1*, an ortholog of the Drosophila *TRIBBLES* gene, which has a developmental role in controlling cell division, was also identified as a HES1 target (Mata et al., 2000). All genes tested by ChIP-qPCR, except *PRDM10,* showed enrichment of HES1 bound chromatin over background (IgG). However, the enrichment profiles were lower than HES1 on its own promoter (Fig 5.2.4 A) with the % Input ranging approximately from 1.1 for *NEUROG3* to 0.3 for *ASCL1*.

HES1 binding sites were identified in its promoter, which matched the regions identified in independent human HES1 ChIP-seq data (Lichtenberg et al., 2018). These binding sites are displayed against the corresponding input in (Fig 4.2.4 B) using integrated genome browser (IGV). The HES1 peaks for *HES1* binding were

consistent across all 4 samples (GFP 1-3, FLAG 1). Visualisation of HES1 promoter peaks for FLAG 2 and GFP-Trap showed a high amount of random peaks for all genes tested so are not presented here. However, there was some inconsistency between samples for the genes selected for validation of the ChIP-seq data as peak quality varies across samples. For example, peaks for NEUROG3 are only observed in GFP 1 and 2 ChIP samples. Combined with the ChIP-qPCR data this data suggests that after release from nocodazole arrest HES1 binds its own promoter more strongly than other HES1 targets in early G1. It may also suggest that HES1 binding to its promoter is a temporally distinct event relative to its binding of non-*HES1* loci, with the 4 hour timepoint after nocodazole release reflecting this.

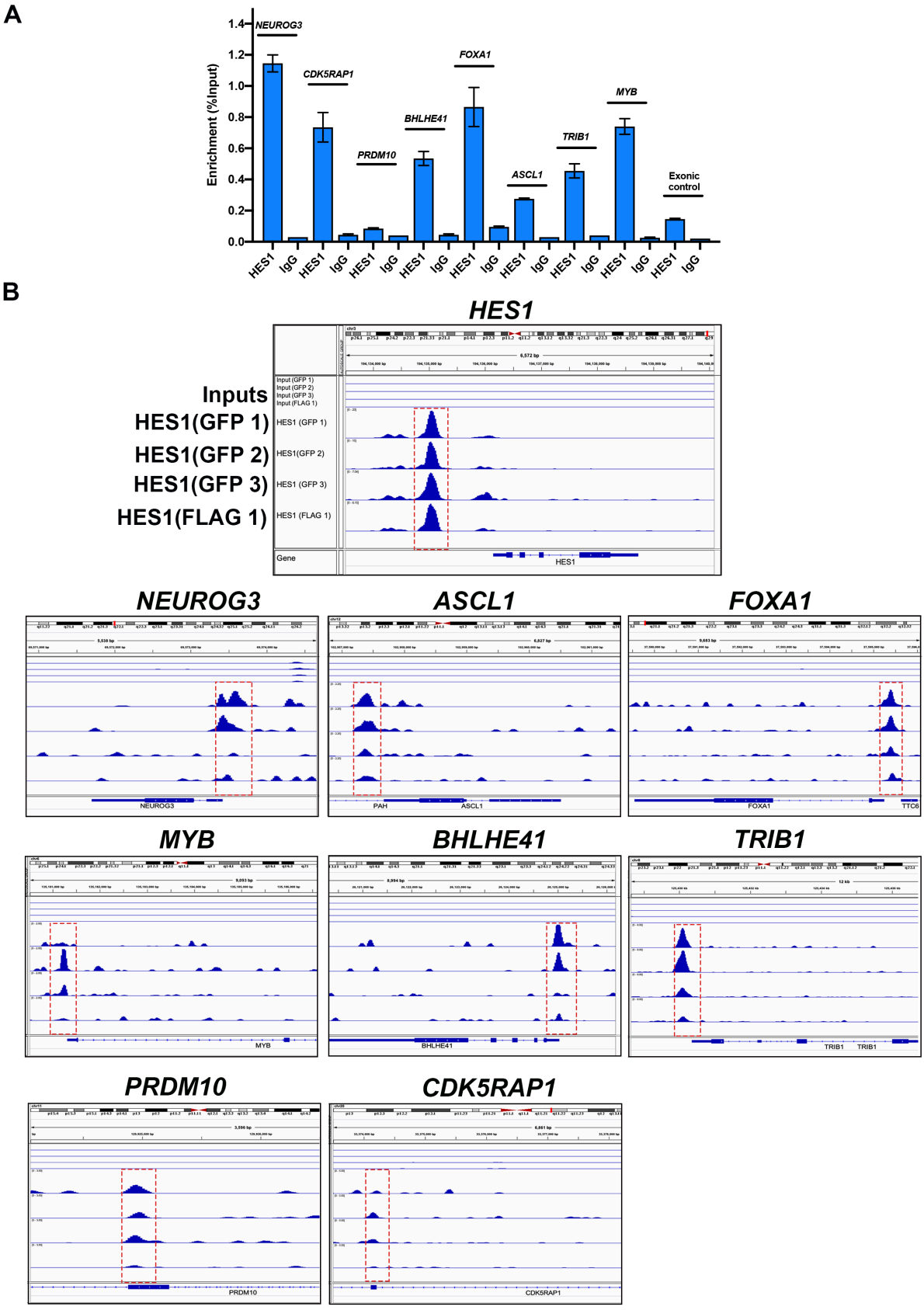

Fig 5.2.4 Validation of HES1 ChIP-seq targets (overleaf). (A) ChIP-qPCR analysis of HES1 enrichment at sites identified by ChIP-seq. Primers were designed to amplify HES1 binding sites in each gene. Enrichment was calculated as measure of recovered

input for each gene. Non-specific IgG is used as a negative control. Non-specific primers were also used to amplify an exonic region in the HES1 gene as a negative control (furthest right bar chart on graph). Representative enrichment values from 1 experiment. Error bars represent ± SEM from 2 technical replicates **(B)** Read density for HES1 peaks identified by ChIP-seq for *HES1* and the genes listed above was visualized in the integrative genome browser (IGV). Dashed, red boxes indicate regions where ChIP-qPCR primers were designed for each gene.

4.2.3 Impact of JI051 on Hes1 target binding

Prior to Hes1 ChIP-seq analysis, I demonstrated that JI051 treatment of MCF7 cells decreased the enrichment of HES1 on its own promoter. To assess if this effect extends to the enrichment of HES1 at the genomic loci presented in Fig 4.2.4, I analysed the enrichment of HES1 at these sites in JI051 treated samples by ChIP-qPCR. No significant decrease in HES1 binding was observed for the targets analysed in JI051-treated cells. With regards to *MYB* and its role in *CCNB1* activation, there was a decrease in HES1 binding to *MYB* from 0.5 to 0.2 % enrichment, but this was not significant due to variability within samples, as 2 out of 6 control samples showed low enrichment. For all other genes, 3-5 control samples were analysed. No significant difference in HES1 enrichment on the promoters for these genes was observed for control versus JI051 treated samples, although a trend of slightly lower enrichment was observed for all genes except for *PRDM10*. No enrichment of HES1 at *PRDM10* loci was detected in control samples.

The data may reflect the differential targeting of HES1 to its own promoter versus other target genes during mitosis exit and in early G1. If HES1 DNA binding is primarily directed to its own promoter after release from nocodazole, the difference in enrichment compared to JI051 arrested cells may be more appreciable for HES1 compared to non-*HES1* target genes where HES1 binding isn't as enriched. Taking this data as a measure for inhibition of HES1 target binding, it suggests that it is largely unaffected for non-*HES1* loci. Therefore, it is not possible to say whether the potential repression of these genes by HES1 would also be relieved.

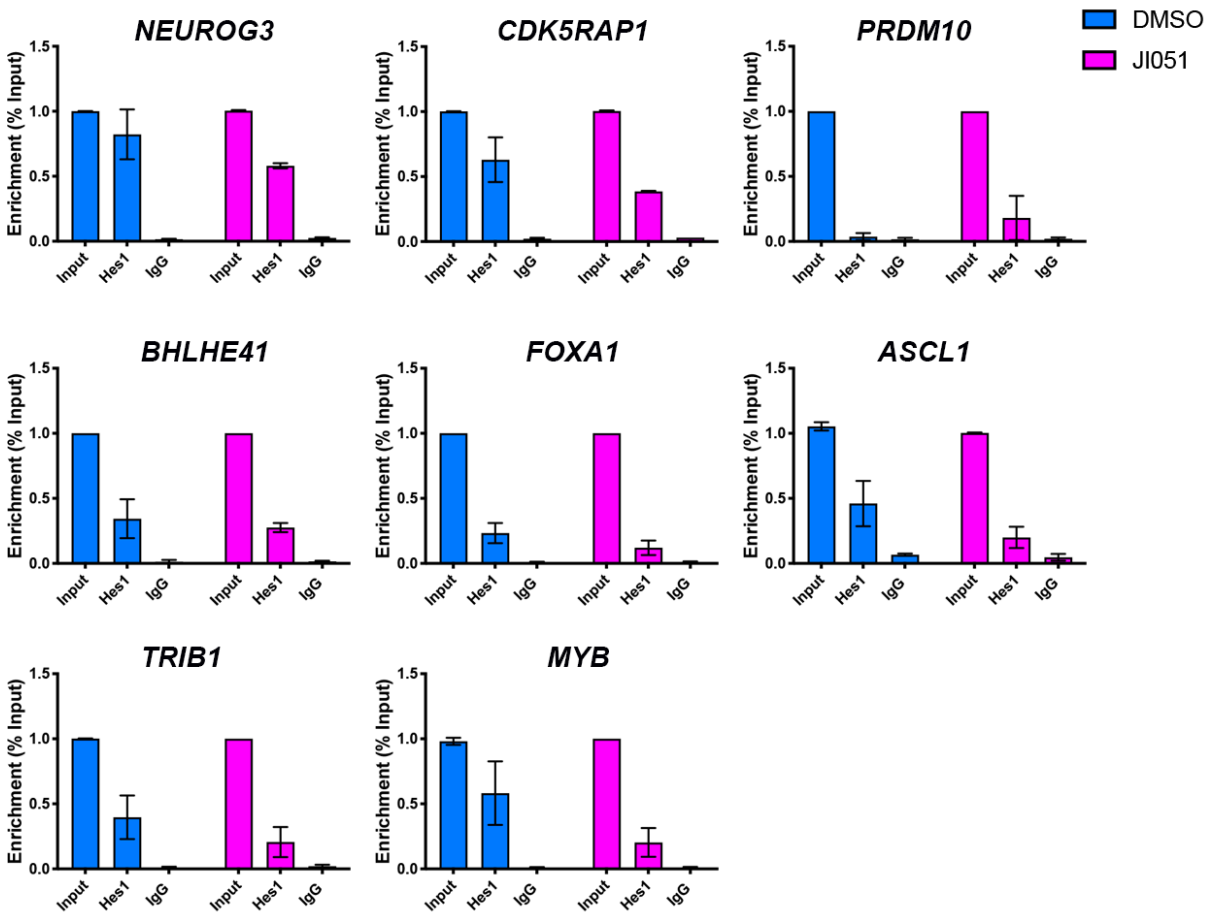

Fig. 5.2.5 Evaluation of HES1 bound loci in JI051 treated cells. ChIP-qPCR was used to compare the enrichment of HES1 bound loci between control and JI051 treated cells for the genes listed above. Enrichment was calculated as measure of recovered input for each gene. Non-specific IgG was used as a negative control. Data for all genes is represented as mean ± SEM from at least 3 biological replicates. (JI051 n=2 for *NEUROG3*, *CDK5RAP1*, *PRDM10*, *BHLHE41*, *ASCL1*, *FOXA1*, *TRIB1*)

5.2.4 Transcriptomic analysis of JI051 treated cells reveals upregulation of mitotic genes

To assess the extent of JI051 treatment on gene expression, RNA-sequencing (RNA-seq) was performed to evaluate global gene expression changes in mitosis that occur during JI051 treatment. RNA-seq was performed in prometaphase (nocodazole arrested) cells, and control and JI051 treated cells 4 hours post-nocodazole washout in 3 biological replicates. Downstream analysis of gene expression changes was performed separately under three comparisons: (1) DMSO vs. nocodazole, a control comparison that allowed me to assess changes in gene expression that occur as cells

exit mitosis and enter G1. (2) JI051 vs nocodazole, and (3) DMSO vs JI051. The latter two comparisons allowed me to assess gene expression profiles to differentiate between the nocodazole arrest state and the JI051 arrest state and also identify differentially genes that can inform on JI051-mediated mitotic arrest state. For comparison 1, 1270 genes were identified as differentially expressed (> 1.5 Log2 fold-change) with high significance (q value < 0.05). For comparison 2 and 3, changes in gene expression were not as statistically significant and were instead selected based on a smaller p value (< 0.01). 177 and 159 differentially expressed genes were identified for comparison 2 and 3, respectively.

Gene expression changes for all three groups are presented in the context of the cell cycle in Fig. 5.2.6. Two broad differential expression profiles can be identified, which are highlighted in the figure. Group one, highlights genes which are down-regulated upon entry into G1. This group includes genes which have roles during the G2/M transition and in mitosis e.g. *CCNB1*, *FOXM1*, *AURKA*. Group two are a subset of genes which are up-regulated upon entry into G1, these include; *CCND1*, *CDKN1A*, *JUN* and *MYC* and also CDK1 inhibitors *WEE1* and *GADD45A* (McGowan & Russell, 1993; Zhan et al., 1999). Both of these groups reflect changes in gene expression that occur during the M/G1 transition, indicating that 4 hours after nocodazole washout control cells have largely exited mitosis. JI051 arrested cells exhibit an expression profile that appears to sit in-between control cells and nocodazole arrested cells. The late cell cycle genes in group one remain up-regulated compared to control cells in G1, indicating that the JI051 arrest is associated with a broad upregulation of mitotic genes. This may simply be a correlation with the mitotic arrest state or an indication that a mechanistic basis for the JI051 arrest lies in sustained expression of the late cell cycle transcriptional programme, as I discussed in chapter 4 with regards to *CCNB1*.

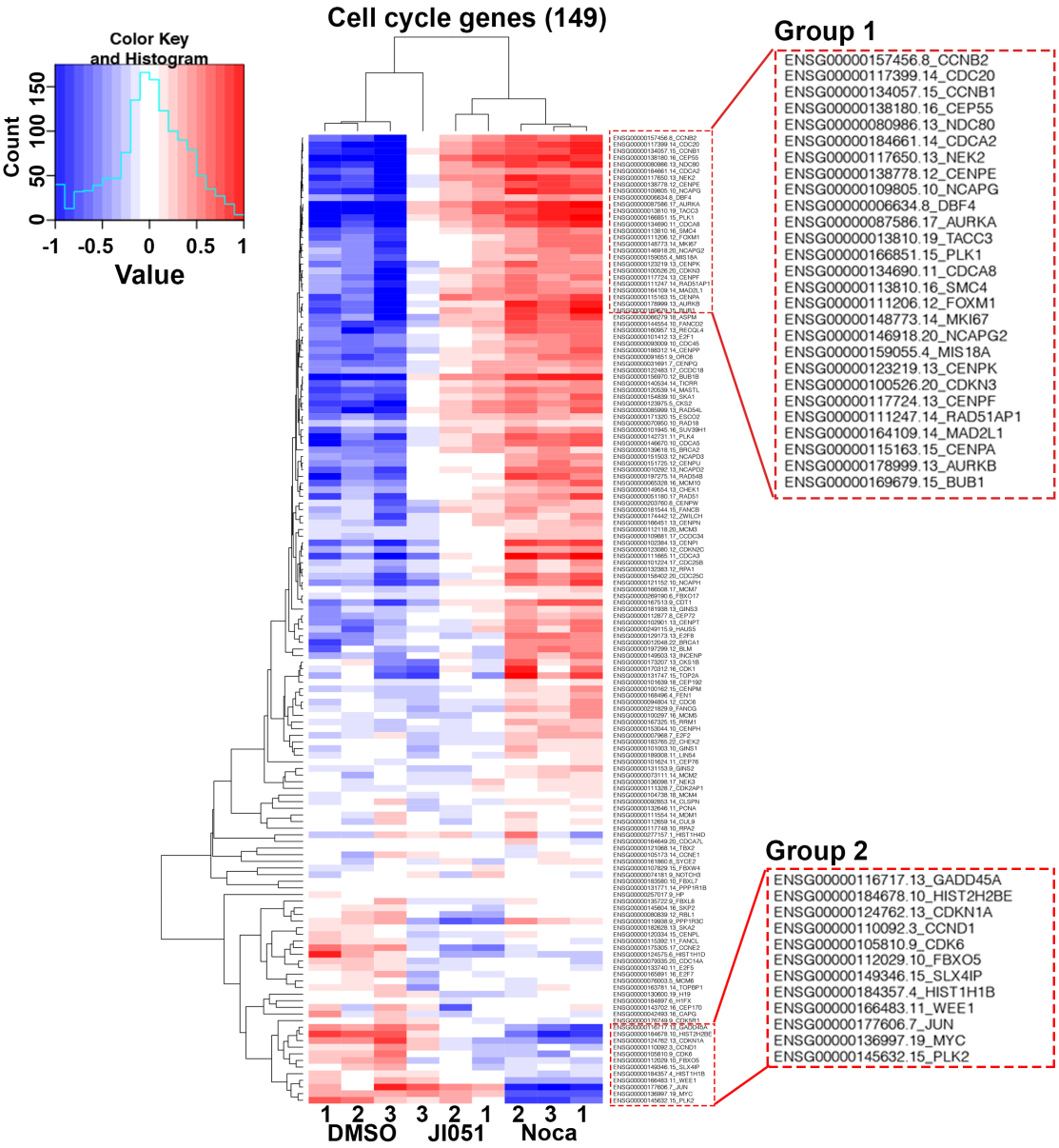

Fig 5.2.6 Heatmap of differential expression for 149 'cell cycle' genes

Cell cycle gene expression for nocodazole (noca) arrested cells, control (DMSO) and JI051-treated cells (JI051) presented as normalised z-scores. DMSO and JI051 samples refer to analysis performed on RNA extracted from cells 4 hours after release from nocodazole arrest and treated with 1µM JI051 or DMSO. Numbers 1-3 at bottom of heatmap refer the biological replicate for each treatment group. 'Group 1' and 'Group 2' to the right of heatmap refer to gene expression patterns of interest. Group 1 highlights genes that are down-regulated upon exit from mitosis and Group 2 highlights genes that are up-regulated upon G1 entry. RNA-seq analysis was performed by Dr. Soumita Ghosh, a former member of Dr. Hyungwon Choi's lab at National University Singapore.

Having established that JI051 causes widespread changes in gene expression, I next sought to identify the most significant differentially expressed (DE) genes that are up/down-regulated in JI051 arrested cells compared to DMSO control cells in early G1 and prometaphase arrested cells. The top 20 DE genes (highest Log2 fold-change and $p < 0.01$) for each comparison are listed in Table(s) 1 and the corresponding gene expression changes are displayed alongside the 'control' expression profile (DMSO/Noca) for each gene in Fig. 5.2.7. I have also indicated whether each gene was identified as a HES1 target from the ChIP-seq data. The top 5 up-regulated genes in JI051 cells compared to control cells were *AURKA*, *BUB1B* (BUBR1), *TACC3*, *PIMREG*, and *KIF14.* Many of the up-regulated genes have the potential to maintain a mitotic arrest. For example, transforming acidic coiled coil 3 (*TACC3*) is an AURORA A substrate and its phosphorylation is required for recruitment to the mitotic spindle where it is involved in microtubule assembly and stabilisation. Increased microtubule stabilisation is known to reduce tension at kinetochore-microtubule attachments thereby preventing the meta/anaphase transition (Burgess et al., 2015; Fanale et al., 2015; Lioutas & Vernos, 2013). *AURKA* was identified in one of the HES1 ChIP-seq samples, however visualization of the identified binding site using the Integrative Genomics Viewer (IGV) in the *AURKA* promoter showed it to be non-specific. The over-expression of BUBR1 could delay mitosis due its role in opposing the APC/C. Other notable up-regulated genes include, *NDC80* and *KNSTRN*, two kinetochore-associated proteins, important for establishing connections with microtubules (Kern et al., 2017). Due to its down-regulation in JI051-treated cells compared to noca and DMSO cells (Table 1 page 146), the beta-tubulin protein gene *TUBB* is interesting, as it suggests that microtubule assembly could be affected in JI051-treated cells (Ferreira et al., 2018).

JI051/DMSO

A Up-regulated

	Gene	HES1 target	p-value	q-value	log2FC
1	*AURKA*	Yes	0.0057	0.0553	1.67
2	*BUB1B*	No	0.0004	0.0476	1.56
3	*TACC3*	No	0.0019	0.0532	1.54
4	*PIMREG*	No	0.0079	0.0591	1.53
5	*KIF14*	No	0.0038	0.0536	1.53
6	*ESPL1*	No	0.0015	0.0520	1.37
7	*GAS2L3*	No	0.0050	0.0553	1.33
8	*NDC80*	No	0.0076	0.0587	1.27
9	*KNSTRN*	No	0.0037	0.0536	1.27
10	*GPSM2*	No	0.0025	0.0534	1.23
11	*SPAG5*	No	0.0007	0.0501	1.23
12	*KIF18B*	No	0.0030	0.0534	1.20
13	*IQGAP3*	No	0.0037	0.0536	1.17
14	*UBE2S*	No	0.0004	0.0476	1.17
15	*DDIAS*	No	0.0008	0.0501	1.11
16	*NDE1*	No	0.0046	0.0547	1.11
17	*DIAPH3*	No	0.0072	0.0578	1.10
18	*CKS2*	No	0.0035	0.0536	1.10
19	*RAD54L*	No	0.0014	0.0516	1.08
20	*CEP128*	Yes	0.0035	0.0536	1.04

B Down-regulated

	Gene	HES1 target	p-value	q-value	log2FC
1	*TUBB*	No	0.0003	0.0476	-1.28
2	*HIST1H2AC*	No	0.0012	0.0511	-1.07
3	*H1F0*	No	0.0006	0.0487	-0.91
4	*CCNE2*	No	0.0038	0.0536	-0.86
5	*SPACA6*	No	0.0084	0.0600	-0.84
6	*PLEKHS1*	No	0.0066	0.0566	-0.84
7	*C9orf152*	No	0.0050	0.0553	-0.83
8	*HIST1H2BJ*	No	0.0055	0.0553	-0.82
9	*SMARCD3*	No	0.0053	0.0553	-0.80
10	*TGFB3*	No	0.0004	0.0476	-0.80
11	*PPP1R3C*	No	0.0025	0.0534	-0.79
12	*VAMP2*	No	0.0023	0.0532	-0.78
13	*ZNF587B*	No	0.0073	0.0579	-0.76
14	*PPP1R3D*	No	0.0044	0.0544	-0.74
15	*FBXO46*	No	0.0018	0.0532	-0.73
16	*MAT2A*	No	0.0072	0.0579	-0.72
17	*THAP2*	No	0.0025	0.0534	-0.72
18	*CLDND2*	No	0.0078	0.0590	-0.72
19	*ZNF121*	No	0.0100	0.0630	-0.71
20	*EDA2R*	No	0.0042	0.0540	-0.70

JI051/Nocodazole

C Up-regulated

	Gene	HES1 target	p-value	q-value	log2FC
1	*CYP1A1*	No	0.0003	0.0544	3.36
2	*CYP1B1*	No	0.0003	0.0544	2.42
3	*MALL*	No	0.0036	0.0706	2.25
4	*EGR1*	No	0.0013	0.0624	2.13
5	*RASD1*	No	0.0004	0.0557	2.07
6	*PHLDA1*	Yes	0.0011	0.0619	2.04
7	*F2RL1*	No	0.0098	0.0846	1.93
8	*EDN1*	No	0.0041	0.0714	1.74
9	*CLDN1*	No	0.0032	0.0691	1.63
10	*MYADM*	No	0.0020	0.0652	1.61
11	*NEDD9*	No	0.0042	0.0714	1.54
12	*CCN1*	No	0.0004	0.0557	1.51
13	*GBP1*	No	0.0053	0.0732	1.46
14	*MACC1*	No	0.0002	0.0544	1.46
15	*OXTR*	No	0.0077	0.0791	1.46
16	*CCN2*	No	0.0001	0.0544	1.45
17	*RAB7B*	Yes	0.0042	0.0714	1.42
18	*KCNF1*	No	0.0001	0.0544	1.41
19	*THBS1*	No	0.0010	0.0607	1.40
20	*DKK1*	No	0.0021	0.0652	1.39

D Down-regulated

	Gene	HES1 target	p-value	q-value	log2FC
1	*GNL1*	No	0.00629	0.07541	-2.44
2	*PSCA*	No	0.00499	0.07322	-0.86
3	*PPP1R3C*	No	0.00237	0.06524	-0.80
4	*AURKB*	No	0.00657	0.07632	-0.69
5	*BLM*	No	0.00285	0.06691	-0.65
6	*PLCH1*	Yes	0.00054	0.0584	-0.64
7	*E2F8*	No	0.00479	0.0729	-0.62
8	*PRR15L*	No	0.0078	0.07946	-0.62
9	*PSRC1*	No	0.00096	0.06074	-0.61
10	*PTPRU*	Yes	0.00634	0.07541	-0.59
11	*LRRC75B*	No	0.00796	0.08029	-0.56
12	*RMI2*	No	0.00924	0.08344	-0.56
13	*CDK2*	No	0.0045	0.07137	-0.56
14	*FANCG*	No	0.00337	0.06921	-0.55
15	*WDR90*	Yes	0.00725	0.07825	-0.55
16	*BDH1*	No	0.00573	0.07329	-0.55
17	*ANKRD35*	No	0.00287	0.06691	-0.54
18	*ARHGEF2*	No	0.00204	0.06524	-0.54
19	*TUBB*	No	0.00177	0.06524	-0.53
20	*E2F2*	No	0.00021	0.05444	-0.53

Table(s) 1. Differentially expressed genes in JI051-arrested cells as measured by RNA-seq Tables (A-B) list the top 20 up/down-regulated genes in JI051 arrested cells compared to control cells 4 hours after nocodazole release (DMSO) and prometaphase cells (Noca). Genes were selected based on significance ($p < 0.01$) and fold change as represented by Log2FC.

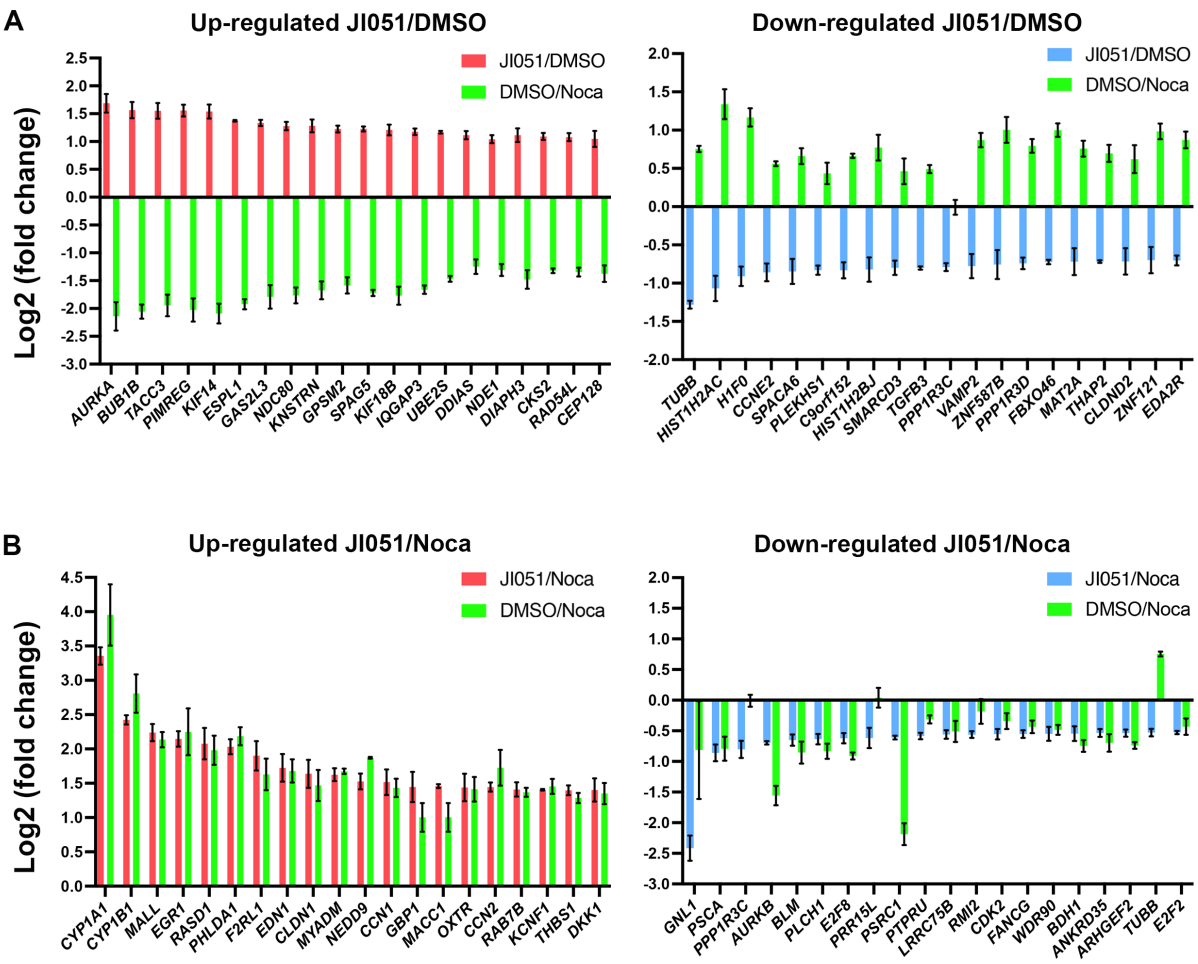

Fig 5.2.7 Top 20 up/down-regulated genes in JI051-arrested cells

The log2FC for genes is presented for significant genes ($p < 0.01$) up/down-regulated in JI051-treated cells compared to DMSO **(A)** and nocodazole **(B)**. The log2FC for each gene is also presented for the control DMSO/Noca group (green bars). Error bars indicate mean ± SEM for 3 biological replicates.

As well, as investigating the most significantly DE genes, I assessed the effect of the JI051 arrest on genes belonging to core components of mitotic regulation. I divided this analysis into three groups relating to the mitotic kinases, *CCNB1* and known activators of *CCNB1* expression, and the mitotic checkpoint complex. The data represents Log2FC comparing expression in early G1 to prometaphase (DMSO/Noca), considered the control group, and JI051 arrest to early G1 (JI051/DMS0) (Fig. 4.2.8).

In control cells, expression was down-regulated for *CCNB1* (-1.75), *FOXM1* (-1.1), and *B-MYB* (-0.78) upon exit from mitosis. In JI051 arrested cells expression is sustained

for *CCNB1* (1.4), *FOXM1* (0.68), and *B-MYB* (0.44). indicating that the expression of these genes decreases marginally after release from nocodazole. *C-MYB* expression across samples was relatively stable (DMSO/Noca: 0.12, JI051/DMSO: 0.04). *MYC* expression was upregulated in control cells and JI051 arrested cells and there was no difference in expression between JI051/DMSO. As both JI051 and control cells were released into fresh media from nocodazole arrest, the upregulation of *MYC* likely reflects a serum response. This data agrees with my previous qPCR data for *CCNB1* expression. For its potential transcriptional activators, beyond their sustained expression, this data does not strongly indicate up-regulation for any of these genes that might contribute to sustained *CCNB1* transcription in JI051 treated cells. Apart from *MYB*, which showed no significant change in expression for both groups, no other *CCNB1* activator was identified as a HES1 target.

Gene expression is presented for the mitotic kinases; *CDK1*, *AURKA, AURKB*, *PLK1*, *MASTL*, and *NEK2.* As discussed in the introduction to chapter 4, these proteins play critical roles in regulating mitosis. *CDK1* holds a hierarchical position in the initiation of early mitotic events. The aurora kinases, *AURKA* and *AURKB* are important for regulating spindle assembly and attachment of microtubules to sister chromatids alongside *PLK1* which also plays a role in regulating sister chromatid cohesion (Kettenbach et al., 2011). *MASTL* prevents premature inactivation of the SAC through negative regulation of the phosphatase PP2A/B55 (Diril et al., 2016). *NEK2* also plays a role in microtube attachment to the kinetochore through phosphorylation of NDC80 (Du et al., 2008). In control cells the expression of the mitotic kinases was down-regulated upon G1 entry: *CDK1* (-0.7) *AURKA* (-2.1)*, AURKB* (-1.6), *PLK1* (-2.0), *PLK4* (-1.36), *MASTL* (-1.2), and *NEK2* (-1.85). In JI051 treated cells, there was no difference between JI051 and DMSO expression. For the rest of the mitotic kinases, their gene expression was sustained in JI051-treated cell compared to control cells. *AURKA* (1.68)*, AURKB* (0.86), *PLK1* (1.5), *PLK4* (0.86), *MASTL* (0.87), and *NEK2* (1.22).

Overall, it is difficult to say whether the sustained, but slightly lower than prometaphase, gene expression observed for mitotic genes during the JI051 arrest is indicative of impaired function or simply a decrease that occurs when cells are

released from prometaphase. In chapter 4 I showed that a similar level of CDK substrate phosphorylation in nocodazole and JI051 arrested cells, indicating that CDK1 is functional. Assessing the kinase activity of the mitotic kinases individually in JI051-arrested conditions would inform on whether these proteins are impaired or functional. Furthermore, assessing the correct localisation of proteins involved in kinetochore/microtubule assembly in mitotic cells would inform on whether JI051-arrested cells can establish kinetochore-microtubule attachments.

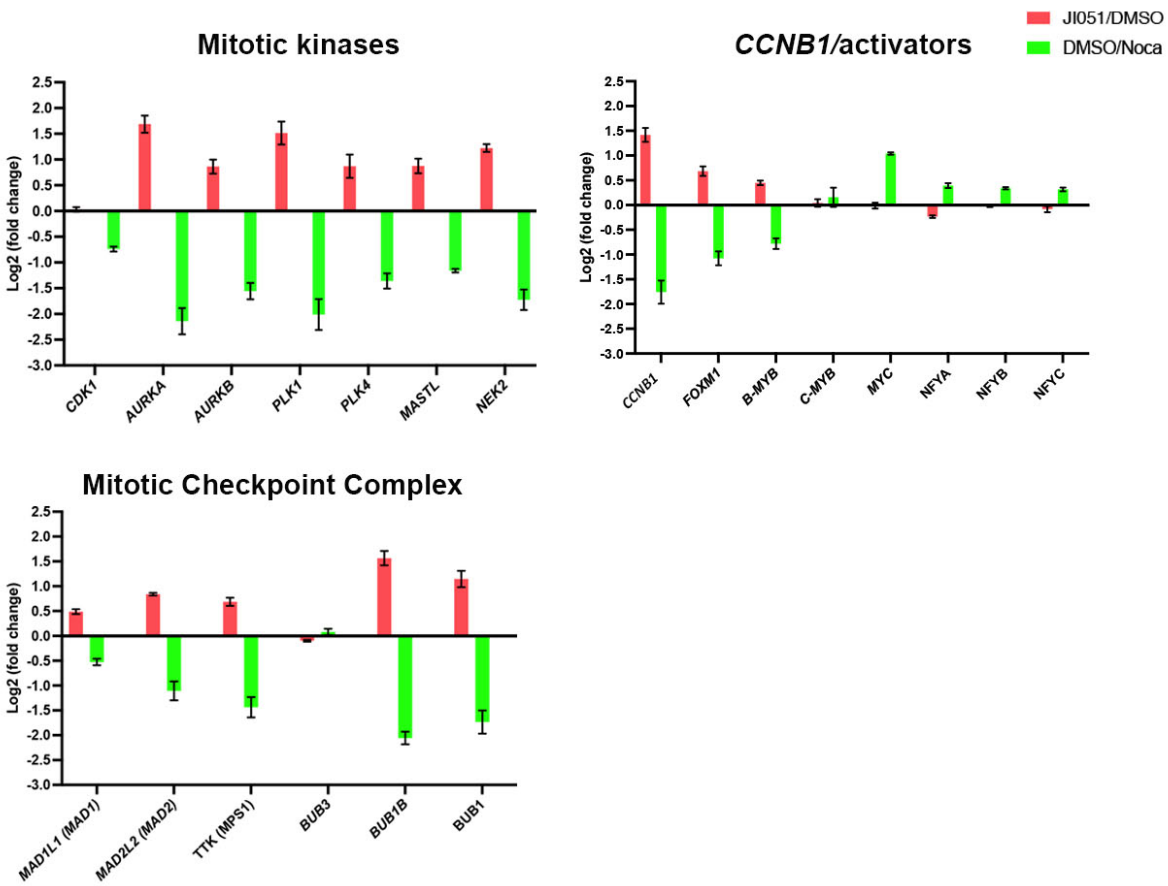

Fig. 5.2.8 RNA-seq analysis of mitotic gene expression

Log2FC of genes associated with mitotic kinases (top left), *CCNB1* and its activators (top right) and mitotic checkpoint genes (bottom left). Log2FC is presented for two groups JI051 vs DMSO (red) and the control group DMSO vs Noca (green). Error bars indicate mean ± SEM for 3 biological replicates

In line with the original aim set out at the beginning of this chapter, I sought to identify HES1 targets whose expression could potentially be up-regulated due to JI051 inhibition of HES1 repression. For this, I used high confidence HES1 targets to consolidate a list of 308 unique genes, which were in at least one IDR dataset. For the 308 genes merged from the GFP IDR datasets, I identified HES1 targets that were found to be differentially expressed based on the RNA-seq data. For this, I used the entire RNA-seq data and did not limit identification to genes that showed either $p < 0.01$ or $q < 0.05$ as described in 5.2.4. The entire RNA-seq dataset consisted of 15323 protein coding transcripts, 528 not annotated (NA) transcripts, 7 long non-coding RNAs (LncRNA), 6 transcribed unitary pseudogenes, and 9 transcribed unprocessed pseudogenes (Fig 5.2.9 A). Of the 15873 DE genes 234 were HES1 targets (Fig 5.2.9 A). I then sorted this list to identify the genes that were upregulated in JI051-arrested cells compared to DMSO (JI051/DMSO) and nocodazole arrested cells JI051/Noca. The top 20 DE genes based on Log2 fold change for each group are presented here alongside the Log2 fold change for control cells (DMSO/Noca) (Fig 5.2.9 B). As mentioned on page 145/146, identifying significantly expressed genes was performed using the following criteria: $q < 0.05$ or $p < 0.05$ significance threshold combined with a log2 fold-change of 1.5. No HES1 target passed the 1.5 Log2FC and not all targets passed the $p < 0.05$ significance threshold. Genes ($p < 0.05$) upregulated in JI051-treated cells compared to control cells in G1 included: *CHTF18*, *FOXN3*, *SYT7*, *TBC1D5*, and *YWHAH.* Genes ($p < 0.05$) upregulated in JI051-treated cell compared to nocodazole-arrested cells included: *NHSL2*, *SMAD3*, *TRIB1*, *ADAMTS9*, *ATP2B1*, *HES1*, *SPRED2*, *SEMA3C*, and *ARID5B.* That high-confidence HES1 targets did not meet the more stringent RNA-seq criteria for differential gene expression (Log2 fold change above 1.5 or $q < 0.05$ significance) indicates that inhibition of HES1 target repression is not a prominent feature of the JI051 mitotic arrest.

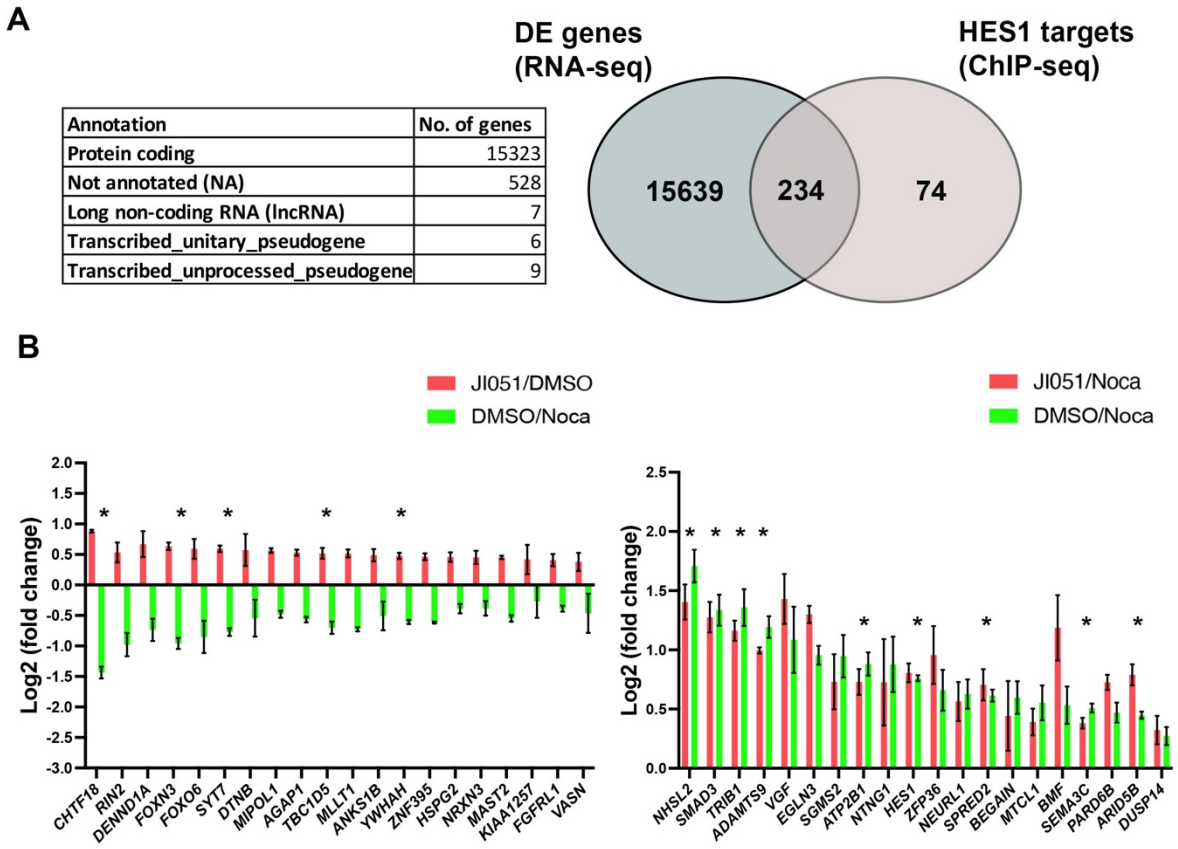

Annotation	No. of genes
Protein coding	15323
Not annotated (NA)	528
Long non-coding RNA (lncRNA)	7
Transcribed_unitary_pseudogene	6
Transcribed_unprocessed_pseudogene	9

Fig 5.2.9 RNA-seq analysis of HES1 target genes

(A) Left, table displaying number of different biotypes in RNA-seq datase. Right, Venn diagram showing overlap of HES1 targets with differentially expressed genes identified by RNA-seq. Only high confidence HES1 targets ($q < 0.05$ MACS2 peak-calling and IDR analysis) from the 3 GFP ChIP biological replicates were used for comparison with RNA-seq data. **(B)** Right, Log2FC of HES1 targets in JI051-arrested cells vs control cells (JI051/DMSO). Left, Log2FC of HES1 targets in JI051-arrested cells vs prometaphase cells (JI051/Noca). In both comparisons the corresponding 'control' gene expression fold-change DMSO/Noca is shown. Genes that passed the $p < 0.5$ significance threshold are marked by an asterisk. Error bars indicate ± SEM from 3 biological replicates. Biotype characterisation of RNA-seq dataset was performed by Dr. Soumita Ghosh, a former member of Dr. Hyungwon Choi's lab at National University Singapore.

5.3 Discussion

5.3.1 HES1 autoregulation in G1 and identification of novel HES1 targets

In this chapter, I demonstrated by ChIP-seq that HES1 binds to its own promoter upon entry into G1. In chapter 4 I showed that *HES1* exhibits a distinct pattern of expression during the M-G1 transition where *HES1* expression increases and peaks at 2 hours followed by a period of down-regulation between 2 and 4 hours after release from nocodazole (Fig 4.2.2). The concurrent binding of HES1 to its own promoter at 4 hours is supportive of a role for negative feedback in the down-regulation of *HES1* in early G1 in MCF7 cells. This is result is reminiscent of earlier studies that first showed autoregulatory control of *HES1* and cyclic expression expression of HES1 at mRNA and protein levels in fibroblast released from serum starvation (Hirata et al., 2002). However, as the RNA timecourse in Fig 4.2.2 was not performed beyond four hours in RNA expression in this thesis, whether or not *HES1* expression exhibits oscillatory expression cannot be concluded. The enrichment of HES1 on its own promoter was also variable, with increased enrichment observed at 4 hours compared to 8 hours after release from nocodazole arrest (Fig 5.2.1 C). If HES1 binding to its own promoter mediates down-regulation of *HES1*, the degree to which it binds could be influenced by the preceding expression of *HES1.* A continuation of the timecourse in 4.2.2 extending from 4 to 8 hours to examine *HES1* expression between 4 and 8 hours could provide information on the relationship between HES1 promoter binding and the levels of *HES1* expression. In general, identification of HES1 binding to its own promoter in MCF7 cells is significant as it provides evidence that HES1 can regulate its own expression in MCF7 cells. Experimental and computational modeling have demonstrated how autoregulatory control of *HES1* expression is a core component of the regulatory network that enables oscillatory *HES1* expression (Hirata et al., 2002; Monk 2003; Momiji & Monk 2008). The differential binding of HES1 to its promoter at 4 and 8 hours could also reflect how *HES1* is subsequently expressed during cell cycle progression. Although, my smFISH data in Chapter 2, largely demonstrates the substantial cell-to-cell heterogeneity in *HES1* expression, a trend of increasing mRNA abundance was highlighted inferred to occur in a cell cycle dependent manner. Changes in the

strength of HES1 negative feedback during the cell cycle is one method by which *HES1* levels could be modulated during the cell cycle.

HES1 enrichment on its promoter was significantly reduced in JI051-treated cells 4 hours after release from nocodazole. However, the fact that the enrichment of HES1 in JI051-treated cells was comparable to nocodazole arrested cells (Fig 5.2.1) suggests that this could be more a consequence of cells being arrested in mitosis rather than inhibition of HES1 binding to its own promoter by JI051. Moreover, the upregulated targets of HES1 in JI051-treated cells (Fig 5.2.9) represent genes that are more highly expressed during G2/M, indicating that the expression profile for these genes is more a reflection of the mitotic arrest state. Of the targets I validated *TRIB1* was significantly upregulated in JI051 cells compared to nocodazole arrested cells. It was also upregulated in control cells (DMSO/Noca) at a similar level to JI051-treated cells, indicating that JI051 had a negligible effect on its expression.

Identification of known HES1 targets such as *HES1*, *NEUROG3*, and *ASCL1* in the ChIP-seq data served as validation for the ChIP-seq experiment. The initial aim of ChIP-sequencing was to identify potential HES1 targets that could regulate the sustained expression of mitotic genes, such as *CCNB1* during JI051 treatment. The identification of *MYB* (c-MYB) as a HES1 target provided a link between indirect HES1 regulation of *CCNB1* expression as c-MYB has been shown to activate *CCNB1* expression (Nakata et al., 2007; Okada et al., 2002). *MYB* has also been implicated in promoting breast cancer proliferation in ER+ cells. In response to β-estradiol *MYB* expression was found to be upregulated in MCF7 cells (Drabsch et al., 2007). In a separate study, the opposite effect was observed for *HES1* expression after 17β-estradiol treatment of MCF7 cells (Müller et al., 2002). Although indirect, this inverse relationship is supportive of the idea that HES1 may repress *MYB*. The broad up-regulation of mitotic genes revealed by RNA-seq demonstrated a correlation between mitotic gene expression and the mitotic arrest, suggesting that sustained *CCNB1* is a consequence rather than a cause of the arrest. Furthermore, HES1 enrichment on the *MYB* promoter was not significantly decreased in JI051-treated cells and *MYB* expression was not significantly altered in JI051-treated cells, ruling

out inhibition of HES1 repression of *MYB* as a potential cause for sustained *CCNB1* expression during JI051 treatment. Nonetheless, the identification of *MYB* as a HES1 target is important for future investigation into indirect links between HES1 and cell cycle control. ChIP-seq analysis of c-MYB targets in MCF7 cells identified numerous genes with known cell cycle functions including *CCNB1*, *CCNE1*, *myc*, and *KLF4*, with *CCNB1* and *KLF4* showing increased expression after c-MYB binding in response to estradiol (Quintana et al., 2011). Further study to clarify the potential effect of HES1 binding to the *MYB* promoter on *MYB* expression will be useful to assess how HES1 could indirectly influence the expression of cell cycle targets of c-MYB. Interestingly, HES1 and c-MYB have previously been identified as binding partners in a protein dimer that repressed CD4 expression in T-cells (Allen et al., 2001).

A notable HES1 target discovered here, which to my knowledge has not been described before was *TRIB1*, a homolog of the Drosophila *tribbles* pseudokinase (Eyers et al. 2017). *TRIB1* was upregulated in JI051-arrested cells compared to cells in prometaphase but wasn't differentially expressed compared to control cells in G1. *TRIB1* has previously been identified as an immediate-early genes so the upregulation of *TRIB1* observed in this experiment may reflect a response to mitotic cells being re-plated in fresh media (Aitken et al., 2015). In a developmental setting Tribbles has been shown to regulate the timing of mitotic entry during Drosophila oogenesis by promoting the degradation of CDC25 (Mata et al., 2000). In a mammalian context TRIB1 has been implicated in a diverse range of signaling pathways (Eyers et al., 2017). TRIB1 has been identified as a tumorigenic factor in a number of different cancers, including acute myelogenous leukemia (AML), hepatocellular carcinoma and breast cancer, and has also been shown to negatively regulate p53 (Gendelman et al., 2017; Ye et al., 2017).

Two intriguing HES1 targets identified by ChIP-seq were the basic helix-loop-helix transcription factors *BHLHE40* and *BHLHE41*, with *BHLHE41* being verified as a HES1 target by ChIP-qPCR (Fig 5.2.4). *BHLHE40* and *BHLHE41*, otherwise known as *DEC1* and *DEC2*, respectively, are both involved in the molecular regulation of the circadian

clock, where they inhibit CLOCK/BMAL1 activation of genes such as *Per1* through competitivebinding to E-boxes in gene promoters or by binding to the CLOCK/BMAL1 complex (Butler et al., 2004; Honma et al., 2002). The molecular machinery of the circadian clock and the cell cycle have been shown to interact with each other and alterations to circadian signaling have been implicated in cancer development (Lin & Farkas, 2018; Savvidis & Koutsilieris, 2012). CLOCK/BMAL1 regulation of *wee1*, *Cdkn1a,* and *Ccnb1* has been demonstrated to control entry into mitosis, suggesting that components of circadian signaling 'gate' cell division (Farshadi et al., 2019; Gréchez-Cassiau et al., 2008; Matsuo et al., 2003). Furthermore, studies have investigated synchronisation between circadian and cell cycle oscillations and the influence this may have on tumorigenesis when either of the two processes is dysregulated (Feillet et al., 2014, 2015; Nagoshi et al., 2004). Using luciferase reporters of BMAL2 and PER2 expression, circadian oscillations were observed for these genes in MCF7 cells but not MDA-MB-231 cells (Lellupitiyage Don et al., 2019). HES1 oscillations in the MCF7-HES1-mVENUS line used here were described as 'circadian-like' due to their ~26 hour periodicity (Sabherwal et al., 2021). Combined with the identification of components of circadian signaling (*BHLHE40* and *BHLHE41*) as HES1 targets, the potential for cross-talk between HES1, circadian, and cell cycle dynamics is an alluring area of further study.

With a growing body of evidence supporting a role for HES1 in various aspects of cancer development (Liu et al., 2015), identifying HES1 targets, especially targets with known oncogenic functions, will be critical to enhance descriptions of HES1 in a cancer context. To this end, my identification of HES1 targets in the MCF7 ER+ breast cancer cell line provides useful information on the regulatory pathways that HES1 could influence in breast cancer.

5.3.2 The effect of JI051-induced gene expression changes on mitotic signaling

Overall, the RNA-seq results reveal a sustained upregulation of mitotic gene expression in JI051 arrested cells. It is therefore difficult to pinpoint a specific cause for the mitotic arrest based solely on gene-expression, as the sustained expression of numerous genes will likely be a correlation with the mitotic arrest rather than a cause. Moreover, the up-regulation of mitotic kinases does not inform on their activity. For example, *AURORA A* was the most up-regulated mitotic kinase in JI051-arrested cells 4 hours after release from nocodazole arrest. However, the sustained expression of *AURORA A* in JI051-arrested cells was lower than *AURORA A* levels in prometaphase. This introduces an uncertainty/conundrum as to whether JI051-arrested cells have diminished AURORA A function, due to lower expression, with respect to cells in prometaphase or sustained AURORA A activity. Both over-expression and inhibition of AURORA A is associated with mitotic defects and genomic instability. In HeLa cells, over-expression of AURORA A causes defects in mitosis that lead to cell tetraploidization and which are associated with centrosome amplification (Meraldi et al., 2002). On the other hand, AURORA A inhibition can also cause defects in mitotic progression. An increase in mis-aligned chromosomes in mitotic cells was observed in HeLa cells expressing siRNAs against *AURORA A* as well as increased numbers of multi-nucleated cells. In the same study, injection of anti-AURORA A antibodies into prometaphase-arrested cells resulted in reduced chromosome congression at the metaphase plate (Marumoto et al., 2003). Use of AURORA A kinase inhibitors, such as MLN8054 (ATP-competitive inhibitor), revealed defects in chromosome alignment and subsequently lagging chromosomes during anaphase resulting in aneuploidy in treated HCT-116 cells. These defects were also accompanied by a delay in mitosis from 1 to 2 hours, which is shorter than the 6 hour + delay I showed in chapter 3 for JI051-treated cells (Hoar et al., 2007), However, a separate AURORA A inhibitor, LY3295668, has been shown to induce a sustained mitotic arrest that ultimately leads to apoptosis (Du et al., 2019). In this study the AURORA A substrate TACC3 was also one of the most upregulated genes in JI051-arrested cells compared to controls cells in early G1 (Fig 5.2.7). TACC3 functions by binding to microtubules and recruiting ch-TOG to promote microtubule stabilisation, which requires AURORA A phosphorylation of TACC3 (Gergely et al., 2003; Kinoshita

et al., 2005). If the sustained expression of *AURORA A* and *TACC3* contributes to sustained microtubule stabilisation it could prevent the transition to anaphase A, which is dependent on microtubule depolymerisation to induce chromosome segregation (Asbury, 2017). *AURORA B* showed sustained expression in JI051-treated cells compared to control cells in G1 but was significantly down-regulated compared to nocodazole arrested cells (Fig 5.2.7/Table 1). Use of AURORA B inhibitors and siRNA has been shown to induce defects associated with polyploidisation (Ditchfield et al., 2003; Hauf et al., 2003; Wilkinson et al., 2007). However, these defects are not associated with prolonged mitotic arrests. Also, the sustained phosphorylation of ser10 on HISTONE H3, a substrate of AURORA B, shown in the western blots in Fig 4.2.2 is indicative of functional AURORA B signalling, ruling out compromised AURORA B signalling as a cause of JI051-induced mitotic defects. Indeed, a similar co-treatment experiment like the JI051+R03306 performed in Fig 4.2.3 but using an AURORA B inhibitor like Hesperadin, which overrides the SAC, could be performed. If the JI051-induced arrest was reversed in this case, it would provide further evidence that the arrest occurs due to activation of the SAC. PLK1 inhibition has been shown to induce prolonged prometaphase arrest, associated with reduced γ-tubulin levels and the formation of monopolar spindles (Lénárt et al., 2007; Rudolph et al., 2009). In this way, the effect of JI051 more closely resembles mitotic defect phenotypes that occur due to prolonged activation of the SAC.

To decipher the origin of the JI051 mitotic arrest, proteomic studies could be employed to assess changes in protein abundance and the phospho-proteome in JI051-arrested cells. Previous studies have described the mitotic phospho-proteome and detailed changes in phosphorylation during progression through mitosis (Ly et al., 2017; Nousiainen et al., 2006; Olsen et al., 2010). Furthermore, phospho-proteomics have been performed in mitotic cells treated with inhibitors for the mitotic kinases (Kettenbach et al., 2011; Petrone et al., 2016). Comparison of a potential JI051-arrested phospho-proteome with these datasets could help identify the signaling pathways JI051 interferes with during mitosis.

The β-tubulin gene *TUBB* was a notable DE gene in JI051-arrested cells, as it showed decreased expression compared to prometaphase and control cells (Fig 5.2.7). Microtubule polymerisation in mitosis occurs when β-tubulin and α-tubulin heterodimers are assembled into protofilaments by multiprotein γ-tubulin complexes, known as γ-TuRCs (Tovey & Conduit, 2018). The subsequent formation of microtubules and their interaction with sister chromatids is fundamental to a successful mitosis (Meunier & Vernos, 2012). The mRNA stability of tubulin genes is known to be affected by microtubule depolymerisation, with treatments like colchicine and nocodazole leading to reduced expression (Cleveland 1989; Ben-Ze'ev et al., 1979). Therefore, continued down-regulation of *TUBB* in JI051-treated cells after release from nocodazole may reflect a situation where microtubules remain depolymerised. Down-regulation of *TUBB* has been reported in RPE1 cells treated with the microtubule destabliser, Combretastatin A-4, however this experiment was performed in quiescent cells (Gasic et al., 2019). I have performed a preliminary immunofluorescent experiment to assess chromatin structure and HES1 localisation in cells released from nocodazole into JI051. In this experiment I did not detect any JI051-treated cells that had progressed beyond a prometaphase-like chromatin structure. In control cells, metaphase and anaphase cells could be identified based on DAPI staining of congressed and segregated chromosomes at 2 and 4 hours after release (Fig 5.3.1). This preliminary data suggests that JI051 cells are delayed, if not arrested completely in prometaphase. Perron, et al also noted an increase in mitotic cells after 24 hours of JI051 treatment alongside an increase in G2 cells identified by FUCCI (Perron et al., 2018). Again, this suggests that JI051-treated cells arrest due to SAC activation. This could be due to cells not being able to establish proper kinetochore-microtubule attachments, which could result from incomplete assembly of the mitotic spindle or incomplete kinetochore formation. Sustained microtubule depolymerisation would also contribute the arrest observed in Fig 5.3.1 supporting identification of *TUBB* down-regulation as a useful insight into the JI051 arrest. Immunofluorescent experiments should be performed to fully assess the integrity of the mitotic spindle in JI051-arrested cells. This would be done using antibodies against either β-tubulin or α-tubulin alongside staining for kinetochore proteins to assess their localisation.

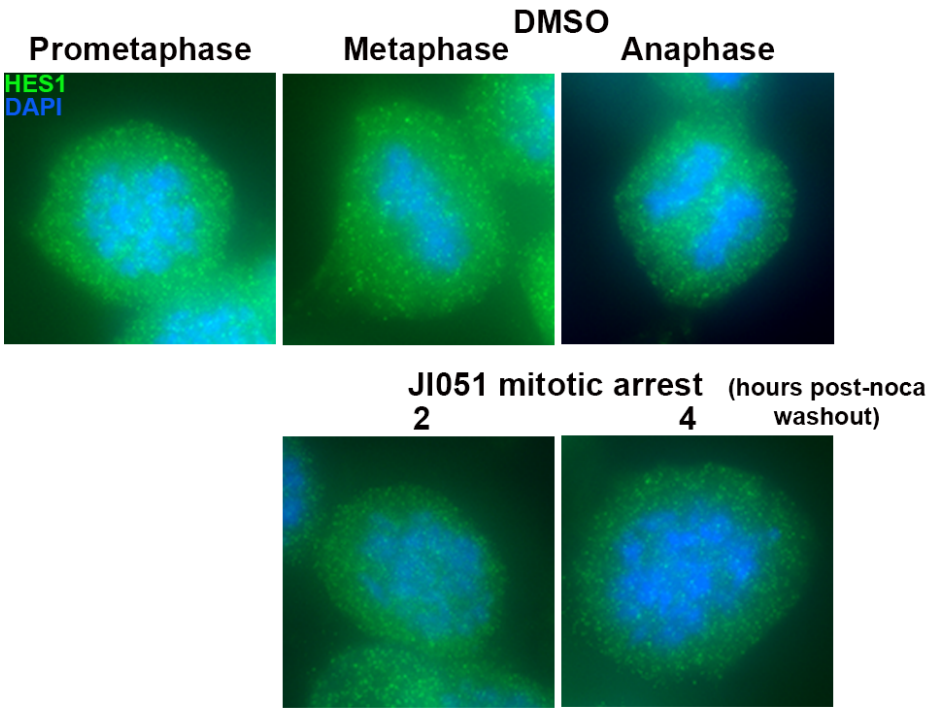

Fig 5.3.1 Preliminary analysis of progression through mitosis in JI051-treated cells
Mitotic and JI051-treated MCF7-HES1-mVENUS cells. Z-projections of 41 images taken at 0.2 µm intervals. Top panel left to right, cell in prometaphase (nocodazole-arrested), control metaphase cell, control anaphase cell. Bottom panel, 2 and 4 hours after release from nocodazole JI051 do not exhibit chromosome congression at the metaphase plate. Images acquired using widefield microscope. HES1-mVENUS was detected using GFP antibody recognising VENUS tag

5.3.3 Potential involvement of dysregulated PHB2 function in the mitotic arrest

Consideration must also be given to the potential role of de-regulated PHB2 signaling in the mitotic arrest observed after JI051 treatment. As JI051 was determined to stabilise a HES1-PHB2 complex, PHB2 signaling independent of HES1 function may also be disrupted. PHB2 has found to be involved in the regulation of a number of cellular process, such as transcription, apoptosis and metabolism (Bavelloni et al., 2015). Although no mitotic defects were reported after PHB2 siRNA knockdown by Perron et al 2018 in HEK293 cells, indicating that the mitotic defects observed upon JI051 treatment did not occur through PHB2 signaling alone, there are previous reports that do support a role for PHB2 in regulating mitosis. Contradictory reports have observed an increase in mitotic cells after PHB2 siRNA knockdown in HeLa cells

(Takata et al., 2007; Lee et al., 2011). In HeLa cells PHB2 localisation was observed on chromosomes during prophase and prometaphase. When PHB2 was depleted chromosomes did not align properly at the metaphase plate. Metaphase-chromosome spreads of PHB2 depleted cells showed that sister chromatids were separated along the entire length of the chromosome. In this study PHB2 was concluded to play a protective role in preventing early phosphorylation of centromeric cohesion by PLK1 (Takata et al., 2007). Another study reported an increase in prometaphase cells upon PHB2 knockdown and a reduction in HEC1 and CENP-F kinetochore localisation in HeLa cells. Over-expression of Lamprey PHB2 in HeLa cells was found to increase the proportion of G2/M cells. This was associated with decreased protein levels of Cyclin B1, CDK1, PLK1, CDC25C and phosphorylated Cyclin B1 and CDK1, suggesting that normal PHB2 signaling may be important for the G2/M transition, however, no mechanism for how PHB2 regulates the above proteins was presented (Shi et al., 2018). PHB2 has also previously been reported to act as a transcriptional repressor of *E2F1* through direct binding with Rb leading to a decrease in cell proliferation in T47D cells (Wang et al., 1999). Expression of PHB2 mutants incapable of binding RB reversed repression of *E2F1* transcription (Wang et al., 1999). PHB2 was also found to translocate to the nucleus of HeLa and MCF7 cells in the presence of estradiol to mediate transcriptional repression of ER target genes (Kasashima et al., 2006; Montano et al., 1999). PHB2 has also been reported to interact with histone deacetylases (Kurtev et al., 2004) This information suggests that impairment of PHB2 function due to stabilisation of HES1-PHB2 complexes could also lead to defects in transcriptional repression, and most relevant to the results presented here, defects in mitosis progression.

5.3.3 Concluding remarks

The aim of the final chapter of this thesis was to examine further whether the mitotic arrest observed in JI051-treated cells could arise due to inhibition of HES1 transcriptional repression. To this end, HES1 ChIP-seq and RNA-seq was performed to identify HES1 targets that could lead to sustained activation of *CCNB1* and subsequent CDK1 activity. Identification of *MYB* an transcriptional activator of *CCNB1* as a HES1 target provided a link to sustained *CCNB1* expression. However,

HES1 binding to *MYB* was not significantly decreased in JI051-arrested cells, nor was *MYB* expression changed. Widespread up-regulation of mitotic genes revealed by RNA-seq indicates that *CCNB1* expression was more likely a correlation with the mitotic arrest than an initial cause. Decreased expression of the β-tubulin gene *TUBB* suggested that microtubule defects could be involved in the arrest. My preliminary data demonstrating that JI051 cells do not exhibit chromosome congression after release from nocodazole is supportive of this. My ChIP-qPCR validation of novel HES1 targets identified by ChIP-seq in MCF7 cells will be informative for further study of HES1 in a breast cancer context.

Chapter 6: General discussion, summary and suggestions for future work

6.1 Overview of findings

In the thesis introduction, I posed 3 broad questions that stood as motivation for the experimental work undertaken in this thesis. These 3 questions were:

1. How is *HES1* expression coupled with the temporal events of the cell cycle?
2. Does HES1 expression have a functional role in controlling cell cycle progression?
3. Can HES1 targets related to this function be identified?

The first question was motivated by the aim to better understand how HES1 signaling dynamics relate to cellular decisions based on proliferation. HES1 has been extensively studied in developmental contexts, such as neurogenesis and pancreatic development (Hatakeyama et al., 2004; Kobayashi & Kageyama, 2014; Seymour et al., 2020). Premature differentiation of progenitor cells upon loss of *Hes1* or aberrant control of progenitor pools due to elevated HES1 function, highlight the importance of HES1 in controlling the proliferative capacity of stem cells (Ishibashi et al., 1995; Ohtsuka and Kageyama 2021; Shimojo et al., 2008). The elucidation of the *Hes1* regulatory network, based on autoregulatory control of *Hes1* transcription and negative regulation by miR-9 (Hirata et al*.,* 2002; Bonev et al., 2012), provided a molecular framework that could explain how HES1 ultradian dynamics, observed in *in vitro* settings, are generated (Shimojo et al., 2008; Kobayashi et al., 2009). Experimental manipulation of HES1 dynamics has since demonstrated the functional importance of HES1 signaling dynamics in controlling cell fate and regulating the proliferation versus quiescence decision in neural progenitors (Imayoshi et al., 2013; Marinopoulou et al., 2021; Sueda et al., 2019).

A key question emerging from the study of HES1 in developmental systems is how HES1 expression dynamics are integrated with the cell cycle. Numerous studies have provided evidence that HES1 controls the expression of cell cycle regulators, notably

both positive and negative regulators of the cell cycle e.g. *CDKN1B*, *E2F1*, *CCND1* (Hartman et al., 2004; Murata et al., 2005; Kabos et al., 2002; Noda et al., 2011; Georgia et al., 2006; Shimojo et al., 2008). Thus, it seems intuitive to ascribe targeting of different cell cycle genes to upstream HES1 dynamics, with oscillatory HES1 expression in proliferating cells indicating repression of negative regulators of the cell cycle. However, this is a relatively simplistic view, and other factors will also influence HES1 function. For example, *E2F1* repression by HES1 in T47D cells was determined to occur through HES1 as part of a heterodimer with HERP1-2 (Hartman et al., 2004). Additionally, repression of *CDKN1B* by HES1 in HeLa cells was not affected by mutation of the WRPW domain that enables binding of the TLE co-repressor, indicating that different HES1 co-repressors may also dictate gene repression (Murata et al., 2005). Multiple binding partners of HES1 have been identified, which are likely to influence gene targeting in different contexts (Fischer and Gessler 2007; Iso et al., 2001), Moreover, imaging of transcription factor dynamics has revealed the 'noise' that can exist within oscillatory signals, in terms of frequency and amplitude, which can in turn influence the cell response (Purvis & Lahav 2013; Loewer et al., 2010; Reyes et al., 2018; Sueda et al., 2019). Additionally, the outcome of transcription factor signaling can be influenced by a cell's position in the cell cycle, as has been demonstrated for the NF-κB inflammation response and SMAD signalling in hESCs (Ankers et al., 2016; Pauklin & Vallier, 2013).

With these points in mind, a more refined view of how *HES1* dynamics potentially influence cell cycle control, can be obtained by observing how *HES1* is expressed within the temporal framework of the cell cycle. This was the guiding principle used as motivation to study *HES1* expression in the ER+ breast cancer MCF7 cells, where HES1 has previously been found to both inhibit and promote proliferation (Müller et al., 2002; Li et al., 2018). Recent research in the Papalopulu lab has since demonstrated the value of this approach in a paper that examined HES1 expression in MCF7 cells and determined distinct dynamics of HES1 protein expression during the cell cycle (Sabherwal et al., 2021).

Two insights I made in this thesis, towards understanding the temporal expression of *HES1* during the cell cycle in MCF7 cells was first, the identification that *HES1* exhibits cell-to-cell variability in transcription and mRNA abundance, which I inferred to be modulated in a cell cycle dependent manner. (Fig 2.2.6, 2.2.7). Secondly, I demonstrated that HES1 binds its own promoter and is differentially enriched at distinct timepoints after entry into G1 from prometaphase arrest indicating that the degree of HES1 negative feedback may be altered during the cell cycle, which could in turn modulate *HES1* expression during the cell cycle (Fig 5.2.1)

In terms of non-genetic heterogeneity, my results in MCF7 cells can be compared to what has been observed for *Hes1* expression in mouse neural progenitor cells (Phillips et al., 2016). Using evidence from smFISH that *Hes1* expression is stochastic, Phillips et al, modelled the effect of low molecule numbers for *Hes1* mRNA, HES1 protein and miR-9 on HES1 oscillations and determined that stochasticity increases the variability of the amplitude and period of HES1 oscillations (Phillips et al., 2016). It is therefore intriguing to think that the stochasticity in *HES1* expression I observed in MCF7 cells can relate to different HES1 protein dynamics. A common understanding of stochasticity in gene expression is that cells within a population will respond to environmental changes or stimuli in different ways based on their underlying gene expression states (Kærn et al., 2005). In cancer, stochasticity or non-genetic heterogeneity has been linked to treatment resistance (Kumar et al., 2019; Pisco & Huang, 2015). Notch signaling has been implicated in tumour reoccurrence in breast cancer with *HES1* expression often a readout of Notch (Abravanel et al., 2015; Jordan et al., 2016; Simões et al., 2015). Describing *HES1* expression dynamics in this context represents an initial step in understanding the potential role of *HES1* dynamics in cell state changes in cancer. That HES1 binds its own promoter was further evidence that supports the occurrence of oscillatory *HES1* expression in MCF7 cells, as this is a regulatory requirement to produce oscillations (Hirata et al., 2002; Momiji & Monk 2008; Goodfellow et al., 2014).

My third question related to the identification of HES1 targets. A desirable goal would be to identify different genes that are targeted by HES1 according to its upstream dynamics or during specific phases of the cell cycle. Differential target binding and gene expression due to protein dynamics has been demonstrated for p53 and NF-κB (Lane et al., 2017; Purvis et al., 2012). Here, I identified HES1 targets in G1 after cells exited mitosis from a nocodazole arrest, which removes the dynamic aspect that would be associated with asynchronously cycling cells. Nonetheless, ChIP-seq revealed HES1 binding to its own promoter, which I validated by qPCR along with several other novel HES1 targets. As discussed in 5.3.1, identifying HES1 targets in a breast cancer cell line could aid understanding of the role for HES1 in breast cancer. I validated my ChIP-seq experiment by ChIP-qPCR for known HES1 targets such as *NEUROG3*, *ASCL1* (Sueda et al., 2019; Sumazaki et al., 2004). The identification and ChIP-qPCR validation of HES1 binding to *MYB* provides yet another route for HES1 to potentially control the cell cycle as c-MYB has been found to activate *CCNB1* expression in MCF7 and hematopoietic cells (Nakata et al., 2007; Quintana et al., 2011).

6.2 Assessment of JI051 as a HES1 inhibitor

The second question I asked at the start of this thesis related to the functional role of HES1 in the cell cycle. To address this, I examined the effect of a recently published inhibitor of HES1 (Perron et al., 2018) on cell cycle progression and HES1 expression in iMEF and MCF7 cells. From my experiments, the dominant effect of JI051 appears to be a prolonged mitosis in cells exposed to JI051 during interphase and a failure of nocodazole released cells to exit mitosis in the presence of the JI051. This evidence strongly suggests that JI051 interferes primarily with regulatory events during mitosis. Although, I observed a down-regulation of HES1 in a small number of cells, this did not significantly impair cell cycle progression prior to the mitotic arrest. Moreover, regardless of whether cells exhibited a decrease in HES1 expression from S-G2 or normal HES1 dynamics, every cell treated with JI051 entered a prolonged mitotic arrest. This suggests that the dominant effect of JI051 might be independent of HES1 signaling in interphase. Citing the undesirable effects of broad spectrum

gamma-secretase inhibitors in treating Notch-driven cancers (Ran et al., 2017), Perron et al sought to identify inhibitors of HES1 to target Notch signaling specifically (Perron et al., 2018). Their aim was to identify compounds that blocked HES1 binding to its co-repressor TLE1. Instead stabilisation of HES1 with PROHIBITIN2 (PHB2) was identified (Perron et al., 2018) Based on the results I have presented in this thesis, I would recommend caution in the use of JI051 as a HES1 inhibitor due to the uncertain role of HES1 in the dominant effect of JI051 (prolonged mitotic arrest) as the information I presented in 5.3.3 suggests mitotic defects can occur upon PHB2 knockdown (Takata et al., 2007; Lee et al., 2011). Other HES1 inhibitors have been reported but their experimental use in the wider scientific community appears limited (Arai et al., 2009, 2016, 2020). These inhibitors are natural products that have been found to prevent HES1 dimerisation using fluorescent-plate assays for HES1 dimerisation. Multipotent mouse neural stem cells (MEB5) treated with one of these natural products, agalloside, differentiated into neurons after 4 days of treatment as verified by staining for neuronal markers GFAP and Tuj1. The pro-neural genes *Mash1*, *Neurog2* and *NeuroD1* were also found to be upregulated by qPCR, indicating that HES1 repression of these genes was potentially inhibited (Arai et al., 2016). Considering the link between modulation of the cell cycle and differentiation (Liu et al., 2019), the use of agalloside could be useful to study whether it slows proliferation in other cells.

An important clarification I think needs to be made for future use of JI051 concerns the interaction between HES1 and PHB2. In untreated cells HEK293 cells, immunoprecipitation of PHB2-FLAG showed coimmunoprecipitation with HES1 that was increased by the addition of increasing amounts of JI051 (Perron et al., 2018). Identifying when HES1 and PHB2 potentially interact in normal cells could be informative for future use of JI051. I would first approach this in a cell cycle dependent manner to assess whether HES1 and PHB2 interact during specific phases of the cell cycle. This could be achieved by co-immunoprecipitation studies in synchronised cells at specific cell cycle phases or by immunofluorescence study of HES1 and PHB2 in combination with cell cycle markers. Knowing if and when HES1 and PHB2 interact could inform on a novel biological role for both proteins, for

example if the interaction occurred in G2 it may suggest that HES1 and PHB2 have a yet to be described role in G2 or mitosis. This would then allow an appraisal of whether JI051 inhibits HES1 and PHB2 together to cause a mitotic arrest or only impairs the function of one of these proteins. As mentioned in 5.3.1 phospho-proteomic analysis of JI051-treated cells could be useful to inform on the signaling pathways that are impaired due to JI051. Furthermore, immunofluorescent experiments assessing microtubule assembly and kinetochore formation will be necessary to assess the integrity of the mitotic spindle after JI051 treatment.

A follow up experiment I would like to perform would be to try and increase the time interphase cells can be live-imaged during JI051 treatment. A drawback of the prolonged mitotic arrest caused by JI051 and the fact that it appears to have an instant effect at preventing mitotic exit, was that it limited the amount of time HES1 dynamics could be imaged to make a better assessment of whether they were affected by JI051. One way to delay entry into mitosis could be to co-treat cells with JI051 and a cell cycle inhibitor. While treatment with a cell cycle inhibitor is an experiment in itself that would examine whether HES1 dynamics are coupled with the cell cycle, a comparison could still be made. This comparison would be made between HES1 dynamics in cell cycle inhibited cells and HES1 dynamics in cell cycle inhibited and JI051-treated cells to assess if JI051 had a distinct effect. Example drugs that could be used include the roscovitine which inhibits CDK2 and has been shown to reduce proliferation MCF7 cells (Nair et al., 2011) Arrest at the G2/M border could also be achieved by use of the CDK1 inhibitor R03306 (Vassilev, 2006). Cell synchronisation methods, such as double thymidine block could also be used.

6.3 Suggestions for future work

Here I will discuss some refinements to the experiments I performed in this thesis that could improve understanding of the results presented. I will also identify future experiments worth pursuing that could utilise data obtained in this thesis.

I used the results of my *HES1* smFISH experiments to infer how HES1 protein is expressed and suggested that the increase in transcription I observed could explain the S/G2 HES1 protein observed expression in MCF7-HES1-mVENUS cells. The comparison between parental (non-CRISPR modified) MCF7 and MCF7-HES1-mVENUS cells comes with the caveat that MCF7-HES1-mVENUS cells are a hemizygous line, as genotyping of the clonal line indicated that one allele had a premature stop codon after CRISPR modification. This could affect the transcriptional dynamics of *HES1* between the parental MCF7 and MCF7-HES1-mVENUS cells. Furthermore, I concluded that in the absence of cell cycle markers, distinguishing G1 and S-phase MCF7 cells by DAPI or nuclear area alone, is not possible. To address these concerns, I have performed a preliminary *HES1* smFISH experiment in MCF7-HES1-mVENUS cells using PCNA immunofluorescence to mark S-phase cells specifically. In this experiment, I was able to identify S-phase cells based on the characteristic PCNA foci. G1 and G2 cells were categorised based on DAPI content similarly to how I described in 2.2.8. Non-S-phase cells below the 6.5 A.U sum of DAPI threshold were categorised as G1 while those above the threshold as G2. In this experiment S-phase cells have the largest percentage of cells that are not actively transcribing (0 *HES1* TSS). 57 and 54 % of G1 and G2 cells did not have any active *HES1* TSS. 38% of G1 cells had 1 *HES1* TSS compared to 23% in G2. G2 cells had the highest percentage of cells with 2 *HES1* TSS (23%). The lower amount of *HES1* TSS may represent the fact that the line is hemizygous for *HES1*. It still, however, recapitulates my MCF7 result where G2 cells showed increased transcription. The preliminary data here also suggests that *HES1* is less transcriptionally active during S-phase, which could support a role for transcriptional down-regulation for the corresponding down-regulation of HES1 protein during S-phase.

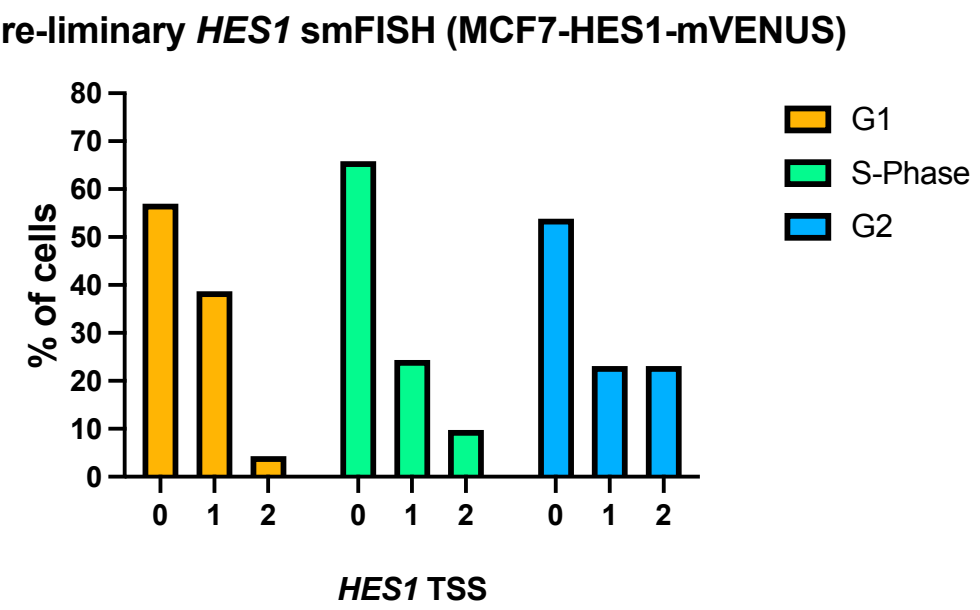

Fig 6.1 Preliminary analysis of *HES1* transcription in MCF7-HES1-mVENUS cells
HES1 transcription during the cell cycle was analysed in the MCF7-HES1-mVENUS cell line using smFISH and PCNA immunostaining. Cells were characterised as S-phase based on detection of PCNA foci in cell nuclei. Cells with diffuse PCNA expression were characterised as G1 and G2 based on a sum of DAPI intensity threshold (G1 = <6.5 A.U., G2 = > 6.5 A.U). The number of active *HES1* TSS in cell nuclei was quantified by smFISH. The percent of cell with 0, 1, or 2 *HES1* TSS was then calculated for each cell cycle phase.

Following on from the above, to obtain a better relationship between *HES1* expression and HES1 protein levels, smFISH can be combined with HES1 immunofluorescence to examine how *HES1* transcription and mRNA numbers correlate with HES1 protein levels in individual cells. This experimental approach has been utilized in HeLa and iPSC cells (Popovic et al., 2018)

To more accurately monitor *HES1* transcription over the cell cycle, the MS2 system can be employed to visualise transcription by live-imaging. The MS2 system is based on fusion of an MS2 binding sequence to the coding sequence of a gene. The MS2-stem loops are bound by the MS2 binding protein after transcription. When the MS2 binding protein is fused to a fluorescent protein transcription can be directly visualised in live cells (Fouts et al., 1997; Bertrand et al., 1998). This system has previously been used to monitor *CCND1* and *CDKN1A* transcription during the cell

cycle (Hafner et al., 2020; Yunger et al., 2010). Live-imaging of *CDKN1A* transcription, was performed in MCF7 cells in combination with live-reporters for p21 and p53 proteins, which enabled a quantitative readout of how upstream protein dynamics of p53 contributed to the activation of *CDKN1A* transcription. The use of a p21 protein reporter enabled a readout of how *CDKN1A* transcription dynamics are related to the temporal expression of p21 protein (Hafner et al., 2020). In this thesis, I demonstrated the utility of the MCF7-HES1-mVENUS cell line for monitoring HES1 protein dynamics over the cell cycle (Sabherwal et al., 2021). Modification of the *HES1* C-terminal locus in this line by CRISPR gene-editing to include an MS2 stem sequence could be used to monitor *HES1* transcription and protein expression concurrently. Observing *HES1* transcription dynamics in real-time would allow me to assess how they change during the cell cycle. This system could therefore verify the smFISH results I presented in this thesis that *HES1* mRNA abundance and transcription increase in a cell-cycle and cell size dependent manner. The ability to simultaneously monitor HES1 protein expression would also inform on the relationship between *HES1* transcription and protein expression. Evidence that CDK1 and CDK2 target NICD for degradation in a cell-cycle dependent manner in HeLa cells (Carrieri et al., 2019), suggests that Notch-activated *HES1* transcription could be attenuated in a similar manner. This is one possible explanation for the S-phase down-regulation of HES1 observed in MCF7-HES1-mVENUS cells (Sabherwal et al., 2021). However, without first establishing the kinetic relationship between *HES1* transcription and HES1 protein.

Utilising information I obtained in my HES1 ChIP-seq experiments on the regions HES1 binds its own promoter in MCF7 cells could inform experiments aimed at altering the *HES1* regulatory network, either by introducing silent mutations in these binding sites or by interfering with HES1 binding. Mutation of N-box sequences has been a staple of experiments investigating HES1 target repression (Hartman et al., 2004; Murata et al., 2005; Takebayashi et al., 1994). Reversible blocking of HES1 to its own promoter would also be very desirable. A CRISPR system has recently been described using guide RNAs (gRNAs) to target catalytically-inactive Cas9 (dCas9) to promoter sequences to block transcription factor binding (Shariati et al., 2019). As

proof-of-principle for this method, OCT4 binding to the *Nanog* promoter was disrupted in mESCs, which resulted in decreased *Nanog* expression and a decrease in cell proliferation (Shariati et al., 2019). Inhibition of HES1 binding to its promoter at sites I identified in this study followed by analysis of *HES1* transcription in MCF7 either by smFISH or MS2 live-imaging could inform on the degree to which HES1 regulates its own expression in MCF7 cells. If an effect on *HES1* transcription dynamics was observed subsequent analysis of the cell cycle could establish a functional connection between the two processes.

Chapter 7: Materials and Methods

7.1 Cell culture, cell lines and cell cycle synchronisation

MCF7 and iMEF cells were cultured in a humdified, 37^{o}C 5% CO_2 and 20% O_2 atmosphere. MCF7 cells were propagated in 10% FBS (Gibco 10500064) high glucose DMEM (Dulbecco's Modified Eagles Medium, Sigma 6429) media supplemented with 1% Penicillin/Streptomycin (Pen/Strep, Sigma P4333). iMEF cells were propagated in 10% FBS (Gibco #26140-07) DMEM (GE Healthcare Life Sciences #SH30081.02) supplemented with 1% Penicillin/Streptomycin (Nacalai Tesque #09367-34).

iMEF and MCF7 cells were passaged passed 2-3 times weekly. Media was aspirated from culture vessels and cells were washed 1x with 1xPBS before the addition of TrypLE (Gibco 12605036) to dissociate cells from culture vessels. Trypsin was deactivated with 10% serum DMEM and cells were pelleted by centrifugation at 1300g for 3mins. Cells were resuspended in an appropriate amount of media and seeded into new culture vessels.

The iMEFs cell line was generated previously in the Kaldis lab from primary MEFs immortalised by serial passaging for 30 times according to established methods (Diril et al., 2016; Todaro & Green, 1963).

MCF7-HES1-mVENUS cell line was generated by Dr Nitin Sabherwal using CRISPR-Cas9. The N-terminal locus of *HES1* was targeted using a guide RNA (gRNA) 5'-gaaaaattcctcgtccccggtgg3-' to facilitate the integration of donor sequence in a pUC57 backbone. Donor sequence consisted of 800bps upstream of *HES1* start codon (5' homology arm), 800bps of downstream of *HES1* start codon (3' homology arm). Homology arms flanked an mVENUS cassette, consisting of ATG-3xFLAG-mVENUS-linker-HA. Silent mutations were inserted in PAM site of 5' homology arm to prevent further CRISPR targeting after integration. *HES1* gRNA, donor plasmid and Cas9 protein were electroporated into MCF7 cells. Post-electroporation, cells were cultured and subsequently FACS sorted for mVENUS-positive signal. Single cell clones were genotyped after expansion. MCF7-HES1-mVENUS line used in this study was

identified as being hemizygous for *HES1* by PCR and sequence-based genotyping. One allele was found to have correct integration of mVENUS cassette. Premature codon was identified on second allele. Further information can be found at (Sabherwal et al., 2021).

For G0/G1 synchronisation of iMEFs, cells were cultured to ~80-90% confluency. At this point 10% serum DMEM was removed, and cells were washed 2x with 1XPBS and 0.1% serum DMEM media supplemented with 1% Penicillin/Streptomycin was added to cells. Cells were cultured in 0.1% serum media for 72 hours to achieve a G0/G1 synchronised population.

For prometaphase arrest of MCF7 cells, cells were seeded into 100mm or 150mm Nunclon^{TM} cell culture dishes (Thermo Scientific) to yield ~70% confluent cultures at the time of treatment. The following day cells were treated with 200nM nocodazole (Sigma Aldrich, M1404) for 15 hours. Mitotic cells were collected by mitotic shake-off and washed 2x in DMEM to clear nocodazole before re-plating cells in 10% serum DMEM media. Nocodazole-released cells were treated with 10 µM R03306 (Calbiochem 217699) or 1 µM JI051 (generously provided by Amelie Perron, Kyoto University).

7.2 RNA extraction and quantitative RT-PCR

RNA isolation was performed using a NucleoSpin RNA II kit (Macherey- Nagel, 740955) according to the manufacturer's protocol and RNA was eluted in 35 µl DNase/Rnase-free H_2O. 1 µg of total RNA was used in each RT-PCR reaction for cDNA synthesis using Maxima Reverse Transcriptase (ThermoScientific #EP0741). cDNA was diluted to 10 ng/µl for use in qPCR reactions.

Relative fold-changes for each gene analysed were calculated using the $2^{-\Delta\Delta Ct}$ method after normalisation of CT values to housekeeping genes eukaryotic elongation factor 2 (*eef2*) for mouse samples and 18s ribosomal RNA(*18srRNA*) for human samples (Livak & Schmittgen, 2001). qPCR reactions were performed using

either a CFX96 or CFX384 TouchTM Real-Time PCR Detection System (Biorad #1855195/#1855485). Primers used in qPCR experiments are listed in table 2**.**

Gene	Oligo ID	Sequence	Species
eEF2	PKO3215	Fwd: CACTTACCATCCCCCGTCAC	*Mus. musculus*
	PKO3216	Rev: CTTTGGGGTCGCAGCTCTTA	
p53	PKO2805	Fwd: TCCGAAGACTGGATGACT	*Mus. musculus*
	PKO2806	Rev: TGAGGTGATGGCAGGATAT	
Cdkn1a	PKO2308	Fwd: CCTTGTCGCTGTCTTGCACT	*Mus. musculus*
	PKO2309	Rev: AATCTGTCAGGCTGGTCTGC	
Ccne1	PKO2316	Fwd: GAGCTTCTAGACCTGTGCGT	*Mus. musculus*
	PKO2317	Rev: CGCACCACTGATAACCTGAG	
Ccna2	PKO2861	Fwd: CAACCCCGAAAAACTGGCGC	*Mus. musculus*
	PKO2862	Rev: AAGAGGAGCAACCCGTCGAG	
Ccnb1	PKO2863	Fwd: GCAGAACAGTTGTGTGCCCA	*Mus. musculus*
	PKO2864	Rev: GTCACAAAGGCGAAGTCACC	
Cdk1	PKO2069	Fwd: CTTCAGAGCTCTGGGCACTC	*Mus. musculus*
	PKO2070	Rev: GGTTCTTGACGTGGGATGCG	
Atm	PKO3286	Fwd: CGAAGCGACCTGGGTTTG	*Mus. musculus*
	PKO3287	Rev: TCATGCTCTAACTGCCGG	
Atr	PKO3298	Fwd: CCTGAACTGATGGCTGATTA	*Mus. musculus*
	PKO3299	Rev: GGTCCCATCAACTTCATCAA	
Fancc	PKO3282	Fwd: TAAGAGAGTCATTCCTGCCT	*Mus. musculus*
	PKO3283	Rev: GATGTGAAAACCTGAAGAGC	
Hes1	PKO3801	Fwd: CCCTGTCTACCTCTCTCCTT	*Mus. musculus*
	PKO3802	Rev: TCAGTCCCCAGAGAATTTTA	
Plk1	PKO1643	Fwd: GGCAAGAGGAGGCTGAGGAT	*Mus. musculus*
	PKO1644	Rev: CACAGCTGATACCCAAGGCC	
18sRNA	PKO6542	Fwd:GGATGTAAAGGATGGAAAATACA	*Homo. sapiens*
	PKO6543	Rev: TCCAGGTCTTCACGGAGCTTGTT	

HES1	SHNP02	Fwd: GAGCAAGAATAAATGAAAGT	*Homo.*
	SHNP03	Rev: CTTGGAATGCCGCGAGCTAT	*sapiens*
CCNB1	PKO6586	Fwd: TTCTGGATAATGGTGAATGGAC	*Homo.*
	PKO6587	Rev: ATGTGGCATACTTGTTCTTGAC	*sapiens*
MASTL	PKO5458	Fwd: TGGTCCTGCGGTAGACTG	*Homo.*
	PKO5459	Rev: GATAACTTTTCTTCACCTTCTGGC	*sapiens*
PLK1	PKO6709	Fwd: AACACGCCTCATCCTCTACAAT	*Homo.*
	PKO6710	Rev: AGGAGGGTGATCTTCTTCATCA	*sapiens*
CDC20	PKO6787	Fwd: GACCACTCCTAGCAAACCTGG	*Homo.*
	PKO6788	Rev: GGGCGTCTGGCTGTTTTCA	*sapiens*
FOXM1	PKO6885	Fwd: TCCTCCACCCCGAGCAA	*Homo.*
	PKO6886	Rev: CGTGAGCCTCCAGGATTCAG	*sapiens*
MYBL2	PKO6887	Fwd: CAAGTGCAAGGTCAAATGG	*Homo.*
(B-MYB)	PKO6888	Rev: CTTCTTAACCAGCTCGATGA	*sapiens*
MYB	PKO7090	Fwd: CTCTCCAAGAACTCCTAC	*Homo.*
(C-MYB)	PKO7091	Rev: GATTCCACCTCTTGTTTG	*sapiens*

Table 2: qPCR primers used in study

7.3 Protein extraction, quantification and western blotting

Total protein was extracted from cells by lysing cells in RIPA buffer (20mM Tris HCl pH8, 150mM NaCl, 0.1% SDS, 0.5% Sodium Deoxycholate, 1% Triton X-100 supplemented with 10mg/mL pepstatin, 10mg/mL leupeptin and 10mg/mL chymostatin). For cells attached to plates, extraction was performed by aspirating media, washing cells 1x with PBS and adding 200 µl of ice-cold RIPA buffer directly to the plate. The volume of RIPA buffer was pipetted multiple times over the surface of the plate to lyse the cells. Detachment of cells was aided by scraping the cells with a plastic scraper (Corning® CLS3008). The lysate was pipetted up and down in the plate before transfer to an Eppendorf on ice for 10 minutes. In the case of protein extraction from nocodazole-arrested cells, mitotic were first collected by mitotic shake-off, pelleted by centrifugation and ice-cold RIPA buffer was added directly to the cell pellet. Lysis was facilitated by pipetting the lysate up and down before

transfer of lysate to an Eppendorf for further incubation on ice for 10 minutes. The lysate was then snap frozen in liquid nitrogen and stored at -80^{o}C until further processing. Prior to protein quantification, the protein lysate was sonicated using a Diagenode Biorupter. Sonication was performed using 5 cycles (30-seconds-on-30-seconds-off) at 4^{o}C. The sonicated lysate was then centrifuged at 10,000G for 10 minutes at 4^{o}C. Protein quantification was performed using a BCA assay (Pierce #23225). 10 µg of protein was used for western blotting. Protein extracts were separated by Sodium Dodecyl Sulfate Polyacrylamide Gel Electrophoresis (SDS-PAGE) using 8-12% polyacrylamide gels. After separation gels were washed briefly with transfer buffer (24.7mM Tris Base pH8, 20% Methanol, 192mM Glycine). Separated protein was transferred to 0.2 µm nitrocellulose membranes by wet transfer at 100V for 2 hours at 4^{o}C. After transfer, nitrocellulose membranes were blocked for 1 hour by washing at room temperature in Tris-Buffered Saline 0.1% Tween-20 solution (TBST) containing 4% milk (Biorad, 1706404). Membranes were incubated overnight at 4^{o}C with primary antibodies listed in table 3. The following day blots were washed with TBST (3x10 minutes) and incubated with the appropriate HRP-conjugated secondary antibody for 1 hour at room temperature. The 3x10 minute TBST was repeated after incubation with secondary antibody. Blots were then incubated with Immobilon chemiluminescent HRP substrate (Millipore #WBKLS0500). The chemiluminescent signal was detected on Super RX-N X-Ray films (Fujifilm #47410). Protein expression was quantified by densiometric analysis in FIJI, with relative protein abundance calculated based on comparison with HSP90 loading control expression.

Protein detected	**Species**	**Company**	**Catalogue No.**	**Dilution used**
HSP90	Mouse	BD Transduction Laboratories	610418	1:5000
Cyclin B1	Mouse	Cell Signalling	4135	1:2000
PLK1	Mouse	Upstate	05-844	1:3000
CDK1	Rabbit	Homemade PRK Lab	N/A	1:5000

PLK1	Mouse	Millipore	05-844	1:3000
MASTL	Rabbit	Homemade pRK Lab	N/A	1:10000
Phospho-HISTONE-H3 (ser10)	Rabbit	Cell Signalling	9701S	1:500
CDC20	Rabbit	Cell Signalling	4823	1:500
HES1 (FLAG)	Mouse	WAKO	018-22383	1:10000
Phospho-CDK Substrate [pTPXK]	Rabbit	Cell Signalling	14371	1:500
Goat Anti-Mouse HRP (Secondary)	-	Pierce	31432	1:1000-1:20,000
Goat Anti-Rabbit (Secondary)	-	Pierce	31462	1:1000-1:20,000

Table 3. Primary and Secondary antibodies used in western blotting

7.4 Immunofluorescent staining

For immunostaining performed in (2.2.5) MCF7 cells were seeded onto glass coverslips in 6-well plates containing two mls DMEM. Coverslips were stored in 70% ethanol and were washed 2x with millipore H_2O prior to use. 16-24 hours later, coverslips were removed with a sterile forceps and placed into a new 6-well plate containing 2mls 1XPBS to wash media from coverslip. PBS was aspirated from wells by tilting the plate and aspirating from the walls of each well to minimise disruption to cells on each coverslip. 1ml fixation buffer was added to each well and plate were incubated at room temperature (RT) for 15 minutes with gentle rocking. Fixation buffer consisted of paraformaldehyde (Pierce™ 16% Formaldehyde (w/v), Methanol-free) diluted to 4% in a 10XPBS and DNase/RNase free H_2O solution. After fixation coverslips were washed 2x with 1xPBS (1-2 minute washes). To permeabilise cells 2mls of 70% ethanol was added to each well and plates were kept at 4^{o}C overnight.

Prior to staining, coverslips were washed 2x with 1xPBS to remove ethanol. Cells were blocked by adding 1ml 1XPBS+1X western blocking reagent (WBR) (Merck #11921673001) to coverslips and incubating for 15 mins at RT. During blocking, primary antibody master mixes were made in 0.5ml 1XPBS+1XWBR. The 0.5 ml primary antibody mix was added directly onto coverslips in 6 well plates. Cells were incubated with primary antibody mixes for 45 mins with gentle rocking (Cyclin B1 Santa Cruz 245, mouse monoclonal, 1:250 dilution; PCNA DakoCytomation M0879, monoclonal, 1:500 dilution). After incubation with primary antibody mixes, cells were washed 3x5 mins with 3ml PBT (1xPBS+0.05% Tween-20). Secondary antibody mixes were made in 1ml 1XPBS+1XWBR (1:1000 Alexa 488 A-11029). Secondary antibody mix was added onto cells and incubated in the dark for 30 mins at RT. Following secondary antibody incubation, cells were washed 3x5 mins with 3ml PBT. For the last 5 minute wash cells were counterstained with 0.5 μg/ml DAPI dilution. A final 1X PBS wash was performed. Coverslips were washed 2x with 3ml Millipore H_2O for ~1 min to remove salt and allow complete drying of coverslips. After drying coverslips were mounted on 1 drop of Invitrogen ProLong Gold antifade (Thermo Scientific P36934) on a glass slide. Slides were let dry in the dark overnight at RT.

7.5 Proliferation assays

For alamarBlue proliferation assays, $2x10^3$ MCF7 cells were seeded in quintuplicate in 96-well plates in 150 µl DMEM. The following day media was replaced with media supplemented with 10% alamarBlue reagent (Bio-Rad BUF012B) and incubated at 37 for 4 hours. After incubation fluorescence was measured using a microplate reader SPECTRAmax M2 (Molecular Devices) with excitation wavelength 560nm and emission wavelength 590 nm.

For incucyte live-imaging of cell growth, an equal number of MCF7 cells were plated in triplicate per condition in 12 well plates and cultured in a humdified, 37^oC 5% CO_2 and 20% O_2 atmosphere. Cells were imaged with a 4x objective every 45 mins for up to 4 days. Images were analysed using Incucyte ZOOM software. At each timepoint

cell density (measured by %confluence) was measured by overlaying a 'mask' on cells.

7.6 FACS analysis

For FACS analysis of cells, 100 µM BrdU (BD Pharmingen, 550891) was added to cell cultures one hour before collection. Cells were collected by either trypsinisation or mitotic shake-off and pelleted (after neutralisation with DMEM 10% FBS for trypsinised cells) by centrifugation and washed 1x with ice-cold PBS in 15 ml falcon tubes. Cells were fixed in ice-cold 70% ethanol. Ethanol was added drop-wise to cells with gentle vortexing. Fixed cells were stored at 4^{o}C for at least one hour prior to FACS staining. Fixed cells were pelleted by centrifugation at 1300xg for 3 mins and blocked by resuspension in 3ml 1XPBS+1% Bovine Serum Albumin (BSA, Sigma Aldrich, A7906) for 5 mins at RT. Cells were pelleted by centrifugation at 1300g for 3 mins, 1XPBS+1%BSA was removed by aspiration and DNA was denatured by treating cells with 1ml 2N HCL/0.5% Triton X-100 for 20 mins at RT, followed by centrifugation by addition of 1ml 0.1M sodium tetraborate, pH 8.5 for 10 mins at RT. Cells were pelleted by centrifugation as described above and permeabilised by the addition of 1ml 1XPBS-1%BSA-0.5% Triton X-100 for 5 mins at RT. Cells were incubated with anti-BrdU antibody (BD Pharmingen, 555627, clone 3D4) diluted 1:500 in 1 ml 1XPBS-1%BSA for 90 mins at RT. After antibody incubation, cells were washed 2x with 1ml 1XPBS-1%BSA. Cells were incubated with Alexa647-conjugated goat anti-mouse secondary antibody (Invitrogen, A21235) diluted 1:400 in 1XPBS-1%BSA for 1 hour at RT in the dark. Following secondary antibody incubation cells were washed 2x with 1ml 1xPBS 1%BSA and resuspended in PBS supplemented with 2.5µg/ml propidium iodide (Merck, 537059) and 20µg/ml RNase A (Sigma Aldrich, R6513). The cell suspension was filtered through a 40 µm strainer. Cells were analysed with a LSRII flow cytometer (BD Bioscience). Analysis of BrdU incorporation and cell cycle distribution was performed using FlowJo^{TM} software.

7.7 Single-molecule Fluorescence *in situ* Hybridisation (smFISH)

MCF7 cells were cultured as described as described in **7.1.** MCF7 cells were seeded onto coverslips in 6-well plates at equal density. 16 - 24 hours later cells were fixed

and permeabilised overnight in 70% ethanol as described in 7.4 Prior to hybridisation of coverslips with smFISH probes, a plastic container was lined with wet paper towels and placed at 37^{o}C to create a humidified chamber for subsequent hybridisation. 25 µM stock smFISH probes were thawed at RT in the dark and mixed by pipetting before dilution. smFISH probe master mixes were made by diluting 0.8 µl of 25 µM stock in 200 µl hybridisation buffer (100mg/ml dextran sulfate and 10% formamide in 2X SSC). 70% ethanol was removed from coverslips by tilting plates and aspirating from the wall of each well. 3ml of wash buffer was added to each well and the plate was left stand at RT for 2mins. Wash buffer was aspirated and another 3mls of wash buffer was added to each well. A clean lid from a 6 well plate was placed in the pre-warmed plastic container. For each coverslip, a 200 µl aliquot of smFISH probe mixture was transferred onto the clean 6-well plate lid. Using a sterile forceps, coverslips were removed from wash buffer and the edges of the coverslip were dabbed gently on a Kim wipe to remove excess liquid. Coverslips were placed cell-side down on top of the 200 µl smFISH probe mixture. A negative 'no probe' control was also used. In this case a coverslip was placed cell side down on 200 µl of hybridisation buffer without the addition of smFISH probes (See Fig 7.1 for no probe control comparison with *HES1* exonic smFISH probe image). The clean lid of another 6-well plate as placed on top of the first lid and the pre-warmed plastic box was sealed with its own lid. The humidified container was wrapped in tinfoil and placed at 37 ^{o}C for 16 hours. Following hybridisation, coverslips were transferred by sterile forceps, to the wells of a new 6-well plate with 3mls wash buffer for 2 minutes. Wash buffer removed and another 3mls of wash buffer was added. The 6-well plate was incubated at 37 ^{o}C for 45 mins. After the incubation at 37 ^{o}C, wash buffer was removed from wells and another 3mls of wash buffer was added and the 6-well plate was incubated at RT for 30 mins. Coverslips were washed 2x 5 min with 3ml 2X SSC. For the second wash coverslips were counterstained with 0.5 µg/ml DAPI. A final 5 min PBS wash was performed after DAPI staining. Coverslips were then washed 2x ~1min with Millipore H_2O to remove salt to allow complete drying of coverslips. Coverslip were let dry in the dark at RT. After drying coverslips were mounted on 1 drop of Invitrogen ProLong Gold antifade (Thermo Scientific P36934) on a glass slide. Slides were let dry in the dark overnight at RT.

Human *HES1* Stallaris smFISH probes targeting exonic and intronic *HES1* sequences were synthesized by LGC Biosearch Technologies and labelled with Quasar 570 (*HES1* exon) and Quasar 670 (*HES1* intron). Human *GAPDH* probes targeting *GAPDH* exons were ordered directly from LGC Biosearch Technologies (SMF-2019-1)

HES1 smFISH probe sequences are listed in table 4.

	***HES1* intron (5' to 3')**	***HES1* exon (5' to 3')**
1	cgcccttacctttctgtg	gattccgctgttatcagcac
2	gaggggctgcaaagagat	aggaccaaggagagaggtag
3	cccaacccctacttaatt	ctacttggtgatcagtagcg
4	ccggggtttcaagacaga	actactgagcaagtgctgag
5	gagttctgtgttcccatg	ggggacgaggaatttttctc
6	tccccacttacatctttc	tgtcgtgttgacactggctg
7	ggggggtttcactcttag	cagatgctgtctttggttta
8	ggagaacgcagtaccagc	ggctttgatgactttctgtg
9	ctggaccccagcgaataa	tcttcgtcttttctccataa
10	cacggagcgcaagcatta	gctcagactttcatttattc
11	agctgcttcagagtgctg	ccaaaatcagtgttttcagc
12	aaggaaagtgagccccgt	gagctatctttcttcagagc
13	cgcgagctctgcatagag	cttcactgtcatttccagaa
14	gaaatcaccgcgaggcga	cgttcatgcactcgctgaag
15	aaccacgggcggaagtct	tgcgcacctcggtattaacg
16	tgtagctgaatgcctctc	taggtcatggcattgatctg
17	gagtgagccaaggcagta	gaagcctccaaacaccttag
18	aataagccccagaccgtg	tgaggaaagcaaactggcca
19	aacttggagttgtggcta	gtgtagacggggatgacagg
20	tccctttccggaacagta	tggaaggtgacactgcgttg
21	gcggctgcaacctctttc	gagtttaggaggaggggtgg
22	agtcctaagtcctttcgc	gagggaagagaggtgggttg
23	ctccacgcagttccaaac	tcaagttcctgtttagagtc

24	gtgctaaaccagtgaccc	aaaaagtcctcttctctccc
25	cccttctgcaacgggaag	tgcatggtcagtcacttaat
26	aatccatcatccaagcct	atacaaaggcgcaatccaat
27	gtgaccttggacaatgcc	acgaaatgtcatctgagctt
28	ctatctcagccccagatc	attttcaaacatctttggca
29	tccctgtagctgcattta	acttccccaaaggaagatat
30	caaaagccgagccactcc	ttctggaagaatcagttcga
31	ctctccacactagcgttg	tccaccaaaagccttttttac
32	cagggagggtgagatggg	agtcaattcctgaattacca
33	catgcgcccgtgaaactg	
34	cagacgggtcaccgaacg	
35	agctgcgggccagaaaga	

Table 4. *HES1* Stellaris smFISH probe sequences

7.8 *HES1* smFISH: Image acquisition and mRNA quantification

Cells were imaged using an Olympus IX83 inverted microscope using Blue Lumencor LED excitation, a *60x/ 1.42 Plan Apo* objective and the *Sedat* filter set Chroma [*89000*]. The images were collected using a *R6 (Qimaging)* CCD camera with a Z optical spacing of (0.2µm) Raw images were then deconvolved using Huygens Pro software (SVI). Cells were imaged using DAPI, TRITC and Cy5 channels. For all channels digital gain was set to 2. For DAPI exposure never exceeded 100 ms, while exposure times for the TRITC and Cy5 channels ranged from 500 ms to 2 seconds

Images were analysed using FISH-quant, a programme run via a custom graphical user interface in Matlab (F. Mueller et al., 2013). Using FISH-quant, single cells and nuclei were outlined, and single mRNA transcripts were quantified by setting a pixel intensity threshold for each mRNA 'spot'. After cells are outlined multiple images were automatically analysed using the 'Batch' mode option in FISH-quant to give a quantification of RNA molecules in each cell.
(https://bitbucket.org/muellerflorian/fish_quant/src/master/)

Images were displayed as XY- maximum intensity projections. Individual cells were segmented in the 'Define outlines' interface by manually drawing around the cell and nuclear surfaces. Images were filtered using a Gaussian filter to reduce noise and enhance the signal-to-noise ratio. After image filtering, individual RNA spots and regions of the cell with no RNA spots are inspected in FISH-quant to assess the pixel intensity of RNA spots. This is done for a number of spots to gauge the range in spot in intensity in order to set a minimum and maximum pixel intensity value for spot detection. The integrated fluorescence intensities of all spots within this range were then fitted to a 3D Gaussian to determine to number of spots in each cell.

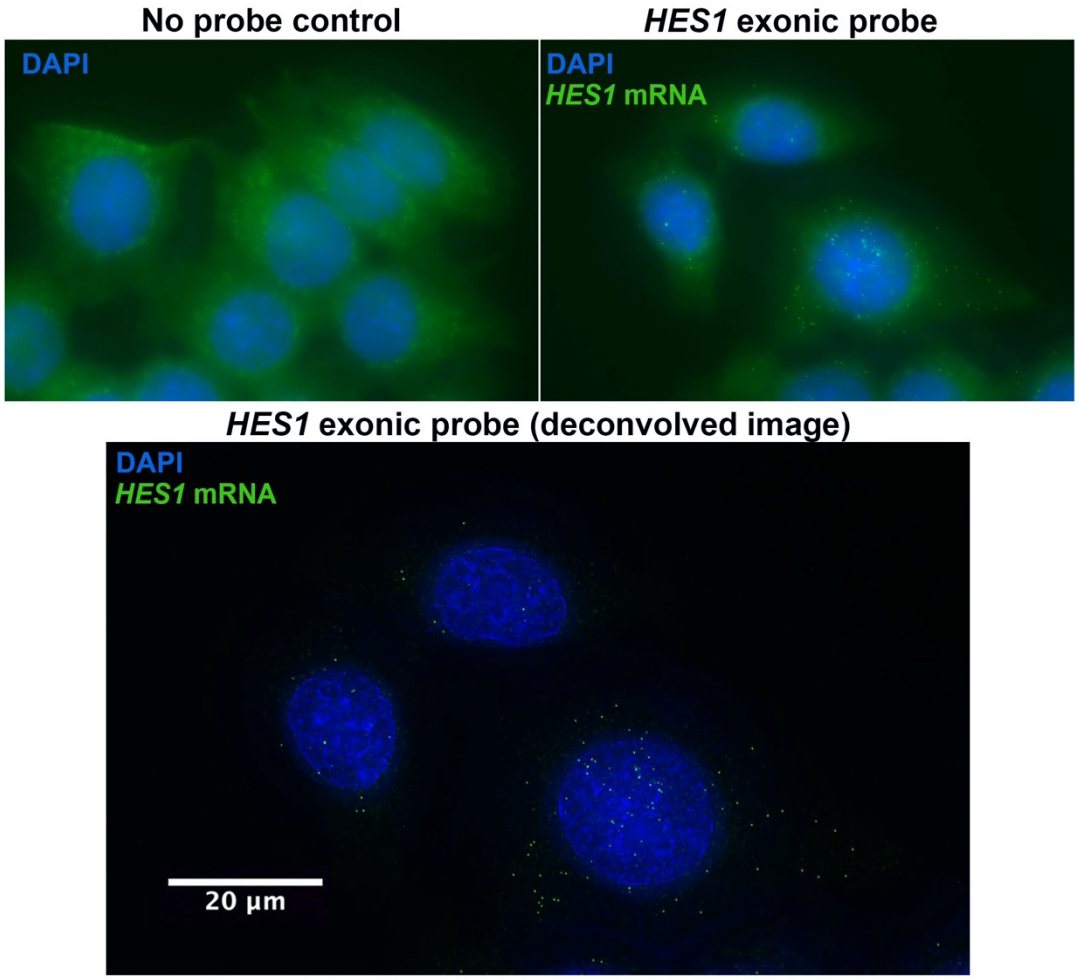

Fig 7.1 Example no probe smFISH control in MCF7 cells
Top feft, example image of fixed MCF7 cells where no smFISH hybridization was performed. Coverslips with negative control cells were incubated on droplets of hybridisation buffer 200 µl of hybridisation buffer without the addition of 0.8 µl of 25 µM *HES1* smFISH probe. Top right, raw image of MCF7 cells from *HES1* smFISH exonic probe hybridisation. As described in 7.7 coverslips with MCF7 cells were

incubated at 37 °C for 16 hours cell side down on droplets of hybridisation buffer 200 µl of hybridisation buffer with the addition of 0.8 µl of 25 µM *HES1* smFISH probe to hybridisation buffer. Bottom centre, deconvolved image of top right image.

7.9 Live-cell imaging and IMARIS analysis

MCF7-HES1-mVENUS cells were seeded into chambered polymer coverslips (ibidi 80826) prior to imaging. Cells were imaged every 20 minutes using a Nikon A1 confocal microscope in an environmental control chamber (37°C 5% CO_2 and normoxia conditions). At each time point 11 images were collected at 2.4 µM intervals. Time-lapse movies were z-stacked and analysed using IMARIS software. To generate data for single cell traces of HES1 intensity over time. Cell nuclei were manually tracked using the 'spot' function in IMARIS to obtain mean values in arbitrary units (A.U.) for HES1 intensity at each timepoint, which represent changes in HES1 concentration in over time. Discrimination of cell cycle phases was achieved by identifying by eye the appearance of PCNA foci as cells entered S-phase and a return to 'smooth' PCNA expression upon entry into G2. The 'surface' function in IMARIS was used to manually segment cell nuclei and cell surfaces to obtain values for cell size and HES1 intensity in mitotic cells

7.10 Chromatin immunoprecipitation (ChIP) in MCF7-HES1-mVENUS cells

MCF7-HES1-mVENUS cells were seeded in 150mm culture dishes 24 hours prior to nocodazole treatment to yield ~70% confluent cultures at the time of treatment. Cells were then synchronised in prometaphase by the addition of 200nM nocodazole to each plate and incubation for 15 hours. Mitotic cells were collected by physically detaching the 'rounded-up' cells by pipetting up and down the media in the plate. During this process plates were inspected under a light microscope to assess the detachment of mitotic cells. The mitotic cell-containing media was collected in 50 ml falcon tubes. Cells were washed of nocodazole by centrifugation at 1300rpm for 3 minutes and resuspension of the cell pellet in fresh DMEM. This process was repeated twice. Cells were counted using a [insert cell counter name]. 5 million cells were plated into 3 150cm^2 dishes with 20 mls of fresh DMEM per condition (DMSO or 1µM JI051). Four hours post-nocodazole washout and release cells were fixed by adding 37% formaldehyde (Sigma Aldrich #252549) directly to the plate at a final

concentration of 0.75%. Each plate was swirled gently at room temperature for 10 minutes. Fixation was stopped by the addition of 2.5M glycine (Biorad #1610718) dissolved in H_2O to a final concentration of 125mM and gently shaking plates at room temperature for 5 minutes. The cells were then washed twice with ice-cold PBS. Cells were lysed directly in each 150 plate by pipetting 1ml of lysis buffer supplemented with protease inhibitors (10 mg/mL pepstatin, 10 mg/mL leupeptin and 10mg/mL chymostatin). Cells were detached from each plate using a cell scraper and the 1ml lysate was collected in a 2ml Eppendorf tube. Each tube was sonicated in a 4°C water bath within a Diagenode Bioruptor at high power (30 seconds on-30 seconds off). 18-20 cycles were used to shear chromatin to approximately 300-500bp. After sonication 50 µl of lysate was removed to assess sonication. This was reverse cross-linked (described below) and DNA was extracted using a QIAquickPCR purification kit (Qiagen #28104). The concentration of chromatin was measured using a nanodrop 8000 spectrometer (Thermo Scientific #ND-8000-GL). The correct shearing of chromatin was verified by running DNA on a 1% agarose gel.

For fixation and lysis of mitotic cells, nocodazole-arrested cells (post 15 hours nocodazole treatment) were detached as described above and collected in 50 mls falcons. Cells were fixed in suspension by the addition of 37% formaldehyde and rolling the tube for 10 minutes at room temperature. Fixation was quenched by the addition of 125mM glycine and continued rolling of the falcon tube for 5 minutes at room temperature. The cells were then pelleted by centrifugation at 1300rpm for 3 minutes and washed with ice-cold PBS. The cell pellet was then resuspended in 1ml IP buffer. The lysate was subjected to sonication and the concentration of chromatin was described as above.

The following ChIP protocol was based on methods described originally described in (Guccione et al., 2006) and subsequently adapted in (Palmer et al., 2019). Based on the DNA concentration of the sonicated lysate a volume approximating 20 µg of DNA based on nanodrop readings was collected and made up to a final volume of 1ml in IP buffer. From this 10 µl (1% of 20 µg in 1ml) was collected and stored at 4 ^{o}C for subsequent DNA extraction to produce 1% input samples used in ChIP-sequencing

and ChIP-qPCR enrichment analysis. Each sonicated sample used for immunoprecipitation was pre-cleared by adding 20 µl of protein A beads (Invitrogen #15910-014) and rotating each sample for one hour at 4°C. Samples were then centrifuged at 100G for 6 minutes at 4°C to pellet the Protein A beads. The supernatant was transferred to new 1.5 eppendorffs. Samples were incubated with antibodies against endogenous, CRISPR-modified HES1 or with a negative control IgG antibody (see **Table 4**) overnight at 4°C with constant rotation. Following overnight incubation samples were centrifuged at 10,000g for 30 minutes. The supernatant was transferred to new tubes and 40 µl of pre-blocked protein A beads were added to each sample. Pre-blocked protein A beads were prepared prior to this by washing beads 3 times with 1ml lysis IP buffer containing 3% BSA. Each sample was incubated at 4°C with constant rotation. After the four hour incubation with antibody-incubated lysate, protein A beads were pelleted by centrifugation and the supernatant was removed. Protein A beads underwent 4 washes described below. In between each wash protein A beads were centrifuged at 100g for 4 minutes at 4°C and the supernatant was aspirated using a 30 gauge needle to prevent loss of beads. Each wash consisted of 1ml of the washes described below.

First wash:

Mixed Micelle Wash Buffer (20mM Tris HCl pH8, 150mM NaCl, 5mM EDTA, 0.02% Sodium Azide, 0.2% SDS, 0.5% Triton X-100, 10.5% w/v Sucrose, 10mg/mL pepstatin, 10mg/mL leupeptin and 10mg/mL chymostatin, diluted in water).

Second wash:

LiCl Detergent wash buffer (5mM Tris-HCl pH8, 0.5% deoxycholic acid, 1mM EDTA, 250mM LiCl, 0.5% NP40, 0.02% Sodium Azide, 10mg/mL pepstatin, 10mg/mL leupeptin and 10mg/mL chymostatin, diluted in water).

Third wash:

Two times in 1mL of Buffer 500: (50mM HEPES pH7, 0.1% deoxycholic acid, 1mM EDTA, 1% Triton X-100, 0.02% Sodium Azide, 10µg/mL pepstatin, 10mg/mL leupeptin and 10mg/mL chymostatin, diluted in water).

Fourth wash:

Two times in 1mL of TE buffer: (10mM Tris HCl, 1mM EDTA, 10µg/mL pepstatin, 10mg/mL leupeptin and 10mg/mL chymostatin, diluted in water).

Following the above washes reverse-crosslinking of protein-bound DNA from protein A beads was performed by adding 260 reverse-crosslinking buffer (0.1M NaHCO3, 1% SDS) containing RNase A, (to a final concentration of 200ng/mL), (Sigma Aldrich #R4642) to the beads. The 1% input samples taken from sonicated lysate prior to immunoprecipitation was also reverse cross-linked at this point. Input and immunoprecipitated samples were then incubated with to a final concentration of at 65 ^{o}C overnight. The following day Proteinase K (Invitrogen #AM2542) was added to each sample to a final concentration of 350 µg/ml and incubated for 1 hour at 60 ^{o}C. Extraction of DNA for downstream ChIP-seq and ChIP-qPCR analysis was performed using a ChIP DNA Clean & Concentrator kit as per manufacturer's instructions (Zymo Research #D5205).

7.11 ChIP-qPCR

Equal amounts of immunoprecipitated DNA and corresponding 1% input DNA were amplified using PowerUP SYBR green master mix (ThermoFisher #A25918). All ChIP-qPCR reactions were performed in either a 9-well plate (CFX96) or 384-well plate (CFX384) TouchTM Real-Time PCR Detection System (Biorad #1855195/#1855485)
Enrichment of HES1 binding at specific loci was calculated using the % input method, which determines the percentage of recovered input. Here amplification observed in ChIP DNA is compared to amplification in the 1% input used for immunoprecipitation and is determined using the following calculation: [100*2^ (Adjusted input - Ct (IP)]

7.12 HES1 ChIP-sequencing and bioinformatic analysis

DNA libraries were prepared using the TruSeq ChIPSample Prep kit (Illumina #P-202-1012), as per the manufacturer's instructions, and sequenced on Illumina HiSeq platforms at Genome Institute Singapore (GIS). Subsequent bioinformatic analysis

was performed by Soumita Ghoush of Dr Hyungwon Choi's Lab at the National University of Singapore according to the following protocol.

FASTQC (https://www.bioinformatics.babraham.ac.uk/projects/fastqc/) was used to get a quick pre-alignment impression of the raw sequenced data. For the ChIP-seq analysis, two iterations of analysis were performed, each round with a different alignment method and subsequently stringent or relaxed thresholds for the peak-calling step. For the first iteration, the sequenced reads were aligned to genomic positions using Bowtie (Langmead et al., 2009), allowing uniquely mapped reads only. The reference indexes for Bowtie were built using the GRCh38 assembly of the Human genome (Harrow et al., 2012). The output of the alignment step was text-based SAM, which was converted to binary BAM and sorted using Samtools (Li et al. 2009). The Burrows-Wheeler Aligner (BWA) (Li and Durbin 2009) was used instead of Bowtie in the second iteration which improved the alignment rate. Only uniquely mapped reads from the BWA aligner were retained, with duplicate reads marked using Picard (http://broadinstitute.github.io/picard/) and subsequently sorted and filtered out using Samtools.

Peak calling was performed on the treated samples to detect areas in the genome enriched with aligned reads compared to its input/control sample using MACS2 (Model-based Analysis of ChIP-seq) (Y. Zhang et al., 2008). This was performed twice, using a default q-value threshold of 0.05 and a relaxed p-value threshold of 0.05. The MACS2 outputs were exported as BED files and explored in IGV (Thorvaldsdóttir et al., 2013) along with the sorted BAM files to visually verify that densely aligned regions have been identified as peaks by the peak caller. Peak selection by a relaxed p-value threshold in the second iteration resulted in several thousand peaks. To assess the concordance of peak calls and retain only reproducible peaks between replicates, the Irreproducibility Discovery Rate (IDR) framework (Li et al. 2011) was used. Downstream analysis such as annotation of peaks to the nearest gene, summarisation, and visualisation of peaks coverage was performed using the R/Bioconductor package ChIPseeker (Yu et al., 2015). To identify enriched sequence motifs at HES1-bound chromatin sequence data was further analysed using DREME from the MEME-suite (Bailey et al., 2009) software in the first round. The discovered

motifs were compared against known motifs from the JASPAR database using Tomtom (S. Gupta et al., 2007) to produce an alignment for each significant match. The same was achieved using the HOMER motif discovery algorithm (Heinz et al., 2010) in the second round.

7.13 RNA-Sequencing

Total RNA isolation from MCF7 cells was performed as described in 7.2. RNA samples from 3 biological replicates were submitted to the Genome Institute of Singapore. Subsequent bioinformatic analysis was performed by Soumita Ghoush of Dr Hyungwon Choi's Lab at the National University of Singapore according to the following protocol.

Pre-alignment quality assessment of raw sequenced reads were performed using FASTQC. The STAR algorithm (Dobin et al., 2013) was used to map the reads to the GRCh38 assembly of the Human genome. The RSEM algorithm (B. Li & Dewey, 2011) is used to quantify expression of transcripts from the mapped reads in Fragments Per Kilobase of transcript per Million mapped reads (FPKM). Differential expression analysis was performed using the EBprotV2 (Koh et al., 2019) software.

To IP:	**Species**	**Company/Cat #**	**Amount used/IP (µg)**
HES1-VENUS (anti-GFP)	Rabbit	Abcam/290	2
HES1-VENUS (Anti DYKDDDDK)	Mouse	FUJIFILM Wako/ 018-22383	2
Non-specific IgG	Mouse	Santa Cruz/sc-2025	1

Table 5. Antibodies used for chromatin immunoprecipitation

Gene	Primer ID	Sequence (5'-3')		Region targeted
HES1	PKO6858	Fwd	ACGCACACACACATCCTCCC	Promoter
	PKO6859	Rev	CTCCTTCACCACCCTTTCCC	
NEUROG3	PKO7030	Fwd	CACGCTTTATCTGCTTCGCC	Promoter
	PKO7031	Rev	GGCCCTTTGTCCGGAATC	
CDK5RAP1	PKO7040	Fwd	CTCTCCAAGCAAGCCTGACC	Promoter
	PKO7041	Rev	TGTTTCATCAGGTTCTGCAGC	
BHLHE41	PKO70444	Fwd	GCGCTGGTAGTTTGCTCTCA	Promoter
	PKO7045	Rev	CCGCGGATGGTACGTTCC	
ASCL1	PKO7047	Fwd	AGAGCCATTTGTCCCTCCTG	Promoter
	PKO7048	Rev	CAGCTGGGTTTGTTGTTGCA	
FOXA1	PKO7051	Fwd	TGAGCTGATGTGGATCTTACGT	Promoter
	PKO7052	Rev	TGCACCTCGGGCTTTGTAG	
TRIB1	PKO7057	Fwd	CAGCCACCTCATTGCACAAC	Promoter
	PKO7058	Rev	ACTGTGAGTGAGTGTGAGCG	
MYB	PKO7074	Fwd	AGCTCTTTGTTTGATGGCATCT	Promoter
	PKO7075	Rev	AAGAGGAGGAGGAGGTCACG	
PRDM10	PKO7042	Fwd	AGTTGGGCAGGTGAAGTAGC	Exon
	PKO7043	Rev	AGCAGCACATCCTTGGAGAG	

Table 6. Primers used for ChIP-qPCR

7.14 Statistical analysis and data visualisation

All figures were designed and assembled using Adobe Photoshop or Illustrator. Throughout the thesis data are presented as mean ± standard error of the mean (SEM) Graphs were generated and data was statistically analysed using GraphPad Prism. Statistical tests used are indicated in figure legends.

References

Abravanel, D. L., Belka, G. K., Pan, T. C., Pant, D. K., Collins, M. A., Sterner, C. J., & Chodosh, L. A. (2015). Notch promotes recurrence of dormant tumor cells following HER2/neu-targeted therapy. *Journal of Clinical Investigation*, *125*(6), 2484–2496.

Aitken, S., Magi, S., Alhendi, A. M. N., Itoh, M., Kawaji, H., Lassmann, T., Daub, C. O., Arner, E., Carninci, P., Forrest, A. R. R., Hayashizaki, Y., Consortium, the F., Khachigian, L. M., Okada-Hatakeyama, M., & Semple, C. A. (2015). Transcriptional Dynamics Reveal Critical Roles for Non-coding RNAs in the Immediate- Early Response. *PLoS Computational Biology*, *11*(4), 1010–1014.

Akazawa, C., Sasai, Y., Nakanishi, S., & Kageyama, R. (1992). Molecular characterization of a rat negative regulator with a basic helix- loop-helix structure predominantly expressed in the developing nervous system. *Journal of Biological Chemistry*, *267*(30), 21879–21885.

Al-Hajj, M., Wicha, M. S., Benito-Hernandez, A., Morrison, S. J., & Clarke, M. F. (2003). Prospective identification of tumorigenic breast cancer cells. *Proceedings of the National Academy of Sciences of the United States of America*, *100*(7), 3983–3988.

Alblas, J., Slager-Davidov, R., Steenbergh, P. H., Sussenbach, J. S., & Van Der Burg, B. (1998). The role of MAP kinase in TPA-mediated cell cycle arrest of human breast cancer cells. *Oncogene*, *16*(1), 131–139.

Alfieri, C., Chang, L., Zhang, Z., Yang, J., Maslen, S., Skehel, M., & Barford, D. (2016). Molecular basis of APC/C regulation by the spindle assembly checkpoint. *Nature*, *536*(7617), 431–436.

Allen, R. D., Kim, H. K., Sarafova, S. D., & Siu, G. (2001). Negative Regulation of CD4 Gene Expression by a HES-1–c-Myb Complex. *Molecular and Cellular Biology*, *21*(9), 3071–3082.

Ankers, J. M., Awais, R., Jones, N. A., Boyd, J., Ryan, S., Adamson, A. D., Harper, C. V., Bridge, L., Spiller, D. G., Jackson, D. A., Paszek, P., Sï¿½e, V., & White, M. R. H. (2016). Dynamic NF-κb and E2F interactions control the priority and timing of inflammatory signalling and cell proliferation. *ELife*, *5*, 1–35.

Anna M. Bentley, Guillaume Normand, Jonathan Hoyt, and R. W. K. (2007). Distinct Sequence Elements of Cyclin B1 Promote Localization to Chromatin, Centrosomes, and Kinetochores during Mitosis. *Molecular Biology of the Cell*, *18*, 986–994.

Arai, M. A., Ishikawa, N., Tanaka, M., Uemura, K., Sugimitsu, N., Suganami, A., Tamura, Y., Koyano, T., Kowithayakorn, T., & Ishibashi, M. (2016). Hes1 inhibitor isolated by target protein oriented natural products isolation (TPO-NAPI) of differentiation activators of neural stem cells. *Chemical Science*, *7*(2), 1514–1520.

Arai, M. A., Masada, A., Ohtsuka, T., Kageyama, R., & Ishibashi, M. (2009). The first Hes1 dimer inhibitors from natural products. *Bioorganic and Medicinal Chemistry Letters*, *19*(19), 5778–5781.

Arai, M. A., Morita, K., Kawano, H., Makita, Y., Hashimoto, M., Suganami, A., Tamura, Y., Sadhu, S. K., Ahmed, F., & Ishibashi, M. (2020). Target protein-oriented isolation of Hes1 dimer inhibitors using protein based methods. *Scientific Reports*, *10*(1), 1–9.

Asbury, C. L. (2017). Anaphase A: Disassembling microtubules move chromosomes toward spindle poles. *Biology*, *6*(1). 15.

Attwooll, C., Denchi, E. L., & Helin, K. (2004). The E2F family: Specific functions and overlapping interests. *EMBO Journal*, *23*(24), 4709–4716.

Awasthi, P., Foiani, M., & Kumar, A. (2015). ATM and ATR signaling at a glance. *Journal of cell science*, *128*(23), 4255-4262.

Babaei Khalili, M., Yazdanparast, R., & Nowrouzi, A. (2018). Induction of transient cell

cycle arrest by H2O2 via modulation of ultradian oscillations of Hes1, Socs3, and p-Stat3 in fibroblast cells. *Journal of Cellular Biochemistry*, *119*(2), 1453–1462.
Baek, J. H., Hatakeyama, J., Sakamoto, S., Ohtsuka, T., & Kageyama, R. (2006). Persistent and high levels of Hes1 expression regulate boundary formation in the developing central nervous system. *Development*, *133*(13), 2467–2476.
Bailey, T. L., Boden, M., Buske, F. A., Frith, M., Grant, C. E., Clementi, L., Ren, J., Li, W. W., & Noble, W. S. (2009). MEME Suite: Tools for motif discovery and searching. *Nucleic Acids Research*, *37*(SUPPL. 2), 202–208.
Baldwin, A. S. (1996). The NF-κB and IκB proteins: New discoveries and insights. *Annual Review of Immunology*, *14*, 649–681.
Banin, S., Moyal, L., Shieh, S. Y., Taya, Y., Anderson, C. W., Chessa, L., Smorodinsky, N. I., Prives, C., Reiss, Y., Shiloh, Y., & Ziv, Y. (1998). Enhanced phosphorylation of p53 by ATM in response to DNA damage. *Science*, *281*(5383), 1674–1677.
Bar-Or, R. L., Maya, R., Segel, L. A., Alon, U., Levine, A. J., & Oren, M. (2000). Generation of oscillations by the p53-Mdm2 feedback loop: A theoretical and experimental study. *Proceedings of the National Academy of Sciences of the United States of America*, *97*(21), 11250–11255.
Barr, A. R., Cooper, S., Heldt, F. S., Butera, F., Stoy, H., Mansfeld, J., Novák, B., & Bakal, C. (2017). DNA damage during S-phase mediates the proliferation-quiescence decision in the subsequent G1 via p21 expression. *Nature Communications*, *8*, 1-17.
Bartel, D. B. (2004). MicroRNAs: Genomics, Biogenesis, Mechanism, and Function. *Cell*, *116*, 281–297.
Batty, P., & Gerlich, D. W. (2019). Mitotic Chromosome Mechanics: How Cells Segregate Their Genome. *Trends in Cell Biology*, *29*(9), 717–726.
Bavelloni, A., Piazzi, M., Raffini, M., Faenza, I., & Blalock, W. L. (2015). Prohibitin 2: At a communications crossroads. *IUBMB Life*, *67*(4), 239–254.
Beach, D., Durkacz, B., & Nurse, P. (1982). Functionally homologous cell cycle control genes in budding and fission yeast. *Nature*, *300*(5894), 706–709.
Ben-Ze'ev, A., Farmer, S. R., & Penman, S. (1979). Mechanisms of Regulating Tubulin Synthesis in Cultured Mammalian Cells. *Cell*, *17*, 319–325.
Bertoli, C., Skotheim, J. M., & De Bruin, R. A. M. (2013). Control of cell cycle transcription during G1 and S phases. *Nature Reviews Molecular Cell Biology*, *14*(8), 518–528.
Bertrand, E., Chartrand, P., Schaefer, M., Shenoy, S. M., Singer, R. H., & Long, R. M. (1998). Localization of ASH1 mRNA particles in living yeast. *Molecular Cell*, *2*(4), 437–445.
Bertrand, N., Castro, D. S., & Guillemot, F. (2002). Proneural genes and the specification of neural cell types. *Nature Reviews Neuroscience*, *3*(7), 517–530.
Bhat, R., Glimm, T., Linde-Medina, M., Cui, C., & Newman, S. A. (2019). Synchronization of Hes1 oscillations coordinates and refines condensation formation and patterning of the avian limb skeleton. *Mechanisms of Development*, *156*, 41–54.
Blagosklonny, M. V., & Pardee, A. B. (2002). The restriction point of the cell cycle. *Cell Cycle*, *1*(2), 102–109.
Blake-Hodek, K. A., Williams, B. C., Zhao, Y., Castilho, P. V., Chen, W., Mao, Y., Yamamoto, T. M., & Goldberg, M. L. (2012). Determinants for Activation of the Atypical AGC Kinase Greatwall during M Phase Entry. *Molecular and Cellular Biology*, *32*(8), 1337–1353.
Bonev, B., Pisco, A., & Papalopulu, N. (2011). MicroRNA-9 Reveals Regional Diversity of Neural Progenitors along the Anterior-Posterior Axis. *Developmental Cell*, *20*(1), 19–32.
Bonev, B., Stanley, P., & Papalopulu, N. (2012). MicroRNA-9 modulates hes1 ultradian

oscillations by forming a double-negative feedback loop. *Cell Reports*, *2*(1), 10–18.
Borggrefe, T., & Oswald, F. (2009). The Notch signaling pathway: Transcriptional regulation at Notch target genes. *Cellular and Molecular Life Sciences*, *66*(10), 1631–1646.
Boström, J., Sramkova, Z., Salašová, A., Johard, H., Mahdessian, D., Fedr, R., Marks, C., Medalová, J., Souček, K., Lundberg, E., Linnarsson, S., Bryja, V., Sekyrova, P., Altun, M., & Andäng, M. (2017). Comparative cell cycle transcriptomics reveals synchronization of developmental transcription factor networks in cancer cells. *PLoS ONE*, *12*(12), 1–24.
Botz, J. R., Zerfass-Thome, K., Spitkovsky, D., Delius, H., Vogt, B., Eilers, M., Hatzigeorgiou, A., Pidder, A., Rr, J.-D., Tumorvirologie, F. A., & Bioinformatik, F. (1996). Cell Cycle Regulation of the Murine Cyclin E Gene Depends on an E2F Binding Site in the Promoter. *Molecular and Cellular Biology*, *16*(7), 3401–3409.
Bravo, R., Frank, R., Blundell, P. A., & Macdonald-Bravo, H. (1987). Cyclin/PCNA is the auxiliary protein of DNA polymerase-delta. *Nature*, *326*. 515–517.
Brito, D. A., & Rieder, C. L. (2006). Mitotic Checkpoint Slippage in Humans Occurs via Cyclin B Destruction in the Presence of an Active Checkpoint. *Current Biology*, *16*(12), 1194–1200.
Burgess, S. G., Peset, I., Joseph, N., Cavazza, T., Vernos, I., Pfuhl, M., Gergely, F., & Bayliss, R. (2015). Aurora-A-Dependent Control of TACC3 Influences the Rate of Mitotic Spindle Assembly. *PLoS Genetics*, *11*(7).
Butler, M. P., Honma, S., Fukumoto, T., Kawamoto, T., Fujimoto, K., Noshiro, M., Kato, Y., & Honma, K. I. (2004). Dec1 and Dec2 Expression Is Disrupted in the Suprachiasmatic Nuclei of Clock Mutant Mice. *Journal of Biological Rhythms*, *19*(2), 126–134.
Buttitta, L. A., & Edgar, B. A. (2007). Mechanisms controlling cell cycle exit upon terminal differentiation. *Current Opinion in Cell Biology*, *19*(6), 697–704.
Carrieri, F. A., Murray, P. J., Ditsova, D., Ferris, M. A., Davies, P., & Dale, J. K. (2019). CDK1 and CDK2 regulate NICD1 turnover and the periodicity of the segmentation clock. *EMBO Reports*, e46436.
Carroll, S. B., Laughon, A., & Thalley, B. S. (1988). Expression, function, and regulation of the hairy segmentation protein in the Drosophila embryo. *Genes & Development*, *2*(7), 883–890.
Catchpole, S., Tavner, F., Le Cam, L., Sardet, C., & Watson, R. J. (2002). A B-myb promoter corepressor site facilitates in vivo occupation of the adjacent E2F site by p107·E2F and p130·E2F complexes. *Journal of Biological Chemistry*, *277*(41), 39015–39024.
Cave, J. W., Loh, F., Surpris, J. W., Xia, L., & Caudy, M. A. (2005). A DNA Transcription Code for Cell-Specific Gene Activation by Notch Signaling. *Current Biology*, *15*, 94–104.
Cenciarelli, C., Marei, H. E., Zonfrillo, M., Casalbore, P., Felsani, A., Giannetti, S., Trevisi, G., Althani, A., & Mangiola, A. (2017). The interference of Notch1 target Hes1 affects cell growth, differentiation and invasiveness of glioblastoma stem cells through modulation of multiple oncogenic targets. *Oncotarget*, *8*(11), 17873–17886.
Cenciarelli, C., Marei, H. E., Zonfrillo, M., Casalbore, P., Felsani, A., Giannetti, S., ... & Mangiola, A. (2017). The interference of Notch1 target Hes1 affects cell growth, differentiation and invasiveness of glioblastoma stem cells through modulation of multiple oncogenic targets. *Oncotarget*, *8*(11), 17873.
Chae, H. B., Yun, J., Bang, Y. J., & Shin, D. Y. (2004). Cdk2-dependent phosphorylation of the NF-Y transcription factor is essential for the expression of the cell cycle-regulatory genes and cell cycle G1/S and G2/M transitions. *Oncogene*, *23*(23), 4084–4088.
Chao, H. X., Fakhreddin, R. I., Shimerov, H. K., Kedziora, K. M., Kumar, R. J., Perez, J., Limas, J. C., Grant, G. D., Cook, J. G., Gupta, G. P., & Purvis, J. E. (2019). Evidence

that the human cell cycle is a series of uncoupled, memoryless phases. *Molecular Systems Biology*, *15*(3), 1–19.
Chen, G., Fernandez, J., Mische, S., & Courey, A. J. (1999). A functional interaction between the histone deacetylase Rpd3 and the corepressor Groucho in Drosophila development. *Genes and Development*, *13*(17), 2218–2230.
Chen, H., Thiagalingam, A., Chopra, H., Borges, M. W., Feder, J. N., Nelkin, B. D., Baylin, S. B., & Ball, D. W. (1997). Conservation of the Drosophila lateral inhibition pathway in human lung cancer: A hairy-related protein (HES-1) directly represses achaete-scute homolog-1 expression. *Proceedings of the National Academy of Sciences of the United States of America*, *94*(10), 5355–5360.
Chen, J., Lin, J., & Levine, A. J. (1995). Regulation of transcription functions of the p53 tumor suppressor by the mdm-2 oncogene. *Molecular Medicine (Cambridge, Mass.)*, *1*(2), 142–152.
Chen, Q., Zhang, X., Jiang, Q., Clarke, P. R., & Zhang, C. (2008). Cyclin B1 is localized to unattached kinetochores and contributes to efficient microtubule attachment and proper chromosome alignment during mitosis. *Cell Research*, *18*(2), 268–280.
Cheung, T. H., & Rando, T. A. (2013). Molecular regulation of stem cell quiescence. *Nature Reviews Molecular Cell Biology*, *14*(6), 329–340.
Chiou, H. Y. C., Liu, S. Y., Lin, C. H., & Lee, E. H. (2014). Hes-1 SUMOylation by protein inhibitor of activated STAT1 enhances the suppressing effect of Hes-1 on GADD45α expression to increase cell survival. *Journal of Biomedical Science*, *21*(1), 1–23.
Chu, Y., Yao, P. Y., Wang, W., Wang, D., Wang, Z., Zhang, L., Huang, Y., Ke, Y., Ding, X., & Yao, X. (2011). Aurora B kinase activation requires survivin priming phosphorylation by PLK1. *Journal of Molecular Cell Biology*, *3*(4), 260–267.
Cisneros, E., Latasa, M. J., García-Flores, M., & Frade, J. M. (2008). Instability of Notch1 and Delta1 mRNAs and reduced Notch activity in vertebrate neuroepithelial cells undergoing S-phase. *Molecular and Cellular Neuroscience*, *37*(4), 820–831.
Cleveland, D. W. (1989). Autoregulated control of tubilin synthesis in animal cells. *Current Opinion in Cell Biology*, *1*(1), 10–14.
Clijsters, L., Van Zon, W., Ter Riet, B., Voets, E., Boekhout, M., Ogink, J., Rumpf-Kienzl, C., & Wolthuis, R. M. F. (2014). Inefficient degradation of cyclin B1 re-activates the spindle checkpoint right after sister chromatid disjunction. *Cell Cycle*, *13*(15), 2370–2378.
Cobrinik, D. (2005). Pocket proteins and cell cycle control. *Oncogene*, *24*(17), 2796–2809.
Cogswell, J. P., Godlevski, M. M., Bonham, M., Bisi, J., & Babiss, L. (1995). Upstream stimulatory factor regulates expression of the cell cycle-dependent cyclin B1 gene promoter. *Molecular and Cellular Biology*, *15*(5), 2782–2790.
Coller, H. A., Sang, L., & Roberts, J. M. (2006). A new description of cellular quiescence. *PLoS Biology*, *4*(3), 0329–0349.
Comșa, Ș., Cîmpean, A. M., & Raica, M. (2015). *Mcf7 Cell Line Story*. *3154*, 3147–3154.
Crews, S. T., & Pearson, J. C. (2009). Transcriptional autoregulation in development. *Current Biology*, *19*(6), 241–246.
Cundell, M. J., Bastos, R. N., Zhang, T., Holder, J., Gruneberg, U., Novak, B., & Barr, F. A. (2013). The BEG (PP2A-B55/ENSA/Greatwall) Pathway Ensures Cytokinesis follows Chromosome Separation. *Molecular Cell*, *52*(3), 393–405.
Dagogo-Jack, I., & Shaw, A. T. (2018). Tumour heterogeneity and resistance to cancer therapies. *Nature Reviews Clinical Oncology*, *15*(2), 81–94.
Dawson, K. B., Madoc-Jones, H., & Field, E. O. (1965). Variations in the Generation Times of a Strain of Rat Sarcoma Cells in Culture. *Experimental Cell Research*, *38*, 75–84.
Dawson, S. R., Turner, D. L., Weintraub, H., & Parkhurst, S. M. (1995). Specificity for the

hairy/enhancer of split basic helix-loop-helix (bHLH) proteins maps outside the bHLH domain and suggests two separable modes of transcriptional repression. *Molecular and Cellular Biology*, *15*(12), 6923–6931.

de Cárcer, G., Venkateswaran, S. V., Salgueiro, L., El Bakkali, A., Somogyi, K., Rowald, K., Montañés, P., Sanclemente, M., Escobar, B., de Martino, A., McGranahan, N., Malumbres, M., & Sotillo, R. (2018). Plk1 overexpression induces chromosomal instability and suppresses tumor development. *Nature Communications*, *9*(1), 1-14.

De Pietri Tonelli, D., Pulvers, J. N., Haffner, C., Murchison, E. P., Hannon, G. J., & Huttner, W. B. (2008). miRNAs are essential for survival and differentiation of newborn neurons but not for expansion of neural progenitors during early neurogenesis in the mouse embryonic neocortex. *Development*, *135*(23), 3911–3921.

De Strooper, B., Annaert, W., Cupers, P., Saftig, P., Craessaerts, K., Mumm, J. S., Schroeter, E. H., Schrijvers, V., Wolfe, M. S., Ray, W. J., Goate, A., & Kopan, R. (1999). A presenilin-1-dependent γ-secretase-like protease mediates release of notch intracellular domain. *Nature*, *398*(6727), 518–522.

DeGregori, J., Kowalik, T., & Nevins, J. R. (1995). Cellular targets for activation by the E2F1 transcription factor include DNA synthesis- and G1/S-regulatory genes. *Molecular and Cellular Biology*, *15*(8), 4215–4224.

Dhuppar, S., & Mazumder, A. (2020). Investigating cell cycle-dependent gene expression in the context of nuclear architecture at single-allele resolution. *Journal of Cell Science*, *133*(12).

Diril, M. K., Bisteau, X., Kitagawa, M., Caldez, M. J., & Wee, S. (2016). *Loss of the Greatwall Kinase Weakens the Spindle Assembly Checkpoint*. 1–26.

Ditchfield, C., Johnson, V. L., Tighe, A., Ellston, R., Haworth, C., Johnson, T., Mortlock, A., Keen, N., & Taylor, S. S. (2003). Aurora B couples chromosome alignment with anaphase by targeting BubR1, Mad2, and Cenp-E to kinetochores. *Journal of Cell Biology*, *161*(2), 267–280.

Dobin, A., Davis, C. A., Schlesinger, F., Drenkow, J., Zaleski, C., Jha, S., Batut, P., Chaisson, M., & Gingeras, T. R. (2013). STAR: Ultrafast universal RNA-seq aligner. *Bioinformatics*, *29*(1), 15–21.

Dohadwala, M., Da Cruz Silva, E. E. F., Hall, F. L., Williams, R. T., Carbonaro-Hall, D. A., Nairn, A. C., Greengard, P., & Berndt, N. (1994). Phosphorylation and inactivation of protein phosphatase 1 by cyclin- dependent kinases. *Proceedings of the National Academy of Sciences of the United States of America*, *91*(14), 6408–6412.

Dolatabadi, S., Candia, J., Akrap, N., Vannas, C., Tomic, T. T., Losert, W., Landberg, G., Åman, P., & Ståhlberg, A. (2017). Cell cycle and cell size dependent gene expression reveals distinct subpopulations at single-cell level. *Frontiers in Genetics*, *8*.

Drabsch, Y., Hugo, H., Zhang, R., Dowhan, D. H., Miao, Y. R., Gewirtz, A. M., Barry, S. C., Ramsey, R. G., & Gonda, T. J. (2007). Mechanism of and requirement for estrogen-regulated MYB expression in estrogen- receptor-positive breast cancer cells. *Proceedings of the National Academy of Sciences*, *104*(34), 13762–13767.

Du, J., Cai, X., Yao, J., Ding, X., Wu, Q., Pei, S., Jiang, K., Zhang, Y., Wang, W., Shi, Y., Lai, Y., Shen, J., Teng, M., Huang, H., Fei, Q., Reddy, E. S., Zhu, J., Jin, C., & Yao, X. (2008). The mitotic checkpoint kinase NEK2A regulates kinetochore microtubule attachment stability. *Oncogene*, *27*(29), 4107–4114.

Du, J., Yan, L., Torres, R., Gong, X., Bian, H., Marugan, C., Boehnke, K., Baquero, C., Hui, Y. H., Chapman, S. C., Yang, Y., Zeng, Y., Bogner, S. M., Foreman, R. T., Capen, A., Donoho, G. P., Van Horn, R. D., Barnard, D. S., Dempsey, J. A., … Campbell, R. M. (2019). Aurora A–selective inhibitor LY3295668 leads to dominant mitotic arrest, apoptosis in cancer cells, and shows potent preclinical antitumor efficacy. *Molecular*

Cancer Therapeutics, *18*(12), 2207–2219.
Ekholm, S. V., & Reed, S. I. (2000). Regulation of G1 cyclin-dependent kinases in the mammalian cell cycle. *Current Opinion in Cell Biology*, *12*(6), 676–684.
Elowitz, M. B., Levine, A. J., Siggia, E. D., & Swain, P. S. (2002). Stochastic gene expression in a single cell. *Science*, *297*(5584), 1183–1186.
Espert, A., Uluocak, P., Bastos, R. N., Mangat, D., Graab, P., & Gruneberg, U. (2014). PP2A-B56 opposes Mps1 phosphorylation of Knl1 and thereby promotes spindle assembly checkpoint silencing. *Journal of Cell Biology*, *206*(7), 833–842.
Espinosa, J. M., & Emerson, B. M. (2001). Transcriptional regulation by p53 through intrinsic DNA/chromatin binding and site-directed cofactor recruitment. *Molecular Cell*, *8*(1), 57–69.
Evans, T., Rosenthal, E. T., Youngblom, J., Distel, D., & Hunt, T. (1983). Cyclin: A protein specified by maternal mRNA in sea urchin eggs that is destroyed at each cleavage division. *Cell*, *33*(2), 389–396.
Eyers, P. A., Keeshan, K., & Kannan, N. (2017). Tribbles in the 21st Century: The Evolving Roles of Tribbles Pseudokinases in Biology and Disease. *Trends in Cell Biology*, *27*(4), 284–298.
Fanale, D., Bronte, G., Passiglia, F., Calò, V., Castiglia, M., Di Piazza, F., Barraco, N., Cangemi, A., Catarella, M. T., Insalaco, L., Listì, A., Maragliano, R., Massihnia, D., Perez, A., Toia, F., Cicero, G., & Bazan, V. (2015). Stabilizing versus destabilizing the microtubules: A double-edge sword for an effective cancer treatment option? *Analytical Cellular Pathology*, *2015*.
Farina, A., Manni, I., Fontemaggi, G., Tiainen, M., Cenciarelli, C., Bellorini, M., Mantovani, R., Sacchi, A., & Piaggio, G. (1999). Down-regulation of cyclin B1 gene transcription in terminally differentiated skeletal muscle cells is associated with loss of functional CCAAT-binding NF-Y complex. *Oncogene*, *18*(18), 2818–2827.
Farshadi, E., Yan, J., Leclere, P., Goldbeter, A., Chaves, I., & van der Horst, G. T. J. (2019). The positive circadian regulators CLOCK and BMAL1 control G2/M cell cycle transition through Cyclin B1. *Cell Cycle*, *18*(1), 16–33.
Feillet, C., Krusche, P., Tamanini, F., Janssens, R. C., Downey, M. J., Martin, P., Teboul, M., Saito, S., Lévi, F. A., Bretschneider, T., Van Der Horst, G. T. J., Delaunay, F., & Rand, D. A. (2014). Phase locking and multiple oscillating attractors for the coupled mammalian clock and cell cycle. *Proceedings of the National Academy of Sciences of the United States of America*, *111*(27), 9828–9833.
Feillet, C., van der Horst, G. T. J., Levi, F., Rand, D. A., & Delaunay, F. (2015). Coupling between the circadian clock and cell cycle oscillators: Implication for healthy cells and malignant growth. *Frontiers in Neurology*, *6*, 1–7.
Ferreira, L. T., Figueiredo, A. C., Orr, B., Lopes, D., & Maiato, H. (2018). Dissecting the role of the tubulin code in mitosis. *Methods in Cell Biology*, *144*, 33–74.
Fischer, A., & Gessler, M. (2007). Delta-Notch-and then? Protein interactions and proposed modes of repression by Hes and Hey bHLH factors. *Nucleic Acids Research*, *35*(14), 4583–4596.
Fischer, M., & Müller, G. A. (2017). Cell cycle transcription control: DREAM/MuvB and RB-E2F complexes. *Critical Reviews in Biochemistry and Molecular Biology*, *52*(6), 638–662.
Fisher, A. L., Ohsako, S., & Caudy, M. (1996). The WRPW motif of the hairy-related basic helix-loop-helix repressor proteins acts as a 4-amino-acid transcription repression and protein-protein interaction domain. *Molecular and Cellular Biology*, *16*(6), 2670–2677.
Foley, E. A., & Kapoor, T. M. (2013). Microtubule attachment and spindle assembly checkpoint signalling at the kinetochore. *Nature Reviews Molecular Cell Biology*, *14*(1),

25–37.
Fouts, D. E., True, H. L., & Celander, D. W. (1997). Functional recognition of fragmented operator sites by R17/MS2 coat protein, a translational repressor. *Nucleic Acids Research*, *25*(22), 4464–4473.
Froese, G. (1964). The distribution and interdependence of generation times of HeLa cells. *Experimental Cell Research*, *35*(2), 415–419.
Fujimitsu, K., Grimaldi, M., & Yamano, H. (2016). Cyclin-dependent kinase 1–dependent activation of APC/C ubiquitin ligase. *Science*, *352*(6289), 1121-1124.
Fukuda, A., Kawaguchi, Y., Furuyama, K., Kodama, S., Horiguchi, M., Kuhara, T., Koizumi, M., Boyer, D. F., Fujimoto, K., Doi, R., Kageyama, R., Wright, C. V. E., & Chiba, T. (2006). Ectopic pancreas formation in Hes1-knockout mice reveals plasticity of endodermal progenitors of the gut, bile duct, and pancreas. *Journal of Clinical Investigation*, *116*(6), 1484–1493.
Fung, T. K., & Poon, R. Y. C. (2005). A roller coaster ride with the mitotic cyclins. *Seminars in Cell and Developmental Biology*, *16*(3), 335–342.
Gao, F., Zhang, Y., Wang, S., Liu, Y., Zheng, L., Yang, J., Huang, W., Ye, Y., Luo, W., & Xiao, D. (2014). Hes1 is involved in the self-renewal and tumourigenicity of stem-like cancer cells in colon cancer. *Scientific Reports*, *4*.
Gascoigne, K. E., & Taylor, S. S. (2008). Cancer Cells Display Profound Intra- and Interline Variation following Prolonged Exposure to Antimitotic Drugs. *Cancer Cell*, *14*(2), 111–122.
Gasic, I., Boswell, S. A., & Mitchison, T. J. (2019). Tubulin mRNA stability is sensitive to change in microtubule dynamics caused by multiple physiological and toxic cues. *PLoS Biology*, 1–23.
Gautier, J., Norbury, C., Lohka, M., Nurse, P., & Maller, J. (1988). Purified maturation-promoting factor contains the product of a Xenopus homolog of the fission yeast cell cycle control gene cdc2+. *Cell*, *54*(3), 433–439.
Gavet, O., & Pines, J. (2010). Progressive Activation of CyclinB1-Cdk1 Coordinates Entry to Mitosis. *Developmental Cell*, *18*(4), 533–543.
Gendelman, R., Xing, H., Mirzoeva, O. K., Sarde, P., Curtis, C., Feiler, H. S., McDonagh, P., Gray, J. W., Khalil, I., & Korn, W. M. (2017). Bayesian network inference modeling identifies TRIB1 as a novel regulator of cell-cycle progression and survival in cancer cells. *Cancer Research*, *77*(7), 1575–1585.
Georgia, S., Soliz, R., Li, M., Zhang, P., & Bhushan, A. (2006). p57 and Hes1 coordinate cell cycle exit with self-renewal of pancreatic progenitors. *Developmental Biology*, *298*(1), 22–31.
Gérard, C., & Goldbeter, A. (2009). Temporal self-organization of the cyclin/Cdk network driving the mammalian cell cycle. *Proceedings of the National Academy of Sciences of the United States of America*, *106*(51), 21643–21648.
Gergely, F., Draviam, V. M., & Raff, J. W. (2003). The ch-TOG/XMAP215 protein is essential for spindle pole organization in human somatic cells. *Genes and Development*, *17*(3), 336–341.
Geva-Zatorsky, N., Rosenfeld, N., Itzkovitz, S., Milo, R., Sigal, A., Dekel, E., Yarnitzky, T., Liron, Y., Polak, P., Lahav, G., & Alon, U. (2006). Oscillations and variability in the p53 system. *Molecular Systems Biology*, *2*, 1–13.
Gharbi-Ayachi, A., Labbé, J.-C., Burgess, A., Vigneron, S., Strub, J.-M., Brioudes, E., Van-Dorsselaer, A., Castro, A., & Lorca, T. (2010). The Substrate of Greatwall Kinase, Arpp19, Controls Mitosis by Inhibiting Protein Phosphatase 2A. *Science*, *330*, 1673–1677.
Gibbs, H. C., Chang-Gonzalez, A., Hwang, W., Yeh, A. T., & Lekven, A. C. (2017).

Midbrain-hindbrain boundary morphogenesis: At the intersection of wnt and Fgf signaling. *Frontiers in Neuroanatomy*, *11*, 1–17.
Ginestier, C., Hur, M. H., Charafe-Jauffret, E., Monville, F., Dutcher, J., Brown, M., Jacquemier, J., Viens, P., Kleer, C. G., Liu, S., Schott, A., Hayes, D., Birnbaum, D., Wicha, M. S., & Dontu, G. (2007). ALDH1 Is a Marker of Normal and Malignant Human Mammary Stem Cells and a Predictor of Poor Clinical Outcome. *Cell Stem Cell*, *1*(5), 555–567.
Ginzberg, M. B., Chang, N., D'souza, H., Patel, N., Kafri, R., & Kirschner, M. W. (2018). Cell size sensing in animal cells coordinates anabolic growth rates and cell cycle progression to maintain cell size uniformity. *ELife*, *7*, 1–27.
Giraldez, A. J., Cinalli, R. M., Glasner, M. E., Enright, A. J., Thomson, J. M., Baskerville, S., Hammond, S. M., Bartel, D. P., & Schier, A. F. (2005). MicroRNAs regulate brain morphogenesis in zebrafish. *Science*, *308*(5723), 833–838.
Golsteyn, R. M., Mundt, K. E., Fry, A. M., & Nigg, E. A. (1995). Cell cycle regulation of the activity and subcellular localization of PLK1, a human protein kinase implicated in mitotic spindle function. *Journal of Cell Biology*, *129*(6), 1617–1628.
Gong, D., Pomerening, J. R., Myers, J. W., Gustavsson, C., Jones, J. T., Hahn, A. T., Meyer, T., & Ferrell, J. E. (2007). Cyclin A2 Regulates Nuclear-Envelope Breakdown and the Nuclear Accumulation of Cyclin B1. *Current Biology*, *17*(1), 85–91.
Goodfellow, M., Phillips, N. E., Manning, C., Galla, T., & Papalopulu, N. (2014). MicroRNA input into a neural ultradian oscillator controls emergence and timing of alternative cell states. *Nature Communications*, *5*. 1-10.
Gorr, I. H., Boos, D., & Stemmann, O. (2005). Mutual inhibition of separase and Cdk1 by two-step complex formation. *Molecular Cell*, *19*(1), 135–141.
Goto, H., Yasui, Y., Nigg, E. A., & Inagaki, M. (2002). Aurora-B phosphorylates Histone H3 at serine28 with regard to the mitotic chromosome condensation. *Genes to Cells*, *7*(1), 11–17.
Granada, A. E., Jiménez, A., Stewart-Ornstein, J., Blüthgena, N., Reber, S., Jambhekar, A., & Lahav, G. (2020). The effects of proliferation status and cell cycle phase on the responses of single cells to chemotherapy. *Molecular Biology of the Cell*, *31*(8), 845–857.
Grant, G. D., Brooks, L., Zhang, X., Mahoneya, J. M., Martyanov, V., Wood, T. A., Sherlock, G., Cheng, C., & Whitfield, M. L. (2013). Identification of cell cycle-regulated genes periodically expressed in U2OS cells and their regulation by FOXM1 and E2F transcription factors. *Molecular Biology of the Cell*, *24*(23), 3634–3650.
Grbavec, D., & Stifani, S. (1996). Molecular interaction between TLE1 and the carboxyl-terminal domain of HES-1 containing the WRPW motif. *Biochemical and Biophysical Research Communications*, *223*(3), 701–705.
Gréchez-Cassiau, A., Rayet, B., Guillaumond, F., Teboul, M., & Delaunay, F. (2008). The circadian clock component BMAL1 is a critical regulator of p21 WAF1/CIP1 expression and hepatocyte proliferation. *Journal of Biological Chemistry*, *283*(8), 4535–4542.
Gruneberg, U., Neef, R., Honda, R., Nigg, E. A., & Barr, F. A. (2004). Relocation of Aurora B from centromeres to the central spindle at the metaphase to anaphase transition requires MKlp2. *Journal of Cell Biology*, *166*(2), 167–172.
Gu, J., Xia, X., Yan, P., Liu, H., Podust, V. N., Reynolds, A. B., & Fanning, E. (2004). Cell Cycle-dependent Regulation of a Human DNA Helicase That Localizes in DNA Damage Foci. *Molecular Biology of the Cell*, *15*, 3320–3332.
Gu, Y., Rosenblatt, J., & Morgan, D. O. (1992). Cell cycle regulation of CDK2 activity by phosphorylation of Thr160 and Tyr15. *EMBO Journal*, *11*(11), 3995–4005.
Guccione, E., Martinato, F., Finocchiaro, G., Luzi, L., Tizzoni, L., Dall' Olio, V., Zardo, G.,

Nervi, C., Bernard, L., & Amati, B. (2006). Myc-binding-site recognition in the human genome is determined by chromatin context. *Nature Cell Biology*, *8*(7), 764–770.
Guiley, K. Z., Iness, A. N., Saini, S., Tripathi, S., Lipsick, J. S., Litovchick, L., & Rubin, S. M. (2018). Structural mechanism of Myb-MuvB assembly. *Proceedings of the National Academy of Sciences of the United States of America*, *115*(40), 10016–10021.
Gupta, P. B., Fillmore, C. M., Jiang, G., Shapira, S. D., Tao, K., Kuperwasser, C., & Lander, E. S. (2011). Stochastic state transitions give rise to phenotypic equilibrium in populations of cancer cells. *Cell*, *146*(4), 633–644.
Gupta, S., Stamatoyannopoulos, J. A., Bailey, T. L., & Noble, W. S. (2007). Quantifying similarity between motifs. *Genome Biology*, *8*(2).
Gut, G., Tadmor, M. D., Pe'Er, D., Pelkmans, L., & Liberali, P. (2015). Trajectories of cell-cycle progression from fixed cell populations. *Nature Methods*, *12*(10), 951–954.
Guttridge, D. C., Albanese, C., Reuther, J. Y., Pestell, R. G., & Baldwin, A. S. (1999). NF-κB Controls Cell Growth and Differentiation through Transcriptional Regulation of Cyclin D1. *Molecular and Cellular Biology*, *19*(8), 5785–5799.
Hafner, A., Reyes, J., Stewart-Ornstein, J., Tsabar, M., Jambhekar, A., & Lahav, G. (2020). Quantifying the Central Dogma in the p53 Pathway in Live Single Cells. *Cell Systems*, 1–11.
Hagting, A., Den Elzen, N., Vodermaier, H. C., Waizenegger, I. C., Peters, J. M., & Pines, J. (2002). Human securin proteolysis is controlled by the spindle checkpoint and reveals when the APC/C switches from activation by Cdc20 to Cdh1. *Journal of Cell Biology*, *157*(7), 1125–1137.
Hahn, A. T., Jones, J. T., & Meyer, T. (2009). Quantitative analysis of cell cycle phase durations and PC12 differentiation using fluorescent biosensors. *Cell Cycle*, *8*(7), 1044–1052.
Harrow, J., Frankish, A., Gonzalez, J. M., Tapanari, E., Diekhans, M., Kokocinski, F., Aken, B. L., Barrell, D., Zadissa, A., Searle, S., Barnes, I., Bignell, A., Boychenko, V., Hunt, T., Kay, M., Mukherjee, G., Rajan, J., Despacio-Reyes, G., Saunders, G., … Hubbard, T. J. (2012). GENCODE: The reference human genome annotation for the ENCODE project. *Genome Research*, *22*(9), 1760–1774.
Hartman, J., Müller, P., Foster, J. S., Wimalasena, J., Gustafsson, J. Å., & Ström, A. (2004). HES-1 inhibits 17β-estradiol and heregulin-β1-mediated upregulation of E2F-1. *Oncogene*, *23*(54), 8826–8833.
Hatakeyama, J., Bessho, Y., Katoh, K., Ookawara, S., Fujioka, M., Guillemot, F., & Kageyama, R. (2004). Hes genes regulate size, shape and histogenesis of the nervous system by control of the timing of neural stem cell differentiation. *Development*, *131*(22), 5539–5550.
Hauf, S., Cole, R. W., LaTerra, S., Zimmer, C., Schnapp, G., Walter, R., Heckel, A., Van Meel, J., Rieder, C. L., & Peters, J. M. (2003). The small molecule Hesperadin reveals a role for Aurora B in correcting kinetochore-microtubule attachment and in maintaining the spindle assembly checkpoint. *Journal of Cell Biology*, *161*(2), 281–294.
Hauf, S., Waizenegger, I. C., & Peters, J. M. (2001). Cohesin cleavage by separase required for anaphase and cytokinesis in human cells. *Science*, *293*(5533), 1320–1323.
Haupt, Y., Mayat, R., Kazazt, A., & Orent, M. (1997). Mdm2 promotes the rapid degradation of p53. *Nature*, *387*, 296–299.
Hayward, D., Alfonso-Pérez, T., Cundell, M. J., Hopkins, M., Holder, J., Bancroft, J., Hutter, L. H., Novak, B., Barr, F. A., & Gruneberg, U. (2019). CDK1-CCNB1 creates a spindle checkpoint-permissive state by enabling MPS1 kinetochore localization. *Journal of Cell Biology*, *218*(4), 1182–1199.
Hégarat, N., Crncec, A., Suarez Peredo Rodriguez, M. F., Echegaray Iturra, F., Gu, Y.,

Busby, O., Lang, P. F., Barr, A. R., Bakal, C., Kanemaki, M. T., Lamond, A. I., Novak, B., Ly, T., & Hochegger, H. (2020). Cyclin A triggers Mitosis either via the Greatwall kinase pathway or Cyclin B. *The EMBO Journal*, *39*(11), 1–23.

Heinz, S., Benner, C., Spann, N., Bertolino, E., Lin, Y. C., Laslo, P., Cheng, J. X., Murre, C., Singh, H., & Glass, C. K. (2010). Simple Combinations of Lineage-Determining Transcription Factors Prime cis-Regulatory Elements Required for Macrophage and B Cell Identities. *Molecular Cell*, *38*(4), 576–589.

Hendzel, M. J., Wei, Y., Mancini, M. A., Van Hooser, A., Ranalli, T., Brinkley, B. R., Bazett-Jones, D. P., & Allis, C. D. (1997). Mitosis-specific phosphorylation of histone H3 initiates primarily within pericentromeric heterochromatin during G2 and spreads in an ordered fashion coincident with mitotic chromosome condensation. *Chromosoma*, *106*(6), 348–360.

Hirata, H., Tomita, K., Bessho, Y., & Kageyama, R. (2001). Hes1 and Hes3 regulate maintenance of the isthmic organizer and development of the mid/hindbrain. *EMBO Journal*, *20*(16), 4454–4466.

Hirata, H., Yoshiura, S., Ohtsuka, T., Bessho, Y., Harada, T., Yoshikawa, K., & Kageyama, R. (2002). Oscillatory expression of the BHLH factor Hes1 regulated by a negative feedback loop. *Science*, *298*(5594), 840–843.

Hoar, K., Chakravarty, A., Rabino, C., Wysong, D., Bowman, D., Roy, N., & Ecsedy, J. A. (2007). MLN8054, a Small-Molecule Inhibitor of Aurora A, Causes Spindle Pole and Chromosome Congression Defects Leading to Aneuploidy. *Molecular and Cellular Biology*, *27*(12), 4513–4525.

Holder, J., Poser, E., & Barr, F. A. (2019). Getting out of mitosis: spatial and temporal control of mitotic exit and cytokinesis by PP1 and PP2A. *FEBS Letters*, *593*(20), 2908–2924.

Honma, S., Kawamoto, T., Takagi, Y., Fujimoto, K., Sato, F., Noshiro, M., Kato, Y., & Honma, K. I. (2002). Dec1 and Dec2 are regulators of the mammalian molecular clock. *Nature*, *419*(6909), 841–844.

Housden, B. E., Fu, A. Q., Krejci, A., Bernard, F., Fischer, B., Tavaré, S., Russell, S., & Bray, S. J. (2013). Transcriptional Dynamics Elicited by a Short Pulse of Notch Activation Involves Feed-Forward Regulation by E(spl)/Hes Genes. *PLoS Genetics*, *9*(1), 13–16.

Huang, Q., Raya, A., DeJesus, P., Chao, S.-H., Quon, K. C., Caldwell, J. S., Chanda, S. K., Izpisua-Belmonte, J. C., & Schultz, P. G. (2004). Identification of p53 regulators by genome-wide functional analysis. *Proceedings of the National Academy of Sciences*, *101*(10), 3456–3461.

Huber, M. D., & Gerace, L. (2007). The size-wise nucleus: Nuclear volume control in eukaryotes. *Journal of Cell Biology*, *179*(4), 583–584.

Hümmer, S., & Mayer, T. U. (2009). Cdk1 Negatively Regulates Midzone Localization of the Mitotic Kinesin Mklp2 and the Chromosomal Passenger Complex. *Current Biology*, *19*(7), 607–612.

Imayoshi, I., Isomura, A., Harima, Y., Kawaguchi, K., Kori, H., Miyachi, H., Fujiwara, T., Ishidate, F., & Kageyama, R. (2013). Oscillatory control of factors determining multipotency and fate in mouse neural progenitors. *Science*, *342*(6163), 1203–1208.

Ingham, P. W., Howard, K. R., & Ish-Horowicz, D. (1985). Transcription pattern of the Drosophila segmentation gene hairy. *Nature*, *318*(6045), 439–445.

Innocente, S. A., Abrahamson, J. L. A., Cogswell, J. P., & Lee, J. M. (1999). p53 regulates a G2 checkpoint through cyclin B1. *Proceedings of the National Academy of Sciences of the United States of America*, *96*(5), 2147–2152.

Ishibashi, M., Ang, S.-L., Shiota, K., Nakanishi, S., Kageyama, R., & Guillemot, F. (1995).

Targeted disruption of mammalian hairy hehx-loop-.hellx factors, premature leads to up-regulation and Enhancer of split homolog-1 (HES-1) of neural neurogenesls, and severe neural tube defects. *Genes & Development*, *1*, 3136–3148.

Iso, T., Sartorelli, V., Poizat, C., Iezzi, S., Wu, H.-Y., Chung, G., Kedes, L., & Hamamori, Y. (2001). HERP, a Novel Heterodimer Partner of HES/E(spl) in Notch Signaling. *Molecular and Cellular Biology*, *21*(17), 6080–6089.

Izumi, T., & Maller, J. L. (1993). Elimination of cdc2 phosphorylation sites in the cdc25 phosphatase blocks initiation of M-phase. *Molecular Biology of the Cell*, *4*(12), 1337–1350.

Jeknić, S., Kudo, T., & Covert, M. W. (2019). Techniques for studying decoding of single cell dynamics. *Frontiers in Immunology*, *10*, 1–12.

Jensen, J., Pedersen, E. E., Galante, P., Hald, J., Heller, R. S., Ishibashi, M., Kageyama, R., Guillemot, F., Serup, P., & Madsen, O. D. (2000). Control of endodermal endocrine development by Hes-1. *Nature Genetics*, *24*(1), 36–44.

Jordan, N. V., Bardia, A., Wittner, B. S., Benes, C., Ligorio, M., Zheng, Y., Yu, M., Sundaresan, T. K., Licausi, J. A., Desai, R., O'Keefe, R. M., Ebright, R. Y., Boukhali, M., Sil, S., Onozato, M. L., Iafrate, A. J., Kapur, R., Sgroi, D., Ting, D. T., … Haber, D. A. (2016). HER2 expression identifies dynamic functional states within circulating breast cancer cells. *Nature*, *537*(7618), 102–106.

Joshi, I., Minter, L. M., Telfer, J., Demarest, R. M., Capobianco, A. J., Aster, J. C., Sicinski, P., Fauq, A., Golde, T. E., & Osborne, B. A. (2009). Notch signaling mediates G 1/S cell-cycle progression in T cells via cyclin D3 and its dependent kinases. *Blood* (Vol. 113, Issue 8, pp. 1689–1698).

Joukov, V., De Nicolo, A., Rodriguez, A., Walter, J. C., & Livingston, D. M. (2010). Centrosomal protein of 192 kDa (Cep192) promotes centrosome-driven spindle assembly by engaging in organelle-specific Aurora A activation. *Proceedings of the National Academy of Sciences of the United States of America*, *107*(49), 21022–21027.

Joukov, V., Walter, J. C., & De Nicolo, A. (2014). The Cep192-Organized Aurora A-Plk1 Cascade Is Essential for Centrosome Cycle and Bipolar Spindle Assembly. *Molecular Cell*, *55*(4), 578–591.

Kabos, P., Kabosova, A., & Neuman, T. (2002). Blocking HES1 expression initiates GABAergic differentiation and induces the expression of p21CIP1/WAF1 in human neural stem cells. *Journal of Biological Chemistry*, *277*(11), 8763–8766.

Kadauke, S., Udugama, M. I., Pawlicki, J. M., Achtman, J. C., Jain, D. P., Cheng, Y., Hardison, R. C., & Blobel, G. A. (2012). Tissue-specific mitotic bookmarking by hematopoietic transcription factor GATA1. *Cell*, *150*(4), 725–737.

Kærn, M., Elston, T. C., Blake, W. J., & Collins, J. J. (2005). Stochasticity in gene expression: From theories to phenotypes. *Nature Reviews Genetics*, *6*(6), 451–464.

Kageyama, R., Ohtsuka, T., & Kobayashi, T. (2007). The Hes gene family: Repressors and oscillators that orchestrate embryogenesis. *Development*, *134*(7), 1243–1251.

Kaldis, P. (1999). The cdk-activating kinase (CAK): From yeast to mammals. *Cellular and Molecular Life Sciences*, *55*(2), 284–296.

Karlsson, J., Kroneis, T., Jonasson, E., Larsson, E., & Ståhlberg, A. (2017). Transcriptomic Characterization of the Human Cell Cycle in Individual Unsynchronized Cells. *Journal of Molecular Biology*, *429*(24), 3909–3924.

Kasashima, K., Ohta, E., Kagawa, Y., & Endo, H. (2006). Mitochondrial functions and estrogen receptor-dependent nuclear translocation of pleiotropic human prohibitin 2. *Journal of Biological Chemistry*, *281*(47), 36401–36410.

Katula, K. S., Wright, K. L., Paul, H., Surman, D. R., Nuckolls, F. J., Smith, J. W., Ting, J. P. Y., Yates, J., & Cogswell, J. P. (1997). Cyclin-dependent kinase activation and S-phase

induction of the cyclin B1 gene are linked through the CCAAT elements. *Cell Growth and Differentiation*, *8*(7), 811–820.
Kempe, H., Schwabe, A., Crémazy, F., Verschure, P. J., & Bruggeman, F. J. (2015). The volumes and transcript counts of single cells reveal concentration homeostasis and capture biological noise. *Molecular Biology of the Cell*, *26*(4), 797–804.
Kern, D. M., Wilson-Kubalek, E. M., & Cheeseman, I. M. (2017). Astrin-SKAP complex reconstitution reveals its kinetochore interaction with microtubule-bound Ndc80. *Elife*, *6*, e26866.
Kettenbach, A. N., Schweppe, D. K., Faherty, B. K., Pechenick, D., Pletnev, A. A., & Gerber, S. A. (2011). Quantitative phosphoproteomics identifies substrates and functional modules of Aurora and Polo-like kinase activities in mitotic cells. *Science Signaling*, *4*(179).
Kiecker, C., & Lumsden, A. (2005). Compartments and their boundaries in vertebrate brain development. *Nature Reviews Neuroscience*, *6*(7), 553–564.
King, R. W., Peters, J. M., Tugendreich, S., Rolfe, M., Hieter, P., & Kirschner, M. W. (1995). A 20s complex containing CDC27 and CDC16 catalyzes the mitosis-specific conjugation of ubiquitin to cyclin B. *Cell*, *81*(2), 279–288.
Kinoshita, K., Noetzel, T. L., Pelletier, L., Mechtler, K., Drechsel, D. N., Schwager, A., Lee, M., Raff, J. W., & Hyman, A. A. (2005). Aurora A phosphorylation of TACC3/maskin is required for centrosome-dependent microtubule assembly in mitosis. *Journal of Cell Biology*, *170*(7), 1047–1055.
Kishi, K., van Vugt, M. A. T. M., Okamoto, K., Hayashi, Y., & Yaffe, M. B. (2009). Functional Dynamics of Polo-Like Kinase 1 at the Centrosome. *Molecular and Cellular Biology*, *29*(11), 3134–3150.
Klein, E. A., & Assoian, R. K. (2008). Transcriptional regulation of the cyclin D1 gene at a glance. *Journal of Cell Science*. *121*(23), 3853-3857
Kobayashi, T., Iwamoto, Y., Takashima, K., Isomura, A., Kosodo, Y., Kawakami, K., Nishioka, T., Kaibuchi, K., & Kageyama, R. (2015). Deubiquitinating enzymes regulate Hes1 stability and neuronal differentiation. *FEBS Journal*, *282*(13), 2475–2487.
Kobayashi, T., & Kageyama, R. (2014). Expression dynamics and functions of Hes factors in development and diseases. *Current Topics in Developmental Biology* (1st ed., Vol. 110).
Kobayashi, T., Mizuno, H., Imayoshi, I., Furusawa, C., Shirahige, K., & Kageyama, R. (2009). The cyclic gene Hes1 contributes to diverse differentiation responses of embryonic stem cells. *Genes and Development*, *23*(16), 1870–1875.
Koh, H. W. L., Zhang, Y., Vogel, C., & Choi, H. (2019). EBprotV2: A Perseus Plugin for Differential Protein Abundance Analysis of Labeling-Based Quantitative Proteomics Data. *Journal of Proteome Research*, *18*(2), 748–752.
Kreso, A., & Dick, J. E. (2014). Evolution of the cancer stem cell model. *Cell Stem Cell*, *14*(3), 275–291.
Kufer, T. A., Silljé, H. H. W., Körner, R., Gruss, O. J., Meraldi, P., & Nigg, E. A. (2002). Human TPX2 is required for targeting Aurora-A kinase to the spindle. *Journal of Cell Biology*, *158*(4), 617–623.
Kumar, N., Cramer, G. M., Dahaj, S. A. Z., Sundaram, B., Celli, J. P., & Kulkarni, R. V. (2019). Stochastic modeling of phenotypic switching and chemoresistance in cancer cell populations. *Scientific Reports*, *9*(1), 1–10.
Kunitoku, N., Sasayama, T., Marumoto, T., Zhang, D., Honda, S., Kobayashi, O., Hatakeyama, K., Ushio, Y., Saya, H., & Hirota, T. (2003). CENP-A phosphorylation by Aurora-A in prophase is required for enrichment of Aurora-B at inner centromeres and for kinetochore function. *Developmental Cell*, *5*(6), 853–864.
Kurtev, V., Margueron, R., Kroboth, K., Ogris, E., Cavailles, V., & Seiser, C. (2004).

Transcriptional regulation by the repressor of estrogen receptor activity via recruitment of histone deacetylases. *Journal of Biological Chemistry*, *279*(23), 24834–24843.
Kwon, J. S., Everetts, N. J., Wang, X., Wang, W., Della Croce, K., Xing, J., & Yao, G. (2017). Controlling Depth of Cellular Quiescence by an Rb-E2F Network Switch. *Cell Reports*, *20*(13), 3223–3235.
Labit, H., Fujimitsu, K., Bayin, N. S., Takaki, T., Gannon, J., & Yamano, H. (2012). Dephosphorylation of Cdc20 is required for its C-box-dependent activation of the APC/C. *EMBO Journal*, *31*(15), 3351–3362.
Lake, R. J., Tsai, P. F., Choi, I., Won, K. J., & Fan, H. Y. (2014). RBPJ, the Major Transcriptional Effector of Notch Signaling, Remains Associated with Chromatin throughout Mitosis, Suggesting a Role in Mitotic Bookmarking. *PLoS Genetics*, *10*(3).
Lam, E. W., & Watson, R. J. (1993). An E2F-binding site mediates cell-cycle regulated repression of mouse B-myb transcription. *The EMBO Journal*, *12*(7), 2705–2713.
Lane, K., Van Valen, D., DeFelice, M. M., Macklin, D. N., Kudo, T., Jaimovich, A., Carr, A., Meyer, T., Pe'er, D., Boutet, S. C., & Covert, M. W. (2017). Measuring Signaling and RNA-Seq in the Same Cell Links Gene Expression to Dynamic Patterns of NF-κB Activation. *Cell Systems*, *4*(4), 458-469.e5.
Langmead, B., Trapnell, C., Pop, M., & Salzberg, S. L. (2009). Ultrafast and memory-efficient alignment of short DNA sequences to the human genome. *Genome Biology*, *10*(3).
Laoukili, J., Alvarez, M., Meijer, L. A. T., Stahl, M., Mohammed, S., Kleij, L., Heck, A. J. R., & Medema, R. H. (2008). Activation of FoxM1 during G2 Requires Cyclin A/Cdk-Dependent Relief of Autorepression by the FoxM1 N-Terminal Domain. *Molecular and Cellular Biology*, *28*(9), 3076–3087.
Lee, J. C., Smith, S. B., Watada, H., Lin, J., Scheel, D., Wang, J., ... & German, M. S. (2001). Regulation of the pancreatic pro-endocrine gene neurogenin3. *Diabetes*, *50*(5), 928-936.
Lee, K., & Rhee, K. (2011). PLK1 phosphorylation of pericentrin initiates centrosome maturation at the onset of mitosis. *Journal of Cell Biology*, *195*(7), 1093–1101.
Lee, M. G., & Nurse, P. (1987). Complementation used to clone a human homologue of the fission yeast cell cycle control gene cdc2. *Nature*, *327*(6117), 31–35.
Lee, M. H., Lin, L., Equilibrina, I., Uchiyama, S., Matsunaga, S., & Fukui, K. (2011). ASURA (PHB2) is required for kinetochore assembly and subsequent chromosome congression. *Acta Histochemica et Cytochemica*, *44*(6), 247–258.
Lellupitiyage Don, S. S., Lin, H. H., Furtado, J. J., Qraitem, M., Taylor, S. R., & Farkas, M. E. (2019). Circadian oscillations persist in low malignancy breast cancer cells. *Cell Cycle*, *18*(19), 2447–2453.
Lénárt, P., Petronczki, M., Steegmaier, M., Di Fiore, B., Lipp, J. J., Hoffmann, M., Rettig, W. J., Kraut, N., & Peters, J. M. (2007). The Small-Molecule Inhibitor BI 2536 Reveals Novel Insights into Mitotic Roles of Polo-like Kinase 1. *Current Biology*, *17*(4), 304–315.
Leonhardt, H., Rahn, H. P., Weinzierl, P., Sporbert, A., Cremer, T., Zink, D., & Cardoso, M. C. (2000). Dynamics of DNA replication factories in living cells. *Journal of Cell Biology*, *149*(2), 271–279.
Leung, T. W. C., Lin, S. S. W., Tsang, A. C. C., Tong, C. S. W., Ching, J. C. Y., Leung, W. Y., Gimlich, R., Wong, G. G., & Yao, K. M. (2001). Over-expression of FoxM1 stimulates cyclin B1 expression. *FEBS Letters*, *507*(1), 59–66.
Li, B., & Dewey, C. N. (2011). RSEM: accurate transcript quantification from RNA-Seq data with or without a reference genome. *BMC Bioinformatics*, *12*(1), 323.
Li, D. W., Yang, Q., Chen, J. T., Zhou, H., Liu, R. M., & Huang, X. T. (2005). Dynamic distribution of Ser-10 phosphorylated histone H3 in cytoplasm of MCF-7 and CHO cells

during mitosis. *Cell Research*, *15*(2), 120–126.
Li, H., & Durbin, R. (2009). Fast and accurate short read alignment with Burrows-Wheeler transform. *Bioinformatics*, *25*(14), 1754–1760.
Li, H., Handsaker, B., Wysoker, A., Fennell, T., Ruan, J., Homer, N., Marth, G., Abecasis, G., & Durbin, R. (2009). The Sequence Alignment/Map format and SAMtools. *Bioinformatics*, *25*(16), 2078–2079.
Li, Q., Brown, J. B., Huang, H., & Bickel, P. J. (2011). Measuring reproducibility of high-throughput experiments. *Annals of Applied Statistics*, *5*(3), 1752–1779.
Li, X., Cao, Y., Li, M., & Jin, F. (2018). Upregulation of HES1 promotes cell proliferation and invasion in breast cancer as a prognosis marker and therapy target via the AKT pathway and EMT process. *Journal of Cancer*, *9*(4), 757–766.
Liang, K., Woodfin, A. R., Slaughter, B. D., Unruh, J. R., Box, A. C., Rickels, R. A., Gao, X., Haug, J. S., Jaspersen, S. L., & Shilatifard, A. (2015). Mitotic Transcriptional Activation: Clearance of Actively Engaged Pol II via Transcriptional Elongation Control in Mitosis. *Molecular Cell*, *60*(3), 435–445.
Lichtenberg, K. H. de, Funa, N. S., Nakic, N., Ferrer, J., Zhu, Z., Huangfu, D., & Serup, P. (2018). Genome-Wide Identification of HES1 Target Genes Uncover Novel Roles for HES1 in Pancreatic Development. *BioRxiv*, 335869.
Lin, H. H., & Farkas, M. E. (2018). Altered Circadian rhythms and breast cancer: From the human to the molecular level. *Frontiers in Endocrinology*, *9*, 219.
Lindqvist, A., Rodríguez-Bravo, V., & Medema, R. H. (2009). The decision to enter mitosis: feedback and redundancy in the mitotic entry network. *Journal of Cell Biology*, *185*(2), 193–202.
Lindqvist, A., Van Zon, W., Rosenthal, C. K., & Wolthuis, R. M. F. (2007). Cyclin B1-Cdk1 activation continues after centrosome separation to control mitotic progression. *PLoS Biology*, *5*(5), 1127–1137.
Lioutas, A., & Vernos, I. (2013). Aurora A kinase and its substrate TACC3 are required for central spindle assembly. *EMBO Reports*, *14*(9), 829–836.
Liu, D., Vader, G., Vromans, M. J. M., Lampson, Mi. A., & Lens, S. M. A. (2009). Sensing Chromosome Bi-Orientation by Spatial Separation of Aurora B Kinase from Kinetochore Substrates. *Science*, *323*, 1350–1354.
Liu, L., Michowski, W., Kolodziejczyk, A., & Sicinski, P. (2019). The cell cycle in stem cell proliferation, pluripotency and differentiation. *Nature Cell Biology*, *21*(9), 1060–1067.
Liu, S., Cong, Y., Wang, D., Sun, Y., Deng, L., Liu, Y., Martin-Trevino, R., Shang, L., McDermott, S. P., Landis, M. D., Hong, S., Adams, A., D'Angelo, R., Ginestier, C., Charafe-Jauffret, E., Clouthier, S. G., Birnbaum, D., Wong, S. T., Zhan, M., … Wicha, M. S. (2014). Breast cancer stem cells transition between epithelial and mesenchymal states reflective of their normal counterparts. *Stem Cell Reports*, *2*(1), 78–91.
Liu, S., Ginzberg, M. B., Patel, N., Hild, M., Leung, B., Chen, Y. C., Li, Z., Chang, N., Diena, S., Wang, Y., Trimble, W., Wasserman, L., Jenkins, J., Marc, W. K., & Kafri, R. (2018). Size uniformity of animal cells is actively maintained by a p38 MAPK-dependent regulation of G1-length. *ELife*, *7*(e26947), 1–27.
Liu, Z. H., Dai, X. M., & Du, B. (2015). Hes1: A key role in stemness, metastasis and multidrug resistance. *Cancer Biology and Therapy*, *16*(3), 353–359.
Livak, K. J., & Schmittgen, T. D. (2001). Analysis of relative gene expression data using real-time quantitative PCR and the 2-ΔΔCT method. *Methods*, *25*(4), 402–408.
Loewer, A., Batchelor, E., Gaglia, G., & Lahav, G. (2010). Basal Dynamics of p53 Reveal Transcriptionally Attenuated Pulses in Cycling Cells. *Cell*, *142*(1), 89–100.
Lohka, M. J., Hayes, M. K., & Maller, J. L. (1988). Purification of maturation-promoting factor, an intracellular regulator of early mitotic events. *Proceedings of the National*

Academy of Sciences of the United States of America, *85*(9), 3009–3013.
Louvi, A., & Artavanis-Tsakonas, S. (2006). Notch signalling in vertebrate neural development. *Nature Reviews Neuroscience*, *7*(2), 93–102.
Lundberg, A. S., & Weinberg, R. A. (1998). Functional Inactivation of the Retinoblastoma Protein Requires Sequential Modification by at Least Two Distinct Cyclin-cdk Complexes. *Molecular and Cellular Biology*, *18*(2), 753–761.
Ly, T., Whigham, A., Clarke, R., Brenes-Murillo, A., Estes, B., Wadsworth, P., & Lamond, A. I. (2017). Proteomic analysis of cell cycle progression in asynchronous cultures, including mitotic subphases, using PRIMMUS. *ELife*, *6*(27574), 1–35.
Mahdessian, D., Cesnik, A. J., Gnann, C., Danielsson, F., Stenström, L., Arif, M., Zhang, C., Le, T., Johansson, F., Shutten, R., Bäckström, A., Axelsson, U., Thul, P., Cho, N. H., Carja, O., Uhlén, M., Mardinoglu, A., Stadler, C., Lindskog, C., … Lundberg, E. (2021). Spatiotemporal dissection of the cell cycle with single-cell proteogenomics. *Nature*, *590*(7847), 649–654.
Malumbres, M., & Barbacid, M. (2005). Mammalian cyclin-dependent kinases. *Trends in Biochemical Sciences*, *30*(11), 630–641.
Manni, I., Mazzaro, G., Gurtner, A., Mantovani, R., Haugwitz, U., Krause, K., Engeland, K., Sacchi, A., Soddu, S., & Piaggio, G. (2001). NF-Y Mediates the Transcriptional Inhibition of the cyclin B1, cyclin B2, and cdc25C Promoters upon Induced G2 Arrest. *Journal of Biological Chemistry*, *276*(8), 5570–5576.
Manni, I., Tunici, P., Cirenei, N., Albarosa, R., Colombo, B. M., Roz, L., Sacchi, A., Piaggio, G., & Finocchiaro, G. (2002). Mxi1 inhibits the proliferation of U87 glioma cells through down-regulation of cyclin B1 gene expression. *British Journal of Cancer*, *86*(3), 477–484.
Marguerat, S., & Bähler, J. (2012). Coordinating genome expression with cell size. *Trends in Genetics*, *28*(11), 560–565.
Marinopoulou, E., Sabherwal, N., Biga, V., Desai, J., Adamson, A. D., & Papalopulu, N. (2021). HES1 protein oscillations are necessary for neural stem cells to exit from quiescence. *Bior*, 6.
Martínez-Alonso, D., & Malumbres, M. (2020). Mammalian cell cycle cyclins. *Seminars in Cell and Developmental Biology*, *107*, 28–35.
Martinez, C. A., & Arnosti, D. N. (2008). Spreading of a Corepressor Linked to Action of Long-Range Repressor Hairy. *Molecular and Cellular Biology*, *28*(8), 2792–2802.
Marumoto, T., Honda, S., Hara, T., Nitta, M., Hirota, T., Kohmura, E., & Saya, H. (2003). Aurora-A Kinase Maintains the Fidelity of Early and Late Mitotic Events in HeLa Cells. *Journal of Biological Chemistry*, *278*(51), 51786–51795.
Masui, Y., & Markert, C. (1971). Cytoplasmic control of nuclear behavior during meiotic maturation of frog oocytes. *Journal of Experimental Zoology*, *177*(2), 129–145.
Mata, J., Curado, S., Ephrussi, A., & Rørth, P. (2000). Tribbles coordinates mitosis and morphogenesis in Drosophila by regulating string/CDC25 proteolysis. *Cell*, *101*(5), 511-522.
Matsuo, T., Yamaguchi, S., Mitsui, S., Emi, A., Shimoda, F., & Okamura, H. (2003). Control mechanism of the circadian clock for timing of cell division in vivo. *Science*, *302*(5643), 255–259.
Matthews, H. K., Delabre, U., Rohn, J. L., Guck, J., Kunda, P., & Baum, B. (2012). Changes in Ect2 Localization Couple Actomyosin-Dependent Cell Shape Changes to Mitotic Progression. *Developmental Cell*, *23*(2), 371–383.
McGowan, C. H., & Russell, P. (1993). Human Wee1 kinase inhibits cell division by phosphorylating p34(cdc2) exclusively on Tyr15. *EMBO Journal*, *12*(1), 75–85.
Meacham, C. E., & Morrison, S. J. (2013). Tumour heterogeneity and cancer cell plasticity.

Nature, *501*(7467), 328–337.
Mena, A. L., Lam, E. W. F., & Chatterjee, S. (2010). Sustained spindle-assembly checkpoint response requires de novo transcription and translation of cyclin B1. *PLoS ONE*, *5*(9).
Meraldi, P., Honda, R., & Nigg, E. A. (2002). Aurora-A overexpression reveals tetraploidization as a major route to centrosome amplification in p53-/- cells. *EMBO Journal*, *21*(4), 483–492.
Meunier, S., & Vernos, I. (2012). Microtubule assembly during mitosis - from distinct origins to distinct functions? *Journal of Cell Science*, *125*(12), 2805–2814.
Miettinen, T. P., Pessa, H. K. J., Caldez, M. J., Fuhrer, T., Diril, M. K., Sauer, U., Kaldis, P., & Björklund, M. (2014). Identification of transcriptional and metabolic programs related to mammalian cell size. *Current Biology*, *24*(6), 598–608.
Miller, I., Min, M., Yang, C., Tian, C., Gookin, S., Carter, D., & Spencer, S. L. (2018). Ki67 is a Graded Rather than a Binary Marker of Proliferation versus Quiescence. *Cell Reports*, *24*(5), 1105-1112.e5.
Minchington, T. G., Griffiths-Jones, S., & Papalopulu, N. (2020). Dynamical gene regulatory networks are tuned by transcriptional autoregulation with microRNA feedback. *Scientific Reports*, *10*(1), 1–13.
Minshull, J., Blow, J. J., & Hunt, T. (1989). Translation of cyclin mRNA is necessary for extracts of activated Xenopus eggs to enter mitosis. *Cell*, *56*(6), 947–956.
Minshull, J., Golsteyn, R., Hill, C. S., & Hunt, T. (1990). The A- and B-type cyclin associated cdc2 kinases in Xenopus turn on and off at different times in the cell cycle. *The EMBO Journal*, *9*(9), 2865–2875.
Mitchison, T. J., & Salmon, E. D. (2001). Mitosis: A history of division. *Nature Cell Biology*, *3*(1), 17–21.
Mochida, S., Maslen, S. L., Skehel, M., & Hunt, T. (2010). Greatwall Phosphorylates an Inhibitor of Protein Phosphatase 2A That Is Essential for Mitosis. *Science*, *330*, 1670–1673.
Momiji, H., & Monk, N. A. M. (2008). Dissecting the dynamics of the Hes1 genetic oscillator. *Journal of Theoretical Biology*, *254*(4), 784–798.
Mondal, G., Sengupta, S., Panda, C. K., Gollin, S. M., Saunders, W. S., & Roychoudhury, S. (2007). Overexpression of Cdc20 leads to impairment of the spindle assembly checkpoint and aneuploidization in oral cancer. *Carcinogenesis*, *28*(1), 81–92.
Monk, N. A. M. (2003). Oscillatory Expression of Hes1, p53, and NF-B Driven by Transcriptional Time Delays. *Current Biology*, *13*, 1409–1412.
Montano, M. M., Ekena, K., Delage-Mourroux, R., Chang, W., Martini, P., & Katzenellenbogen, B. S. (1999). An estrogen receptor-selective coregulator that potentiates the effectiveness of antiestrogens and represses the activity of estrogens. *Proceedings of the National Academy of Sciences of the United States of America*, *96*(12), 6947–6952.
Morgan, D. O. (1999). Regulation of the APC and the exit from mitosis. *Nature Cell Biology*, *1*(2), E47–E53.
Morin, V., Prieto, S., Melines, S., Hem, S., Rossignol, M., Lorca, T., Espeut, J., Morin, N., & Abrieu, A. (2012). CDK-dependent potentiation of MPS1 kinase activity is essential to the mitotic checkpoint. *Current Biology*, *22*(4), 289–295.
Mueller, F., Senecal, A., Tantale, K., Marie-Nelly, H., Ly, N., Collin, O., Basyuk, E., Bertrand, E., Darzacq, X., & Zimmer, C. (2013). FISH-quant: Automatic counting of transcripts in 3D FISH images. *Nature Methods*, *10*(4), 277–278.
Mueller, P. R., Coleman, T. R., Kumagai, A., & Dunphy, W. G. (1995). Myt1: A membrane-associated inhibitory kinase that phosphorylates Cdc2 on both threonine-14 and tyrosine-15. *Science*, *270*(5233), 86–90.

Müller, G. A., & Engeland, K. (2010). The central role of CDE/CHR promoter elements in the regulation of cell cycle-dependent gene transcription: Review article. *FEBS Journal*, *277*(4), 877–893.
Müller, G. A., Wintsche, A., Stangner, K., Prohaska, S. J., Stadler, P. F., & Engeland, K. (2014). The CHR site: Definition and genome-wide identification of a cell cycle transcriptional element. *Nucleic Acids Research*, *42*(16), 10331-10350.
Müller, P., Kietz, S., Gustafsson, J. Å., & Ström, A. (2002). The anti-estrogenic effect of all-trans-retinoic acid on the breast cancer cell line MCF-7 is dependent on HES-1 expression. *Journal of Biological Chemistry*, *277*(32), 28376–28379.
Munsky, B., Neuert, G., & Van Oudenaarden, A. (2012). Using gene expression noise to understand gene regulation. *Science*, *336*(6078), 183–187.
Murata, K., Hattori, M., Hirai, N., Hirata, H., Kageyama, R., Shinozuka, Y., Sakai, T., & Minato, N. (2005). Hes1 Directly Controls Cell Proliferation through the Transcriptional Repression of p27 Kip1. *Molecular and Cellular Biology*, *25*(10), 4262–4271.
Murray, A. W., Solomon, M. J., & Kirschner, M. W. (1989). The role of cyclin synthesis and degradation in the control of maturation promoting factor activity. *Nature, 339(6222), 280-286.*
Musacchio, A., & Salmon, E. D. (2007). The spindle-assembly checkpoint in space and time. *Nature Reviews Molecular Cell Biology*, *8*(5), 379–393.
Nagoshi, E., Saini, C., Bauer, C., Laroche, T., Naef, F., & Schibler, U. (2004). Circadian gene expression in individual fibroblasts: Cell-autonomous and self-sustained oscillators pass time to daughter cells. *Cell*, *119*(5), 693–705.
Nair, B. C., Vallabhaneni, S., Tekmal, R. R., & Vadlamudi, R. K. (2011). Roscovitine confers tumor suppressive effect on therapy-resistant breast tumor cells. *Breast Cancer Research*, *13*(3).
Nakata, Y., Shetzline, S., Sakashita, C., Kalota, A., Rallapalli, R., Rudnick, S. I., Zhang, Y., Emerson, S. G., & Gewirtz, A. M. (2007). c-Myb Contributes to G 2 / M Cell Cycle Transition in Human Hematopoietic Cells by Direct Regulation of. *Molecular and Cellular Biology*, *27*(6), 2048–2058.
Nakojima, H., Toyoshima-Morimoto, F., Taniguchi, E., & Nishida, E. (2003). Identification of a consensus motif for PlK (Polo-like kinase) phosphorylation reveals Myt1 as a Plk1 substrate. *Journal of Biological Chemistry*, *278*(28), 25277–25280.
Nam, Y., Sliz, P., Pear, W. S., Aster, J. C., & Blacklow, S. C. (2007). Cooperative assembly of higher-order Notch complexes functions as a switch to induce transcription. *Proceedings of the National Academy of Sciences of the United States of America*, *104*(7), 2103–2108.
Narasimha, A. M., Kaulich, M., Shapiro, G. S., Choi, Y. J., Sicinski, P., & Dowdy, S. F. (2014). Cyclin D activates the Rb tumor suppressor by mono-phosphorylation. *ELife*, *3*, 1–21.
Nelson, D. E., Ihekwaba, A. E. C., Elliott, M., Johnson, J. R., Gibney, C. A., Foreman, B. E., Nelson, C., See, V., Horton, C. A., Spiller, D. G., Edwards, S. W., McDowell, H. P., Unitt, J. F., Sullivan, E., Grimley, R., Benson, N., Broomhead, D., Kell, D. B., & White, M. R. H. (2004). Oscillations in NF-κB signaling control the dynamics of gene expression. *Science*, *306*(5696), 704–708.
Nicklas, R. B. (1997). How cells get the right chromosomes. *Science*, *275*(5300).
Nicolas, D., Phillips, N. E., & Naef, F. (2017). What shapes eukaryotic transcriptional bursting? *Molecular BioSystems*, *13*(7), 1280–1290.
Niedzwiedz, W., Mosedale, G., Johnson, M., Ong, C. Y., Pace, P., & Patel, K. J. (2004). The Fanconi anaemia gene FANCC promotes homologous recombination and error-prone DNA repair. *Molecular Cell*, *15*(4), 607–620.

Nijenhuis, W., Castelmur, E. Von, Littler, D., Marco, V. De, Tromer, E., Vleugel, M., Osch, M. H. J. Van, Snel, B., Perrakis, A., & Kops, G. J. P. L. (2013). A TPR domain–containing N-terminal module of MPS1 is required for its kinetochore localization by Aurora B. *Journal of Cell Biology*, *201*(2), 217–231.

Noda, N., Honma, S., & Ohmiya, Y. (2011). Hes1 is required for contact inhibition of cell proliferation in 3T3-L1 preadipocytes. *Genes to Cells*, *16*(6), 704–713.

Norbury, C., & Nurse, P. (1992). Animal Cell Cycles and Their Control. *Annual Review of Biochemistry*, *61*(1), 441–468.

Nousiainen, M., Silljé, H. H. W., Sauer, G., Nigg, E. A., & Körner, R. (2006). Phosphoproteome analysis of the human mitotic spindle. *Proceedings of the National Academy of Sciences of the United States of America*, *103*(14), 5391–5396.

Novais-Cruz, M., Abad, M. A., van IJcken, W. F. J., Galjart, N., Jeyaprakash, A. A., Maiato, H., & Ferrás, C. (2018). Mitotic progression, arrest, exit or death relies on centromere structural integrity, rather than de novo transcription. *ELife*, *7*, 1–27.

Nugoli, M., Chucana, P., Vendrell, J., Orsetti, B., Ursule, L., Nguyen, C., Birnbaum, D., Douzery, E. J. P., Cohen, P., & Theillet, C. (2003). Genetic variability in MCF-7 sublines: Evidence of rapid genomic and RNA expression profile modifications. *BMC Cancer*, *3*, 1–12.

Nurse, P., & Bissett, Y. (1981). Gene required in G1 for commitment to cell cycle and in G2 for Control of Mitosis in Fission Yeast. *Nature*, *292*(5823), 558–560.

Ochi, S., Imaizumi, Y., Shimojo, H., Miyachi, H., & Kageyama, R. (2020). Oscillatory expression of Hes1 regulates cell proliferation and neuronal differentiation in the embryonic brain. *Development*.

Ohi, R., & Gould, K. L. (1999). Regulating the onset of mitosis. *Current Opinion in Cell Biology*, *11*(2), 267–273.

Ohtani, K., Degregori, J., & Nevins, J. R. (1995). Regulation of the cyclin E gene by transcription factor E2F1. *Proceedings of the National Academy of Sciences of the United States of America*, *92*(26), 12146–12150.

Ohtsuka, T., Ishibashi, M., Gradwohl, G., Nakanishi, S., Guillemot, F., & Kageyama, R. (1999). Hes1 and Hes5 as Notch effectors in mammalian neuronal differentiation. *The EMBO Journal*, *18*(8), 2196–2207.

Ohtsuka, T., & Kageyama, R. (2021). Hes1 overexpression leads to expansion of embryonic neural stem cell pool and stem cell reservoir in the postnatal brain. *Development*, *148*(4).

Okada, M., Akimura, H., Hou, D.-X., Takahashi, T., & Ishii, S. (2002). Myb controls G2/M progression by inducing cyclin B expression in the Drosophila eye imaginal disc. *EMBO Journal*, *21*(4), 675–684.

Olsen, J. V., Vermeulen, M., Santamaria, A., Kumar, C., Miller, M. L., Jensen, L. J., Gnad, F., Cox, J., Jensen, T. S., Nigg, E. A., Brunak, S., & Mann, M. (2010). Quantitative phosphoproteomics revealswidespread full phosphorylation site occupancy during mitosis. *Science Signaling*, *3*(104).

Ong, C. T., Cheng, H. T., Chang, L. W., Ohtsuka, T., Kageyama, R., Stormo, G. D., & Kopan, R. (2006). Target selectivity of vertebrate notch proteins: Collaboration between discrete domains and CSL-binding site architecture determines activation probability. *Journal of Biological Chemistry*, *281*(8), 5106–5119.

Ostroukhova, M., Qi, Z., Oriss, T. B., Dixon-McCarthy, B., Ray, P., & Ray, A. (2006). Treg-mediated immunosuppression involves activation of the Notch-HES1 axis by membrane-bound TGF-β. *Journal of Clinical Investigation*, *116*(4), 996–1004.

Padovan-Merhar, O., Nair, G. P., Biaesch, A. G., Mayer, A., Scarfone, S., Foley, S. W., Wu, A. R., Churchman, L. S., Singh, A., & Raj, A. (2015). Single Mammalian Cells Compensate for Differences in Cellular Volume and DNA Copy Number through

Independent Global Transcriptional Mechanisms. *Molecular Cell*, *58*(2), 339–352.
Pagano, M. (1997). Cell cycle regulation by the ubiquitin pathway. *The FASEB Journal*, *11*(13), 1067–1075.
Palaparti, A., Baratz, A., & Stifani, S. (1997). The Groucho/transducin-like enhancer of split transcriptional repressors interact with the genetically defined amino-terminal silencing domain of histone H3. *Journal of Biological Chemistry*, *272*(42), 26604–26610.
Palmer, N., Talib, S. Z. A., Ratnacaram, C. K., Low, D., Bisteau, X., Si Lee, J. H., Pfeiffenberger, E., Wollmann, H., Loong Tan, J. H., Wee, S., Sobota, R., Gunaratne, J., Messerschmidt, D. M., Guccione, E., & Kaldis, P. (2019). CDK2 regulates the NRF1/Ehmt1 axis during meiotic prophase I. *Journal of Cell Biology*, *218*(9), 2896–2918.
Palozola, K. C., Donahue, G., Liu, H., Grant, G. R., Becker, J. S., Cote, A., Yu, H., Raj, A., & Zaret, K. S. (2017). Mitotic transcription and waves of gene reactivation during mitotic exit. *Science*, *358*(6359), 119–122.
Pardee, A. B. (1974). A restriction point for control of normal animal cell proliferation. *Proceedings of the National Academy of Sciences of the United States of America*, *71*(4), 1286–1290.
Park, H. J., Wang, Z., Costa, R. H., Tyner, A., Lau, L. F., & Raychaudhuri, P. (2008). An N-terminal inhibitory domain modulates activity of FoxM1 during cell cycle. *Oncogene*, *27*(12), 1696–1704.
Parsons, G. G., & Spencer, C. A. (1997). Mitotic repression of RNA polymerase II transcription is accompanied by release of transcription elongation complexes. *Molecular and Cellular Biology*, *17*(10), 5791–5802.
Pauklin, S., & Vallier, L. (2013). The cell-cycle state of stem cells determines cell fate propensity. *Cell*, *155*(1), 135–147.
Pennycook, B. R., & Barr, A. R. (2020). Restriction point regulation at the crossroads between quiescence and cell proliferation. *FEBS Letters*, *594*, 2046–2060.
Pérez-Roger, I., Solomon, D. L. C., Sewing, A., & Land, H. (1997). Myc activation of cyclin E/Cdk2 kinase involves induction of cyclin E gene transcription and inhibition of p27(Kip1) binding to newly formed complexes. *Oncogene*, *14*(20), 2373–2381.
Perron, A., Nishikawa, Y., Iwata, J., Shimojo, H., Takaya, J., Kobayashi, K., Imayoshi, I., Mbenza, N. M., Takenoya, M., Kageyama, R., Kodama, Y., & Uesugi, M. (2018). Small-molecule screening yields a compound that inhibits the cancer-associated transcription factor Hes1 via the PHB2 chaperone. *Journal of Biological Chemistry*, *293*(21), 8285–8294.
Petrone, A., Adamo, M. E., Cheng, C., & Kettenbach, A. N. (2016). Identification of candidate cyclin-dependent kinase 1 (Cdk1) substrates in mitosis by quantitative phosphoproteomics. *Molecular and Cellular Proteomics*, *15*(7), 2448–2461.
Pfeuty, B. (2015). A computational model for the coordination of neural progenitor self-renewal and differentiation through Hes1 dynamics. *Development*, *142*(3), 477–485.
Phillips, N. E., Manning, C. S., Pettini, T., Biga, V., Marinopoulou, E., Stanley, P., Boyd, J., Bagnall, J., Paszek, P., Spiller, D. G., White, M. R. H., Goodfellow, M., Galla, T., Rattray, M., & Papalopulu, N. (2016). Stochasticity in the miR-9/Hes1 oscillatory network can account for clonal heterogeneity in the timing of differentiation. *ELife*, *5*, 1–33.
Piggott, J. R., Rai, R., & Carter, B. L. A. (1982). A bifunctional gene product involved in two phases of the yeast cell cycle. *Nature*, *298*(5872), 391–393.
Pines, J., & Hunter, T. (1989). Isolation of a human cyclin cDNA: Evidence for cyclin mRNA and protein regulation in the cell cycle and for interaction with p34cdc2. *Cell*, *58*(5), 833–846.

Pines, J., & Hunter, T. (1994). The differential localization of human cyclins A and B is due to a cytoplasmic retention signal in cyclin B. *EMBO Journal*, *13*(16), 3772–3781.
Pisco, A. O., & Huang, S. (2015). Non-genetic cancer cell plasticity and therapy-induced stemness in tumour relapse: "What does not kill me strengthens me." *British Journal of Cancer*, *112*(11), 1725–1732.
Podhorecka, M., Skladanowski, A., & Bozko, P. (2010). H2AX phosphorylation: Its role in DNA damage response and cancer therapy. *Journal of Nucleic Acids*, *2010*.
Popovic, D., Koch, B., Kueblbeck, M., Ellenberg, J., & Pelkmans, L. (2018). Multivariate Control of Transcript to Protein Variability in Single Mammalian Cells. *Cell Systems*, *7*(4), 398-411.e6.
Puck, T. T., & Steffen, J. (1963). Life Cycle Analysis of Mammalian Cells: I. A Method for Localizing Metabolic Events within the Life Cycle, and Its Application to the Action of Colcemide and Sublethal Doses of X-Irradiation. *Biophysical Journal*, *3*(5), 379–397.
Purvis, J. E., Karhohs, K. W., Mock, C., Batchelor, E., Loewer, A., & Lahav, G. (2012). P53 Dynamics Control Cell Fate. *Science*, *336*(6087), 1440–1444.
Purvis, J. E., & Lahav, G. (2013). Encoding and decoding cellular information through signaling dynamics. *Cell*, *152*(5), 945–956.
Qian, J., Lesage, B., Beullens, M., Van Eynde, A., & Bollen, M. (2011). PP1/repo-man dephosphorylates mitotic histone H3 at T3 and regulates chromosomal aurora B targeting. *Current Biology*, *21*(9), 766–773.
Qian, Y. W., Erikson, E., Taieb, F. E., & Maller, J. L. (2001). The polo-like kinase Plx1 is required for activation of the phosphatase Cdc25C and cyclin B-Cdc2 in Xenopus oocytes. *Molecular Biology of the Cell*, *12*(6), 1791–1799.
Quintana, A. M., Liu, F., O'Rourke, J. P., & Ness, S. A. (2011). Identification and Regulation of c-Myb Target Genes in MCF-7 Cells. *BMC Cancer*, *11*.
Raj, A., Peskin, C. S., Tranchina, D., Vargas, D. Y., & Tyagi, S. (2006). Stochastic mRNA synthesis in mammalian cells. *PLoS Biology*, *4*(10), 1707–1719.
Raj, A., & van Oudenaarden, A. (2008). Nature, Nurture, or Chance: Stochastic Gene Expression and Its Consequences. *Cell*, *135*(2), 216–226.
Ramkumar, N., & Baum, B. (2016). Coupling changes in cell shape to chromosome segregation. *Nature Reviews Molecular Cell Biology*, *17*(8), 511–521.
Ran, Y., Hossain, F., Pannuti, A., Lessard, C. B., Ladd, G. Z., Jung, J. I., Minter, L. M., Osborne, B. A., Miele, L., & Golde, T. E. (2017). γ-Secretase inhibitors in cancer clinical trials are pharmacologically and functionally distinct. *EMBO Molecular Medicine*, *9*(7), 950–966.
Reed, S. I. (2003). Ratchets and clocks: The cell cycle, ubiquitylation and protein turnover. *Nature Reviews Molecular Cell Biology*, *4*(11), 855–864.
Reiter, V., Matschkal, D. M. S., Wagner, M., Globisch, D., Kneuttinger, A. C., Müller, M., & Carell, T. (2012). The CDK5 repressor CDK5RAP1 is a methylthiotransferase acting on nuclear and mitochondrial RNA. *Nucleic Acids Research*, *40*(13), 6235–6240.
Rellos, P., Ivins, F. J., Baxter, J. E., Pike, A., Nott, T. J., Parkinson, D. M., Das, S., Howell, S., Fedorov, O., Qi, Y. S., Fry, A. M., Knapp, S., & Smerdon, S. J. (2007). Structure and regulation of the human Nek2 centrosomal kinase. *Journal of Biological Chemistry*, *282*(9), 6833–6842.
Reyes, J., Chen, J. Y., Stewart-Ornstein, J., Karhohs, K. W., Mock, C. S., & Lahav, G. (2018). Fluctuations in p53 Signaling Allow Escape from Cell-Cycle Arrest. *Molecular Cell*, *71*(4), 581-591.e5.
Rogers, S., McCloy, R. A., Parker, B. L., Gallego-Ortega, D., Law, A. M. K., Chin, V. T., Conway, J. R. W., Fey, D., Millar, E. K. A., O'Toole, S., Deng, N., Swarbrick, A., Chastain, P. D., Cesare, A. J., Timpson, P., Caldon, C. E., Croucher, D. R., James, D. E.,

Watkins, D. N., & Burgess, A. (2018). MASTL overexpression promotes chromosome instability and metastasis in breast cancer. *Oncogene*, *37*(33), 4518–4533.
Rosasco-Nitcher, S. E., Lan, W., Khorasanizadeh, S., & Stukenberg, P. T. (2008). Centromeric Aurora-B activation requires TD-60, microtubules, and substrate priming phosphorylation. *Science*, *319*(5862), 469–472.
Rudolph, D., Steegmaier, M., Hoffmann, M., Grauert, M., Baum, A., Quant, J., Haslinger, C., Garin-Chesa, P., & Adolf, G. R. (2009). BI 6727, a polo-like kinase inhibitor with improved pharmacokinetic profile and broad antitumor activity. *Clinical Cancer Research*, *15*(9), 3094–3102.
Rushlow, C. A., Hogan, A., Pinchin, S. M., Howe, K. M., Lardelli, M., & Ish-Horowicz, D. (1989). The Drosophila hairy protein acts in both segmentation and bristle patterning and shows homology to N-myc. *The EMBO Journal*, *8*(10), 3095–3103.
Ryl, T., Kuchen, E. E., Bell, E., Shao, C., Flórez, A. F., Mönke, G., Gogolin, S., Friedrich, M., Lamprecht, F., Westermann, F., & Höfer, T. (2017). Cell-Cycle Position of Single MYC-Driven Cancer Cells Dictates Their Susceptibility to a Chemotherapeutic Drug. *Cell Systems*, *5*(3), 237-250.e8.
Sabherwal, N., Rowntree, A., Kursawe, J., & Papalopulu, N. (2021). Phase-register of non-ultradian Hes1 oscillations ER + breast cancer cells . *BioRxiv*.
Sadasivam, S., & DeCaprio, J. A. (2013). The DREAM complex: Master coordinator of cell cycle-dependent gene expression. *Nature Reviews Cancer*, *13*(8), 585–595.
Sadasivam, S., Duan, S., & DeCaprio, J. A. (2012). The MuvB complex sequentially recruits B-Myb and FoxM1 to promote mitotic gene expression. *Genes and Development*, *26*(5), 474–489.
Samuel, T., Weber, H. O., & Funk, J. O. (2002). Linking DNA damage to cell cycle checkpoints. *Cell Cycle*, *1*(3), 161–167.
Sandler, O., Mizrahi, S. P., Weiss, N., Agam, O., Simon, I., & Balaban, N. Q. (2015). Lineage correlations of single cell division time as a probe of cell-cycle dynamics. *Nature*, *519*(7544), 468–471.
Sang, L., Coller, H. A., & Roberts, J. M. (2008). Control of the reversibility of cellular quiescence by the transcriptional repressor HES1. *Science*, *321*(5892), 1095–1100.
Santoni-Rugiu, E., Falck, J., Mailand, N., Bartek, J., & Lukas, J. (2000). Involvement of Myc Activity in a G1/S-Promoting Mechanism Parallel to the pRb/E2F Pathway. *Molecular and Cellular Biology*, *20*(10), 3497–3509.
Sarmento, L. M., Huang, H., Limon, A., Gordon, W., Fernandes, J., Tavares, M. J., Miele, L., Cardoso, A. A., Classon, M., & Carlesso, N. (2005). Notch1 modulates timing of G1-S progression by inducing SKP2 transcription and p27Kip1 degradation. *Journal of Experimental Medicine*, *202*(1), 157–168.
Sasai, Y., Kageyama, R., Tagawa, Y., Shigemoto, R., & Nakanishi, S. (1992). Two mammalian helix-loop-helix factors structurally related to Drosophila hairy and Enhancer of split. *Genes and Development*, *6*(12 B), 2620–2634.
Satyanarayana, A., & Kaldis, P. (2009). Mammalian cell-cycle regulation: Several cdks, numerous cyclins and diverse compensatory mechanisms. *Oncogene*, *28*(33), 2925–2939.
Savvidis, C., & Koutsilieris, M. (2012). Circadian rhythm disruption in cancer biology. *Molecular Medicine*, *18*(9), 1249–1260.
Schade, A. E., Oser, M. G., Nicholson, H. E., & DeCaprio, J. A. (2019). Cyclin D–CDK4 relieves cooperative repression of proliferation and cell cycle gene expression by DREAM and RB. *Oncogene*, *38*(25), 4962–4976.
Schmidt, E. E., & Schibler, U. (1995). Cell size regulation, a mechanism that controls cellular RNA accumulation: Consequences on regulation of the ubiquitous transcription factors

Oct1 and NF-Y, and the liver-enriched transcription factor DBP. *Journal of Cell Biology*, *128*(4), 467–483.
Schmoller, K. M., Turner, J. J., Kõivomägi, M., & Skotheim, J. M. (2015). Dilution of the cell cycle inhibitor Whi5 controls budding-yeast cell size. *Nature*, *526*(7572), 268–272.
Schnell, S. A., Ambesi-Impiombato, A., Sanchez-Martin, M., Belver, L., Xu, L., Qin, Y., Kageyama, R., & Ferrando, A. A. (2015). Therapeutic targeting of HES1 transcriptional programs in T-ALL. *Blood*, *125*(18), 2806–2814.
Schulze, A., Zerfass, K., Spitkovsky, D., Middendorp, S., Bergès, J., Helin, K., Jansen-Dürr, P., & Henglein, B. (1995). Cell cycle regulation of the cyclin A gene promoter is mediated by a variant E2F site. *Proceedings of the National Academy of Sciences of the United States of America*, *92*(24), 11264–11268.
Schwarz, C., Johnson, A., Kõivomägi, M., Zatulovskiy, E., Kravitz, C. J., Doncic, A., & Skotheim, J. M. (2018). A Precise Cdk Activity Threshold Determines Passage through the Restriction Point. *Molecular Cell*, *69*(2), 253-264.e5.
Sciortino, S., Gurtner, A., Manni, I., Fontemaggi, G., Dey, A., Sacchi, A., Ozato, K., & Piaggio, G. (2001). The cyclin B1 gene is actively transcribed during mitosis in HeLa cells. *EMBO Reports*, *2*(11), 1018–1023.
Seong, C. H., Chiba, N., Kusuyama, J., Subhan Amir, M., Eiraku, N., Yamashita, S., Ohnishi, T., Nakamura, N., & Matsuguchi, T. (2021). Bone morphogenetic protein 9 (BMP9) directly induces Notch effector molecule Hes1 through the SMAD signaling pathway in osteoblasts. *FEBS Letters*, *595*(3), 389–403.
Seymour, P. A., Collin, C. A., Egeskov-Madsen, A. la R., Jørgensen, M. C., Shimojo, H., Imayoshi, I., de Lichtenberg, K. H., Kopan, R., Kageyama, R., & Serup, P. (2020). Jag1 Modulates an Oscillatory Dll1-Notch-Hes1 Signaling Module to Coordinate Growth and Fate of Pancreatic Progenitors. *Developmental Cell*, *52*(6), 731-747.e8.
Shariati, S. A., Dominguez, A., Xie, S., Wernig, M., Qi, L. S., & Skotheim, J. M. (2019). Reversible Disruption of Specific Transcription Factor-DNA Interactions Using CRISPR/Cas9. *Molecular Cell*, *74*(3), 622-633.e4.
Sherr, C. J., & Roberts, J. M. (1999). CDK inhibitors: Positive and negative regulators of G1-phase progression. *Genes and Development*, *13*(12), 1501–1512.
Shi, Y., Guo, S., Wang, Y., Liu, X., Li, Q., & Li, T. (2018). Lamprey Prohibitin2 Arrest G2/M Phase Transition of HeLa Cells through Down-regulating Expression and Phosphorylation Level of Cell Cycle Proteins. *Scientific Reports*, *8*(1), 1–8.
Shimojo, H., Ohtsuka, T., & Kageyama, R. (2008). Oscillations in Notch Signaling Regulate Maintenance of Neural Progenitors. *Neuron*, *58*(1), 52–64.
Simões, B. M., O'Brien, C. S., Eyre, R., Silva, A., Yu, L., Sarmiento-Castro, A., Alférez, D. G., Spence, K., Santiago-Gómez, A., Chemi, F., Acar, A., Gandhi, A., Howell, A., Brennan, K., Rydén, L., Catalano, S., Andó, S., Gee, J., Ucar, A., … Clarke, R. B. (2015). Anti-estrogen Resistance in Human Breast Tumors Is Driven by JAG1-NOTCH4-Dependent Cancer Stem Cell Activity. *Cell Reports*, *12*(12), 1968–1977.
Skinner, S. O., Xu, H., Nagarkar-Jaiswal, S., Freire, P. R., Zwaka, T. P., & Golding, I. (2016). Single-cell analysis of transcription kinetics across the cell cycle. *ELife*, *5*, 1–24.
Solomon, M. J., Lee, T., & Kirschner, M. W. (1992). Role of phosphorylation in p34cdc2 activation: Identification of an activating kinase. *Molecular Biology of the Cell*, *3*(1), 13–27.
Soni, D. V., Sramkoski, R. M., Lam, M., Stefan, T., & Jacobberger, J. W. (2008). Cyclin B1 is rate limiting but not essential for mitotic entry and progression in mammalian somatic cells. *Cell Cycle*, *7*(9), 1285–1300.
Sonnen, K. F., & Aulehla, A. (2014). Dynamic signal encoding-From cells to organisms. *Seminars in Cell and Developmental Biology*, *34*, 91–98.

Sosa, M. S., Bragado, P., & Aguirre-Ghiso, J. A. (2014). Mechanisms of disseminated cancer cell dormancy: An awakening field. *Nature Reviews Cancer*, *14*(9), 611–622.
Soufi, A., & Dalton, S. (2016). Cycling through developmental decisions: How cell cycle dynamics control pluripotency, differentiation and reprogramming. *Development (Cambridge)*, *143*(23), 4301–4311.
Spellman, P. T., Sherlock, G., Zhang, M. Q., Iyer, V. R., Anders, K., Eisen, M. B., Brown, P. O., Botstein, D., & Futcher, B. (1998). Comprehensive identification of cell cycle-regulated genes of the yeast Saccharomyces cerevisiae by microarray hybridization. *Molecular Biology of the Cell*, *9*(12), 3273–3297.
Spencer, S. L., Cappell, S. D., Tsai, F. C., Overton, K. W., Wang, C. L., & Meyer, T. (2013). The proliferation-quiescence decision is controlled by a bifurcation in CDK2 activity at mitotic exit. *Cell*, *155*(2), 369.
Stanyte, R., Nuebler, J., Blaukopf, C., Hoefler, R., Stocsits, R., Peters, J. M., & Gerlich, D. W. (2018). Dynamics of sister chromatid resolution during cell cycle progression. *Journal of Cell Biology*, *217*(6), 1985–2004.
Stemmann, O., Zou, H., Gerber, S. A., Gygi, S. P., & Kirschner, M. W. (2001). Dual inhibition of sister chromatid separation at metaphase. *Cell*, *107*(6), 715–726.
Stewart-Ornstein, J., Cheng, H. W. (Jacky), & Lahav, G. (2017). Conservation and Divergence of p53 Oscillation Dynamics across Species. *Cell Systems*, *5*(4), 410-417.e4.
Ström, A., Arai, N., Leers, J., & Gustafsson, J. Å. (2000). The Hairy and Enhancer of Split homologue-1 (HES-1) mediates the proliferative effect of 17β-estradiol on breast cancer cell lines. *Oncogene*, *19*(51), 5951–5953.
Sturrock, M., Hellander, A., Aldakheel, S., Petzold, L., & Chaplain, M. A. J. (2014). The Role of Dimerisation and Nuclear Transport in the Hes1 Gene Regulatory Network. *Bulletin of Mathematical Biology*, *76*(4), 766–798.
Sudakin, V., Chan, G. K. T., & Yen, T. J. (2001). Checkpoint inhibition of the APC/C in HeLa cells is mediated by a complex of BUBR1, BUB3, CDC20, and MAD2. *Journal of Cell Biology*, *154*(5), 925–936.
Sueda, R., Imayoshi, I., Harima, Y., & Kageyama, R. (2019). High Hes1 expression and resultant Ascl1 suppression regulate quiescent vs. active neural stem cells in the adult mouse brain. *Genes & Development*, 1–13.
Sumazaki, R., Shiojiri, N., Isoyama, S., Masu, M., Keino-Masu, K., Osawa, M., Nakauchi, H., Kageyama, R., & Matsui, A. (2004). Conversion of biliary system to pancreatic tissue in Hes1-deficient mice. *Nature Genetics*, *36*(1), 83–87.
Summers, M. K., Pan, B., Mukhyala, K., & Jackson, P. K. (2008). The Unique N Terminus of the UbcH10 E2 Enzyme Controls the Threshold for APC Activation and Enhances Checkpoint Regulation of the APC. *Molecular Cell*, *31*, 544–556.
Sun, S. C., Ganchi, P. A., Ballard, D. W., & Greene, W. C. (1993). NF-κB controls expression of inhibitor IκBα: Evidence for an inducible autoregulatory pathway. *Science*, *259*(5103), 1912–1915.
Sun, X. M., Bowman, A., Priestman, M., Bertaux, F., Martinez-Segura, A., Tang, W., Whilding, C., Dormann, D., Shahrezaei, V., & Marguerat, S. (2020). Size-Dependent Increase in RNA Polymerase II Initiation Rates Mediates Gene Expression Scaling with Cell Size. *Current Biology*, *30*(7), 1217-1230.e7.
Takata, H., Matsunaga, S., Morimoto, A., Ma, N., Kurihara, D., Ono-Maniwa, R., Nakagawa, M., Azuma, T., Uchiyama, S., & Fukui, K. (2007). PHB2 Protects Sister-Chromatid Cohesion in Mitosis. *Current Biology*, *17*(15), 1356–1361.
Takebayashi, K., Sasai, Y., Sakai, Y., Watanabe, T., Nakanishi, S., & Kageyama, R. (1994). Structure, chromosomal locus, and promoter analysis of the gene encoding the mouse helix-loop-helix factor HES-1. Negative autoregulation through the multiple N box

elements. *Journal of Biological Chemistry*, *269*(7), 5150–5156.
Tang, Y., Zhao, W., Chen, Y., Zhao, Y., & Gu, W. (2008). Acetylation Is Indispensable for p53 Activation. *Cell*, *133*(4), 612–626.
Taniguchi, K., & Karin, M. (2018). NF-κB, inflammation, immunity and cancer: Coming of age. *Nature Reviews Immunology*, *18*(5), 309–324.
Thorvaldsdóttir, H., Robinson, J. T., & Mesirov, J. P. (2013). Integrative Genomics Viewer (IGV): High-performance genomics data visualization and exploration. *Briefings in Bioinformatics*, *14*(2), 178–192.
Tibbetts, R. S., Brumbaugh, K. M., Williams, J. M., Sarkaria, J. N., Cliby, W. A., Shieh, S. Y., Taya, Y., Prives, C., & Abraham, R. T. (1999). A role for ATR in the DNA damage-induced phosphorylation of p53. *Genes and Development*, *13*(2), 152–157.
Todaro, G. J., & Green, H. (1963). Quantitative studies of the growth of mouse embryo cells in culture and their development into established lines. *Journal of Cell Biology*, *17*, 299–313.
Tovey, C. A., & Conduit, P. T. (2018). Microtubule nucleation by γ-tubulin complexes and beyond. *Essays in Biochemistry*, *62*(6), 765–780.
Tremblay. (2009). HES1 is a novel interactor of the Fanconi anemia core complex (Blood (2008) 112, 5(2062-2070)). *Blood*, *114*(18), 3974.
Tsukahara, T., Tanno, Y., & Watanabe, Y. (2010). Phosphorylation of the CPC by Cdk1 promotes chromosome bi-orientation. *Nature*, *467*(7316), 719–723.
Tzur, A., Kafri, R., LeBleu, V. S., Lahav, G., & Kirschner, M. W. (2009). Cell Growth and Size Homeostasis in Proliferating Animal Cells. *Science*, *325*(5937), 167–171.
Van Horn, R. D., Chu, S., Fan, L., Yin, T., Du, J., Beckmann, R., Mader, M., Zhu, G., Toth, J., Blanchard, K., & Ye, X. S. (2010). Cdk1 activity is required for mitotic activation of Aurora A during G 2/M transition of human cells. *Journal of Biological Chemistry*, *285*(28), 21849–21857.
Vassilev, L. T. (2006). Cell cycle synchronization at the G2/M phase border by reversible inhibition of CDK1. *Cell Cycle*, *5*(22), 2555–2556.
Vassilev, L. T., Tovar, C., Chen, S., Knezevic, D., Zhao, X., Sun, H., Heimbrook, D. C., & Chen, L. (2006). Selective small-molecule inhibitor reveals critical mitotic functions of human CDK1. *Proceedings of the National Academy of Sciences of the United States of America*, *103*(28), 10660–10665.
Wall, D. S., Mears, A. J., McNeill, B., Mazerolle, C., Thurig, S., Wang, Y., Kageyama, R., & Wallace, V. A. (2009). Progenitor cell proliferation in the retina is dependent on Notch-independent Sonic hedgehog/Hes1 activity. *Journal of Cell Biology*, *184*(1), 101–112.
Wang, S.-C., Lin, X.-L., Wang, H.-Y., Qin, Y.-J., Chen, L., Li, J., Jia, J.-S., Shen, H.-F., Yang, S., Xie, R.-Y., Wei, F., Gao, F., Rong, X.-X., Yang, J., Zhao, W.-T., Zhang, T.-T., Shi, J.-W., Yao, K.-T., Luo, W.-R., … Xiao, D. (2015). Hes1 triggers epithelial-mesenchymal transition (EMT)-like cellular marker alterations and promotes invasion and metastasis of nasopharyngeal carcinoma by activating the PTEN/AKT pathway. *Oncotarget*, *6*(34), 36713–36730.
Wang, S., Nath, N., Adlam, M., & Chellappan, S. (1999). Prohibitin, a potential tumor suppressor, interacts with RB and regulates E2F function. *Oncogene*, *18*(23), 3501–3510.
Wasner, M., Tschöp, K., Spiesbach, K., Haugwitz, U., Johne, C., Mössner, J., Mantovani, R., & Engeland, K. (2003). Cyclin B1 transcription is enhanced by the p300 coactivator and regulated during the cell cycle by a CHR-dependent repression mechanism. *FEBS Letters*, *536*(1–3), 66–70.
Watanabe, N., Arai, H., Iwasaki, J., Shiina, M., Ogata, K., Hunter, T., & Osada, H. (2005). *Cyclin-dependent kinase (CDK) phosphorylation destabilizes somatic Wee1 via multiple*

pathways. *102*(33), 11663–11668.
Welburn, J. P. I., Vleugel, M., Liu, D., Iii, J. R. Y., Lampson, M. A., & Fukagawa, T. (2010). Aurora B Phosphorylates Spatially Distinct Targets to Differentially Regulate the Kinetochore-Microtubule Interface. *Molecular Cell*, *38*(3), 383–392.
Weng, A. P., Millholland, J. M., Yashiro-Ohtani, Y., Arcangeli, M. L., Lau, A., Wai, C., Del Bianco, C., Rodriguez, C. G., Sai, H., Tobias, J., Li, Y., Wolfe, M. S., Shachaf, C., Felsher, D., Blacklow, S. C., Pear, W. S., & Aster, J. C. (2007). c-Myc is an important direct target of Notch1 in T-cell acute lymphoblastic leukemia/lymphoma (Genes and Development (2006) 20, (2096-2109)). *Genes and Development*, *21*(5), 625.
Whitfield, M. L., Sherlock, G., Saldanha, A. J., Murray, J. I., Ball, C. A., Alexander, K. E., Matese, J. C., Perou, C. M., Hurt, M. M., Brown, P. O., Botstein, D., & Carolina, N. (2002). Human Cell Cycle and Their Expression in Tumors. *Molecular Biology of the Cell*, *13*, 1977–2000.
Wieczorek, M., Bechstedt, S., Chaaban, S., & Brouhard, G. J. (2015). Microtubule-associated proteins control the kinetics of microtubule nucleation. *Nature Cell Biology*, *17*(7), 907–916.
Wilkinson, R. W., Odedra, R., Heaton, S. P., Wedge, S. R., Keen, N. J., Crafter, C., Foster, J. R., Brady, M. C., Bigley, A., Brown, E., Byth, K. F., Barrass, N. C., Mundt, K. E., Foote, K. M., Heron, N. M., Jung, F. H., Mortlock, A. A., Boyle, F. T., & Green, S. (2007). AZD1152, a selective inhibitor of Aurora B kinase, inhibits human tumor xenograft growth by inducing apoptosis. *Clinical Cancer Research*, *13*(12), 3682–3688.
Wolf, F., Wandke, C., Isenberg, N., & Geley, S. (2006). Dose-dependent effects of stable cyclin B1 on progression through mitosis in human cells. *EMBO Journal*, *25*(12), 2802–2813.
Wu, X., Bayle, J. H., Olson, D., & Levine, A. J. (1993). The p53-mdm-2 autoregulatory feedback loop. *Genes & Development*, *53*, 1126–1132.
Yamagishi, Y., Yang, C. H., Tanno, Y., & Watanabe, Y. (2012). MPS1/Mph1 phosphorylates the kinetochore protein KNL1/Spc7 to recruit SAC components. *Nature Cell Biology*, *14*(7), 746–752.
Yang, H. W., Cappell, S. D., Jaimovich, A., Liu, C., Chung, M., Daigh, L. H., Pack, L. R., Fan, Y., Regot, S., Covert, M., & Meyer, T. (2020). Stress-mediated exit to quiescence restricted by increasing persistence in cdk4/6 activation. *ELife*, *9*, 1–16.
Yang, H. W., Chung, M., Kudo, T., & Meyer, T. (2017). Competing memories of mitogen and p53 signalling control cell-cycle entry. *Nature*, *549*(7672), 404–408.
Yang, Q., & Ferrell, J. E. (2013). The Cdk1-APC/C cell cycle oscillator circuit functions as a time-delayed, ultrasensitive switch. *Nature Cell Biology*, *15*(5), 519–525.
Yano, S., Zhang, Y., Miwa, S., Tome, Y., Hiroshima, Y., Uehara, F., Yamamoto, M., Suetsugu, A., Kishimoto, H., Tazawa, H., Zhao, M., Bouvet, M., Fujiwara, T., & Hoffman, R. M. (2014). Spatial-temporal FUCCI imaging of each cell in a tumor demonstrates locational dependence of cell cycle dynamics and chemoresponsiveness. *Cell Cycle*, *13*(13), 2110–2119.
Ye, Y., Wang, G., Wang, G., Zhuang, J., He, S., Song, Y., Ni, J., Xia, W., & Wang, J. (2017). The oncogenic role of Tribbles 1 in hepatocellular carcinoma is mediated by a feedback loop involving microRNA-23a and p53. *Frontiers in Physiology*, *8*, 789.
Yin, X. Y., Grove, L., Datta, N. S., Katula, K., Long, M. W., & Prochownik, E. V. (2001). Inverse regulation of cyclin B1 by c-Myc and p53 and induction of tetraploidy by cyclin B1 overexpression. *Cancer Research*, *61*(17), 6487–6493.
Yoshiura, S., Ohtsuka, T., Takenaka, Y., Nagahara, H., Yoshikawa, K., & Kageyama, R. (2007). Ultradian oscillations of Stat, Smad, and Hes1 expression in response to serum. *Proceedings of the National Academy of Sciences of the United States of America*,

104(27), 11292–11297.
Young, D. W., Hassan, M. Q., Yang, X. Q., Galindo, M., Javed, A., Zaidi, S. K., Furcinitti, P., Lapointe, D., Montecino, M., Lian, J. B., Stein, J. L., Van Wijnen, A. J., & Stein, G. S. (2007). Mitotic retention of gene expression patterns by the cell fate-determining transcription factor Runx2. *Proceedings of the National Academy of Sciences of the United States of America*, *104*(9), 3189–3194.
Yu, G., Wang, L. G., & He, Q. Y. (2015). ChIP seeker: An R/Bioconductor package for ChIP peak annotation, comparison and visualization. *Bioinformatics*, *31*(14), 2382–2383.
Yunger, S., Rosenfeld, L., Garini, Y., & Shav-Tal, Y. (2010). Single-allele analysis of transcription kinetics in living mammalian cells. *Nature Methods*, *7*(8), 631–633.
Zaidi, S. K., Nickerson, J. A., Imbalzano, A. N., Lian, J. B., Stein, J. L., & Stein, G. S. (2018). Mitotic gene bookmarking: An epigenetic program to maintain normal and cancer phenotypes. *Molecular Cancer Research*, *16*(11), 1617–1624.
Zatulovskiy, E., Berenson, D. F., Topacio, B. R., & Skotheim, J. M. (2020). Cell growth dilutes the cell cycle inhibitor Rb to trigger cell division. *Science*, *369*, 466–471.
Zhan, Q., Antinore, M. J., Wang, X. W., Carrier, F., Smith, M. L., Harris, C. C., & Fornace, A. J. (1999). Association with Cdc2 and inhibition of Cdc2/Cyclin B1 kinase activity by the p53-regulated protein Gadd45. *Oncogene*, *18*(18), 2892–2900.
Zhang, S., Chang, L., Alfieri, C., Zhang, Z., Yang, J., Maslen, S., Skehel, M., & Barford, D. (2016). Molecular mechanism of APC/C activation by mitotic phosphorylation. *Nature*, *533*(7602), 260–264.
Zhang, Y., Liu, T., Meyer, C. A., Eeckhoute, J., Johnson, D. S., Bernstein, B. E., Nussbaum, C., Myers, R. M., Brown, M., Li, W., & Shirley, X. S. (2008). Model-based analysis of ChIP-Seq (MACS). *Genome Biology*, *9*(9), 1-9.
Zhao, Y., Ge, C. C., Wang, J., Wu, X. X., Li, X. M., Li, W., Wang, S. S., Liu, T., Hou, J. Z., Sun, H., Fang, D., & Xie, S. Q. (2017). MEK inhibitor, PD98059, promotes breast cancer cell migrationby inducing β-catenin nuclear accumulation. *Oncology Reports*, *38*(5), 3055–3063.
Zhou, L., Tian, X., Zhu, C., Wang, F., & Higgins, J. M. (2014). Polo-like kinase-1 triggers Histone phosphorylation by Haspin in mitosis. *EMBO Reports*, *15*(3), 273–281.
Zhurinsky, J., Leonhard, K., Watt, S., Marguerat, S., Bähler, J., & Nurse, P. (2010). A coordinated global control over cellular transcription. *Current Biology*, *20*(22), 2010–2015.
Ziebold, U., Bartsch, O., Marais, R., Ferrari, S., & Klempnauer, K. H. (1997). Phosphorylation and activation of B-Myb by cyclin A-Cdk2. *Current Biology*, *7*(4), 253–260.

Supplementary information

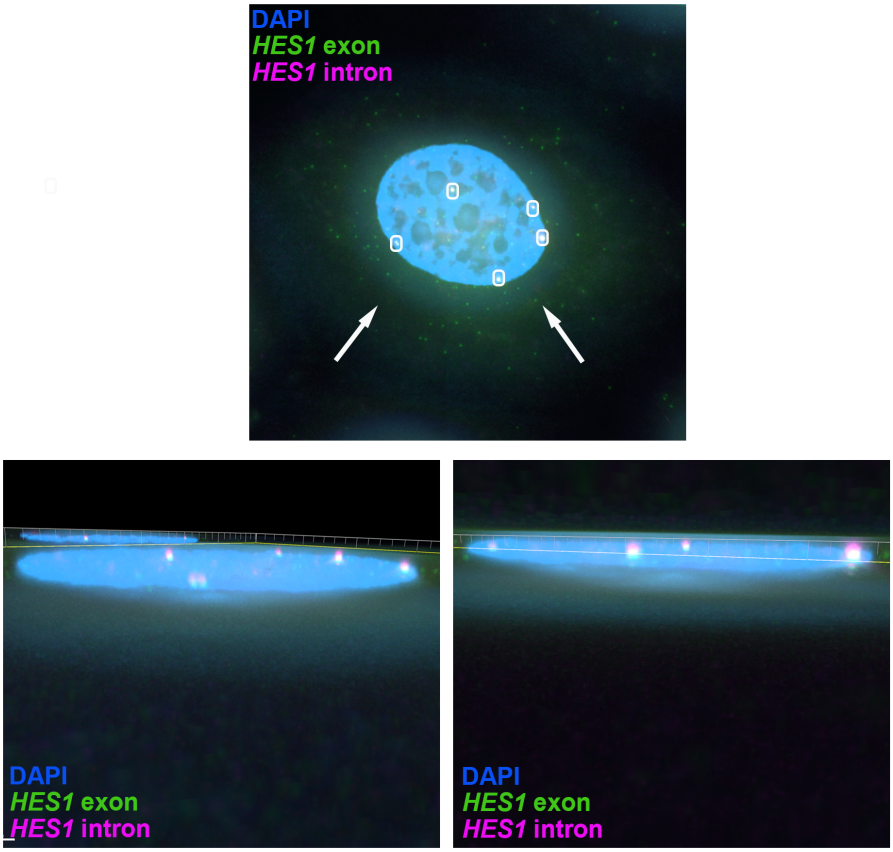

Fig S1 Nuclear localisation of *HES1* intronic and exonic smFISH signal (Fig 2.2.7)
3D IMARIS image of z-projected *HES1* smFISH image presented in Fig 2.2.7. Top panel is viewpoint looking down on cell. The two white arrows represent the side-on viewpoint of the two images in the bottom panel.

GO:0048667 - Cell morphogenesis involved in neuron differentiation
NTNG1 - netrin G1
TNR - tenascin R
LHX4 - LIM homeobox 4
GATA3 - GATA binding protein 3
NEUROG3 - neurogenin 3
PAX6 - paired box 6
THY1 - THY-1 cell surface antigen
CAPRIN2 -caprin family member 2
NRXN3 - neurexin 3
BCL11B - B-cell lymphoma 11B
LINGO1 - leucine rich repeat and IG domain containing 1
ARGHDIA - rho GDP disscociation inhibitor 1
PTPRS - protein tyrosine phosphatase receptor type 5
RAPH1 - ras associated and pleckstrin homology domains containing protein 1
SRC - proto-oncogene tyrosine kinase src
PARD6B - par-6 family cell polarity regulator beta
DOK5 - docking protein 5
BMP7 - bone morphogenetic protein 7
YWHAH - *t*yrosine 3-monooxygenase/tryptophan 5-monooxygenase activation protein eta
WNT7A - WNT family member 7B
TOP2B - DNA topoisomerase II beta
FEZF2 - fez family zinc finger II
SKIL - SKI-like oncogene
HES1 - hairy and enhancer of split 1
ATOH1 - atonal BHLH transcription factor 1
BMPR1B - bone morpohgenetic protein receptor type 1B
SEMA5A - semaphorin
EFNA5 - ephrin A5
SYNGAP1 - synaptic ras GTPase activating protein 1
VEGFA - vascular endothelial factor A
CAMK2B - calcium/calmodulin-dependent protein kinase II beta
SEMA3C - semaphorin 3C
NFIB - nuclear factor 1 B-type
SEMA4D - semaphorin 4D
LHX2 - LIM homeobox 2
SH3KBP1 - SH3 domain-containing kinase binding protein 1

Table S1 Gene ontology (GO) analysis of HES1 target genes

GFP1 GFP2 IDR

Chromosome	Gene name	Start	End	Annotation	Distance To TSS
chr4	RBPJ	26319154	26319792	Promoter (<=1kb)	0
chr8	TRIB1	125429807	125430319	Promoter (<=1kb)	-39
chr14	TNFAIP2	103126970	103127485	Promoter (<=1kb)	-81
chr16	CHTF18	795569	796035	Promoter (<=1kb)	-580
chr17	CBX2	79778008	79778437	Promoter (<=1kb)	0
chr1	TP73	3668672	3669205	Exon (ENST00000443034.1/ENST00000443034.1, exon 1 of 3)	-13161
chr8	GASAL1	102806414	102807110	Promoter (<=1kb)	0
chr3	HES1	194133983	194135355	Promoter (<=1kb)	-793
chr8	TMEM70	73975918	73976354	Promoter (<=1kb)	0
chr3	PROS1	93470343	93470832	Distal Intergenic	415581
chr16	ANKRD26P1	46390271	46390905	Distal Intergenic	87534
chr2	FTCDNL1	199850873	199851527	Promoter (<=1kb)	0
chr3	RYBP	72447127	72447438	Promoter (<=1kb)	-504
chr2	RAPH1	203535157	203535731	Promoter (<=1kb)	0
chr10	NEURL1	103554944	103555378	Promoter (<=1kb)	0
chr19	ZNF296	45076222	45076604	Promoter (<=1kb)	0
chr1	MAST2	45803361	45803731	Promoter (<=1kb)	0
chr10	BNIP3	131981895	131982307	Promoter (<=1kb)	0
chr16	GSE1	85612927	85613378	Promoter (<=1kb)	0
chr5	MAP3K1	56815173	56815599	Promoter (<=1kb)	0
chr3	CDV3	133573503	133573843	Promoter (<=1kb)	0
chr11	LINC02751	15708044	15708397	Intron (ENST00000663676.1/ENST00000663676.1, intron 4 of 7)	102560
chr14	ITPK1	93115135	93115737	Promoter (<=1kb)	0
chr12	RAN	130871595	130872106	Promoter (<=1kb)	0
chr17	B3GNTL1	83050776	83051400	Promoter (<=1kb)	409

chr12	KSR2	117969054	117969612	Promoter (<=1kb)	-64
chr18	LPIN2	3012900	3013578	Promoter (<=1kb)	0
chr4	JAKMIP1	6200311	6200701	Promoter (<=1kb)	0
chr18	MTCL1	8705130	8705442	Promoter (<=1kb)	-219
chr17	BAHCC1	81429381	81429765	Intron (ENST00000675386.2/57597, intron 3 of 27)	-13700
chr14	FOXA1	37595059	37595581	Promoter (<=1kb)	0
chr12	PAWR	79690929	79691466	Promoter (<=1kb)	0
chr3	LINC00886	156816857	156817264	Promoter (<=1kb)	0
chr3	HES1	194141247	194141882	Distal Intergenic	5099
chr16	CCNYL3	34586705	34587056	Distal Intergenic	-205595
chr12	BHLHE41	26124889	26125284	Promoter (<=1kb)	0
chr20	NELFCD	58981086	58981363	Promoter (<=1kb)	0
chr8	RUNX1T1	92103236	92103631	Promoter (<=1kb)	0
chr12	ANKS1B	99984510	99985003	Promoter (<=1kb)	0
chr9	VAV2	133992187	133992759	Promoter (<=1kb)	0
chr14	ACOT2	735696677	73570061	Promoter (<=1kb)	382
chr2	LINC00486	32916242	32916642	Intron (ENST00000414054.5/285045, intron 4 of 4)	-10443
chr17	PPP1R1B	39617655	39617944	Distal Intergenic	-8796
chr3	LINC02028	194070961	194071423	Promoter (<=1kb)	0
chr16	ANKRD26P1	46386304	46386558	Distal Intergenic	91881
chr17	DLX4	49968443	49968891	Promoter (<=1kb)	-79
chr22	TBX1	19806490	19806848	Exon (ENST00000329517.11/54584, exon 6 of 8)	41411
chr2	USP34	61471056	61471342	Promoter (<=1kb)	0
chr14	MIPOL1	37197763	37198130	Promoter (<=1kb)	0
chr9	MYMK	133509543	133510048	Distal Intergenic	14911
chr12	ASCL1	102957226	102957631	Promoter (<=1kb)	-43
chr10	ZMIZ1	79242757	79243186	Promoter (<=1kb)	-483
chr2	PROC	127407949	127408325	Exon (ENST00000657275.1/ENST00000657275.1, exon 1 of 2)	-10102

chr16	ANKRD26P1	46400004	46400231	Distal Intergenic	78208
chr14	PPP1R3E	23301533	23302012	Promoter (<=1kb)	0
chr20	ZNF217	53594258	53594773	Promoter (<=1kb)	-419
chr16	ANKRD26P1	46389558	46390117	Distal Intergenic	88322
chr15	SMAD3	67065297	67065827	Promoter (<=1kb)	0
chr5	PCDHAC2	14096652 5	14096677	Promoter (<=1kb)	49
chr16	ANKRD26P1	46387720	46388055	Distal Intergenic	90384
chr11	GVQW3	76381048	76381345	Promoter (<=1kb)	0
chr9	DENND1A	1239299 13	1239302 74	Promoter (<=1kb)	0
chr16	ANKRD26P1	46398777	46399030	Distal Intergenic	79409
chr2	DTNB	25673147	25673888	Promoter (<=1kb)	0
chr3	MYRIP	39809346	39809669	Promoter (<=1kb)	0
chr4	SEL1L3	25862852	25863073	Promoter (<=1kb)	0
chr5	MIR2277	93677350	93677628	Intron (ENST00000395965.8/83989, intron 10 of 10)	-56562
chr9	PRUNE2	76906073	76906464	Promoter (<=1kb)	0
chrX	APLN	1296543 13	1296547 66	Promoter (<=1kb)	190
chr16	CCNYL3	34582121	34582518	Distal Intergenic	-201011
chr6	FKBP5	35727946	35728473	Promoter (<=1kb)	110
chr16	ANKRD26P1	46394421	46395091	Distal Intergenic	83348
chr16	ANKRD26P1	46400591	46401194	Distal Intergenic	77245
chr1	KCNQ4	40783551	40783910	Promoter (<=1kb)	0
chr16	GSE1	85611729	85612428	Promoter (<=1kb)	320
chr7	LFNG	2524142	2524415	Promoter (<=1kb)	-233
chr14	SPTSSA	34462087	34462368	Promoter (<=1kb)	0
chr2	LPIN1	11746476	11746842	Promoter (<=1kb)	0
chr22	GNB1L	19854731	19855065	Promoter (<=1kb)	0
chr1	HSPG2	21956860	21957293	Exon (ENST00000637118.1/ENST00000637118.1, exon 1 of 2)	-19550

chr9	PRRT1B	131545409	131545729	Promoter (<=1kb)	0
chr16	CCNYL3	34573978	34574406	Distal Intergenic	-192868
chr16	CCNYL3	34587945	34588371	Distal Intergenic	-206835
chr7	PALS2	24573151	24573467	Promoter (<=1kb)	0
chrX	CMC4	155071106	155071341	Promoter (<=1kb)	0
chr9	SEMA4D	89497970	89498300	Promoter (<=1kb)	0
chr2	BIRC6	32356872	32357125	Promoter (<=1kb)	0
chr16	ANKRD26P1	46388587	46389093	Distal Intergenic	89346
chr16	CCNYL3	34592594	34592840	Distal Intergenic	-211484
chr19	ARID3A	935001	935218	Promoter (2-3kb)	2436
chr3	TBC1D5	177425222	177429226	Promoter (<=1kb)	0
chr2	SP3	173963955	173964315	Promoter (<=1kb)	0
chr1	CDK18	205504611	205504940	Promoter (<=1kb)	0
chr19	NFIX	13051576	13052030	Intron (ENST00000592199.6/4784, intron 2 of 10)	-17973
chr1	MAN1C1	25616662	25616937	Promoter (<=1kb)	-531
chr16	MMP2	55480304	55480628	Promoter (<=1kb)	0
chr20	EPB41L1	36154432	36154775	Promoter (<=1kb)	0
chr3	XIRP1	39180948	39181272	Distal Intergenic	11323
chr10	NEUROG3	69573311	69573675	Promoter (<=1kb)	0
chr2	MIR1301	25311343	25311541	Intron (ENST00000264709.7/1788, intron 2 of 22)	17180
chr2	CT75	222319500	222319849	Promoter (<=1kb)	202
chr3	HES1	194135783	194136187	Promoter (<=1kb)	0
chr4	SGMS2	107824747	107824971	Promoter (<=1kb)	0
chr8	ZNF395	28401944	28402281	Intron (ENST00000521548.5/55893, intron 7 of 15)	-15484
chr4	CFAP97	185203977	185204177	Promoter (<=1kb)	0
chr19	ARHGEF1	41904392	41904767	Promoter (<=1kb)	176
chr20	PARD6B	50730889	50731167	Promoter (<=1kb)	-413
chr19	SBK2	55526314	55526642	Distal Intergenic	9661

chr20	NRSN2-AS1	324335	324739	Promoter (<=1kb)	0
chr14	AK7	96391689	96392087	Promoter (<=1kb)	-41
chrY	GYG2P1	11721875	11722114	Distal Intergenic	696180
chr17	SLC25A10	81711721	81712050	Promoter (<=1kb)	-186
chr11	SYT7	61580995	61581328	Promoter (<=1kb)	0
chr14	BEGAIN	100547833	100548183	Promoter (<=1kb)	0
chr17	TNRC6C	77957985	77958176	Promoter (1-2kb)	-1064
chr19	MLLT1	6236981	6237339	Intron (ENST00000252674.9/4298, intron 3 of 11)	-20013
chr6	FOXO3	108559526	108559914	Promoter (<=1kb)	0
chr6	HIVEP2	142944971	142945228	Promoter (<=1kb)	0
chr1	KCNAB2	6026124	6026434	Promoter (<=1kb)	0
chr14	EGLN3	33938366	33938713	Intron (ENST00000250457.9/112399, intron 1 of 4)	-7030
chr2	DUSP2	96145022	96145336	Promoter (<=1kb)	104
chr6	FOXO3	108557932	108558256	Promoter (1-2kb)	-1579
chr14	LINC01303	61568597	61568855	Promoter (1-2kb)	1339
chr11	TMPRSS4	118057706	118057987	Intron (ENST00000636151.1/100526771, intron 3 of 6)	-19025
chr17	PLD6	17206318	17206907	Promoter (<=1kb)	0
chr17	SPAG9	50944469	50944842	Exon (ENST00000501718.2/ENST00000501718.2, exon 1 of 2)	30518
chr1	FOXO6	41353823	41354069	Distal Intergenic	-7853
chr11	VPS37C	61161387	61161674	Promoter (<=1kb)	0
chr11	ASCL2	2257424	2257657	Distal Intergenic	13295
chr17	LINC00511	72640456	72640751	Promoter (<=1kb)	0
chr2	TGFA	70554031	70554306	Promoter (<=1kb)	0
chr3	TPRA1	127591011	127591374	Promoter (<=1kb)	0
chr4	PGRMC2	128287859	128288337	Promoter (<=1kb)	0
chr6	LOC102724511	170026624	170026826	Distal Intergenic	-133780
chr10	MAPK8	48306319	48306565	Promoter (<=1kb)	-74
chr11	PAX6-AS1	31812037	31812321	Promoter (<=1kb)	0

chr14	ANGEL1	76812710	76812952	Promoter (<=1kb)	0
chr5	NREP	111757614	111757988	Promoter (<=1kb)	0
chr6	LOC102724511	170179025	170179397	Exon (ENST00000610240.1/ENST00000610240.1, exon 1 of 1)	18363
chr8	EMC2	108584519	108584760	Intron (ENST00000521504.1/ENST00000521504.1, intron 1 of 2)	110668
chr5	WWC1	168353355	168353582	Intron (ENST00000265293.9/23286, intron 1 of 22)	-17839
chr21	MIR6815	45470912	45471299	Intron (ENST00000651438.1/80781, intron 3 of 41)	-6967
chr1	ELF3	202018802	202019049	Distal Intergenic	5024
chr16	NTHL1	2039588	2039885	Promoter (<=1kb)	583
chrM	MIR12136	11645	16549	Exon (ENST00000361381.2/ENST00000361381.2, exon 1 of 1)	-4131
chr5	EMB	49658614	49658790	Distal Intergenic	753208
chr15	TRPM7	50686714	50686961	Promoter (<=1kb)	0
chr10	MARVELD1	97713675	97714323	Promoter (<=1kb)	0
chr14	MIDEAS	73759973	73760369	Promoter (<=1kb)	0
chr11	CCDC85B	65890519	65890920	Promoter (<=1kb)	0
chr21	KRTAP10-2	44550726	44551153	Promoter (<=1kb)	352
chr16	CCNYL3	34582714	34583227	Distal Intergenic	-201604
chr17	DUSP14	37489586	37489970	Promoter (<=1kb)	0
chr18	ZNF407-AS1	74598067	74598410	Promoter (<=1kb)	0
chr19	KDM4B	5103123	5103340	Intron (ENST00000611640.4/23030, intron 9 of 23)	-9018
chr22	SCARF2	20430946	20431498	Promoter (1-2kb)	-1020
chrX	PDK3	24465106	24465269	Promoter (<=1kb)	-1
chr13	IL17D	20704049	20704425	Promoter (<=1kb)	0
chr1	ATP8B2	154328584	154328852	Promoter (<=1kb)	0
chr10	TM9SF3	96586947	96587167	Promoter (<=1kb)	0
chr14	NRXN3	79279031	79279306	Promoter (<=1kb)	-33
chr14	BCL11B	99274569	99274784	Promoter (2-3kb)	-2372

chr14	LINC02285	101175080	101175259	Distal Intergenic	54240
chr15	USP3-AS1	63600670	63601098	Promoter (<=1kb)	0
chr2	CNNM3	96816526	96816863	Promoter (<=1kb)	258
chr2	AGAP1	235493923	235494143	Promoter (<=1kb)	0
chr3	SKIL	170356740	170357055	Promoter (<=1kb)	-623
chr3	TPRG1	189304796	189305014	Intron (ENST00000433971.5/285386, intron 9 of 10)	-4880
chr4	ATOH1	93828579	93828806	Promoter (<=1kb)	0
chr4	MMAA	145619160	145619541	Promoter (<=1kb)	0
chr5	EFNA5	107557144	107557522	Intron (ENST00000333274.11/1946, intron 1 of 4)	-50953
chr7	MET	116672057	116672462	Promoter (<=1kb)	0
chr7	GIGYF1	100694354	100694570	Promoter (<=1kb)	-104
chr15	IDH3A	78149314	78149639	Promoter (<=1kb)	0
chr9	PBX3	125990981	125991302	Distal Intergenic	125710
chr10	LCOR	96832837	96833076	Promoter (<=1kb)	0
chr20	INSM1	20364414	20364597	Exon (ENST00000623641.1/ENST00000623641.1, exon 1 of 1)	-3507
chr8	PVT1	128025074	128025267	Promoter (2-3kb)	-2242
chr6	DDR1	30884149	30884450	Promoter (<=1kb)	0
chr14	FOXN3	89417155	89417349	Promoter (<=1kb)	0
chr16	LITAF	11612454	11612693	Intron (ENST00000576036.5/9516, intron 1 of 3)	-13954
chr11	POU2AF1	111436743	111437010	Intron (ENST00000531398.1/5450, intron 1 of 4)	12971
chr11	PRDM10	129924863	129925063	Exon (ENST00000358825.9/56980, exon 13 of 22)	17527
chr15	BMF	40103334	40103687	Promoter (2-3kb)	2399
chr17	SP6	47850885	47851204	Promoter (<=1kb)	0
chr9	NFIB	14315259	14315479	Promoter (<=1kb)	-677
chr5	EMB	49659775	49659999	Distal Intergenic	751999
chr16	ZFHX3	72927584	72927818	Intron (ENST00000268489.10/463, intron 3 of 9)	-37750
chr1	TTC39A	51297816	51298140	Promoter (<=1kb)	0

chr2	MIR375	219001696	219002173	Promoter (<=1kb)	0
chr3	TNK2-AS1	195907774	195907990	Promoter (<=1kb)	-86
chr14	ADAM21P1	70254754	70255016	Distal Intergenic	-6953
chr2	STK17B	196171617	196171892	Promoter (<=1kb)	-39
chr5	LINC01184	128083218	128083562	Promoter (<=1kb)	-46
chr6	MYB	135181046	135181325	Promoter (<=1kb)	0
chr9	ANKS6	98796409	98796643	Promoter (<=1kb)	0
chr21	MIR6724-1	8234381	8234609	Distal Intergenic	-14896
chr17	AMZ2P1	64975403	64975595	Promoter (<=1kb)	0
chr7	SEMA3C	80919022	80919375	Promoter (<=1kb)	0
chr6	SPDEF	34546847	34547135	Intron (ENST00000374037.8/25803, intron 1 of 5)	9194
chr22	YWHAH	31944433	31944700	Promoter (<=1kb)	0
chr10	ECHS1	133373547	133373781	Promoter (<=1kb)	-193
chr20	OVOL2	18058912	18059184	Promoter (<=1kb)	0
chr12	FGD6	95217393	95217616	Promoter (<=1kb)	0
chr3	BHLHE40-AS1	4868368	4868598	Intron (ENST00000449914.5/ENST00000449914.5, intron 1 of 3)	37903
chr3	CD47	108090986	108091494	Promoter (<=1kb)	0
chr6	LINC00271	135497561	135497805	Promoter (<=1kb)	0
chr11	CDON	126115999	126116268	Distal Intergenic	-52664
chr12	ZNF664-RFLNA	123973000	123973425	Promoter (<=1kb)	0
chr4	KLF3	38663701	38663994	Promoter (<=1kb)	-203
chr7	NAMPT	106285020	106285359	Promoter (<=1kb)	-37
chr17	HID1	74972146	74972349	Promoter (<=1kb)	367
chr2	ODC1-DT	104484554	104486577	Promoter (<=1kb)	-32
chrX	XPNPEP2	129706480	129706687	Distal Intergenic	-32287
chrY	GYG2P1	11747589	11747825	Distal Intergenic	670469
chr17	DGKE	56833960	56834199	Promoter (<=1kb)	0
chr4	FGFRL1	1010625	1010839	Promoter (<=1kb)	646

chr7	VGF	101163635	101163912	Promoter (1-2kb)	1202
chr20	CYP24A1	54185000	54185261	Distal Intergenic	-11014
chr12	ZDHHC17	76764038	76764214	Promoter (<=1kb)	0
chr16	CCNYL3	34581288	34581660	Distal Intergenic	-200178

GFP1 GFP3 IDR

Chromosome	Gene name	Start	End	Annotation	Distance To TSS
chr4	RBPJ	26319045	26319719	Promoter (<=1kb)	0
chr16	CHTF18	795581	796035	Promoter (<=1kb)	-580
chr8	TRIB1	125429785	125430381	Promoter (<=1kb)	0
chr3	HES1	194133943	194135266	Promoter (<=1kb)	-882
chr8	TMEM70	73975936	73976354	Promoter (<=1kb)	0
chr18	LPIN2	3012900	3013578	Promoter (<=1kb)	0
chr1	TP73	3668672	3669205	Exon (ENST00000443034.1/ENST00000443034.1, exon 1 of 3)	-13161
chr14	TNFAIP2	103126973	103127494	Promoter (<=1kb)	-72
chr8	GASAL1	102806458	102807001	Promoter (<=1kb)	0
chr2	FTCDNL1	199850873	199851527	Promoter (<=1kb)	0
chr2	RAPH1	203535106	203535731	Promoter (<=1kb)	0
chr3	RYBP	72447132	72447449	Promoter (<=1kb)	-509
chrM	MIR12136	16097	16546	Distal Intergenic	-8583
chr16	GSE1	85612954	85613388	Promoter (<=1kb)	0
chr17	CBX2	79778008	79778437	Promoter (<=1kb)	0
chr10	BNIP3	131981920	131982307	Promoter (<=1kb)	0
chr11	LINC02751	15708037	15708387	Intron (ENST00000663676.1/ENST00000663676.1, intron 4 of 7)	102553
chr3	HES1	194135771	194136225	Promoter (<=1kb)	0
chr5	MAP3K1	56815173	56815599	Promoter (<=1kb)	0
chr12	RAN	130871645	130872106	Promoter (<=1kb)	0
chr12	PAWR	79690960	79691475	Promoter (<=1kb)	0
chr9	VAV2	133992187	133992759	Promoter (<=1kb)	0
chr3	LINC00886	156816857	156817317	Promoter (<=1kb)	0
chr19	ZNF296	45076113	45076604	Promoter (<=1kb)	0

chr3	LINC02028	194070943	194071457	Promoter (<=1kb)	0
chr12	KSR2	117969054	117969482	Promoter (<=1kb)	-64
chr14	ACOT2	73569730	73570061	Promoter (<=1kb)	445
chr17	DLX4	49968503	49968866	Promoter (<=1kb)	-104
chr22	TBX1	19806518	19806848	Exon (ENST00000329517.11/54584, exon 6 of 8)	41439
chr14	MIPOL1	37197749	37198173	Promoter (<=1kb)	0
chr9	MYMK	133509539	133510019	Distal Intergenic	14940
chr14	FOXA1	37595117	37595598	Promoter (<=1kb)	0
chr14	ITPK1	93115135	93115801	Promoter (<=1kb)	0
chr9	PRUNE2	76906079	76906415	Promoter (<=1kb)	0
chr17	BAHCC1	81429381	81429765	Intron (ENST00000675386.2/57597, intron 3 of 27)	-13700
chr3	MYRIP	39809350	39809669	Promoter (<=1kb)	0
chr3	HES1	194141247	194142006	Distal Intergenic	5099
chr8	RUNX1T1	92103236	92103624	Promoter (<=1kb)	0
chrX	APLN	129654313	129654766	Promoter (<=1kb)	190
chr3	TPRA1	127590972	127591476	Promoter (<=1kb)	0
chr19	MLLT1	6236981	6237339	Intron (ENST00000252674.9/4298, intron 3 of 11)	-20013
chr5	MIR2277	93677350	93677648	Intron (ENST00000395965.8/83989, intron 10 of 10)	-56562
chr14	PPP1R3E	23301519	23301962	Promoter (<=1kb)	0
chr7	SEMA3C	80919022	80919375	Promoter (<=1kb)	0
chr20	ZNF217	53594423	53594864	Promoter (<=1kb)	-584
chr17	B3GNTL1	83050959	83051340	Promoter (<=1kb)	469
chr3	CDV3	133573503	133573843	Promoter (<=1kb)	0
chr2	DTNB	25673329	25674074	Promoter (<=1kb)	0
chr9	DENND1A	123929950	123930274	Promoter (<=1kb)	0
chr15	BMF	40103334	40103687	Promoter (2-3kb)	2399
chr15	SMAD3	67065306	67065781	Promoter (<=1kb)	0
chr1	MAST2	45803361	45803731	Promoter (<=1kb)	0
chr1	KCNQ4	40783551	40783936	Promoter (<=1kb)	0
chr11	PRDM10	129924838	129925102	Exon (ENST00000358825.9/56980, exon 13 of 22)	17488
chr16	GSE1	85611765	85612144	Promoter (<=1kb)	356
chr1	HSPG2	21956842	21957194	Exon (ENST00000637118.1/ENST00000637118.1, exon 1 of 2)	-19532
chr10	NEURL1	103554944	103555367	Promoter (<=1kb)	0

chr3	LOC105376975	17742516	17742964	Promoter (<=1kb)	0
chr2	SP3	173963962	173964315	Promoter (<=1kb)	0
chr17	PPP1R1B	39617655	39618080	Distal Intergenic	-8660
chr12	ANKS1B	99984443	99984993	Promoter (<=1kb)	0
chr4	JAKMIP1	6200248	6200686	Promoter (<=1kb)	0
chr19	NFIX	13051600	13052030	Intron (ENST00000592199.6/4784, intron 2 of 10)	-17973
chr16	MMP2	55480331	55480585	Promoter (<=1kb)	0
chr20	EPB41L1	36154350	36154775	Promoter (<=1kb)	0
chr3	XIRP1	39180855	39181233	Distal Intergenic	11362
chr19	ARHGEF1	41904343	41904797	Promoter (<=1kb)	127
chr2	CT75	222319500	222319890	Promoter (<=1kb)	202
chrX	XPNPEP2	129706500	129706718	Distal Intergenic	-32256
chr3	PROS1	93470343	93470832	Distal Intergenic	415581
chr6	FOXO3	108559526	108559902	Promoter (<=1kb)	0
chr18	MTCL1	8705061	8705417	Promoter (<=1kb)	-244
chr20	NRSN2-AS1	324405	324677	Promoter (<=1kb)	0
chr9	PRRT1B	131545395	131545679	Promoter (<=1kb)	0
chr1	KCNAB2	6026138	6026476	Promoter (<=1kb)	0
chr14	EGLN3	33938385	33938598	Intron (ENST00000250457.9/112399, intron 1 of 4)	-7049
chr6	FOXO3	108557919	108558153	Promoter (1-2kb)	-1682
chr6	LOC102724511	170026578	170026848	Distal Intergenic	-133758
chr6	FKBP5	35727980	35728459	Promoter (<=1kb)	124
chr11	TMPRSS4	118057636	118057987	Intron (ENST00000636151.1/100526771, intron 3 of 6)	-19025
chr10	ZMIZ1	79242757	79243186	Promoter (<=1kb)	-483
chr13	GTF3A	27424487	27424886	Promoter (<=1kb)	0
chr2	MIR1301	25311343	25311599	Intron (ENST00000264709.7/1788, intron 2 of 22)	17122
chr22	SCARF2	20430946	20431534	Promoter (1-2kb)	-1020
chr1	FOXO6	41353826	41354101	Distal Intergenic	-7821
chr17	LINC00511	72640456	72640760	Promoter (<=1kb)	0
chr9	SEMA4D	89497970	89498261	Promoter (<=1kb)	0
chr14	SPTSSA	34462087	34462370	Promoter (<=1kb)	0
chr11	PAX6-AS1	31812050	31812321	Promoter (<=1kb)	0
chr8	EMC2	108584495	108584801	Intron (ENST00000521504.1/ENST00000521504.1, intron 1 of 2)	110644
chr21	MIR6815	45470930	45471298	Intron (ENST00000651438.1/80781, intron 3 of 41)	-6968

chr16	NTHL1	2039590	2039849	Promoter (<=1kb)	619
chr1	TMEM51-AS2	15200851	15201041	Intron (ENST00000428417.5/55092, intron 1 of 2)	-29534
chr11	CCDC85B	65890532	65890906	Promoter (<=1kb)	0
chr12	ASCL1	102957245	102957503	Promoter (<=1kb)	-171
chr2	DUSP2	96145025	96145336	Promoter (<=1kb)	104
chr21	LINC00322	43287935	43288263	Distal Intergenic	43776
chr22	IL17REL	50027722	50028128	Intron (ENST00000266182.10/164714, intron 12 of 13)	-15063
chr6	LOC102724511	170178935	170179325	Exon (ENST00000610240.1/ENST00000610240.1, exon 1 of 1)	18273
chr7	LFNG	2524114	2524399	Promoter (<=1kb)	-249
chr9	NFIB	14315208	14315546	Promoter (<=1kb)	-626
chrM	MIR12136	12751	15772	Exon (ENST00000361567.2/ENST00000361567.2, exon 1 of 1)	-5237
chr2	BIRC6	32356887	32357105	Promoter (<=1kb)	0
chr15	TRPM7	50686721	50686962	Promoter (<=1kb)	0
chr20	NELFCD	58981108	58981363	Promoter (<=1kb)	0
chr14	MIDEAS	73760073	73760355	Promoter (<=1kb)	0
chr1	FHAD1	15285194	15285392	Promoter (1-2kb)	-1653
chr21	KRTAP10-2	44550876	44551156	Promoter (<=1kb)	349
chr17	SLC25A10	81711721	81712087	Promoter (<=1kb)	-149
chr11	GVQW3	76381084	76381325	Promoter (<=1kb)	0
chr14	NRXN3	79279031	79279252	Promoter (<=1kb)	-87
chr15	USP3-AS1	63600652	63601092	Promoter (<=1kb)	0
chr2	AGAP1	235493933	235494137	Promoter (<=1kb)	0
chr5	EFNA5	107557078	107557545	Intron (ENST00000333274.11/1946, intron 1 of 4)	-50887
chr7	LFNG	2523436	2523644	Promoter (<=1kb)	0
chr7	MET	116672118	116672406	Promoter (<=1kb)	0
chrX	NHSL2	72018462	72018765	Intron (ENST00000633930.1/340527, intron 1 of 7)	-8716
chr1	ATP8B2	154328584	154328745	Promoter (<=1kb)	-54
chr11	VPS37C	61161387	61161684	Promoter (<=1kb)	0
chr19	KDM4B	5103123	5103348	Intron (ENST00000611640.4/23030, intron 9 of 23)	-9010
chr3	TPRG1	189304796	189304998	Intron (ENST00000433971.5/285386, intron 9 of 10)	-4896
chr16	ANKRD26P1	46390271	46390905	Distal Intergenic	87534
chr22	GNB1L	19854671	19855065	Promoter (<=1kb)	0
chr7	KDM7A-DT	140176946	140177349	Promoter (<=1kb)	0

chr20	INSM1	20364414	20364612	Exon (ENST00000623641.1/ENST00000623641.1, exon 1 of 1)	-3492
chr8	PVT1	128025071	128025596	Promoter (1-2kb)	-1913
chr15	IDH3A	78149325	78149611	Promoter (<=1kb)	0
chr2	CNNM3	96816589	96816863	Promoter (<=1kb)	321
chr14	AK7	96391756	96392074	Promoter (<=1kb)	-54
chr3	TNK2-AS1	195907774	195908020	Promoter (<=1kb)	-56
chr19	SMARCA4	10960684	10961009	Promoter (<=1kb)	0
chr16	ZFHX3	72927584	72927873	Intron (ENST00000268489.10/463, intron 3 of 9)	-37750
chr1	TTC39A	51297816	51298126	Promoter (<=1kb)	0
chr10	LCOR	96832837	96833033	Promoter (<=1kb)	0
chr14	LINC01303	61568648	61568984	Promoter (1-2kb)	1210
chr15	MEX3B	82046828	82047110	Promoter (<=1kb)	-810
chr4	ATOH1	93828579	93828808	Promoter (<=1kb)	0
chr4	PGRMC2	128287963	128288328	Promoter (<=1kb)	0
chr5	NREP	111757705	111757997	Promoter (<=1kb)	0
chr3	CADPS	62517157	62517534	Intron (ENST00000612439.4/8618, intron 15 of 27)	-16551
chr10	MARVELD1	97713693	97714618	Promoter (<=1kb)	0
chr13	IL17D	20704049	20704350	Promoter (<=1kb)	0
chr17	AIPL1	6377107	6377309	Distal Intergenic	57770
chr5	LINC01184	128083318	128083575	Promoter (<=1kb)	-146
chr6	MYB	135181046	135181320	Promoter (<=1kb)	0
chr7	VGF	101163679	101164019	Promoter (1-2kb)	1095
chr1	ELF3	202018830	202019248	Distal Intergenic	5052
chr19	SBK2	55526335	55526581	Distal Intergenic	9722
chr12	FGD6	95217393	95217632	Promoter (<=1kb)	0
chr17	PLD6	17206205	17206688	Promoter (<=1kb)	0
chr3	LINC00960	75669161	75669434	Promoter (2-3kb)	-2866
chr20	OVOL2	18058881	18059184	Promoter (<=1kb)	0
chr17	AMZ2P1	64975431	64975644	Promoter (<=1kb)	0
chr11	SYT7	61580995	61581344	Promoter (<=1kb)	0
chr14	ANGEL1	76812793	76812970	Promoter (<=1kb)	0
chr17	DUSP14	37489680	37489970	Promoter (<=1kb)	0
chr3	ATXN7	63937978	63938216	Intron (ENST00000674280.1/6314, intron 4 of 12)	25390
chr4	SGMS2	107824747	107824955	Promoter (<=1kb)	0

chr8	ZNF395	28401993	28402267	Intron (ENST00000521548.5/55893, intron 7 of 15)	-15533
chr3	PRICKLE2	64226682	64227104	Promoter (1-2kb)	-1216
chr3	ADAMTS9	64919997	64920547	Intron (ENST00000650103.1/100507098, intron 4 of 11)	-231997
chr12	RIMKLB	8697699	8698122	Promoter (<=1kb)	0
chr7	NAMPT	106284948	106285397	Promoter (<=1kb)	0
chr20	BMP7	57266310	57267180	Promoter (<=1kb)	0
chr17	TBX2-AS1	61407435	61409101	Promoter (2-3kb)	2454
chr14	FOXN3	89417155	89417350	Promoter (<=1kb)	0
chr17	DGKE	56833966	56834328	Promoter (<=1kb)	0
chr11	POU2AF1	111436743	111437012	Intron (ENST00000531398.1/5450, intron 1 of 4)	12969
chr17	MIR4737	60043182	60043650	Promoter (<=1kb)	-77
chr1	CDK18	205504611	205504902	Promoter (<=1kb)	0
chr2	PROC	127408018	127408349	Exon (ENST00000657275.1/ENST00000657275.1, exon 1 of 2)	-10078
chr10	ARID5B	61903203	61903453	Promoter (1-2kb)	1504
chr3	CD47	108091113	108091494	Promoter (<=1kb)	-82
chr3	SKIL	170356740	170357055	Promoter (<=1kb)	-623
chr17	TBX2-AS1	61405297	61407336	3' UTR	4219
chr15	CCDC33	74245471	74245739	Intron (ENST00000398814.8/80125, intron 2 of 18)	9145
chr1	SYT6	114152812	114153195	Promoter (<=1kb)	0
chr20	CYP24A1	54185048	54185401	Distal Intergenic	-11062
chr18	SMCHD1	2655560	2655877	Promoter (<=1kb)	0
chr11	CDON	126115949	126116240	Distal Intergenic	-52614
chr2	LPIN1	11746483	11746775	Promoter (<=1kb)	0
chrX	PDK3	24465017	24465269	Promoter (<=1kb)	-1

GFP2 GFP3 IDR

Chromosome	Gene name	Start	End	Annotation	Distance To TSS
chr3	HES1	194133943	194135355	Promoter (<=1kb)	-793
chr4	RBPJ	26319045	26319792	Promoter (<=1kb)	0
chr16	CHTF18	795569	795979	Promoter (<=1kb)	-636
chr8	TRIB1	125429785	125430381	Promoter (<=1kb)	0
chr8	TMEM70	73975918	73976314	Promoter (<=1kb)	0

chr2	FTCDNL1	199850959	199851440	Promoter (<=1kb)	0
chr11	LINC02751	157080377	157083977	Intron (ENST00000663676.1/ENST00000663676.1, intron 4 of 7)	102553
chr19	ARHGEF1	41904343	41904797	Promoter (<=1kb)	127
chr2	RAPH1	203535106	203535717	Promoter (<=1kb)	0
chr1	TP73	3668701	3669177	Exon (ENST00000443034.1/ENST00000443034.1, exon 1 of 3)	-13189
chr14	TNFAIP2	103126970	103127494	Promoter (<=1kb)	-72
chrM	MIR12136	3153	4003	Exon (ENST00000387347.2/ENST00000387347.2, exon 1 of 1)	3511
chr8	GASAL1	102806414	102807110	Promoter (<=1kb)	0
chr3	RYBP	72447127	72447449	Promoter (<=1kb)	-504
chr16	GSE1	85612927	85613388	Promoter (<=1kb)	0
chr17	CBX2	79778026	79778421	Promoter (<=1kb)	0
chr12	PAWR	79690929	79691475	Promoter (<=1kb)	0
chr9	VAV2	133992254	133992601	Promoter (<=1kb)	0
chr10	BNIP3	131981895	131982279	Promoter (<=1kb)	0
chr18	LPIN2	3013121	3013557	Promoter (<=1kb)	0
chr9	MYMK	133509539	133510048	Distal Intergenic	14911
chr14	MIPOL1	371977499	371981733	Promoter (<=1kb)	0
chr5	MAP3K1	56815174	56815550	Promoter (<=1kb)	0
chr12	RAN	130871595	130872088	Promoter (<=1kb)	0
chr3	LINC02028	194070943	194071457	Promoter (<=1kb)	0
chr9	DENND1A	123929913	123930231	Promoter (<=1kb)	0
chr3	LINC00886	156816857	156817317	Promoter (<=1kb)	0
chr19	ZNF296	45076113	45076598	Promoter (<=1kb)	0
chr12	KSR2	117969088	117969612	Promoter (<=1kb)	-98
chr14	ACOT2	73569667	73570061	Promoter (<=1kb)	382
chrM	MIR12136	26	1053	Exon (ENST00000387314.1/ENST00000387314.1, exon 1 of 1)	6461

chr17	DLX4	49968443	49968891	Promoter (<=1kb)	-79
chr22	TBX1	19806490	19806814	Exon (ENST00000329517.11/54584, exon 6 of 8)	41411
chr8	EMC2	108584495	108584801	Intron (ENST00000521504.1/ENST00000521504.1, intron 1 of 2)	110644
chrM	MIR12136	6221	6675	Promoter (<=1kb)	839
chr14	FOXA1	37595059	37595598	Promoter (<=1kb)	0
chr1	HSPG2	21956842	21957293	Exon (ENST00000637118.1/ENST00000637118.1, exon 1 of 2)	-19532
chr14	ITPK1	93115157	93115801	Promoter (<=1kb)	0
chr1	KCNQ4	40783572	40783936	Promoter (<=1kb)	0
chr14	PPP1R3E	23301519	23302012	Promoter (<=1kb)	0
chr16	GSE1	85611729	85612428	Promoter (<=1kb)	320
chr17	BAHCC1	81429392	81429725	Intron (ENST00000675386.2/57597, intron 3 of 27)	-13740
chr3	HES1	194141258	194142006	Distal Intergenic	5110
chr8	RUNX1T1	92103306	92103631	Promoter (<=1kb)	-20
chr14	EGLN3	33938366	33938713	Intron (ENST00000250457.9/112399, intron 1 of 4)	-7030
chrM	MIR12136	11645	16549	Exon (ENST00000361381.2/ENST00000361381.2, exon 1 of 1)	-4131
chrM	MIR12136	10550	11510	Exon (ENST00000361335.1/ENST00000361335.1, exon 1 of 1)	-3036
chr17	B3GNTL1	83050776	83051400	Promoter (<=1kb)	409
chr3	CDV3	133573526	133573836	Promoter (<=1kb)	0
chr2	DTNB	25673147	25674074	Promoter (<=1kb)	0
chr3	MYRIP	39809346	39809655	Promoter (<=1kb)	0
chr5	MIR2277	93677384	93677648	Intron (ENST00000395965.8/83989, intron 10 of 10)	-56596
chr9	PRUNE2	76906073	76906464	Promoter (<=1kb)	0
chrX	APLN	129654323	129654662	Promoter (<=1kb)	294
chr15	SMAD3	67065297	67065827	Promoter (<=1kb)	0
chr1	MAST2	45803391	45803713	Promoter (<=1kb)	0

chr11	TMPRSS4	118057636	118057952	Intron (ENST00000636151.1/100526771, intron 3 of 6)	-19060
chr1	TTC39A	51297853	51298140	Promoter (<=1kb)	0
chr19	NFIX	13051576	13052015	Intron (ENST00000592199.6/4784, intron 2 of 10)	-17988
chr3	XIRP1	39180855	39181272	Distral Intergenic	11323
chr16	MMP2	55480304	55480628	Promoter (<=1kb)	0
chr6	MYB	135181105	135181325	Promoter (<=1kb)	0
chr20	BMP7	57189819	57190770	Promoter (2-3kb)	-2663
chr20	PREX1	48828203	48828556	Promoter (<=1kb)	-204
chr17	DGKE	56833960	56834328	Promoter (<=1kb)	0
chr4	LINC01262	189235000	189235431	Distral Intergenic	-424174
chr1	KCNAB2	6026124	6026476	Promoter (<=1kb)	0
chr10	NEURL1	103555018	103555378	Promoter (<=1kb)	0
chr17	RPL23AP87	83189763	83190108	Intron (ENST00000651869.1/ENST00000651869.1, intron 2 of 3)	-36789
chr5	EFNA5	107557078	107557545	Intron (ENST00000333274.11/1946, intron 1 of 4)	-50887
chr6	FOXO3	108557919	108558256	Promoter (1-2kb)	-1579
chr16	NTHL1	2039588	2039885	Promoter (<=1kb)	583
chr1	FOXO6	41353823	41354101	Distral Intergenic	-7821
chr17	TBX2-AS1	61407435	61409101	Promoter (2-3kb)	2454
chr2	SP3	173963955	173964311	Promoter (<=1kb)	0
chr3	LOC105376975	177425116	177429664	Promoter (<=1kb)	0
chr17	PPP1R1B	39617673	39618080	Distral Intergenic	-8660
chr3	PRICKLE2-AS1	64049616	64050160	Distral Intergenic	-17804
chr12	ANKS1B	99984443	99985003	Promoter (<=1kb)	0
chr20	EPB41L1	36154350	36154726	Promoter (<=1kb)	-14
chr4	JAKMIP1	6200248	6200701	Promoter (<=1kb)	0
chr17	TBX2-AS1	61409230	61409789	Promoter (1-2kb)	1766
chr15	USP3-AS1	63600652	63601098	Promoter (<=1kb)	0
chr3	HES1	194135771	194136225	Promoter (<=1kb)	0

chr4	CAMK2D	113636901	113637154	Intron (ENST00000394524.7/817, intron 3 of 17)	-119258
chr17	TBX4	61462414	61464615	Promoter (<=1kb)	0
chr16	SLC12A4	67961700	67962011	Promoter (2-3kb)	2054
chr2	CT75	222319523	222319890	Promoter (<=1kb)	225
chr3	PROS1	93470357	93470824	Distal Intergenic	415589
chr15	TRPM7	50686714	50686962	Promoter (<=1kb)	0
chr2	AGAP1	235493923	235494143	Promoter (<=1kb)	0
chr20	CYP24A1	54185000	54185401	Distal Intergenic	-11014
chr14	MIDEAS	73759973	73760369	Promoter (<=1kb)	0
chr18	MTCL1	8705061	8705442	Promoter (<=1kb)	-219
chr20	BCAS1	53996528	53997154	Promoter (<=1kb)	-599
chr20	NRSN2-AS1	324335	324739	Promoter (<=1kb)	0
chr9	PRRT1B	131545395	131545729	Promoter (<=1kb)	0
chr19	ZFP36	39402476	39402843	Distal Intergenic	-4004
chr19	MLLT1	6236989	6237337	Intron (ENST00000252674.9/4298, intron 3 of 11)	-20021
chr21	KRTAP10-2	44550726	44551156	Promoter (<=1kb)	349
chr6	FOXO3	108559547	108559914	Promoter (<=1kb)	0
chr7	NDUFA4	109403776	109407784	Promoter (<=1kb)	-223
chr6	FKBP5	35727946	35728473	Promoter (<=1kb)	110
chr3	ADAMTS9	64648750	64649355	Intron (ENST00000498707.5/56999, intron 10 of 39)	5324
chr10	ZMIZ1	79242783	79243117	Promoter (<=1kb)	-552
chr11	PAX6	31812037	31812291	Promoter (<=1kb)	0
chr14	NRXN3	79279031	79279306	Promoter (<=1kb)	-33
chr2	MIR1301	253113477	253115999	Intron (ENST00000264709.7/1788, intron 2 of 22)	17122
chr21	MIR6815	45470912	45471299	Intron (ENST00000651438.1/80781, intron 3 of 41)	-6967
chr20	BMP7	57125623	57127107	Distal Intergenic	46482
chrM	MIR12136	5286	5542	Promoter (1-2kb)	1972
chr3	PRICKLE2	64222404	64222717	Promoter (2-3kb)	2749
chr13	LINC00572	29924144	29924397	Promoter (2-3kb)	2254

chr3	TPRA1	127590972	127591476	Promoter (<=1kb)	0
chr6	LOC102724511	170026578	170026848	Distal Intergenic	-133758
chr20	BMP7	57262074	57263129	Promoter (2-3kb)	2649
chr17	LINC00511	72640461	72640760	Promoter (<=1kb)	0
chr9	SEMA4D	89497987	89498300	Promoter (<=1kb)	0
chr14	SPTSSA	34462118	34462370	Promoter (<=1kb)	0
chr18	DLGAP1	3710695	3711094	Intron (ENST00000400147.6/9229, intron 4 of 9)	18284
chr1	PADI4	17340347	17340671	Intron (ENST00000375448.4/23569, intron 6 of 15)	-5363
chr16	ZFHX3	72927590	72927873	Intron (ENST00000268489.10/463, intron 3 of 9)	-37756
chr17	TBX4	61475391	61476004	Promoter (2-3kb)	-2347
chr11	SMIM38	69122762	69122997	Intron (ENST00000637504.1/219931, intron 19 of 19)	-32481
chr12	LOC645485	30754733	30755150	Promoter (<=1kb)	0
chr12	ASCL1	102957226	102957631	Promoter (<=1kb)	-43
chr2	DUSP2	96145022	96145285	Promoter (<=1kb)	155
chr5	LINC01184	128083218	128083575	Promoter (<=1kb)	-46
chr6	DCDC2	24359856	24360122	Promoter (1-2kb)	-1797
chr6	LOC102724511	170178935	170179397	Exon (ENST00000610240.1/ENST00000610240.1, exon 1 of 1)	18273
chr7	LFNG	2524114	2524415	Promoter (<=1kb)	-233
chr7	NAMPT	106284948	106285397	Promoter (<=1kb)	0
chr16	VASN	4374879	4375077	Intron (ENST00000304735.4/114990, intron 1 of 1)	3031
chr20	BMP7-AS1	57218290	57218874	Intron (ENST00000395863.8/655, intron 2 of 6)	3418
chr17	TBX2-AS1	61340666	61341177	Intron (ENST00000407086.8/54828, intron 22 of 23)	52885
chr2	BIRC6	32356872	32357125	Promoter (<=1kb)	0
chr20	LOC101927377	47351724	47354176	Promoter (<=1kb)	0
chr16	CA5A	87925443	87925675	Exon (ENST00000568801.1/763, exon 3 of 3)	10854
chr20	BCAS1	53937945	53938435	3' UTR	57494
chr3	PSMD6-AS2	64006615	64007069	Promoter (2-3kb)	2593

chr3	ADAMTS9-AS2	64684905	64685243	Promoter (<=1kb)	0
chr20	LINC00494	48204304	48204855	Distal Intergenic	-155029
chr20	NELFCD	58981086	58981295	Promoter (<=1kb)	0
chr8	PVT1	128025071	128025596	Promoter (1-2kb)	-1913
chr11	CCDC85B	65890519	65890920	Promoter (<=1kb)	0
chr8	LINC01606	57209784	57210274	Exon (ENST00000521653.6/ENST00000521653.6, exon 7 of 7)	-8002
chr21	PSMG1	39183302	39183682	Promoter (<=1kb)	0
chr20	LINC01522	48018002	48018526	Intron (ENST00000651247.1/ENST00000651247.1, intron 1 of 4)	-27875
chr3	PRICKLE2-AS3	64187183	64188437	Promoter (<=1kb)	0
chrM	MIR12136	9699	9931	Promoter (2-3kb)	-2185
chr12	LRTM2	1837109	1837330	Intron (ENST00000537784.5/93589, intron 4 of 14)	9546
chr14	LINC02691	104373162	104373484	Distal Intergenic	149507
chr22	SCARF2	20430958	20431534	Promoter (1-2kb)	-1032
chr7	MET	116672057	116672462	Promoter (<=1kb)	0
chr17	SLC25A10	81711816	81712087	Promoter (<=1kb)	-149
chr11	GVQW3	76381048	76381345	Promoter (<=1kb)	0
chr20	BMP7-AS1	57217404	57217967	Promoter (2-3kb)	2532
chr3	PRICKLE2-AS1	64055352	64055602	Distal Intergenic	-12362
chr1	DHRS3	12595987	12596184	Promoter (<=1kb)	124
chr1	ATP8B2	154328584	154328852	Promoter (<=1kb)	0
chr11	VPS37C	61161443	61161684	Promoter (<=1kb)	0
chr12	EPS8	157895001	157898880	Promoter (<=1kb)	-101
chr19	KDM4B	5103138	5103348	Intron (ENST00000611640.4/23030, intron 9 of 23)	-9010
chr20	INSM1	20364416	20364612	Exon (ENST00000623641.1/ENST00000623641.1, exon 1 of 1)	-3492
chr3	CFAP92	129003852	129004077	Promoter (1-2kb)	-1162
chr3	TPRG1	189304832	189305014	Intron (ENST00000433971.5/285386, intron 9 of 10)	-4880

chr3	ADAMTS9-AS1	64558839	64559504	Promoter (1-2kb)	-1818
chr3	ADAMTS9	64859083	64859395	Intron (ENST00000650103.1/100507098, intron 3 of 11)	-171083
chr16	ANKRD26P1	46390290	46390883	Distal Intergenic	87556
chr3	PSMD6-AS2	64005774	64006435	Promoter (1-2kb)	1752
chr3	ADAMTS9-AS1	64559849	64560052	Promoter (1-2kb)	-1270
chr20	BMP7	57171283	57172333	Promoter (1-2kb)	1256
chr22	GNB1L	19854671	19855039	Promoter (<=1kb)	0
chr1	NTNG1	107140849	107141699	Promoter (<=1kb)	0
chr17	TBX4	61450791	61451385	Promoter (1-2kb)	-1019
chr20	LINC01523	47895451	47896022	Distal Intergenic	-87382
chr3	ADAMTS9	64604780	64605384	Intron (ENST00000498707.5/56999, intron 23 of 39)	10766
chr3	ADAMTS9	64920704	64921033	Intron (ENST00000650103.1/100507098, intron 4 of 11)	-232704
chr3	PSMD6-AS2	64003778	64005282	Promoter (<=1kb)	0
chr20	BMP7	57263791	57264596	Promoter (1-2kb)	1182
chrM	MIR12136	10087	10391	Promoter (2-3kb)	-2573
chr15	IDH3A	78149314	78149639	Promoter (<=1kb)	0
chr20	BCAS1	53979345	53979733	Intron (ENST00000448484.5/8537, intron 5 of 8)	16196
chr3	PSMD6-AS2	64005402	64005615	Promoter (1-2kb)	1380
chr3	PRICKLE2	64232316	64233453	Intron (ENST00000564377.6/166336, intron 1 of 7)	-6850
chr12	ATP2B1	89709702	89709951	Promoter (<=1kb)	-402
chr2	CNNM3	96816526	96816855	Promoter (<=1kb)	258
chr3	ADAMTS9	64852484	64852683	Intron (ENST00000650103.1/100507098, intron 3 of 11)	-164484
chr20	BMP7	57267359	57269152	Promoter (<=1kb)	-718
chr4	LINC01262	189233838	189234079	Distal Intergenic	-425526
chr14	AK7	96391689	96392087	Promoter (<=1kb)	-41
chr1	SYT6	114215274	114215711	Intron (ENST00000420156.2/ENST00000420156.2, intron 1 of 1)	-61394

chr20	CDK5RAP1	33374021	33374242	Promoter (<=1kb)	-662
chr20	LINC00494	48187294	48187606	Distal Intergenic	-172278
chr20	OVOL2	18058881	18059103	Promoter (<=1kb)	0
chr1	SYT6	114196910	114197179	Distal Intergenic	-43030
chr3	ADAMTS9	64857343	64858035	Intron (ENST00000650103.1/100507098, intron 3 of 11)	-169343
chr17	TBX4	61451787	61452150	Promoter (<=1kb)	-254
chr17	TBX2-AS1	61409974	61410435	Promoter (1-2kb)	1120
chr1	S100A10	151993690	151993941	Promoter (<=1kb)	0
chr1	NTNG1	107256496	107256961	Intron (ENST00000370073.6/22854, intron 2 of 7)	-3842
chr11	PRDM10	129924838	129925102	Exon (ENST00000358825.9/56980, exon 13 of 22)	17488
chr15	BMF	40103373	40103613	Promoter (2-3kb)	2473
chr16	LINC02188	86829386	86829687	Distal Intergenic	94587
chr5	ZSWIM6	61330923	61331142	Promoter (1-2kb)	-1116
chr9	NFIB	14315208	14315546	Promoter (<=1kb)	-626
chr20	BMP7	57156096	57156349	Distal Intergenic	17240
chr16	ZFPM1-AS1	88501101	88501297	Intron (ENST00000319555.8/161882, intron 3 of 9)	29756
chr20	LINC00494	48178666	48179058	Distal Intergenic	-180826
chr10	LCOR	96832872	96833076	Promoter (<=1kb)	0
chr10	FAM53B	124744240	124744571	Promoter (<=1kb)	0
chr14	LINC01303	61568597	61568984	Promoter (1-2kb)	1210
chr18	ZNF516	76348504	76348910	Distal Intergenic	30003
chr4	ATOH1	93828580	93828808	Promoter (<=1kb)	0
chr4	PGRMC2	128287859	128288337	Promoter (<=1kb)	0
chr5	NREP	111757614	111757997	Promoter (<=1kb)	0
chr9	UBE2R2	33816986	33817215	Promoter (<=1kb)	0
chr20	LINC00494	48199820	48200256	Distal Intergenic	-159628
chr3	TNK2-AS1	195907798	195908020	Promoter (<=1kb)	-56

chr17	TBX4	61478350	61479618	Promoter (<=1kb)	0
chr20	BCAS1	53950008	53950403	Intron (ENST00000448484.5/8537, intron 7 of 8)	45526
chr10	MARVELD1	97713675	97714618	Promoter (<=1kb)	0
chr20	SULF2	47662527	47665041	Promoter (<=1kb)	0
chr13	IL17D	20704113	20704425	Promoter (<=1kb)	34
chr20	ZNF217	53592132	53593003	Promoter (<=1kb)	836
chr17	LOC101927855	61400097	61401600	Promoter (<=1kb)	0
chr17	TBX4	61479863	61480333	Promoter (1-2kb)	1500
chr20	PFDN4	54199484	54199674	Distal Intergenic	-8413
chr20	MIR3616	47141593	47143197	Exon (ENST00000357410.7/2139, exon 10 of 14)	-23770
chr20	BMP7	57164935	57165162	Distal Intergenic	8427
chr3	ADAMTS9	64921399	64922352	Intron (ENST00000650103.1/100507098, intron 4 of 11)	-233399
chr1	ELF3	202018802	202019248	Distal Intergenic	5024
chr19	SBK2	55526314	55526642	Distal Intergenic	9661
chr20	BMP7	57233089	57233651	Intron (ENST00000395863.8/655, intron 1 of 6)	-8249
chr3	ATXN7	63995194	63995422	Intron (ENST00000674280.1/6314, intron 11 of 12)	4684
chr3	PRICKLE2-AS1	64060387	64060800	Distal Intergenic	-7164
chr20	LINC00494	48326261	48326685	Exon (ENST00000651871.1/ENST00000651871.1, exon 3 of 3)	-33199
chr8	LOC105375800	143771647	143771880	Promoter (<=1kb)	0
chr17	PLD6	17206205	17206907	Promoter (<=1kb)	0
chr17	TBX4	61464767	61466412	Promoter (<=1kb)	0
chr1	KCND3-IT1	111877397	111877725	Intron (ENST00000369697.5/3752, intron 1 of 5)	-20492
chr7	SEMA3C	80919069	80919375	Promoter (<=1kb)	0
chr3	ADAMTS9	64688052	64688652	Promoter (<=1kb)	-52
chr3	ADAMTS9-AS1	64578436	64579291	Intron (ENST00000626014.2/101929335, intron 1 of 3)	-3252
chr20	PARD6B	50731189	50731501	Promoter (<=1kb)	-79

chr20	BMP7-AS1	57216567	57217294	Promoter (1-2kb)	1695
chr20	LINC00494	48381690	48382755	Distal Intergenic	16043
chr4	MFSD8	127965216	127965429	Promoter (<=1kb)	0
chr3	ADAMTS9-AS1	64563737	64564241	Promoter (2-3kb)	2006
chr3	PRICKLE2	64251280	64251972	Intron (ENST00000564377.6/166336, intron 1 of 7)	16202
chr16	SBK1	28292321	28292505	Promoter (<=1kb)	-20
chr12	FGD6	95217393	95217632	Promoter (<=1kb)	0
chr20	CYP24A1	54152569	54152868	Distal Intergenic	4430
chr20	ZNF217	53583038	53583324	Promoter (<=1kb)	0
chr3	ADAMTS9-AS1	64588307	64588678	Exon (ENST00000594810.3/101929335, exon 3 of 3)	4523
chr17	AMZ2P1	64975403	64975644	Promoter (<=1kb)	0
chr19	ZNF581	55642905	55643118	Promoter (<=1kb)	-531
chr1	ARHGEF11	157045700	157045892	Promoter (<=1kb)	0
chr1	SNAP47	227766210	227766436	Intron (ENST00000366760.5/116841, intron 2 of 3)	18056
chr11	TSPAN4	842818	843071	Promoter (<=1kb)	0
chr11	SYT7	61581012	61581344	Promoter (<=1kb)	0
chr14	ANGEL1	76812710	76812970	Promoter (<=1kb)	0
chr17	DUSP14	37489586	37489925	Promoter (<=1kb)	0
chr21	MIR3648-1	8992276	8992542	Distal Intergenic	5277
chr3	ATXN7	63986039	63986317	Promoter (1-2kb)	-1882
chr4	SGMS2	107824748	107824971	Promoter (<=1kb)	0
chr8	ZNF395	28401944	28402281	Intron (ENST00000521548.5/55893, intron 7 of 15)	-15484
chr17	TBX2-AS1	61387641	61388927	Exon (ENST00000589222.5/54828, exon 25 of 26)	5135
chr1	NTNG1	107160583	107160824	Intron (ENST00000370073.6/22854, intron 2 of 7)	11989
chr3	PRICKLE2	64220848	64221239	Intron (ENST00000638394.2/166336, intron 1 of 7)	4227
chr20	LINC01522	48154876	48155108	Distal Intergenic	-164749
chr1	NTNG1	107326930	107327245	Intron (ENST00000370073.6/22854, intron 3 of 7)	66127
chr20	PPP4R1L	58264792	58265041	Intron (ENST00000650934.1/55370, intron 5 of 17)	7784

chr20	BMP7-AS1	57211992	57212958	Promoter (1-2kb)	-1914
chr3	ADAMTS9	64932817	64933165	Intron (ENST00000650103.1/100507098, intron 4 of 11)	-244817
chr3	PSMD6	64014443	64015078	Promoter (1-2kb)	-1155
chr1	LINC01661	106842744	106842987	Intron (ENST00000659929.1/105378889, intron 4 of 4)	24483
chr3	PRICKLE2	64267891	64268637	Promoter (<=1kb)	0
chr3	ADAMTS9	64603551	64604369	Exon (ENST00000498707.5/56999, exon 24 of 40)	11781
chr5	NPM1	171388486	171388720	Promoter (<=1kb)	0
chr3	PRICKLE2-AS1	64054491	64054758	Distal Intergenic	-13206
chr8	FAM135B	138206163	138206577	Intron (ENST00000395297.6/51059, intron 7 of 19)	-53759
chr20	PREX1	48804527	48804932	Intron (ENST00000371941.4/57580, intron 1 of 39)	23067
chr3	ADAMTS9	64898208	64898566	Intron (ENST00000650103.1/100507098, intron 4 of 11)	-210208
chr17	DHRS13	28903027	28903263	Promoter (<=1kb)	0
chrM	MIR12136	1620	1863	Exon (ENST00000387342.1/ENST00000387342.1, exon 1 of 1)	5651
chr3	PRICKLE2	64331466	64331953	Intron (ENST00000295902.11/166336, intron 2 of 8)	-63292
chr3	ADAMTS9	64724067	64724373	Intron (ENST00000460833.1/100507098, intron 1 of 1)	-36067
chr17	TBX4	61457291	61461126	Promoter (<=1kb)	827
chr20	BCAS1	53991709	53993027	Promoter (2-3kb)	2902
chr17	LINC00511	72634964	72635168	Intron (ENST00000581549.2/400619, intron 2 of 4)	5304
chr17	TBX4	61485211	61485956	Downstream (<=300bp)	6848
chr20	LINC01522	48151754	48152220	Distal Intergenic	-161627
chr20	BCAS1	53983533	53983910	Intron (ENST00000448484.5/8537, intron 5 of 8)	12019
chr20	BMP7	57266310	57267232	Promoter (<=1kb)	0
chr14	FOXN3	89417156	89417350	Promoter (<=1kb)	0
chr17	TBX4	61452540	61452997	Promoter (<=1kb)	118
chr1	SYT6	114113082	114113441	Intron (ENST00000610121.5/148281, intron 3 of 6)	38999

chrX	XPNPEP2	129706480	129706718	Distal Intergenic	-32256
chr3	ADAMTS9	64870702	64871015	Intron (ENST00000650103.1/100507098, intron 4 of 11)	-182702
chr20	ZNF217	53593747	53594864	Promoter (<=1kb)	0
chr17	TBX2-AS1	61389060	61390818	Exon (ENST00000588720.1/ENST00000588720.1, exon 1 of 1)	3244
chr20	LINC01522	48123706	48124258	Intron (ENST00000655183.1/ENST00000655183.1, intron 1 of 3)	-133579
chr1	PRMT6	107031953	107032500	Distal Intergenic	-24174
chr11	POU2AF1	111436753	111437012	Intron (ENST00000531398.1/5450, intron 1 of 4)	12969
chr3	SNTN	63652138	63652561	Promoter (<=1kb)	-114
chr17	MIR4737	60043182	60043548	Promoter (<=1kb)	-77
chr1	CDK18	205504646	205504940	Promoter (<=1kb)	0
chr20	LINC01523	47894714	47895253	Distal Intergenic	-88151
chr20	BCAS1	53997722	53997968	Promoter (1-2kb)	-1793
chr2	PROC	127407949	127408349	Exon (ENST00000657275.1/ENST00000657275.1, exon 1 of 2)	-10078
chr3	SYNPR	63237740	63238013	Intron (ENST00000478456.5/132204, intron 1 of 4)	9425
chr20	LINC00494	48393844	48394122	Distal Intergenic	28197
chr1	KCND3	111983591	111984003	Promoter (<=1kb)	-795
chr2	SPRED2	65431125	65431335	Promoter (1-2kb)	1264
chr22	TBX1	19756755	19757028	Promoter (<=1kb)	52
chr3	LSM3	142489466	142491900	Distal Intergenic	70129
chr3	CD47	108090986	108091291	Promoter (<=1kb)	0
chr3	SKIL	170356748	170357029	Promoter (<=1kb)	-649
chr4	ELF2	139177506	139177760	Promoter (<=1kb)	-288
chr5	AHRR	373656	373988	Intron (ENST00000505113.6/116412618, intron 5 of 12)	30128
chr8	GSR	30727700	30727890	Promoter (<=1kb)	0
chr8	CALB1	90082532	90082954	Promoter (<=1kb)	0

chr1	PRMT6	107030925	107031143	Distal Intergenic	-25531
chr20	PREX1	48635224	48635571	Intron (ENST00000482556.5/57580, intron 15 of 21)	7167
chr20	SULF2	47747857	47748020	Intron (ENST00000359930.8/55959, intron 2 of 20)	9311
chr3	ADAMTS9	64601950	64602707	Exon (ENST00000498707.5/56999, exon 26 of 40)	13443
chr3	PRICKLE2-AS1	64056938	64057221	Distal Intergenic	-10743
chr3	ADAMTS9	64940131	64940696	Intron (ENST00000650103.1/100507098, intron 4 of 11)	-252131
chr20	BMP7	57104270	57104570	Distal Intergenic	69019
chr3	ATXN7	63995572	63996469	Exon (ENST00000674280.1/6314, exon 12 of 13)	5062
chr1	SYT6	114103932	114104238	Intron (ENST00000610121.5/148281, intron 3 of 6)	48202
chr7	VGF	101163635	101164019	Promoter (1-2kb)	1095
chr8	LINC00861	126098841	126099196	Intron (ENST00000651482.1/100130231, intron 3 of 3)	-126730
chr20	SULF2	47657854	47658435	Promoter (1-2kb)	1295
chr20	CYP24A1	54136411	54137520	Distal Intergenic	19778
chr3	PSMD6	64009521	64009903	Exon (ENST00000472046.1/100507062, exon 2 of 3)	3385
chr3	ESYT3	138434383	138434687	Promoter (<=1kb)	0
chr20	BCAS1	53990794	53991171	Intron (ENST00000448484.5/8537, intron 4 of 8)	4758
chr20	TFAP2C	56735224	56735451	Distal Intergenic	104990
chr17	TBX2-AS1	61393472	61395921	Promoter (<=1kb)	0
chr17	TBX4	61454276	61457138	Promoter (<=1kb)	0
chr17	TBX2-AS1	61384877	61385295	Intron (ENST00000407086.8/54828, intron 23 of 23)	8767
chr1	SYT6	114080885	114081259	Distal Intergenic	71181
chr1	LINC01661	106604261	106605002	Distal Intergenic	-213222
chr3	ADAMTS9	64636869	64637050	Intron (ENST00000498707.5/56999, intron 12 of 39)	17629
chr3	ADAMTS9	64737700	64737961	Intron (ENST00000460833.1/100507098, intron 1 of 1)	-49700
chr20	BMP7-AS1	57213911	57216495	Promoter (<=1kb)	0
chr17	ERN1	64043395	64043569	3' UTR	11198

chr3	PRICKLE2	64267091	64267335	Promoter (<=1kb)	839
chr20	BCAS1	53993126	53994530	Promoter (1-2kb)	1399
chr20	CYP24A1	54173924	54174283	Promoter (<=1kb)	0
chr2	ITGA6-AS1	172455243	172455457	Intron (ENST00000412899.5/3655, intron 1 of 6)	10555
chr3	ADAMTS9	64615798	64616348	Promoter (<=1kb)	0
chr20	RIN2	19783955	19784130	Intron (ENST00000432334.2/54453, intron 1 of 3)	-15443
chr3	ADAMTS9	64685866	64686420	Promoter (<=1kb)	190
chr20	BMP7	57177987	57178558	Exon (ENST00000463939.1/655, exon 3 of 3)	-4398
chr20	LINC02910	60053365	60053817	Promoter (2-3kb)	-2036
chr17	TBX2-AS1	61411163	61413758	Promoter (<=1kb)	0
chr11	CDON	126115949	126116268	Distal Intergenic	-52614
chr2	LPIN1	11746476	11746842	Promoter (<=1kb)	0
chr3	LINC00698	62986667	62987099	Intron (ENST00000475886.5/285401, intron 3 of 6)	36196
chr3	ADAMTS9	64637246	64637831	Intron (ENST00000498707.5/56999, intron 12 of 39)	16848
chr20	BMP7	57113661	57114088	Intron (ENST00000652038.1/ENST00000652038.1, intron 1 of 2)	59501
chr20	CYP24A1	54168374	54168563	Intron (ENST00000216862.8/1591, intron 4 of 11)	3390
chr17	TBX2-AS1	61399301	61399629	Promoter (<=1kb)	0
chr3	SYNPR-AS1	63575221	63575407	Intron (ENST00000478300.6/132204, intron 4 of 5)	-25170
chr20	LSM14B	62122039	62122250	Promoter (<=1kb)	-211
chr20	LINC01271	50400244	50400479	Distal Intergenic	-78902
chrM	MIR12136	2153	2475	Exon (ENST00000387347.2/ENST00000387347.2, exon 1 of 1)	5039
chrX	PDK3	24465017	24465265	Promoter (<=1kb)	-5

Table(s) S2 List of high confidence HES1 targets identified by ChIP-seq